Faculty of Engineering

Department of Chemical and Environmental Engineering

Manufacturing & Process Technologies Division

Environmental Fluid Mechanics and Geoprocesses Research Group

Microwave-assisted In-situ Catalytic Upgrading of Heavy Oil

Hossein Anbari

Thesis submitted to the University of Nottingham

for the degree of Doctor of Philosophy

Supervisors:

Professor Sean Rigby

Professor John Robinson

Dr Mohamed Adam

March 2023

Abstract

This work concerns reservoir simulation of heavy oil recovery and experimental studies of downhole oil catalytic upgrading enhanced with microwaves. Numerical simulations are a key tool to investigate the Toe to Heel Air Injection (THAI) operating mechanism due to the limitations in experimental (3D combustion cell) THAI investigations. In this study, the THAI process was numerically studied through reservoir simulations. The starting point of the numerical simulation study was to develop a new experimental scale THAI model. The new experimental scale THAI model was history-matched against previous 3D combustion tube experiments. The experimental scale THAI model was then scaled up to a field scale model. The field scale THAI models were then used to study two types of THAI well arrangements, namely the direct line drive (DLD) and staggered line drive (SLD). The DLD and SLD well arrangements were compared in terms of sweep efficiency, water cut, and oxygen utilisation. Although, the DLD well arrangement resulted in earlier oil production, it was shown that, in terms of overall performance, the SLD well arrangement is superior to the DLD well arrangement.

There are only a limited number of published field scale THAI models in the literature. None of the previously developed field scale THAI models, that considered an underlying bottom water (BW) in the reservoir, was validated against field data. *Ab initio* field-scale model development using a direct history matching of a field-scale THAI process with BW has never been published by other researchers. This was due to insufficient published data concerning the oil production trends experienced in the field. It was also hypothesised (from former numerical studies) that reducing the air injection rate will lead to lower oil production rates. This work, for the first time, presents a field-scale THAI model that was validated against data obtained from the Kerrobert THAI project in Canada. The model includes the existing

relatively thick bottom water in the studied formation. A real life quasi-staggered line drive (QSLD) THAI well configuration was studied through the history-matched model. The history matched model was also used to investigate the effect of the variation in air injection rates on THAI performance in presence of BW. It was demonstrated that extra air ingress from the neighbouring THAI well pair had caused a reduction in oxygen utilisation throughout the process. As a result, the simulated temperature profile declined with an increasing combustion time. An inversely proportional relationship was detected between the coke concentration and the oxygen profile around the HP well. It was found that the size of the steam zone, ahead of the combustion front, differs with variation in air injection rates. It was observed that some of the mobilised oil sank into the BW, leaving a significant amount of oil trapped in the reservoir. To prevent such an event, the location of the HP well was altered as a potential strategy to optimise the THAI efficiency. Consequently, the predicted oxygen utilisation, as well as cumulative oil production, were improved in comparison with the history-matched model.

The CAtalytic upgrading PRocess In situ (CAPRI) is an add-on to the THAI process. The horizontal section of the producer well is surrounded by a catalyst layer in the CAPRI process. Further upgrading occurs as the THAI oil flows through the catalyst layer. The history-matched THAI simulation, developed in this study, showed that the in-situ combustion alone may not provide sufficient heating for downhole catalytic upgrading of heavy oil in the THAI-CAPRI process. Therefore, an extra heating source is required for a successful THAI-CAPRI process. As a strategy to provide the needed heating, a microwave heating technique has been proposed in this study. It was demonstrated that heavy oil can be heated directly with microwaves to 425°C, which is the temperature needed for successful catalytic upgrading. Contrary to previous assertions, the microwave heating of heavy oil was done without the need for an additional microwave susceptor. Two commercially available hydrodesulphurization (HDS) and low temperature shift (LTS) catalysts as well as Alumina support, were each used for

microwave-assisted catalytic upgrading experiments. The characterisation of the treated oil revealed a considerable upgrading performance in terms of API gravity, reduction in viscosity, and reduction in sulphur content.

The characteristics of the THAI process are suitable not only for in-situ upgrading but for hydrogen production downhole. Employing the catalytic add-on of the THAI process (the CAPRI process) could potentially result in even higher in-situ hydrogen production. In this study, a series of microwave-assisted catalytic upgrading experiments were carried out to investigate the hydrogen production potential of the CAPRI process. Two commercial hydrodesulphurization and low shift temperature catalysts were used for the microwave-assisted catalytic hydrogen production experiments. A significant hydrogen content was detected in the gas product using the HDS and LTS catalyst. The produced hydrogen was originated from the catalytic dehydrogenation of heavy oil. The produced hydrogen in-situ within the THAI-CAPRI process can be used to facilitate hydrodesulphurization as well as improving API gravity upgrading by hydrogenation of the treated oil.

Dedication

To my parents, Masoumeh Lesan and Mohammadreza Anbari

To my sisters, Lachin Anbari and Samin Anbari

Acknowledgements

I would like to thank my supervisors, Professor Sean Rigby, Professor John Robinson, and Dr Mohamed Adam. It was a great honour to work under the supervision of a brilliant team of experts in the field of enhanced oil recovery and microwave heating technologies. I am sincerely grateful for their technical insight during my doctoral research. I am also thankful for their support during the unprecedented time of COVID-19 pandemic.

Special thanks to Professor Malcolm Greaves and Mr Konstantin Starkov for their support and insight during the development of the history-matched THAI model. I also wish to thank Dr Alex Turta for providing the Comprehensive Assessment of the THAI Process report.

I truly acknowledge Dr Mohamed Adam for designing the microwave-assisted catalytic upgrading batch reactor system. I thank him for his assistance with electromagnetic simulations, as well as characterising coke and sulphur deposition on the HDS catalyst and sulphur content of the treated oil. Many thanks to Dr Clement Uguna, Mr David Mee, and Mr Theo Ching for their assistance with GC, N_2 adsorption, TGA analysis, respectively.

I would like to thank the University of Nottingham and Natural Environment Research Council Centre for Doctoral Training in Oil & Gas for funding this research project. I am grateful to Computer Modelling Group for their technical support during this project.

Last but not least, I would like to thank my family and friends for their unconditional love and support. Thank you for believing in me.

Table of Contents

Abstract i
Dedication iv
Acknowledgements v
List of Figures x
List of Tables xiv
List of Publications xv
1. Introduction 1
1.1 Thesis outline 3
2. Literature review and aims and objectives of this study 5
2.1 Heavy oil recovery: Principles and Technologies 5
2.2 Thermal Enhanced Oil Recovery 7
2.3 Steam-based Processes 7
2.3.1 Cyclic Steam Stimulation (CSS) 8
2.3.2 Steam Assisted Gravity Drainage (SAGD) 8
2.3.3 Vapour Assisted Petroleum Extraction (VAPEX) 9
2.3.4 Expanding Solvent Steam Assisted Gravity Drainage (ES-SAGD) 10
2.4 In-situ combustion (ISC) 11
2.5 Demand for the development of new in-situ combustion ISC technologies 12
2.6 Toe to Heal Air Injection (THAI) 13
2.7 THAI laboratory work 17
2.7.1 3D combustion cell experiments 17
2.7.2 Limitation of 3D combustion cell experiments 20
2.8 THAI simulation work 22
2.8.1 THAI numerical models in laboratory scale 22
2.8.2 THAI numerical models in field scale 25
2.8.3 Issues with previously developed THAI numerical models in field scale 26
2.9 Limitation of the THAI process 26
2.10 Aims and objectives of this study 31

3. THAI numerical modelling 32
3.1 Introduction 32
3.2 Experimental-scale THAI numerical simulation 32
3.2.1 Model Development 33
3.2.2 PVT and Petrophysical Properties 35
3.2.3 Kinetics scheme 37
3.2.4 Operating conditions 39
3.2.5 Model validation 39
3.2.6 Results and discussions 40
3.3 Field-scale THAI numerical simulation 45
3.3.1 Model Development 46
3.3.2 PVT and Petrophysical Properties 49
3.3.3 Kinetics scheme 51
3.3.4 Operating condition 53
3.3.5 Results and discussions 57
3.3.6 Conclusion 65
4. Field performance and numerical simulation of the Kerrobert THAI pilot 66
4.1 Introduction 67
4.2 Field data analysis 71
4.3 THAI simulation 78
4.3.1 Model development 78
4.3.2 PVT and petrophysical properties 80
4.3.3 Kinetics scheme 82
4.4 Model validation by history matching 84
4.4.1 Modelling the K2 THAI pilot 84
4.4.2 Effect of additional air ingress from KA5 on the overall performance of K2 88
4.5 Results and discussions 90
4.5.1 Combusted zone (swept region) 91
4.5.2 Combustion zone 93
4.5.3 Coke zone 102

4.5.4 Steam zone 106
4.5.5 Mobile oil zone (MOZ) 108
4.6 Conclusion 113

5. In-situ microwave-assisted CAPRI using Hydrodesulphurisation catalyst 115
5.1 Introduction 115

5.2 Microwave (dielectric) heating 123

5.3 Materials and methods 125

5.3.1 Materials 125
5.3.2 Experimental setup 128
5.4 Characterization 133

5.5 Results and discussion 140

5.5.1 Dielectric properties 140
5.5.2 Heating profile 141
5.5.3 Catalytic upgrading and catalyst activity 143
5.5.4 Effect of particle size on upgrading 148
5.6 Conclusion 151

6. In-situ hydrogen production via the microwave-assisted THAI-CAPRI 153
6.1 Introduction 153

6.2 Materials 177

6.2.1 Heavy oil produced through the THAI process 177
6.2.2 Low Temperature Shift (LTS) catalyst 177
6.3 Experimental setup 179

6.4 Characterisation 179

6.5 Results and discussion 182

6.5.1 Dielectric properties 182
6.5.2 Heating profile 184
6.5.3 Catalytic upgrading 186

6.5.4 Effect of particle size on upgrading 194
6.5.5 Effect of coke deposition on catalyst activity 195
6.6 Conclusion 199

7. Conclusion and future work 201
7.1 Conclusion 201

7.2 Future work 203

References 205
Appendices 216
Appendix 1 216

List of Figures

Figure 1.1. Schematic of the THAI-CAPRI process....2
Figure 2.1. Heavy oil formation....5
Figure 2.2. Schematic arrangement in THAI process....14
Figure 2.3. Staggered Line Drive (SLD) (left) and Direct Line Drive (DLD) (right) THAI schematics (VI= Vertical Injector)....15
Figure 2.4. Placement of the injection and producer wells in (Xia, et al., 2003) tests and dimensions of the 3D combustion cell....18
Figure 2.5. Placement of the injection and producer wells in (Xia & Greaves, 2006) (Run 2000-01) and dimensions of the 3D combustion cell.....19
Figure 3.1. Experimental scale THAI model dimensions and HI and HP configuration 34
Figure 3.2. The variation of Athabasca bitumen viscosity with the temperature, taken from (Mojarab, et al., 2011)....36
Figure 3.3. Oil/water relative permeability curve (a) and gas/oil relative permeability curve (b). *Note: K_{rw} and K_{row} are the water and oil relative permeabilities at water saturation S_w, respectively, while K_{rg} and K_{rog} are the gas and oil relative permeabilities at oil saturation S_o, respectively 37
Figure 3.4. Comparison of the experimental and simulated oil production rates at experimental-scale....40
Figure 3.5. Comparison between the experimental and simulated peak temperatures with time at experimental scale.....41
Figure 3.6. Comparison of the experimental and simulated oxygen concentration in produced gas at experimental scale 43
Figure 3.7. The predicted oxygen and coke concentration around the toe section of the horizontal producer 44
Figure 3.8. In-situ combustion upscaling workflow taken from (Nissen, et al., 2015) 45
Figure 3.9. The DLD-THAI well arrangement at field scale....48
Figure 3.10. The SLD-THAI well arrangement at field scale 49
Figure 3.11. Variation of viscosity with temperature taken from Ado (2020) 50
Figure 3.12. The predicted combustion front shape (oxygen mole fraction) for the DLD-THAI (a) and the SLD-THAI (b) processes 57
Figure 3.13. The predicted aerial view of oil saturation profile for the DLD-THAI (a) and the SLD-THAI (b) processes 58
Figure 3.14. The predicted cross-sectional view of the oil saturation profile for the DLD-THAI (a) and the SLD-THAI (b) processes 59
Figure 3.15. The predicted oil production profile for the DLD-THAI and SLD-THAI processes 60
Figure 3.16. The predicted oxygen content in the produced gas for the DLD-THAI and SLD-THAI processes....61
Figure 3.17. The predicted coke deposition profile (in kg/m3) for the DLD-THAI (a) and the SLD-THAI (b) processes 63
Figure 3.18. The predicted in-situ steam generation profile (steam mole fraction) for the DLD-THAI (a) and the SLD-THAI (b) processes 64
Figure 4.1. The location of THAI well pairs (K1-K12, where KA is vertical injector and KP is horizontal producer). Old horizontal wells are marked from 1 to 9 (Turta, et al., 2018) 72

Figure 4.2. Schematics of the Kerrobert THAI project (Petrobank Energy & Resources Ltd, 2012) 74
Figure 4.3. K2 air injection and oil production profiles 75
Figure 4.4. The air injection profile, cumulative air injected, gas production profile, and cumulative gas produced for the K2 (form November 2013 to April 2016) 77
Figure 4.5. Reservoir model dimensions and VI and HP configuration in quasi-staggered line drive (SQLD) fashion. Notes: *The oil layer (pay zone), transition zone, and bottom water zone are shown in grey, dark blue, and light blue, respectively. 80
Figure 4.6. Comparison of simulation results for Model S with field data for the K2 pilot 85
Figure 4.7. Actual variation of temperature along KP2 versus time. Notes: * TC01 is located at the toe of HP. 87
Figure 4.8. Predicted variation of temperature around the toe section of HP in model S against time. Notes: * Order of perforation is from the toe side of HP. 87
Figure 4.9. Model D simulated oil production profile compared with corresponding field data for K2 89
Figure 4.10. Simulated water cut against air injection rates for Model S and Model D 90
Figure 4.11. Areal schematic of zones developed in the THAI process 91
Figure 4.12. Simulated ternary profile for model S and D in vertical midplane view (a) and in 3D (b) in May 2016. Notes: * SO, SW, and SG represent oil saturation, water saturation, and gas saturation, respectively. 93
Figure 4.13. Change in predicted oxygen profile for Model S (left) and Model D (right) at vertical midplane from November 2014 to May 2016 (uninterrupted air injection period) 94
Figure 4.14. Variation over time of injected air rates and predicted change in O2 concentration at toe section of the HP by Model S. Notes: * Order of perforation is from the toe side of the HP. 95
Figure 4.15. Variation over time of injected air rates and predicted change in O2 concentration at the toe section of the HP by Model D. Notes: * Order of perforation is from the toe side of the HP 98
Figure 4.16. Cumulative oxygen injected, cumulative oxygen produced, predicted oxygen utilisation, and oil production profile by Model S and Model D. Notes: * The illustrated parameters are distinguished with different line styles. 99
Figure 4.17. 3D simulated temperature profile by Model S and Model D in (a) March 2014 and (b) July 2015 100
Figure 4.18. Simulated 3D structure of coke zone in Model S and Model D in May 2016 .. 102
Figure 4.19. Predicted coke concentration and oxygen profile around the third perforation from the toe side of HP in Model S and Model D. Notes: *SC stands for standard condition. 104
Figure 4.20. Predicted steam profile by model S and D during THAI process 106
Figure 4.21. Predicted oil saturation profile by model S and D during uninterrupted air injection period 111
Figure 4.22. Predicted oil saturation profile (a and b) and oil production profile by model S with varied HP location (c) 113
Figure 5.1. Schematic of the CAPRI process, taken from (Hart, et al., 2013) 116
Figure 5.2. Schematic of the THAI-CAPRI process 117
Figure 5.3. The predicted temperature profile alongside the HP well in the history matched model (Model S) in July 2015 (a) and May 2016 (b) 119

Figure 5.4. The predicted temperature profile alongside the HP well in Model D in July 2015 (a) and May 2016 (b) 120
Figure 5.5. Selective nature of microwave heating 124
Figure 5.6. Schematic diagram of the laboratory-scale microwave-assisted heavy oil upgrading experiment setup 129
Figure 5.7. Front view of the experimental setup 130
Figure 5.8. Batch reactor 130
Figure 5.9. Front view of the experimental setup with safety shield 131
Figure 5.10. Quartz tube 131
Figure 5.11. Process monitoring and control 132
Figure 5.12. Gas sample vials 133
Figure 5.13. Washing the spent catalyst 133
Figure 5.14. 5 ml Fisherbrand glass pycnometer 134
Figure 5.15. NμLine, ATAC cone and plate viscometer 135
Figure 5.16. Cone and plate geometry for viscometer (ATAC Group, 2023) 135
Figure 5.17. basic flow pattern of gas chromatography (Science Direct, 2023) 136
Figure 5.18. Changes in output value of GC in response to gas sample components (each peak in the graph above represents a different component) 137
Figure 5.19. The Micromeritics 3Flex instrument 138
Figure 5.20. Outgassing and vacuuming the catalyst 138
Figure 5.21. Dielectric loss tangent of the CoMo/γ-Al_2O_3 catalyst and the THAI oil (Adam, et al., 2020) 140
Figure 5.22. A typical power, temperature, and pressure profile during microwave heating of the heavy oil with and without using HDS catalyst 141
Figure 5.23. Effect of holding time at 425 °C on API gravity & viscosity 143
Figure 5.24. Effect of holding time at 425 °C on sulphur content 144
Figure 5.25. Effect of particle size on API gravity, viscosity & desulphurisation 148
Figure 5.26. Effect of particle size on coke and sulphur deposition, and BET surface area of the spent catalyst 148
Figure 5.27. N_2 sorption isotherms for the fresh and spent HDS catalyst 150
Figure 6.1. Hydrogen production technologies (Cho, et al., 2023) 154
Figure 6.2. Bitumen pyrolysis reaction scheme, taken from (Turta, et al., 2020), High Molecular Weight Gas (HMWG) represents all C2+ combustible gases. 158
Figure 6.3. Bitumen aquathermolysis reaction scheme, taken from (Turta, et al., 2020), High Molecular Weight Gas (HMWG) represents all C2+ combustible gases. 160
Figure 6.4. The aquathermolysis and pyrolysis regimes for the system of heavy oil and water (Kapadia, et al., 2012) 161
Figure 6.5. The Whitesands pilot well layout map. The operation of P3 was suspended and P3-B was drilled as a CAPRI well in 2008 (Petrobank Energy & Resources Limited, 2009) 172
Figure 6.6. Horizontal section of P3-B well in the Whitesands pilot, which was converted to a catalytic downhole reactor in the CAPRI testing form August to October 2008 (Turta, et al., 2018) 172
Figure 6.7. West Texas Intermediate (WTI) crude oil price change from 2018 to present (Macrotrends, 2023), the pricing is in US$/bbl 173
Figure 6.8. Schematic of dehydrogenation and hydrogenation within microwave-assisted THAI-CAPRI process 176

Figure 6.9. Schematic diagram of the dielectric properties measurement system.....180
Figure 6.10. Dielectric measurement system setup 181
Figure 6.11. Dielectric properties of the $ZnO/CuO/Al_2O_3$ catalyst. *Error bars represent standard deviation of a set of dielectric properties measurement for the LTS catalyst 182
Figure 6.12. Absorbed power, temperature, and pressure profile during microwave heating of the heavy oil with and without using LTS and HDS catalyst. * The abbreviations T, P and Cat in the legend represent temperature, pressure, and catalyst, respectively. 184
Figure 6.13. Three different points for gas collection during upgrading experiments using LTS catalyst. * T, P and Cat represent temperature, pressure, and catalyst, respectively. 186
Figure 6.14. Effect of holding time at 400 °C on API gravity & viscosity 186
Figure 6.15. Water condensation on the top flange 190
Figure 6.16. Boudouard reaction (Hunt, et al., 2013) 191
Figure 6.17. Effect of the LTS catalyst particle size on API gravity, viscosity.....194
Figure 6.18. N2 sorption isotherms for the fresh and spent HDS and LTS catalyst.....196
Figure 6.19. TGA results for the fresh and spent LTS catalysts and change in loss tangent of the fresh LTS catalyst with temperature 197

List of Tables

Table 2.1. Experimental conditions for the 3D THAI combustion cell experiments 20
Table 3.1. Grid block refinement system for experimental scale THAI model.....33
Table 3.2. Experimental-scale PVT data taken from (Ado, Greaves, & Rigby, 2017) 35
Table 3.3. Properties and initial conditions of the experimental-scale THAI model taken from (Greaves, Dong, & Rigby, 2012 c) 36
Table 3.4 a and b Experimental-scale THAI kinetics scheme. Note*: IC is immobile pseudo-component, MC is Mobile pseudo-component, and LC is light pseudo-component.....38
Table 3.5. Operating condition of the experimental scale THAI simulation.....39
Table 3.6. Injected air properties and injector and production well constrains for the experimental-scale THAI model.....39
Table 3.7. Grid block refinement system for the staggered line drive SLD-THAI model and the direct line drive DLD model at field scale.....47
Table 3.8. Properties and initial conditions of the Field scale THAI model 51
Table 3.9 a and b. Field-scale THAI kinetics scheme. Note*: IC is immobile pseudo-component, MC is Mobile pseudo-component, and LC is light pseudo-component. COx is the inert gas.....53
Table 3.10. Input data for steam assisted pre-ignition heating cycle for field scale THAI simulations.....54
Table 3.11. Operating conditions of DLD-THAI model at field scale 55
Table 3.12. Operating conditions of SLD-THAI model at field scale.....56
Table 4.1. Grid block refinement system.....79
Table 4.2. Properties and initial conditions of the Eastern Kerrobert reservoir 81
Table 4.3. Injected air properties and production well constrains 82
Table 4.4 a and b. THAI Kinetics scheme. Note*: IC is Immobile pseudo-Component, MC is Mobile pseudo-Component, and LC is Light pseudo-Component. 83
Table 4.5. KP2 average gas compositions from 2009 to 2015 in mole% (HMWG represents high molecular weight gas).....96
Table 5.1. Properties of the heavy oil used for this experimental work 125
Table 5.2. SARA analysis of THAI oil used in this study.....126
Table 5.3. Comparison of the performance of CoMo/γ-Al_2O_3 to that of γ-Al_2O_3 (Experiments were run under similar conditions at 425 °C and 15 minutes holding time with particles of 212 – 600 µm size).....146
Table 6.1.Composition of the HDS and LTS catalysts.....187
Table 6.2. The performance of CoMo/γ-Al_2O_3, γ-Al_2O_3 and ZnO/CuO/Al_2O_3 catalysts including the gas composition 189
Table 6.3. The gas composition of the produced gas collected at Point 1, Point 2, and Point 3 in Figure 6.13.....193

List of Publications

- Anbari, H., Robinson, J.P., Greaves, M., Rigby, S.P., 2022. Field performance and numerical simulation study on the toe to heel air injection (THAI) process in a heavy oil reservoir with bottom water. Journal of Petroleum Engineering and Science 220, 111202.
- Adam, M., Anbari, H., Hart, A., Wood, J., Robinson, J.P., Rigby, S.P., 2020. In-situ microwave-assisted catalytic upgrading of heavy oil: Experimental validation and effect of catalyst pore structure on activity. Chemical Engineering Journal 413, 127420

1. Introduction

Extra-heavy oil and bitumen (EHOB) comprises 30 percent (only 4% less than conventional crude oil) of remaining technically recoverable fossil fuel resources on the earth. The attention has been shifting towards unconventional oil resources such as EHOB with the decline in conventional light oil reserves. However, EHOB are difficult to recover due to high intrinsic viscosity. Thermal enhanced oil recovery (EOR) methods are designed to reduce the viscosity of the remaining oil in place by increasing its temperature. Steam-based technologies are typically used to provide the required heat. The main limitation for steam-based methods, is that they are very energy intensive as they use natural gas to provide the required energy. Also, surface steam generation processes can cause release of significant quantities of greenhouse gases. Therefore, alternative energy-efficient and low-carbon technologies must be developed the could (a) eliminate the continuous need for steam injection and (b) deliver the required heat in-situ.

In-situ combustion (ISC) involves injection of air into the reservoir and creation of a combustion front, in which a fraction of the oil in the reservoir is combusted to generate heat downhole. The conventional ISC process suffers from serious operational problems, with gas over-riding and channelling being especially problematic. The Toe to Heel Air Injection (THAI) process is a relatively new ISC technology that has been shown to efficiently recover heavy oil with a reduced environmental footprint. The THAI process integrates ISC with advanced horizontal well concepts. A horizontal producer well is used instead of a vertical producer well (as in conventional ISC), and this difference is the main feature of the THAI process. This means that only short, gravity-driven vertical displacement of oil is necessary compared to the longer, horizontal displacement needed for conventional ISC. Controlled gas

over-ride, high sweep efficiency, production of thermally upgraded heavy oil, and less environmental footprint have been reported as benefits of the THAI process.

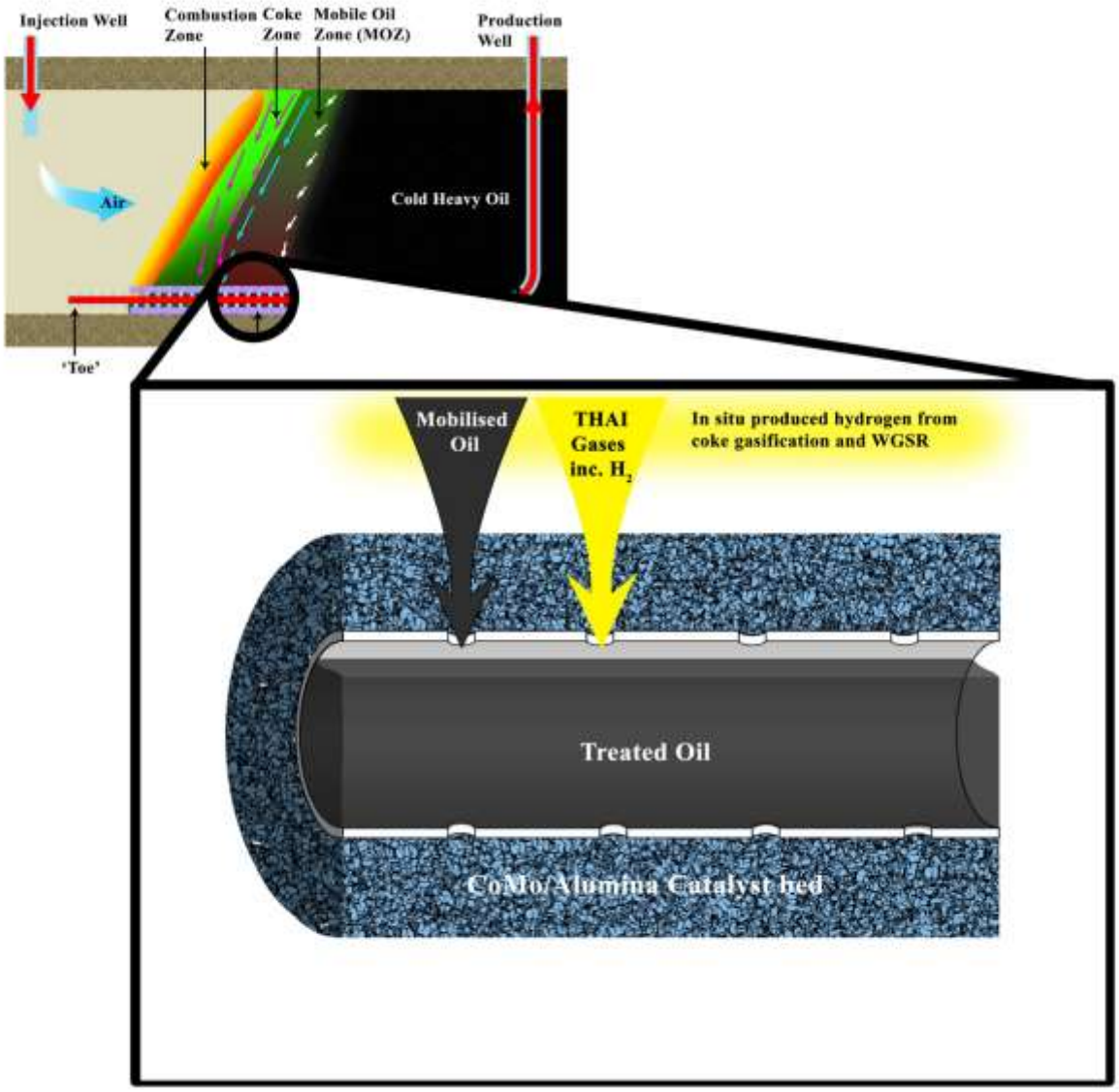


Figure 1.1. Schematic of the THAI-CAPRI process

The CAtalytic upgrading PRocess In situ (CAPRI) is an add-on to the THAI process. In the CAPRI process the horizontal section of the producer well is surrounded by an annular layer of a catalyst. Figure 1.1 shows the schematic of the THAI-CAPRI process. As the partially

cracked THAI oil (first upgrading) flows through the annular catalyst layer, it is further upgraded (second upgrading), before being produced by the horizontal producer well.

The THAI technology exhibits a short-distance character for oil displacement but has a long-distance pathway for high temperature oxidation (HTO) reactions. The toe section of the horizontal well is placed below the shoe section of the injection well. This means a short-distance process for oil flow, from the mobile oil zone (MOZ) to the producer well, while a long-distance process for burning O_2 with thermal cracking of the oil during its approach to the producer well. This characteristic of the THAI process is suitable not only for in-situ upgrading but for hydrogen production downhole. Compared to other commercial and experimental in-situ combustion processes, a combination of the produced hydrogen and methane, at high valumes, has not been seen for competing processes but through the THAI process. Employing the catalytic add-on of the THAI process (the CAPRI process) could potentially result in even higher in-situ hydrogen production.

1.1 Thesis outline

The following is the structure in which this thesis is presented:

Chapter Two outlines heavy oil recovery principles and techniques. Thermal heavy oil recovery technologies and their relative advantages/disadvantages are compared in this chapter. It also provides an introduction to Toe to Heel Air Injection (THAI) technology, the latest in-situ combustion process. Previous experimental and numerical studies of the THAI process are examined as well. The aims and objectives of this study are presented in this chapter.

Chapter Three presents a new experimental scale THAI model that is validated against a 3D combustion cell experiment in the literature. The experimental THAI model is scaled up to a field scale THAI simulation. The new field scale THAI simulation is used to numerically

investigate the performance direct line drive (DLD) and staggered line drive (SLD) THAI well arrangements.

Chapter Four presents field data analysis of a THAI pilot project in Canada. It also presents a history-matched THAI model that considers underlying bottom water in the studied reservoir. The history matched THAI model is used to study operational aspects of the THAI process. This chapter also proposes optimisation scenarios for the existing and forthcoming THAI projects.

Chapter Five focuses on in-situ catalytic upgrading add-on of the THAI process (CAPRI process). This chapter proposes microwave heating technology to provide the extra heat required for a successful CAPRI process. It also presents the results obtained from a series of microwave-assisted catalytic heavy oil upgrading experiment using commercially available hydrodesulphurisation (HDS) and low temperature shift (LTS) catalysts. A range of characterisations are conducted for the fresh and treated oil as well as the fresh and spent catalysts.

Chapter Six investigates potential of in-situ hydrogen production through the THAI-CAPRI process. This chapter presents the gas analysis results obtained during upgrading experiments using the HDS and LTS catalysts. In addition, the effect of operating conditions of microwaved-assisted upgrading experiments on the produced hydrogen content is studied.

Chapter seven utilises findings from this research to draw a general conclusion and to provide some suggestions for future research.

2. Literature review and aims and objectives of this study

2.1 Heavy oil recovery: Principles and Technologies

Heavy Oil is formed from light oil that has lost the light molecule leaving the heavy ones. Most of the hydrogen is in the light ends of oil. Hence, heavy oil is depleted in hydrogen. Hydrogen depletion forms hydrocarbon compounds characterised by long, very complex molecules. The long molecules of heavy oil impart high internal friction resulting in high viscosity (bp, 2011).

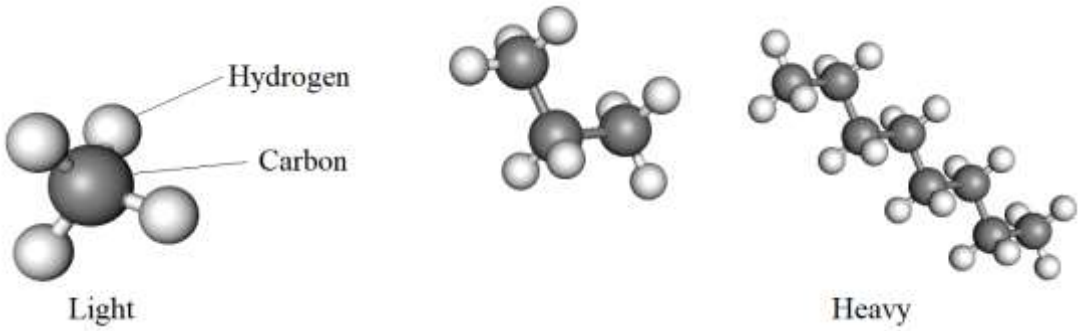


Figure 2.1. Heavy oil formation

Conventionally, the term “oil sand” refers to those highly viscous oil-containing reservoirs in which the oil at reservoir conditions is too viscous to flow to a wellbore and, as such, is uneconomic to produce in volumes without technological intervention. Oil sand contains high saturations of heavy oil and bitumen. If an oil’s API (American Petroleum Institute) gravity is greater than 10, it is less dense than water and will float on it. If an oil’s API gravity is less than 10, it is denser than water and will sink. Heavy oil is defined as oil with 10 to 20° API gravity and a viscosity of more than 100cp. Extra heavy oil includes bitumen as well as oil (tar) sands with less than 10° API and viscosity of more than 10,000 cp. Bitumen is the lowest grade of naturally occurring oil and is a result of biodegradation (large volume of methane and carbon dioxide being produced as oil is degraded for millions of years) of former lighter oil hydrocarbon reservoirs. The main distinction between the terms is that the high viscosity of natural bitumen prevents it from flowing to a wellbore under natural in-situ reservoir

conditions, whereas extra heavy and heavy oil will flow to the wellbore under the same conditions (Larter & Head, 2014). The economic production, the low market value, and the pre-production cost prior to refining hamper heavy oil exploitation. This is due to presence of high molecular weight hydrocarbon and heavy metals (Hart A. , 2014).

Several technologies are already being used for heavy oil extraction with differing levels of success, recovery ranging from as low as 5% (water flooding) through to more than 70% (steam assisted gravity drainage). Enhanced oil recovery techniques can be broadly classified into either thermal or non-thermal methods and their suitability for a particular project is usually dependent on the reservoir location, as well as oil composition (Shah A. , et al., 2010).

The following techniques with their limitations are classified as primary and secondary methods for heavy oil production:

- Surface mining (strictly limited by the depth of reservoir)
- Cold production (severely limited by the suitability of reservoirs, poor recovery factor)
- cold heavy oil production with sand CHOPS (higher recovery factor compared to cold production, however, the major issue is the separation of sand which is both mechanically and economically intensive)
- water flooding (less effective in reservoirs with an absence of underlying water

As the third stage of heavy oil production, when conventional recovery methods are no longer enough to sustain production, enhanced oil recovery EOR techniques are applied in order to extract the significant amount of oil left behind by primary and secondary methods. By reducing the viscosity of heavy oil and pushing it through the reservoir, EOR techniques improve sweep and displacement efficiency in the reservoir. Advances made in directional drilling, and measuring while drilling (MWD), technologies have facilitated development of in-situ technologies for recovery of bitumen such as steam assisted gravity drainage (SAGD),

expanding solvent- SAGD (ES-SAGD), and solvent vapour extraction (VAPEX). These technologies have significantly improved the wellbore-reservoir contact, the sweep efficiencies, and the produced oil rates as well as reducing the production costs (Nasr & Ayodele, 2005). Chemical flooding (Polymer, Surfactant, Alkaline), and cyclic steam simulation (CSS) are other existing enhanced heavy oil recovery methods (Shah A. , et al., 2010).

The degree to which the enhanced oil recovery methods are applicable will depend upon development of improved process technology. It will also depend on improved understanding of fluid chemistry, phase behaviour and physical properties: and on the accuracy of geology and reservoir engineering in characterising the physical nature of individual reservoirs (Borchardt & Yen, 1989).

2.2 Thermal Enhanced Oil Recovery

When the oil in reservoir has a high viscosity (>100 cp), thermal methods for oil recovery have found most use. Oil viscosity is a function of temperature and API gravity. These processes add heat to the reservoir to reduce oil viscosity and/or to vaporize the oil. In both instances, the oil is made more mobile so that it can be more effectively driven to producing wells. In addition to adding heat, EOR techniques provide a driving force to move oil to producing wells (Speight, 2011).

2.3 Steam-based Processes

Many innovative concepts in heavy oil recovery have been developed based on steam injection such as SAGD. The steam processes are the most advanced of all enhanced oil recovery methods in terms of field experience and thus have the least uncertainty in estimating performance, provided that a good reservoir description is available. Steam processes are most often applied in reservoirs containing viscous oils and tar sands, usually in place of rather

following secondary or primary methods. Commercial application of steam process has been underway since the early 1960s (Speight, 2011).

2.3.1 Cyclic Steam Stimulation (CSS)

The cyclic steam stimulation or steam soak or huff 'n' puff technique is a three-stage process starting with the injection of high-pressure steam for around a month's duration. This is followed by the soak stage where the well is shut in (usually for several days), leaving the heat to distribute uniformly (reducing viscosity of oil) before the well is finally put in to production. In addition to heating the reservoir, the high-pressure steam creates fractures in the formation improving fluid flow. The oil production rate increases quickly to a high rate, staying at that level for a short time before gradually declining over several months. When the oil production rate becomes uneconomic, the cycle is then repeated until the flow of oil diminishes to a point of no return (Shah A. , et al., 2010; Speight, 2011).

This process has a main advantage of a fast return during early production. However, oil recovery can be as low as 10 or 20% of the original oil volume (Ghoodjani, Kharrat, Vossoughi, & Bolouri, 2011). CSS in not suited for all reservoirs, particularly those with low reservoir drive such as solution gas drive. CSS might be followed with another thermal recovery operation in order to be able to recover the remaining oil in place (Nasr & Ayodele, 2005).

2.3.2 Steam Assisted Gravity Drainage (SAGD)

Canada has played a leading role in the development and application of the SAGD process. In the SAGD process, two superposed horizontal well are placed 5 m apart near the bottom of the formation. The top horizontal well is used to inject steam, which rises under buoyancy forces and forms a steam chamber above the well. The bottom well is used to collect the produced liquids (formation water, condensates and oil). The process is a counter-current gravity drainage process and therefore depends primarily upon the density difference between the

rising steam and the liquid phase as well as on the effective vertical permeability of the reservoir (Nasr & Ayodele, 2005).

The key benefits of the SAGD process are an improved steam-oil-ratio SOR and high ultimate recovery (on the order of 60% to 70%). Thermally, SAGD is about twice as efficient as cyclic steam stimulation, with a steam-oil-ratio that is approaching two (instead of four for CSS), for similar cases. The outstanding technical issues related to low initial oil rate, artificial lifting of bitumen to the surface, horizontal well operation and extrapolation of the process to reservoirs having low permeability, low pressure or bottom water. For SAGD, ex-situ heat generation is a major economic constraint on the all thermal processes (Speight, 2011). SAGD processes, which require the purchase of external natural gas, would be considerably less economically attractive. Additionally, this process has its considerable environmental impacts from enormous water consumption and the creation of significant quantities of greenhouse gases. Large volumes of water are needed to run SAGD, with between two and ten barrels of water injected as steam for every barrel of oil produced. Assuming that three barrels of water are used to make steam per barrel of oil produced, the approximate amount of carbon dioxide CO_2 generated to supply the latent heat requirement of steam generation was estimated to be ~0.092 tonnes (Shah A. , et al., 2010).

2.3.3 Vapour Assisted Petroleum Extraction (VAPEX)

VAPEX is a non-thermal process that is similar to SAGD except that a vaporised hydrocarbon solvent, or a mixture of hydrocarbon solvents, is injected instead of steam. The solvent diffuses into the oil and reduces its viscosity. This allows the oil to flow into the lower well bore (the producer) (Nasr & Ayodele, 2005). In terms of solvent injection rate, there are parameters that should be taken into account including the dimensions of the system, rock and fluid properties, and breakthrough time of solvent. The higher diffusion coefficient can improve the final

recovery factor, while the solvent penetration into the oil phase occurs faster (Ghoodjani, Kharrat, Vossoughi, & Bolouri, 2011).

The key benefits are significantly lower energy costs, the potential for in-situ upgrading and application of thin reservoirs, with bottom water or reactive mineralogy. VAPEX can be used in conjunction with SAGD methods (Speight, 2011). The added advantage of VAPEX is that the solvent might cause partial upgrade of the oil through de-asphalting. A main disadvantage of the VAPEX process is that the rate of oil production is very low as compared to SAGD (Nasr & Ayodele, 2005). The process was initially found to be a promising alternative to thermal processes. However, the dispersion and diffusion of the solvents are relatively slow and therefore the process is much less efficient than heat. The high cost of solvent is the main economic concern and recovery of solvent is therefore important (Shah A. , et al., 2010). Another important concern in this process, when applied to fracture reservoirs, is early solvent breakthrough through the fracture network without efficient contact with the heavy oil, which can reduce the process efficiency and allow the solvent to escape out of the reservoir (Ghoodjani, Kharrat, Vossoughi, & Bolouri, 2011).

2.3.4 Expanding Solvent Steam Assisted Gravity Drainage (ES-SAGD)

ES-SAGD involves the co-injection of a hydrocarbon solvent and steam to improve recovery from the SAGD process. The hydrocarbon solvent is soluble in bitumen at reservoir conditions and serves to decrease its viscosity, thereby increasing the rate of production and the overall recovery more than a process driven by steam. The additive (which is injected in the vapour form) is selected in such way than can evaporate and condense at water conditions. In this way, solvent can condense with steam close to the steam chamber interface (Orr, 2009). This is a novel approach for combining the benefits of steam and solvents in the recovery of heavy oil and bitumen. ES-SAGD sits between SAGD and VAPEX with the injection of both steam and

solvent in order to increase the energy efficiency compared with VAPEX and reduce the energy costs with respect to SAGD (Shah A. , et al., 2010).

A newly patented ES-SAGD process has been successfully tested and has resulted in improved oil rates and oil-steam-ratio, and lower energy and water requirements as compared to conventional SAGD (Nasr & Ayodele, 2005). Recoveries of 40-60% have been reported along with high production rates. A further way to reduce the high demand of steam is to replace a proportion with a non-condensable gas such as natural gas or nitrogen in what is termed Steam and Gas Push (SAGP) (Sharma, Moore, & Mehta, 2012).

2.4 In-situ combustion (ISC)

In-situ combustion has been recognised for many years as a feasible thermal process for recovery of heavy oil and bitumen deposits. This process has been extensively investigated in both laboratory and field tests (Rahnama, Barrufet, & Mamora, 2017). Fire flooding or ISC is a thermal EOR method in which heat is generated within the reservoir by igniting the formation oil and then propagating a combustion front through the oil-bearing media. The fuel necessary to sustain the combustion front is supplied by the heavy residual material or coke that deposits on the sand grains distillation, thermal cracking, pyrolysis etc. of the crude oil ahead of the combustion front (Greaves & Al-Shamali, 1996). ISC, in principle, is a gas injection, which has additional beneficial effects associated with the propagation of the heat generated by the ISC front (Turta, Lu, bhattacharya, Condrachi, & Hanson, 2005). ISC involves injection of air and the creation of a combustion (oxidation) front or zone within a heavy oil or bitumen reservoir that pushes the fluids (including gases from the injected air e.g. nitrogen and by-products of combustion) ahead of the zone (Nasr & Ayodele, 2005).

Some applications of ISC for heavy oil production in China, were reviewed by Yao, et al (2018). They discussed transformation of the production method from steam flooding to ISC

for some heavy oil fields in China. The ISC pilot test was conducted on Du-66 reservoir in Liaohe oil region from 2006. The field had a single well average daily production of 0.5 t/d before starting of ISC. After converting the thermal production method from steam flooding to ISC, the single well average daily production has increased to 3.8 t/d, and total reservoir daily production has reached 619 t/d. They reported that production costs were greatly reduced too. They also reported that ISC is not limited by reservoir depth, because air flow is hardly influenced by reservoir depth and combustion heat is generated inside the oil layer.

On the other hand, due to gravity override of injected gasses, the combustion front may not advance uniformly in the vertical direction, and the total sweep efficiency may be reduced by the preferential flow of gas to one or more wells of the ISC well pattern. The presence of cold oil bank in front of the mobilized oil is another problem that is frequently encountered in conventional ISC (Rahnama, Barrufet, & Mamora, 2017). Gravity segregation (gas overriding) due to the difference between the gas and oil densities, channelling due to the unfavourable rock heterogeneity and unfavourable gas/oil mobility ratio, are other downsides of conventional ISC (Ghoodjani, Kharrat, Vossoughi, & Bolouri, 2011).

2.5 Demand for the development of new in-situ combustion ISC technologies

The conventional ISC process was widely operated from the 1950s to the 1980s. It is generally considered to be a difficult process to control, and operators have therefore been somewhat reluctant to treat conventional ISC as a main stream thermal heavy oil technology. However, the theoretical promise remains very high. One of the most successful conventional ISC operations has been operating in Romania (Suplacu du Bacu, since 1964), which clearly proves that good reservoir quality (homogeneous formation), good conformance, high oil saturation, preferably dipping, will almost certainly ensure success. However, most heavy oil and bitumen reservoirs do not often possess all the desirable characteristics for successful operation of conventional in-situ combustion (Greaves, Dong, & Rigby, 2012 c). Thus, novel ISC processes

are required to recover heavy oil and bitumen from inappropriate reservoir application having poor control of process.

2.6 Toe to Heal Air Injection (THAI)

THAI is a relatively new enhanced oil recovery process, which integrates in-situ combustion and advanced horizontal well concepts. A horizontal producer well instead of a vertical producer well (conventional ISC) is used, which is the main feature of the THAI process. Also, the toe of the horizontal producer is positioned close to the injection point. Thus, the combustion front propagates along the horizontal production well, from the 'toe' position, to the 'heal' (Greaves, Tuwil, & Bagci, 1993).

The basic mechanism of THAI process for heavy oil recovery is the same as for the conventional ISC process, i.e. burning of a heavy residue, or coke fraction, produces the heat required to increase the temperature of the oil-bearing formation, reducing the in-situ oil viscosity, and thereby, increasing oil mobility. The fuel for the combustion reaction (mainly coke) is generated by thermal cracking of heavy residue (asphaltense, resins and aromatics) (Xia et al, 2003). The combustion front propagates along the horizontal producer well from the 'toe' position to the 'heal' (Shah A. , et al., 2010) as shown schematically in Figure 2.2.

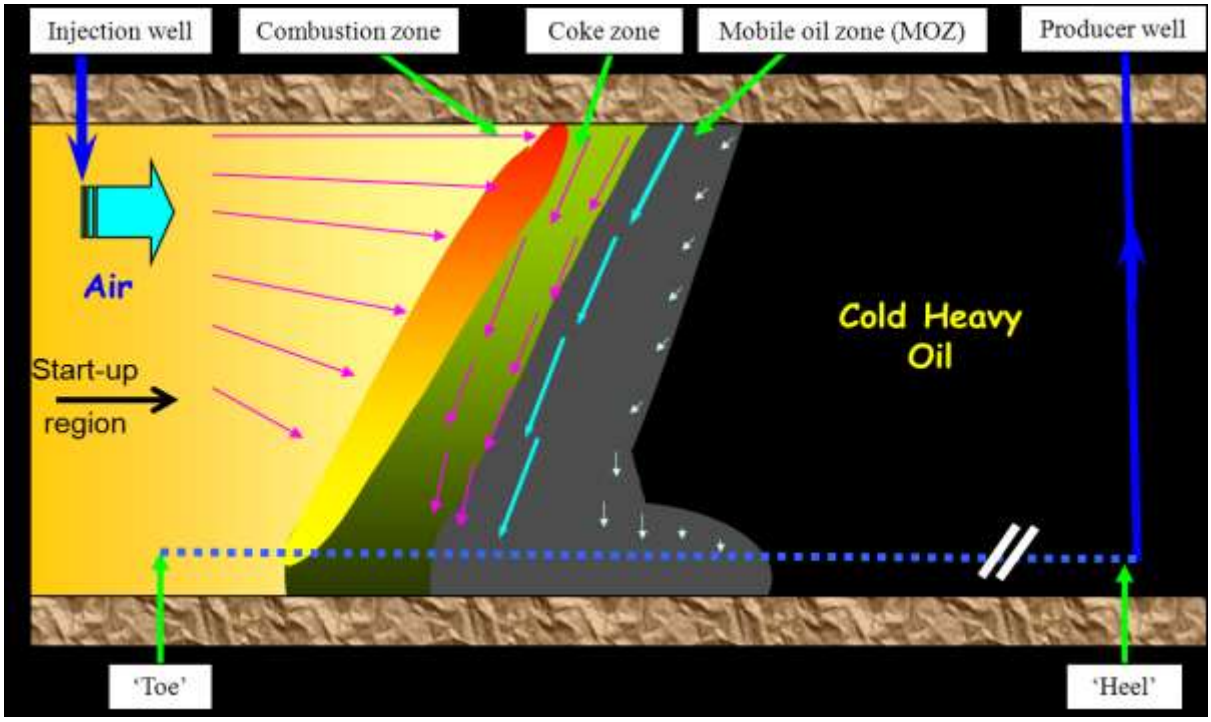


Figure 2.2. Schematic arrangement in THAI process

THAI process has previously typically been applied in two well configurations: either direct line drive (DLD), where the vertical injector is placed in front of the toe of the horizontal producer, or in a staggered line drive (SLD), where the toe of the horizontal producer is located close to line of vertical injectors, but is laterally off-set (Turta, Greaves, & Grabowski, 2018). Figure 2.3 shows the schematics of the DLD and SLD THAI well arrangements.

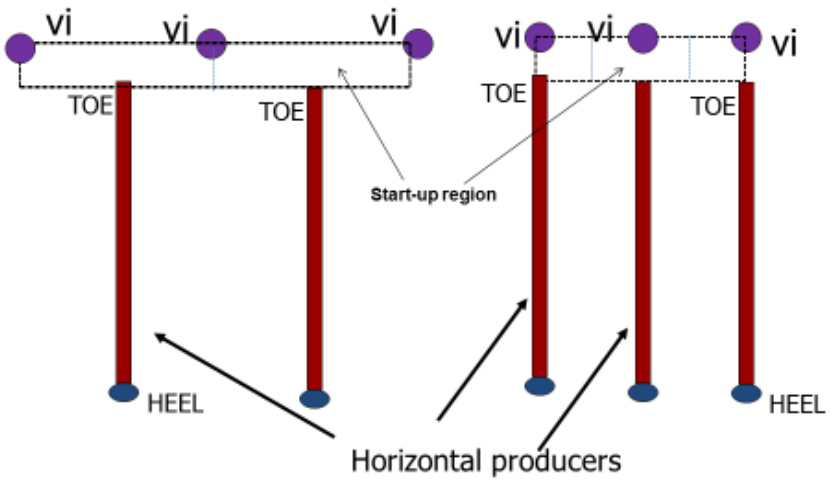


Figure 2.3. Staggered Line Drive (SLD) (left) and Direct Line Drive (DLD) (right) THAI schematics (VI= Vertical Injector)

Xia & Greaves (2006) reported potential benefits of THAI over conventional ISC processes for heavy oil recovery as following;

1. Controlled gas override, results in a quasi-upright in situ combustion front

In conventional ISC process, fluids (gas, steam, water, and mobilised oil) move through the formation horizontally, from the vertical injection well to the vertical producer well. The interwell distance may be 100 to 200 meters in heavy oil reservoir. The difference in density between the gas and oil gives rise to gravity segregation. Thus, gas overriding is inevitable in the conventional ISC. In THAI, the effect of gas overriding is controlled. This is because the horizontal producer well, placed in the bottom of the oil layer, is the only pathway for mobilised fluids to leave the formation. This occurs via a top-to-bottom flow, directly into the horizontal production well (Xia & Greaves, 2006).

2. High air flux maintain process in HTO mode, avoiding LTO reactions

In THAI, the air flux can be varied during operation. Since air injectivity into the reservoir actually increases, owing to depletion in the burned region, a high air flux can be employed to maintain oil production at the desired rate. Not least, using a higher flux maintains the process

in a High Temperature Oxidisation HTO mode, avoiding the complication of Low Temperature Oxidisation LTO reactions (Xia & Greaves, 2006).

3. High sweep efficiency, related to the absence of any gas coning (channelling) in producer well

THAI process proposes good areal and vertical sweep efficiency (Greaves, Dong, & Rigby, 2013). THAI achieves a very stable combustion front propagation from the 'toe' to the 'heal'of the horizontal producer well. This contributes to a very efficient sweep of the reservoir (Xia & Greaves, 2006).

4. Process produces thermally upgraded oil, up to 8-10° API higher than reservoir crude oil

THAI was initiated by Petrobank at their Whitesands pilot project in 2006. The produced oil was partially upgraded in the range of 10.6 to 16.1° API, compared to the original bitumen value of 7.9° API (Shah A. , et al., 2010).

5. Significant environmental benefits due to in-situ removal of sulphur and heavy metals

Experimental and field pilot results indicate sulphur and heavy-metal content is reduced in the produced oil with THAI technology (Petrobank Energy & Resources Limited, 2009).

6. Unique mobile oil zone (MOZ) ahead of the combustion front reduces sensitivity to reservoir heterogeneity in the virgin zone (mainly for extra-heavy reservoirs)

As the combustion front extends and moves further away from the injection well region, heat conduction into the downstream oil region causes the MOZ to develop and increase in size. The short displacement feature of THAI means that gas communication/connectivity is easily established and maintained, so that early oil production is achieved. The overall sensitivity of the process to reservoir heterogeneity effects is also significantly reduced, since the combustion

and oil displacement processes are effectively taking place in a small section of the reservoir (Xia, Greaves, Turta, & Ayasse, 2003).

7. Fluid injectivity is increased due to higher permeability in the burned zone

THAI mainly operates in high temperature oxidation (HTO) mode. It is generally agreed that LTO is undesirable in the ISC process, since it can lead to oil viscosification and reduced gas relative permeability, which can seriously reduce the air injectivity, leading to failure of the process. Operation in a high temperature oxidation (HTO) region, to ensure vigorous combustion, is absolutely vital to avoid this situation developing (Greaves, Dong, & Rigby, 2013).

8. Combustion front tracking capacity via 'toe-to-heal' propagation
9. For a commercial line drive operation, and a fixed well pattern, the number of wells is reduced to almost half due to their use first as producers and then as injectors

2.7 THAI laboratory work

2.7.1 3D combustion cell experiments

Turta, co-inventor of THAI process, has reported that over 100 3D model (box style 60cm*40cm*20cm) laboratory investigations have been carried out by Improved Oil Recovery Group at the University of Bath, UK from 1990 to 2002 (Turta, Greaves, & Grabowski, 2018). The experiments were conducted at low pressure, and, remarkably, they were able to predict most of the main features observed in the THAI pilot operated by Petrobank, at their Athabasca oil sands site, near Colin, Alberta, Canada (Greaves, Dong, & Rigby, 2012 c).

Xia et al, (2003) carried out two three-dimensional combustion tests of THAI. These tests were aimed at understanding the mechanism governing the high oil recovery and thermal upgrading

achieved by THAI. A rectangular stainless-steel combustion cell was used (shown in Figure 2.4) to carry out the ISC tests. The cell was fitted with an array of 76 thermocouples. Wolf lake oil (10.5 API°) and sand was packed into the combustion cell. One dry, and one wet, combustion test were completed using the standard THAI well arrangement, i.e. HIHP (Horizontal Injector Horizontal Producer) (only dry combustion test was explored in the current report). An improved control system was used, in order to achieve a near-adiabatic condition as possible for the 3D cell operation. An electric heating element near to the horizontal injection well was used for ignition. Air was injected (at the rate of 9 m^3 m^{-2} h^{-1}) into the sand pack to start ignition (Xia, Greaves, Turta, & Ayasse, 2003). The experimental arrangements of their 3D cell test are presented in Table 2.1.

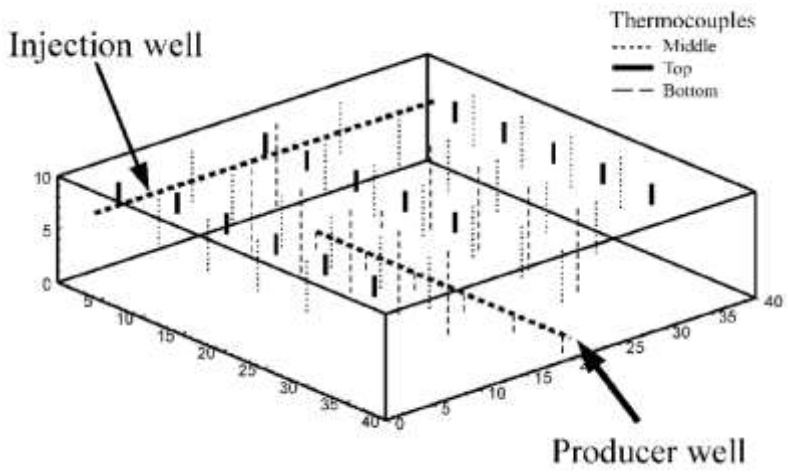


Figure 2.4. Placement of the injection and producer wells in (Xia, Greaves, Turta, & Ayasse, 2003) tests and dimensions of the 3D combustion cell

It was concluded that THAI can achieve a very high oil recovery, (85 % OOIP) which makes it a very attractive EOR method for heavy oil and tar sand bitumen reservoir. A further important benefit of THAI for heavy oil and bitumen applications is that it produces partially upgraded oil. The produced oil had a viscosity of 50 to 500 mPa s at 15° C and an API gravity of 8°, compared with the original Wolf Lake crude oil viscosity of 48,000 mPa s at 15° C and

API gravity of 10.5°.Thermal cracking plays an essential part in the THAI process to maintain: (1) stable combustion; (2) high oil recovery; and (3) upgrading of heavy oil (Xia, Greaves, Turta, & Ayasse, 2003).

Xia and Greaves, (2006) used a 3D combustion cell with slightly different dimensions for another THAI process experimental test (Run 2000 -01) (shown in Figure 2.5). Virgin Athabasca oil sand was packed in the combustion cell. The same well type and well configuration were employed for this test. An electrical coil heater was imbedded into the inlet face of the sand pack. This was also used to preheat the entrance zone of the sand pack up to a temperature of around 500 °C. The air was injected into the sand pack to start ignition. During the first 190 min, the air injection flux was kept at 12 m^3 m^{-2} h^{-1}. Following the first period of dry combustion, the air injection flux was increased to 16 m^3 m^{-2} h^{-1}. This was maintained until the end of the dry combustion period, at 320 min (Greaves, Dong, & Rigby, 2012 c; Xia & Greaves, 2006).

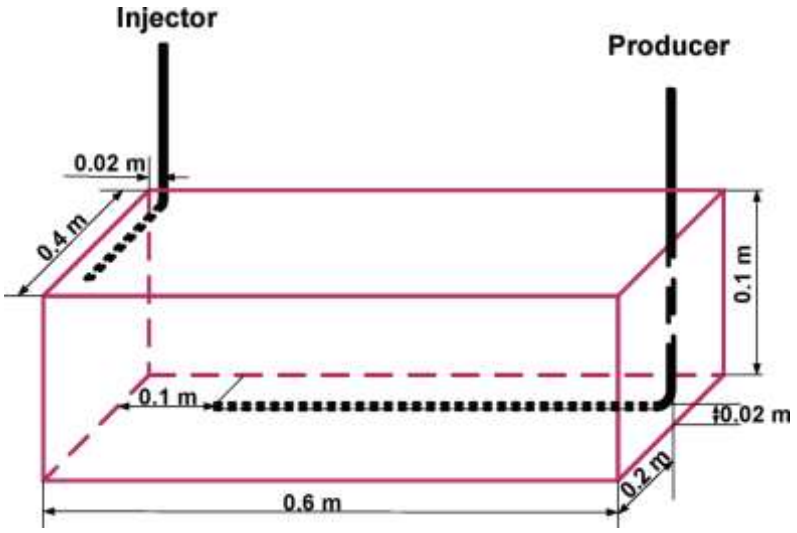


Figure 2.5. Placement of the injection and producer wells in (Xia & Greaves, 2006) (Run 2000- 01) and dimensions of the 3D combustion cell.

Oil recovery of 81.5 % OOIP was achieved. THAI produced thermally upgraded oil from the start of oil production, which was 3° API higher than the original bitumen. Therefore. It increased to 16 to 18° API during the stable operating period of the oil production. This sustainable level of upgrading is sufficient almost to dispense with the need to use diluent for pipeline transportation. No other in-situ heavy oil recovery process, including SAGD, is capable of achieving any significant level of in-situ upgrading. The produced oil viscosity was 50 mPa s at 20 °C compared with virgin Athabasca Tar Sand bitumen that has viscosity of approximately 1,000,000 mPa s at 15 °C (permanent viscosity reduction of 1000 – 10,000). The volumetric sweep of the combustion front approached 50% of the sand pack volume, which is about 66% more than for a conventional ISC experiment in a 3D combustion cell (Xia & Greaves, 2006).

Table 2.1. Experimental conditions for the 3D THAI combustion cell experiments

Run	Xia et al, 2003	2000 - 01
Sandpack	Wolf lake oil	Virgin Athabasca oil sands
Oil Saturation (wt %)	75	13.55
Initial temperature	20	20
Air flux ($m^3\ m^{-2}\ h^{-1}$)	9	12-16
Well type	HIHP	HIHP
Well configuration	DLD	DLD
Back pressure (kPa)	138	170-240

2.7.2 Limitation of 3D combustion cell experiments

A physical 3D combustion cell is of limited size, owing to reasons of cost and safety. It nevertheless is one of the best experimental techniques that can be used to gain insight into the performance of the THAI process. The implication from the laboratory works is that communication between injectors is essential to create an initial large thermal front. Being

relatively small, the communication phase prior to ignition is not a very significant operation in the experiments, whereas in the field, it is very significant. This is one of the limiting factors of the 3D combustion cell (Turta, Greaves, & Grabowski, 2018). The heating of the inlet zone of the 3D combustion cell (between the vertical injector well and the toe of the horizontal producer) simulates the creation of the broad initial burning surface, which is a required pre-condition for the success of the THAI process. Having said that, it is considerably more challenging to achieve such a broad initial combustion front in the field conditions. This is because heat (either through hot gas or electrically) is used to increase the temperature of the inlet zone of the sand pack.

The sweep efficiency of the combustion front is considerably higher in the laboratory (52-68%) compared to the field. This is due to the small sizes of the 3D combustion cell. A comparison of THAI laboratory tests conducted by three independent organizations gave ultimate oil recovery in the range of 70 -80% by the University of Bath, 60-70% by Alberta Innovates Technology Futures (AITF), and 50-60% by Petrobank Energy & Recourses Limited (Turta, Greaves, & Grabowski, 2018). Also, because of small size of the 3D model, results from the THAI experimental work did not allow to make a performance comparison between direct line drive and staggered line drive well arrangements.

Bearing in mind the limitations experienced in THAI laboratory works, the experimental results should not be considered as a full representative of the field conditions. Numerical simulation are developed to overcome challenges experienced by physical aspect of the previous THAI laboratory works. The reservoir engineer must incorporate the knowledge gained from laboratory results and their associated limitations in order to develop detailed numerical simulations (Turta, Greaves, & Grabowski, 2018).

2.8 THAI simulation work

Although experimental studies help in understanding the THAI process mechanisms and provide insight into what will happen in the reservoir, a fuller understanding of THAI's merits and limitations requires sophisticated development of reservoir simulation models that is able to accurately predict reservoir behaviours both in dynamic and steady state conditions (Ado, Greaves, & Rigby, 2017).

Numerical Modelling of THAI is a very challenging reservoir problem. This is due to the strongly coupled interaction between reaction kinetics and fluid flow processes in the reservoir. The kinetics of fuel (coke) deposition and coke combustion remain one of the major sources of uncertainty in modelling THAI, and also conventional in-situ combustion (Ado, Greaves, & Rigby, 2017).

2.8.1 THAI numerical models in laboratory scale

There have been only a relatively small number of papers published on the numerical simulation of ISC at the experimental scale. The availability of more powerful personal computers (PCs) and gathering interests, of late, that ISC could be a very important contributor toward a solution for exploration of the vast reserves of heavy oil and bitumen around the world have intensified efforts on this front (Greaves, Dong, & Rigby, 2012 c). Mostly, Computer Modelling Group's (CMG) STARS thermal simulator has been used for numerical investigations.

Tare and Greaves, (2002) developed a model of a 3D combustion cell experiment for Wolf Lake heavy oil (10.9° API). The predictions were broadly in-line with what was observed experimentally. A robust, stable propagating combustion front (temperature between 500 and 550 °C) was predicted. Also, in-situ upgrading up to 16-17 ° API gravity was obtained numerically. However, a comparison to dynamic parameters (oil production rate, water

production rate, produced gas composition, and variation of the combustion front peak temperature) was not attempted.

Greaves et al, (2012 c) performed a numerical simulation of 3D combustion cell experiment for Virgin Athabasca sands (8° API). Their model predicted some of the dynamic features of THAI. However, it was not able to accurately predict critical parameters such as fuel deposition and the effect of a sudden change in air flux rate on the level of produced oxygen. Their model used a split-cracking kinetics scheme, as opposed to the direct conversion cracking kinetics scheme (reported by Philips et al, who used virgin Athabasca sands to develop a more detailed set of thermal cracking reactions, after conducting a number of experiments). The major disadvantage of split-cracking kinetics is it is heavily dependent on the selected stoichiometric coefficients of the products. They also modelled their combustion cell experiment excluding LTO reactions. The kinetic model is typically represented by the following equations (Greaves, Dong, & Rigby, 2012 c);

Thermal cracking:

Heavy oil → coke + light oil (Equation 2.1)

Coke combustion:

Coke + 1.225O_2 → 0.95CO_2 + 0.05CO + 0.5H_2O (Equation 2.2)

Two other combustion reactions were included:

Heavy oil + O_2 → CO_2 + H_2O (Equation 2.3)

Light oil + O_2 → CO_2 + H_2O (Equation 2.4)

The stoichiometric coefficients in Equation 1 were obtained by tuning the model, using trial and error procedure. The activation energy and the frequency factor for Equation 1 were

obtained from (Phillips, Haidar, & Poon, 1985), while those for Equation 2 are obtained from Greaves et al, 2007. All of the kinetic parameters in Equation 3 and 4 used the default values in STARS for Wolf Lake oil. The sensitivity of the simulation results to grid block size was investigated as well.

There are important elements to be considered when it comes to validation of the numerical models. Coke profile, peak combustion temperature, oil production rate (must be predicated as accurately as possible), produced oxygen (oxygen use is an indicator of combustion performance), and oil upgrading.

It was evident that Greaves et al, (2012 c) simulation predicted the main features of the residual coke profiles quite well. Simulation predicted higher combustion temperatures than experimental values. This may be because the heat loss applied in the simulation does not exactly match that occurring in the experiment. There was a very close overall agreement in terms of oil production rate between experimental and numerical results. Most of the trend changes in terms of coke deposition, produced oxygen, peak temperature were predicted accurately, with the simulation results lagging the experiment by only a very small amount. There was also good agreement in oil upgrading between the predicted and experimental values. However, the model was seriously deficient in that it failed to accurately predict the time when oxygen was first detected at the production well.

Although the 3D combustion cell experiments were conducted at low pressure, they can provide a basic for scaling-up the oil production rate. Using a steady state analysis of the ISC process and assuming that the combustion temperature and fuel in the reservoir is the same as in the experiment, upscaling only depends upon the injected air flux (Greaves, Dong, & Rigby, 2012 c).

Ado et al, (Dynamic Simulation of the Toe-to-Heel Air Injection Heavy Oil recovery Process, 2017) performed a numerical simulation of the THAI process in experimental scale using findings from 3D THAI experiments reported by Tare and Greaves, (2002) (virgin Athabasca bitumen). Phillips et al, (1985) kinetics parameters were slightly adjusted to use in their model. Based on initial boiling point data proposed by Phillips et al, (1985) , the Peng-Robinson Equation of State (PR-EOS) available in Aspen HYSYS software was used for PVT data of the Athabasca bitumen. The frequency factor for the coke combustion reaction and the heat of reaction were adjusted to best match the peak temperature in the experiment. Petrophysical parameters (the porosity and permeability) were taken from (Greaves, Dong, & Rigby, 2012 c). Oil/water relative permeability curve and gas/oil relative permeability cure were adjusted to increase numerical stability consistent with the experimental results. In order to choose the optimum mesh size, the grid sensitivity was analysed too.

In addition to the main validation elements of other abovementioned laboratory-scale THAI numerical models, Ado et al, (2017) achieved a substantial improvement in predicting the fuel laydown and oxygen production during the later stages of the experiment, which was not available previously. Their model also provided better guidance on the operability of the process than previous models.

2.8.2 THAI numerical models in field scale

Coates and Zhao, (2001) were the first to simulate a field scale section of the THAI process. They used kinetics proposed by Belgrave et al, (1993) scheme for Athabasca and Lloydminster crudes, and found that the process had good areal and vertical sweep, producing high oil recovery. Anaya et al, (2010) used kinetic and relative permeability parameters from a combustion tube simulation directly in the field pilot simulation. High oil recovery was claimed but it was only in the range of 30-43 %.

Rahnema and Mamora, (2010) compared THAI and SAGD using a field pilot simulation. They predicted that THAI has lower oil production rate that SAGD. It was due to employing Belgrave kinetics, allowing LTO reactions to produce much more coke than is indicated by thermal cracking alone. Greaves et al (2012 a; 2013) also conducted THAI field scale models using Phillips et al, (1985) kinetics scheme for Athabasca bitumen. Although there is insufficient published data concerning the oil production trends experienced in the Conklin filed pilot, Greaves et al, (2013) constrained a model by aligning predicted oil production with a range of other outcomes (a daily oil production per horizontal well) and simple scale-up of the 3D combustion cell experiment by Tare and Greaves, (2002).

2.8.3 Issues with previously developed THAI numerical models in field scale

Previously developed field-scale THAI models (Rojas, Ruiz, & Jaime, 2010; Coates & Zhao, 2001; Greaves, Dong, & Rigby, 2012 a; Greaves, Dong, & Rigby, 2013; Ado M. R., 2020) used data from 3D combustion cell experiments to first validate their laboratory scale THAI simulation and only then scale-up experimental scale models to field-scale models. However, none of the aforementioned models consider a bottom water zone. Although, Araujo et al. (2016) and Ado (2019) carried out THAI simulations in presence of bottom water in the reservoir, their results were not validated against actual field data. *Ab initio* field-scale model development using direct history matching of a field-scale THAI process has never been tried previously by other workers. This was due to insufficient published data concerning the oil production trends experienced in the field.

2.9 Limitation of the THAI process

The THAI process is an EOR process and usually employed after primary heavy oil recovery processes. A number of old horizontal wells from previous recovery operations is already present in the formation, prior to the THAI process. This could affect the overall THAI performance as injected air might channel towards the old horizontal wells. The field evidences

from the Kerrobert project reported by Turta et al, (2018) showed that, when the air injector well was located very close to an old horizontal well, it was extremely easy for the injected air to flow upwards towards the old horizontal well instead of flowing towards the targeted horizontal producer. Such an effect could be experienced either from very beginning of the THAI operation or after a while when a pathway for air migration is established between the THAI air injector and the nearby old horizontal well.

Operational problems can limit the THAI process as well. The first significant operational issue in terms of oil production is the sand influx (Turta, Greaves, & Grabowski, 2018). The sand flux may cause a severe challenge with pumping the oil to the surface. Therefore, appropriate preventative solutions should be considered from the very beginning in any THAI application to tackle challenges associated with sand influx. Petrobank has stated that modifying well arrangement from direct line drive (DLD) to staggered line drive (SLD) well configuration can slightly decrease the sand influx issue (Turta, Greaves, & Grabowski, 2018). Sand influx also has negative impact on the production pumps used within the THAI process.

Another major operational problem in the THAI process is the short-duration endurance of casing in the horizontal section of the producer to the high temperature of the combustion front. Petrobank reported that in the first of three well sections reservoir temperature reached as high as 800 °C in the Conklin THAI field pilot, Alberta, Canada (Turta, Greaves, & Grabowski, 2018). This peak temperature is higher than in the experiments (630 °C average) and also higher than the simulated value (680 °C average). Both the experimental and simulated experimental cases are affected by heat loses, whereas the field reservoir case is more adiabatic and should therefore operate at somewhat higher temperature (Greaves, Dong, & Rigby, 2012 c). Depending on the well arrangement within the THAI process, the horizontal section of the horizontal producer may be frequently exposed to temperatures as high as 600-800 ºC. This is more likely to happen in the direct line drive (DLD) well configuration compared to the

staggered line drive (SLD) well arrangement in the field. Once the in-situ combustion front touches the casing of the horizontal producer, it remains continuously in contact with the casing throughout the rest of life of the project (Turta, Greaves, & Grabowski, 2018). Nevertheless, the damaged region, which usually is located in the toe section of the horizontal producer, can be isolated. This allows the well to be further used for production. Turta et al (2018) reported that the Kerrobert THAI project has encountered this situation several times.

Applicability of the THAI process in the presence of thick bottom water has not been fully proven yet. Nevertheless, the THAI application could be feasible in the presence of a relatively thin bottom water (thickness of bottom water zone/thickness of pay zone (w/o), in a range of 0.3-0.5) (Turta, Greaves, & Grabowski, 2018). The Kerrobert THAI pilot, in which the formation has an average w/o ratio of 0.6, provided experience for such a situation. Despite a relatively thick bottom water layer, the performance of pilot wells in the Kerrobert project were better than the best conventional ISC applications in a similar bottom water situation (Turta, Greaves, & Grabowski, 2018). Although the Kerrobert THAI pilot shows the potential of the THAI process in presence of a thick bottom water layer, more field development work is needed to examine the overall performance of the THAI process in bottom water situation.

It was earlier discussed that that LTO reaction are undesirable in the ISC process. Therefore, operation in a HTO region, to ensure vigorous combustion, is absolutely vital to avoid challenges associated with LTO reactions. Turta et al (2018) reported that the LTO reaction can be slightly amplified mainly in the SLD well arrangement. The predicted temperature profile for THAI showed reasonably high values after 2 years (ca. 450 °C), but they decreased to 300 °C after 5 years and ca. 275 °C after 7 years. This indicates a lack of air injectivity and that the in-situ combustion process was therefore dying (Greaves, Dong, & Rigby, 2013). Therefore, maintaining the desirable temperature alongside the horizontal producer is another challenge of the THAI process.

Petrobank, (2009) reported a potential of approximately 2000 barrels per day per well for this pilot field. The production rate at their projected commercial May River development was set at a design value of 88 m^3 of oil per day. This was based on the experience from the Conklin project. It needs to be kept in mind, however, that the pilot was not a production unit but was used to explore a variety of operating conditions and gain further insight and knowledge of the THAI process. Further in-situ upgrading within the THAI process is required as high viscosity and impurities make heavy oil and bitumen extraction, transportation and refining difficult and cost intensive.

Produced heavy oil from the THAI process requires further upgrading. Heavy oil upgrading may involve either cokers or hydrocrackers, or both in a refinery unit. Upgraders require huge investments and are built for enormous capacity of at least 100,000-200,000 bbl/day, costing around $5-8 billion (Turta, Greaves, & Grabowski, 2018). In addition, upgraders may become uneconomic when the difference between light and heavy oil prices is small. Hence, several alternative field upgrading techniques have been explored that targeted the reduction of the size of the upgrader in order to minimise capital requirements. Operating costs of a surface upgrader can reach around £100's millions but a downhole or in-situ oil upgrading process may be able to achieve this for a negligible cost (Shah A. , et al., 2010).

The CAtalytic upgrading PRocess In situ (CAPRI) is an add-on to the THAI process, which was developed to provide additional in-situ heavy oil upgrading (Tare & Greaves, 2002). In the CAPRI process, an annular layer of catalyst is emplaced around the casing of the horizontal producer well. This subjects the oil to a second stage of upgrading during the flow of the oil into the borehole (Turta, Greaves, & Grabowski, 2018). There are fewer experimental studies on the CAPRI process than laboratory investigations for the THAI process. Turta et al, (2018) reported that to improve the catalyst performance and advance the CAPRI technology more in-depth considerations are required. Previous studies showed that a temperature of around 425

ºC is needed for a successful CAPRI process (Shah A. , et al., 2011). However, previously developed experimental scale simulation of the THAI process suggested that the temperature of the oil passing through catalyst packing around the horizontal well does not exceed 300 ºC (Ado, Greaves, & Rigby, 2017). Hence, there is a need to provide extra heating for a successful field scale CAPRI process.

2.10 Aims and objectives of this study

In this study, it is aimed to numerically assess and compare the overall performance of the DLD and SLD THAI well arrangements. The operating aspects of the THAI process in the presence of an underlying bottom water is numerically investigated. It is also aimed to provide the additional heating required for a successful CAPRI process, in-situ catalytic add-on of the THAI process. The potential of additional in-situ upgrading, as well as hydrogen production via the CAPRI process are studied.

The objectives of this study are listed as follows:

a) Developing a new field scale THAI model for heavy oil recovery
b) History matching the developed THAI model by utilising field data
c) Numerically studying the impact of fundamental parameters in a successful THAI process
d) Proposing optimisation scenarios for existing and forthcoming THAI projects
e) Providing extra heat required for a successful CAPRI process using microwave heating technology
f) Conducting microwave-assisted catalytic upgrading experiment using various commercially available catalysts
g) Demonstrating upgrading potential of microwave-assisted CAPRI process
h) Examining in-situ hydrogen production via the THAI-CAPRI process

3. THAI numerical modelling

3.1 Introduction

Detailed numerical simulation is the only way to explore various critical factors affecting the design and operation of the THAI process. Adequate analytical models for the field scale THAI process have not been developed so far. This requires setting out a workflow strategy to develop a simulation model, comprising the following three steps (Turta, Greaves, & Grabowski, 2018);

a) The development of the reaction and fluid models
b) Validation by history matching of combustion performance (depending on the scale of simulation, calibrating predicted results with the 3D combustion cell experiments and the field data)
c) Constructing reservoir simulations that can forecast at both the experimental and field scales

THAI numerical study in this research work consists of the following three categories:

1. Experimental-scale THAI simulation
2. Field-scale THAI simulation
3. Field performance and numerical simulation study on the THAI process in a heavy oil reservoir with bottom water (the Kerrobert THAI pilot project)

The following subsections will explain each THAI simulation categories in detail.

3.2 Experimental-scale THAI numerical simulation

The laboratory or experimental scale THAI simulations were the starting point of the numerical investigation during this research work. In this section, it was aimed to model the 3D THAI experiments which were carried out by Tare & Greaves, (2002).

3.2.1 Model Development

The 2018.10 version of STARS software, developed by Computer Modelling Group (CMG) was used to develop THAI simulations at experimental scale. The conservation equations and solution techniques used in STARS will be discussed in Appendix 1. Ado et al, (2017) carried out a grid sensitivity analysis for their THAI model at experimental scale to choose the optimum mesh size. Their simulations were run by using six different grid types. It was done to determine which grid types were sufficient to model the dynamics of the combustion zone. Based on computational efficiency and dynamics of the combustion zones, Ado et al, (2017) proposed the fine dynamic mesh as the optimum grid type for THAI simulations at experimental scale. Table 3.1 shows details of the fine dynamic mesh grid system used for experimental scale THAI simulation in this work, which is based on the proposed grid type by Ado et al, (2017).

Table 3.1. Grid block refinement system for experimental scale THAI model

Combustion cell Dimension (i × j × k)	60cm × 40cm × 10cm
Number of original grid block (i × j × k)	30 × 19 × 7
Number of refined grid block (i × j × k)	90 × 57 × 7
Total number of grid blocks	38298

The simulated combustion cell is a regular Cartesian grid (with 30,19,7 blocks in the i, j, and k directions, respectively). The original/parent grid blocks were then split into 3 refined grid blocks in the i direction, and 3 refined blocks in the j direction. The original grid blocks were not refined in the k direction. In terms of THAI well arrangement, a horizontal injector well

(HI) - horizontal producer well (HP) THAI well configuration was used for the model. Grid refinement was not conducted for the grid blocks in which the HI and HP wells were located. The horizontal sections of both HI and HP wells were perforated. Previous studies on experimental scale THAI models (Ado, Greaves, & Rigby, 2017; Greaves, Dong, & Rigby, 2012 c) employed the discretised wellbore modelling (DW) option for their THAI simulation. However, the DW modelling option was not available in the 2018.10 version of STARS software. The sink/source well model was used for both HI and HP. A single porosity type was assigned for the model with a homogenous oil layer. It was due to the physical properties of 3D THAI experiments by Tare & Greaves, (2002), in which the combustion cell was packed with the Athabasca Tar Sand. The experimental scale does not contain a bottom water section. An electrical heater was used to preheat the inlet zone (around horizontal injector well) of the reservoir and to bring it up to ignition temperature.

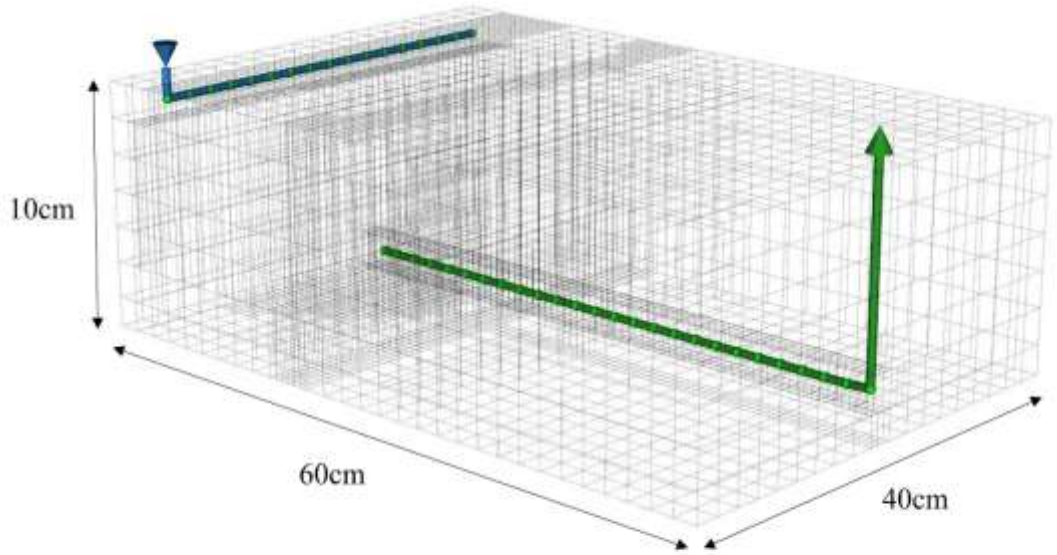


Figure 3.1. Experimental scale THAI model dimensions and HI and HP configuration

3.2.2 PVT and Petrophysical Properties

Ado et al, (2017) used the Peng-Robinson Equation of the State, available in Aspen HYSYS software, to model the properties of the Athabasca bitumen. They used three pseudo-components based on the initial boiling point data, which was proposed by Phillips et al, (1985). Pseudo-components consisted of LC, MC, and IC representing the light, mobile, and immobile components, respectively. Table 3.2 shows pressure, volume and temperature (PVT) data used for the experimental-scale THAI simulation is this study, which is based on PVT data proposed by Ado et al, (2017).

Table 3.2. Experimental-scale PVT data taken from (Ado, Greaves, & Rigby, 2017)

Component	Fraction (mol %)	Molecular Weight (g mol^{-1})	Critical Pressure P_c (kPa)	Critical Temperature T_c (ºC)	Density ρ (kg m^{-3})	Boiling Temperature T_B (ºC)
LC	42.5	210.82	1682.88	464.68	828.24	281.47
MC	23.91	496.81	1038.46	698.53	961.66	549.67
IC	33.59	1017.01	729.22	940.36	1088.04	785.78

Ado et al, (2017) also proposed the variation of Athabasca bitumen viscosity with the temperature. They used the viscosity/temperature relationship for Athabasca reservoirs reported by Mojarab et al, (2011) (shown in Figure 3.2), STARS's default data for light oil and heavy oil (for the viscosity of the LC and MC pseudo-components, respectively), and a linear mixing rule (to estimate the viscosity of the IC pseudo-component). Variation of viscosity at high temperatures (up to 900 °C) is shown later in this chapter (Figure 3.11).

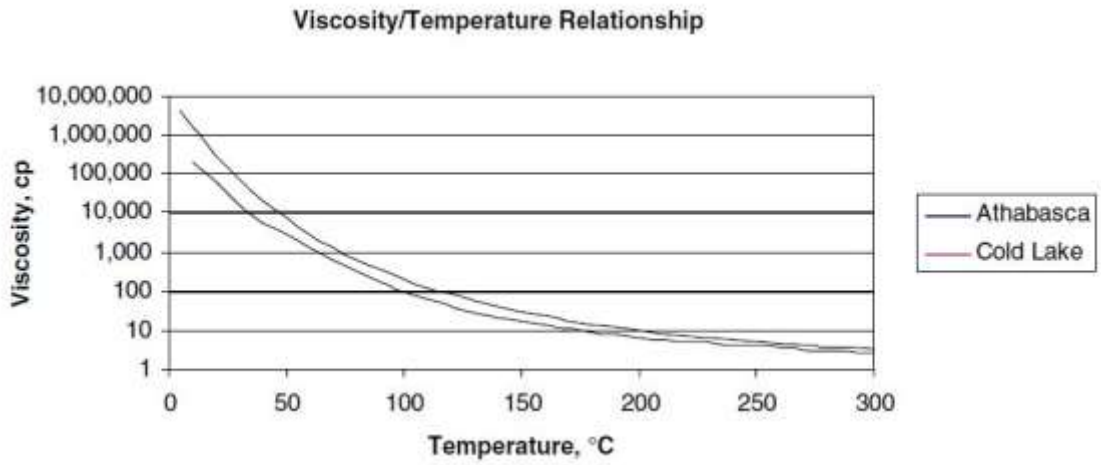


Figure 3.2. The variation of Athabasca bitumen viscosity with the temperature, taken from (Mojarab, Harding, & Maini, 2011)

The petrophysical properties used for the experimental-scale THAI simulation in this study shown in Table 3.3 were taken from study by Greaves et al, (2012 c).

Table 3.3. Properties and initial conditions of the experimental-scale THAI model taken from (Greaves, Dong, & Rigby, 2012 c)

3D combustion cell porosity	0.34
Horizontal permeability, k_h (mD)	11500
Vertical permeability, k_v (mD)	3450
Initial reservoir temperature (°C)	20
Initial reservoir pressure (kPa)	290
Initial oil saturation, S_{oi}	0.85
Initial water saturation, S_{wi}	0.15
Initial gas saturation, S_{gi}	0

The oil/water and gas/water relative permeability curves used for the experimental-scale THAI simulation in this study were taken from study by Ado et al, (2017) (shown in Figure 3.3). The relative permeability curves were slightly adjusted for numerical stability enhancement.

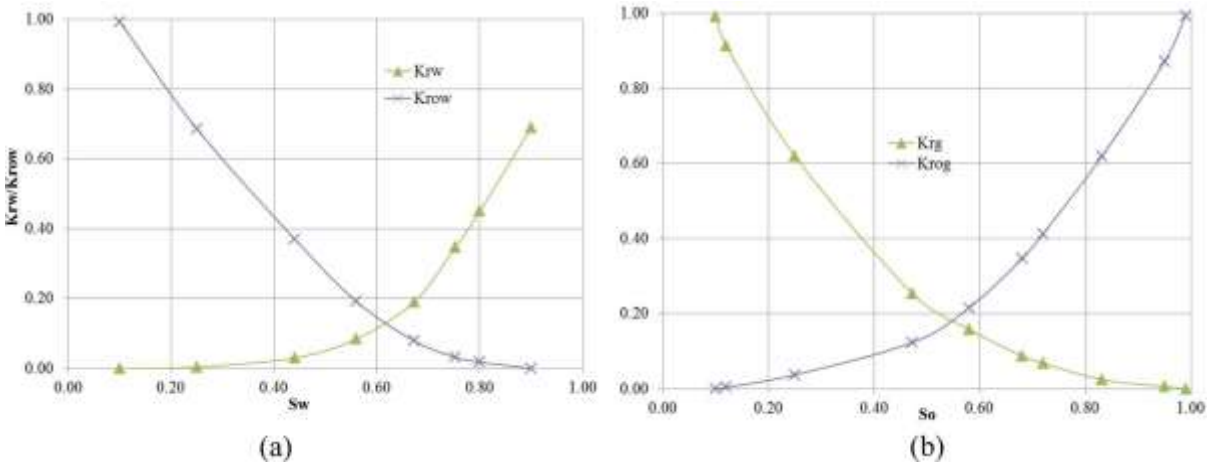


*Figure 3.3. Oil/water relative permeability curve (a) and gas/oil relative permeability curve (b). *Note: K_{rw} and K_{row} are the water and oil relative permeabilities at water saturation S_w, respectively, while K_{rg} and K_{rog} are the gas and oil relative permeabilities at oil saturation S_o, respectively*

3.2.3 Kinetics scheme

Greaves et al, (2012 c) carried out a laboratory level THAI simulation, in which several dynamic parameters for dry combustion were closely predicted compared to results from 3D combustion cell experiments by Tare and Greaves, (2002). However, they did not account for low-temperature oxidation (LTO) reactions in their model because the THAI process predominantly operates in the high-temperature oxidation (HTO) mode. Ado et al, (2017) reported that the direct conversion cracking kinetics proposed by Phillips et al, (1985) accurately predicted the dynamic conditions in 3D combustion cell experiments. They also reported that Phillips et al, (1985) has the advantage of being easily scalable allowing a range of field scenarios to be studied. In addition, the Phillips et al, (1985) has the benefit of being independent of the stoichiometry of the reacting products (Ado, Greaves, & Rigby, 2017).

However, they reported that the rate of coke deposition was not high enough to meet the THAI requirement and to history-match the experimental results by Tare and Greaves, (2002). Consequently, the kinetics parameters for the coke deposition reactions were adjusted in their finally proposed THAI kinetics. They also "tuned" the frequency factors and activation energies for MC and LC pseudo-components to match the experimental results from 3D combustion cell experiments. Table 3.4 a and b shows the experimental-scale THAI kinetics used for this model, which was taken from (Ado, Greaves, & Rigby, 2017).

Table 3.4 a and b Experimental-scale THAI kinetics scheme. Note: IC is immobile pseudo-component, MC is Mobile pseudo-component, and LC is light pseudo-component*

a. Thermal cracking reactions	Frequency factor (min^{-1})	Activation energy ($J\ mole^{-1}$)
IC → 2.0471 MC	3.822×10^{20}	239.01×10^{3}
MC → 0.4884 IC	3.366×10^{18}	215.82×10^{3}
MC → 2.3567 LC	1.132×10^{15}	184.88×10^{3}
LC → 0.4243 MC	1.524×10^{15}	180.45×10^{3}
IC → 77.4563 Coke	2.320×10^{15}	180.88×10^{3}

b. Combustion reactions	Frequency factor ($min^{-1}\ kPa^{-1}$)	Activation energy ($J\ mole^{-1}$)	Heat of Reactions ($J\ mole^{-1}$)
IC + 106.7 O_2 78.9 CO_2 + 4.2 CO + 46.90 H_2O	1.812×10^{8}	138×10^{3}	4×10^{7}
MC + 37.1 O_2 → 28.1 CO_2 + 1.5 CO + 22.4 H_2O	1.812×10^{9}	138×10^{3}	1.6×10^{7}
LC + 32.025 O_2 → 11.2 CO_2 + 0.6 CO + 14.5 H_2O	1.812×10^{10}	138×10^{3}	4.91×10^{7}
Coke + 1.22 O_2 → 0.93 CO_2 + 0.03 CO + 0.57 H_2O	1.000×10^{10}	123×10^{3}	3.9×10^{7}

3.2.4 Operating conditions

The electrical heating method within CMG's Builder was used (for the first 30 minutes) to heat the inlet zone of the combustion cell (around the horizontal injection well). Air injection was then commenced, which was increased during the simulation. Table 3.5 shows the air injection rates and their timeline during the THAI process at experimental scale.

Table 3.5. Operating condition of the experimental scale THAI simulation

Air injection rates (cm^3/min)	Timeline (minutes)
8000	30 — 190
10667	190 — 320

A minimum bottom hole pressure was set as the horizontal injector and producer wells constraints. The composition of air injected into the reservoir, temperature of injected fluid, injector and producer well constraints are shown in Table 3.6.

Table 3.6. Injected air properties and injector and production well constrains for the experimental-scale THAI model

Injected fluid composition (%)	Injected fluid temperature (°C)	Injection well maximum bottom hole pressure (kPa)	Production well minimum bottom hole pressure (kPa)	Production well maximum surface liquid rate (cm^3 min^{-1})
N_2 (79) & O_2 (21)	25	1900	170	25

3.2.5 Model validation

The experimental results from 3D combustion cell experiments carried out by Tare and Greaves, (2002) was utilised to validate the predicted results from experimental-scale THAI

simulation in this work. Oil production rates, oxygen utilisation, and peak temperature profiles were compared between the simulated results and experimental data.

3.2.6 Results and discussions

3.2.6.1 Oil production

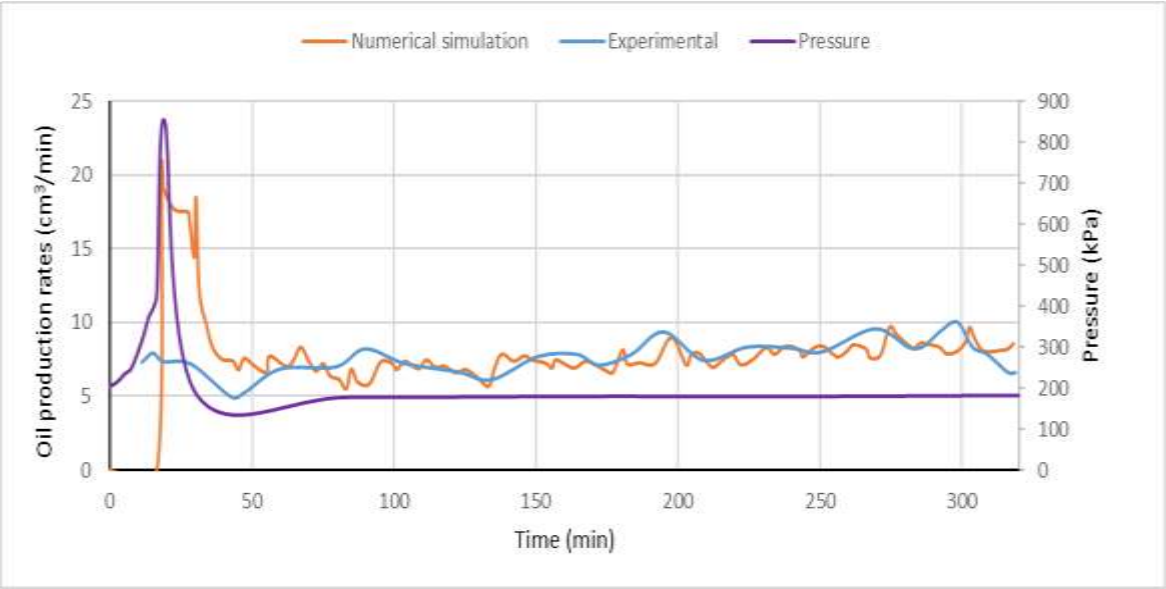


Figure 3.4. Comparison of the experimental and simulated oil production rates at experimental-scale

The oil production rate profile is one of the most important data sets that needs to be predicted as accurately as possible (Greaves, Dong, & Rigby, 2012 c). Figure 3.4 shows the comparison between the experimental and predicted (at experimental scale) oil production profiles. The initial simulated oil production profile shows a deviation in comparison with the experimental results. A similar deviation was shown by Greaves et al, (2012 c) and Ado et al, (2017) , where an initial overshoot in oil production rate was reported for the first 90 and 40 minutes of the dry combustion simulations, respectively. Ado et al, (2017) reported that their experimental scale model for oil production did not show the same overshoot because of the low sampling rate during the experimental measurement of the oil flow rate. No oil was present inside the horizontal producer prior to the pre-ignition heating of the inlet zone (around the horizontal

injection well) in the simulation in this work. The simulation predicted oil production after 16 minutes, when some of the oil around the toe section of the horizontal well was mobile enough to be produced. The initial in-situ oil mobilisation in the model, prior to the air injection, was due to the thermal cracking of the oil originally in place through the heat supplied by electrical heating. This resulted in a considerable overshoot in the predicted oil production rate (up to 22 cm^3/min) for a short period (10 minutes). A direct relationship can be detected between the predicted pressure profile and oil production rate in Figure 3.4. A similar initial spike in oil production rate was reported by Ado et al, (2017). They also reported that formation of thermally cracked products (gaseous and light hydrocarbons) resulted in a pressure build-up around the toe section of the horizontal producer. Apart from the initial stage of simulation, there is a very close overall agreement between the predicted and experimental results until the end of the simulated period (320 minutes).

3.2.6.2 Peak combustion temperature

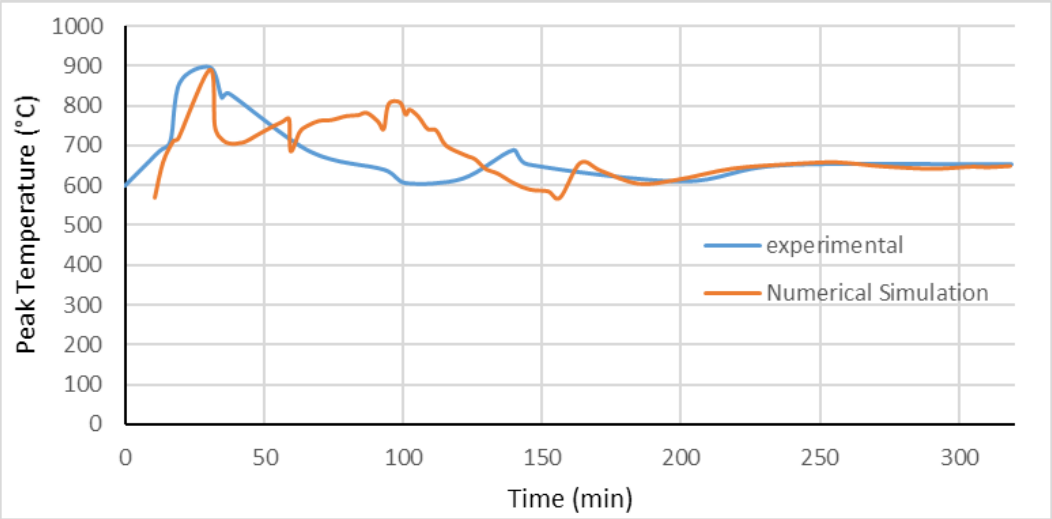


Figure 3.5. Comparison between the experimental and simulated peak temperatures with time at experimental scale.

The experimental-scale THAI numerical study by Greaves et al, (2012 c) showed that after 70 minutes, the predicted temperature lies above the experimental value by 40 to 90 °C, and this

deviation was maintained until the end of the simulated period (320 minutes). They reported that the higher predicted peak temperatures may be due to the difference between the applied heat loss in the simulation and that occurring in the experiments. Figure 3.5 shows the comparison between the experimental and simulated (at experimental scale) peak temperatures profiles with time in this work. It was shown that the simulation predicted the maximum temperature achieved in the experiments very well. The simulated peak temperatures matched closely with experimental results during the higher air injection rate period (190 to 320 minutes). However, there was an evident deviation between the experimental and predicted results during the lower air injection period (30 to 190 minutes). This was due to the use of electrical heater as the pre-ignition heating strategy prior to air injection in the 3D combustion cell experiments. A similar trend for the peak temperature profile was observed in a numerical study by Ado et al (Dynamic Simulation of the Toe-to-Heel Air Injection Heavy Oil recovery Process, 2017). They reported that it is likely that the tape heater control method employed in the experiments by Tare and Greaves, (2002) overcompensated for the heat loss, resulting in temperature rise in the sandpack, and then (later in the experiment) undercompensated, allowing the sandpack temperature to undershoot.

3.2.6.3 Oxygen content in the produced gas

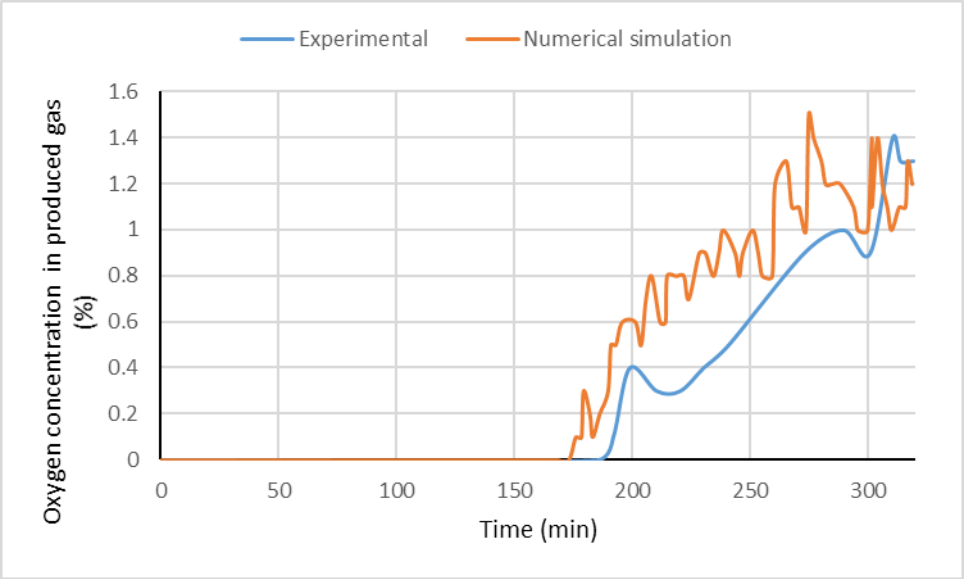


Figure 3.6. Comparison of the experimental and simulated oxygen concentration in produced gas at experimental scale

Oxygen utilisation is another important indicator of combustion performance or, alternatively, how much oxygen is consumed by the HTO reactions. The oxygen content of the produced gas indirectly indicates how efficient the combustion process is (Greaves, Dong, & Rigby, 2012 c). Figure 3.6 shows the comparison between the predicted oxygen content of the produced gas in current study with that from 3D combustion cell experiment. Greaves et al, (2012 c) reported that the first appearance of oxygen was because of the sudden increase in the air injection rate. However, Figure 3.6 shows that the first predicted appearance of oxygen happened before the increase in air injection rate (after 140 minutes of air injection) in the current work. The predicted oxygen content of the produced gas lay above the experimental value by 0.2 to 0.4 %, and this difference was maintained to the end of the simulated period, apart from the last 10 minutes. This is similar to the observation made by Ado et al, (2017) that an increase in air injection rate does cause an increase in oxygen content in the produced gas. They ran their simulation with the higher air injection rate (10667 cm^3/min) for the whole dry combustion

period. Ado et al, (2017) reported that the increase in oxygen content of the produced gas occurred at exactly the same time, regardless of whether the air injection rate was increased or not. However, they recommended further investigation of this aspect of the THAI process. Figure 3.7 shows that there is direct relationship between the predicted coke concentration around the toe section of the horizontal producer and the predicted oxygen content of the produced gas. It was found that high coke concentration around the toe section of the horizontal producer increases the oxygen utilisation, and inversely, low high coke concentration around the toe section of the horizontal producer decreases the oxygen utilisation. This relationship will be investigated further in more detail in 4.5.3 later in this study.

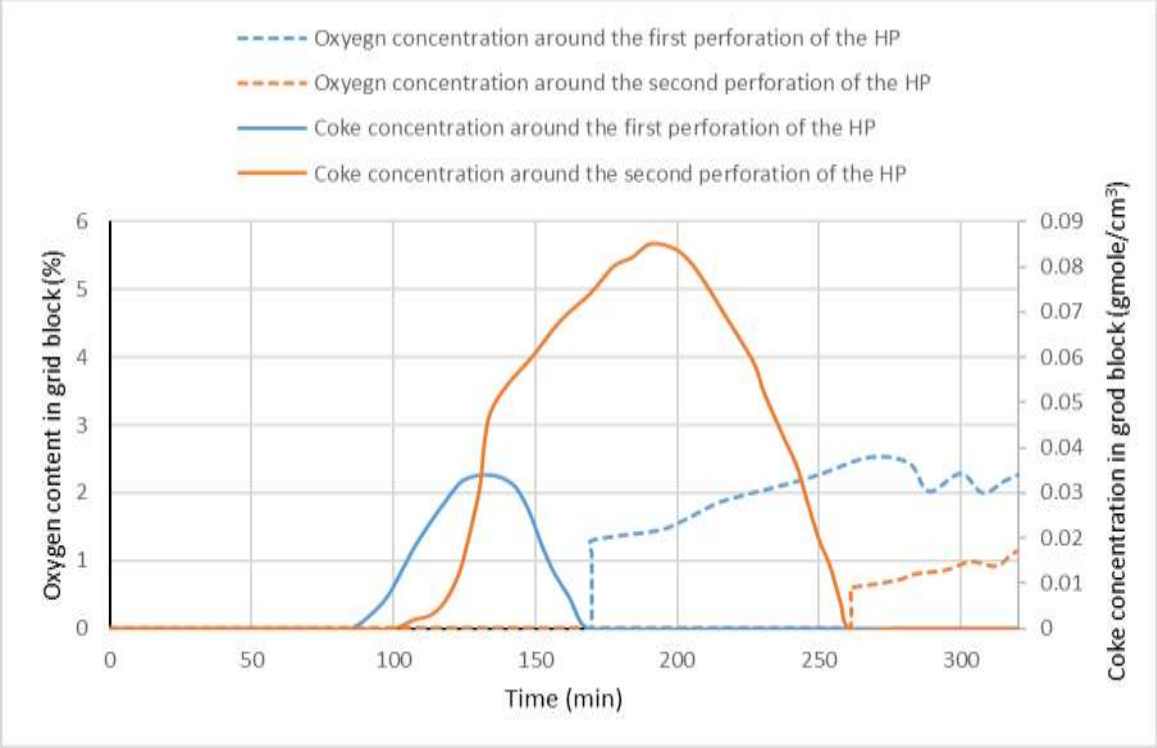


Figure 3.7. The predicted oxygen and coke concentration around the toe section of the horizontal producer

3.3 Field-scale THAI numerical simulation

Only a few published field scale THAI simulation studies are available in literature (shown in Sections 2.8.2 and 2.8.3). Scaling-up the 3D combustion cell experiment by Tare and Greaves, (2002) has been mostly used to construct a mechanistic model of the THAI process in field scale. Nissen et al, (2015) reported a detailed in-situ combustion upscaling workflow that was summarised in Figure 3.8. There is no published research on a history-matched THAI model at field scale in the literature. This is due to the lack of published data from the field pilots and THAI operators. In this section a new field scale THAI model is presented which will be employed to study different THAI well arrangements. The model developed will also be used to study a real-life THAI pilot project in a later chapter (4).

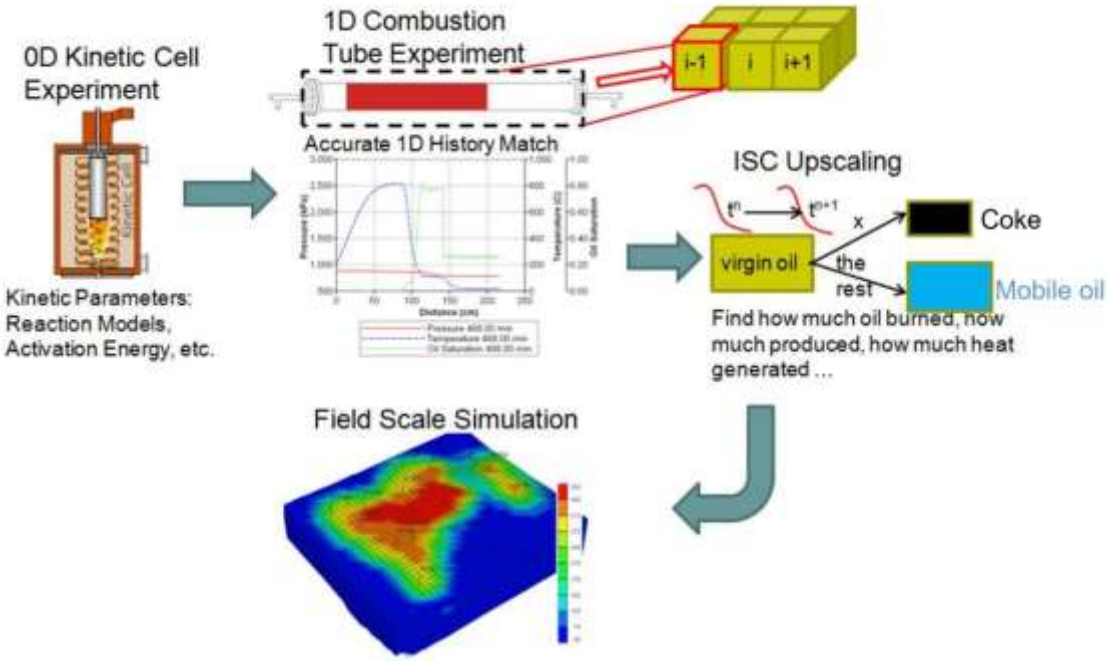


Figure 3.8. In-situ combustion upscaling workflow taken from (Nissen, Zhu, Kovescek, Castanier, & Gerritsen, 2015)

3.3.1 Model Development

The 2019.10 version of STARS software, developed by Computer Modelling Group (CMG) was employed to develop THAI simulations at field scale. In-situ combustion simulations are sensitive to grid block size. The grid blocks represent regions of the order of centimetres in size at experimental scale, whereas they are of the order of metres at field scale THAI simulations. Ado, (2020 a) carried out a grid sensitivity analysis on THAI simulations at field scale. He used sequential volume up scaling to obtain larger-length scale predictions. Ado, (2020 a) proposed a new approach to up-scale experimental scale THAI simulations that were validated against 3D combustion cell experiments. Table 3.7 shows details of the grid system used for field scale THAI simulation in this work, which is based on the proposed grid type by Ado, (2020 a) (Model P). The simulated combustion cell is a regular Cartesian grid (with 30,19,7 blocks in the i, j, and k directions, respectively). The original/parent grid blocks were then split into 3 refined grid blocks in the i direction, and 3 refined blocks in the j direction. The original grid blocks were not refined in the k direction. The total number of grid blocks for grid system slightly varied depending on the applied THAI well arrangement in the simulations. The THAI well arrangement at field scale and its variation will be studies in details in Section 3.3.1.1.

Table 3.7. Grid block refinement system for the staggered line drive SLD-THAI model and the direct line drive DLD model at field scale

Reservoir Dimension (i × j × k)	148m × 98m × 24m
Number of original grid block (i × j × k)	30 × 19 × 7
Number of refined grid block (i × j × k)	90 × 57 × 7
Total number of grid blocks	38442 (SLD-THAI field scale model) 38451 (DLD-THAI field scale model)

3.3.1.1 THAI well arrangement at field scale

The THAI process consists of at least one vertical injector (VI), perforated in the upper part of the oil zone, and a horizontal producer (HP), placed at the lowest possible part of the oil zone, with its toe facing the VI (Turta, Greaves, & Strakov, 2021). The THAI process can be applied in two well arrangements: direct line drive (DLD) and staggered line drive (SLD). Only DLD THAI well arrangement has been employed by THAI operators in field pilots and projects so far (Turta A. , 2021). Based on previous field experiences and THAI simulations, Turta et al, (2018) reported that the main ways to bring substantial improvements to the THAI process are: (a) employing the SLD THAI well arrangement instead of the DLD THAI well arrangement, whenever possible, (b) creating an initial broad in-situ combustion front. A summary of the main differences between the DLD-THAI process and SLD-THAI process have been reported by Turta et al, (2018). In the following sub-section both THAI well arrangement will be employed to numerically study the impact of the well arrangement type on the overall performance of the THAI process at field scale.

3.3.1.1.1 Direct line drive (DLD) THAI well arrangement at field scale

Figure 3.9 shows the DLD THAI well arrangement, which consists of a vertical injector well that is placed in front of the toe section of the horizontal producer well. Turta et al, (2018) reported that the maximum temperature observed by the horizontal section of the producer well is always higher in the DLD-THAI well arrangement compared to that in the SLD-THAI well arrangement. The local coke plugging of the horizontal section of the producer well represents a self-healing feature of the THAI technology (Turta, Greaves, & Grabowski, 2018). This, possibly, will be more established in the in the DLD-THAI well arrangement compared to that in the SLD-THAI well arrangement. This also represents a higher risk of coke blocking of the horizontal section of the producer well employing the DLD-THAI well arrangement.

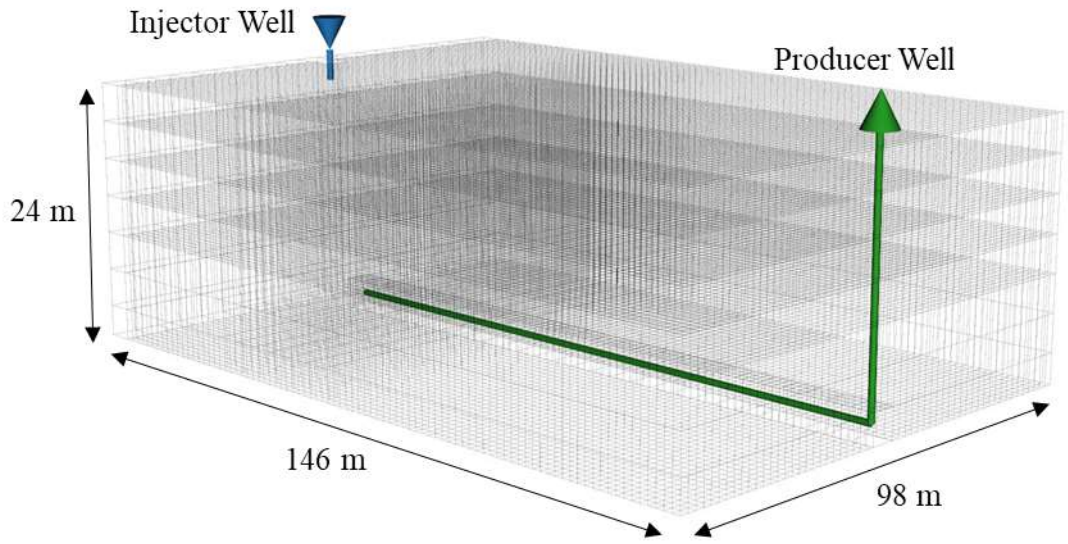


Figure 3.9. The DLD-THAI well arrangement at field scale

3.3.1.1.2 Staggered line drive (SLD) THAI well arrangement at field scale

Figure 3.10 shows the SLD THAI well arrangement, which consists of two vertical injector wells and a horizontal producer well. The toe section of the horizontal producer well is placed close to the line of the vertical injector wells but is laterally offset (Turta, Greaves, & Strakov,

2021). Turta et al (2018) reported that the SLD-THAI well arrangement is associated with a broader oil displacement front resulting in higher air injection and oil production rates in the THAI process. As the air injection well is not placed just above the toe section of the horizontal producer well, the well completion of the vertical air injector well is less critical in the SLD-THAI well arrangement. Also, the risk of water coning is lower in the SLD-THAI well arrangement compared to the DLD-THAI well arrangement. However, establishing communication between the injector wells and the producer well is not straightforward in the SLD-THAI well arrangement. First, the whole start-up regions must be heated to 100 to 120 °C. Secondly, a linear in-situ combustion front must be built along the line uniting the injector wells (Turta, Greaves, & Grabowski, 2018).

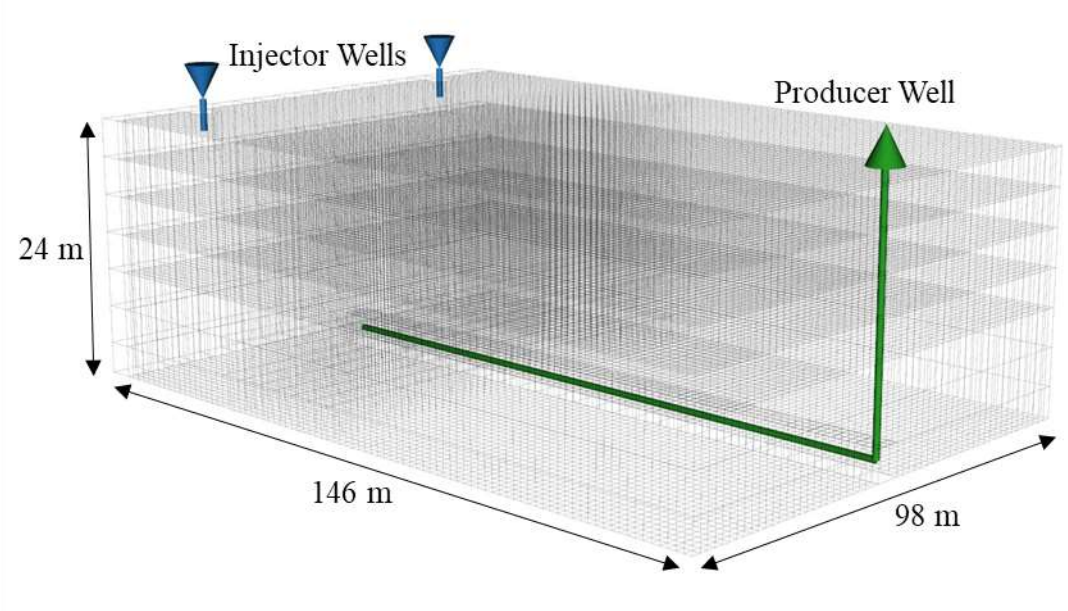


Figure 3.10. The SLD-THAI well arrangement at field scale

3.3.2 PVT and Petrophysical Properties

The PVT properties, shown in Section 3.2.2 (used for the experimental scale THAI simulation in this work), were employed for the field scale THAI simulations in this section.

Figure 3.11 shows the data used for the variation of bitumen viscosity as a function of change in temperature for the filed scale THAI simulation, which was taken from the study by Ado, (2020).

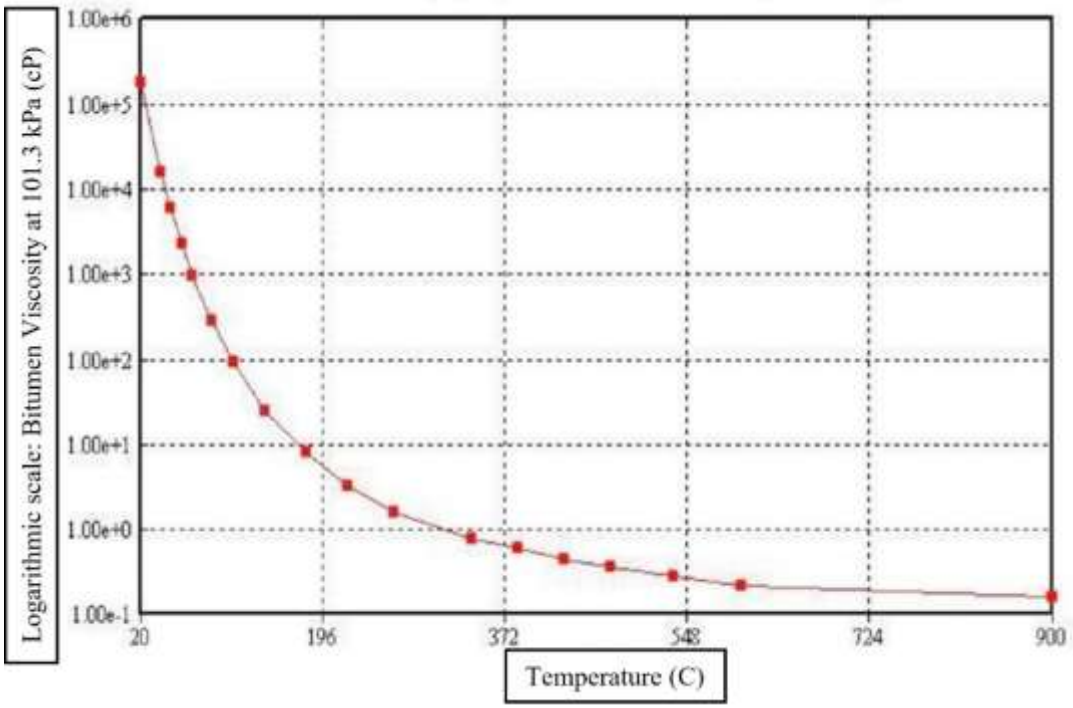


Figure 3.11. Variation of viscosity with temperature taken from Ado, (2020)

Table 3.8 shows the petrophysical properties used for the field scale THAI simulation in this study, which was taken from Petrobank Energy & Resources Limited annual report (2009).

Table 3.8. Properties and initial conditions of the Field scale THAI model

3D combustion cell porosity	0.34
Horizontal permeability, k_h (mD)	6400
Vertical permeability, k_v (mD)	3450
Initial reservoir temperature (°C)	20
Initial reservoir pressure (kPa)	2800
Initial oil saturation, S_{oi}	0.80
Initial water saturation, S_{wi}	0.20
Initial gas saturation, S_{gi}	0

The oil/water and gas/water relative permeability curves used for the experimental-scale THAI simulations, shown in Section 3.2.2, was also employed for the field scale THAI simulations in this work.

3.3.3 Kinetics scheme

The experimental scale THAI kinetics scheme, shown in Section 3.2.3 cannot be directly used for the THAI simulation at field scale. This is due the dimensional differences in lengths scale between the experimental scale models (centimetres) and field scale THAI simulations (meters). Also, the time scale is different in field scale simulations (years) compare to experimental scale models (hours). Nissen et al, (2015) reported that up-scaling experimental scale ISC model to field scale model includes the challenge of how to treat the kinetics of chemical reactions because the reactions rates are many orders of magnitude faster in comparison with the other physiochemical processes, e.g. heat and mass transfer. This means that it is very likely that, at low temperature regions, too much coke is going to be deposited (over coking) in the field scale THAI simulations, if the same experimental scale THAI kinetics

scheme are to be used. Over coking can lead to failure of the process by reducing the air injectivity. The frequency factors of reactions therefore need to be adjusted for upscaling the THAI kinetics scheme. Ado, (2020) carried out a comparative study between the predictions for the two different types of validated kinetics schemes. He proposed a new upscaling procedure, which involved reducing the reaction frequency factors of the experimental scale THAI kinetics scheme. The kinetics scheme used for Model P in the study by Ado, (2020), was used for the field scale THAI simulation in this work, with minor adjustment. Table 3.9 a and b shows the field scale THAI kinetics scheme that was used for the present study.

Table 3.9 a and b. Field-scale THAI kinetics scheme. Note: IC is immobile pseudo-component, MC is Mobile pseudo-component, and LC is light pseudo-component. COx is the inert gas*

a. Thermal cracking reactions	Frequency factor (min^{-1})	Activation energy ($J\ mole^{-1}$)
IC → 2.0471 MC	8.186×10^{16}	239.01×10^{3}
MC → 0.4884 IC	7.2094×10^{14}	215.82×10^{3}
MC → 2.3567 LC	2.42455×10^{11}	184.88×10^{3}
LC → 0.4243 MC	3.26415×10^{11}	180.45×10^{3}
IC → 77.4563 Coke	4.96905×10^{11}	180.88×10^{3}

b. Combustion reactions	Frequency factor ($min^{-1}\ kPa^{-1}$)	Activation energy ($J\ mole^{-1}$)	Heat of Reactions ($J\ mole^{-1}$)
IC + 106.684 O_2 → 83.33 CO_x + 46.904 H_2O	2.77214×10^{3}	138×10^{3}	4×10^{7}
MC + 37.06 O_2 → 29.7495 CO_x + 22.365 H_2O	2.77214×10^{4}	138×10^{3}	1.6×10^{7}
LC + 17.4629 O_2 → 11.8183 CO_x +14.5 H_2O	2.77214×10^{4}	138×10^{3}	4.91×10^{7}
Coke + 1.22 O_2 → 0.9758 CO_x + 0.565 H_2O	1.52988×10^{5}	123×10^{3}	3.9×10^{7}

3.3.4 Operating condition

3.3.4.1 Pre-ignition heating cycle (PIHC)

The start-up operating process for the field scale THAI simulations varies compared to that in the experimental scale THAI models. As it was discussed in Section 3.2.4, electrical heating was used to increase the temperature of the inlet zone of the combustion cell, prior to the air injection, in the experimental scale THAI simulations. In field THAI projects, the communication between the injector and production wells is achieved by steam injection and

the ignition phase can also involve steam injection for heating the surrounding region of the air injection well (Turta, Greaves, & Grabowski, 2018). The pre-ignition heating cycle (PIHC) was carried out by injection of steam into the reservoir for the first 104 days during the field scale THAI simulations. The steam assisted PIHC was carried out for both SLD-THAI and DLD-THAI well arrangements. The data for steam assisted PIHC was taken from Petrobank Energy & Resources Limited annual report (2009) and is shown in Table 3.10.

Table 3.10. Input data for steam assisted pre-ignition heating cycle for field scale THAI simulations

Steam injection rate (m^3/day)	Steam injection pressure (kPa)	Steam quality (%)	Steam temperature (°C)
80	5500	80	270

3.3.4.2 The DLD-THAI operating condition at field scale

Table 3.11 shows the operating condition of the field scale THAI model when the DLD well arrangement was applied. Using an up-scaling factor, Ado (2020 a) up-scaled the experimental scale THAI air injection rate (from 8000 cm^3/min to 20000 m^3/day) for his field scale THAI model. The same air injection rate was considered, throughout, for the field scale DLD-THAI model in this work.

Table 3.11. Operating conditions of DLD-THAI model at field scale

Injected air composition	CO_x (79%) & O_2 (21%)
Number of vertical air injection well	1
Air injection duration	2 years
Air injection rate	20000 m^3/day
Maximum bottom hole pressure of the injection well	9500 kPa
Minimum bottom hole pressure of the producer well	2800 kPa
Maximum surface liquid rate of the producer well	315 m^3/day

3.3.4.3 The SLD-THAI operating condition at field scale

Table 3.12 shows the operating condition of the field scale THAI model when the SLD well arrangement was applied. A constant air injection rate (equal to that in DLD-THAI model) was considered for the field scale SLD-THAI model as well. However, the air injection into the reservoir was carried out through two injector wells.

Table 3.12. Operating conditions of SLD-THAI model at field scale

Injected air composition	CO_x (79%) & O_2 (21%)
Number of vertical air injection well	2
Air injection duration	2 years
Air injection rate (for each injection well)	10000 m^3/day
Maximum bottom hole pressure of the injection well	9500 kPa
Minimum bottom hole pressure of the producer well	2800 kPa
Maximum surface liquid rate of the producer well	315 m^3/day

3.3.5 Results and discussions

3.3.5.1 Combustion front shape

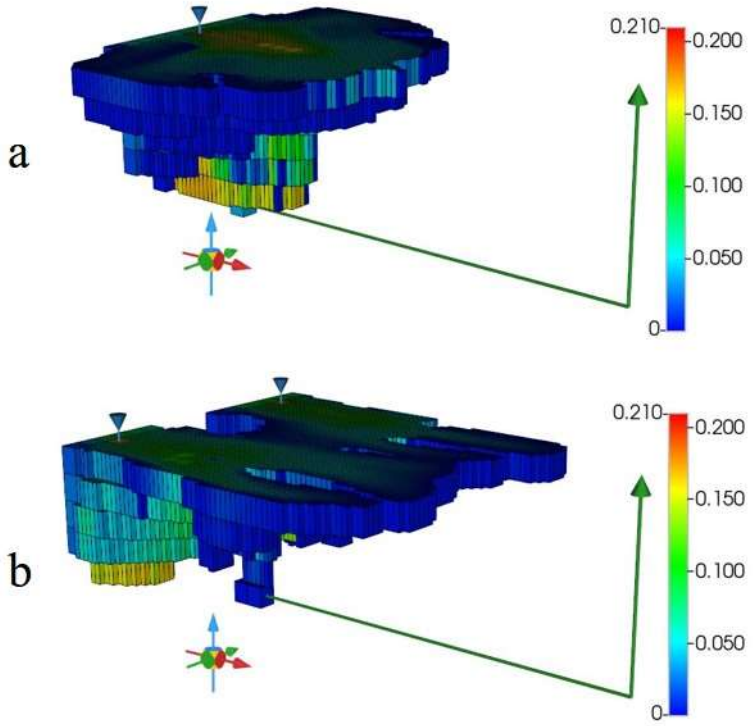


Figure 3.12. The predicted combustion front shape (oxygen mole fraction) for the DLD-THAI (a) and the SLD-THAI (b) processes

The oxygen concentration falls to zero at the leading edge of the oxygen front as it contacts the combustion front. Consequently, the leading edge of the oxygen front is a good indicator of the true shape of the combustion front (Greaves, Dong, & Rigby, 2012 b). Figure 3.12 shows the predicted combustion front shape for the DLD-THAI (a) and the SLD-THAI (b) field scale simulations at the end of the simulated period. It is apparent that both simulations predicted stable combustion process (no oxygen breakthrough ahead of combustion front). This was due to the sealing effect of coke deposition ahead of the combustion front, which will be discussed in chapter 4 later in this study. It can be observed that a broader combustion front propagation was achieved in in the SLD-THAI application compared to that in the DLD-THAI application.

This is directly related to poor oxygen consumption in the DLD-THAI process. This will be studied in detail in Section 3.3.5.4 in this work.

3.3.5.2 Oil saturation

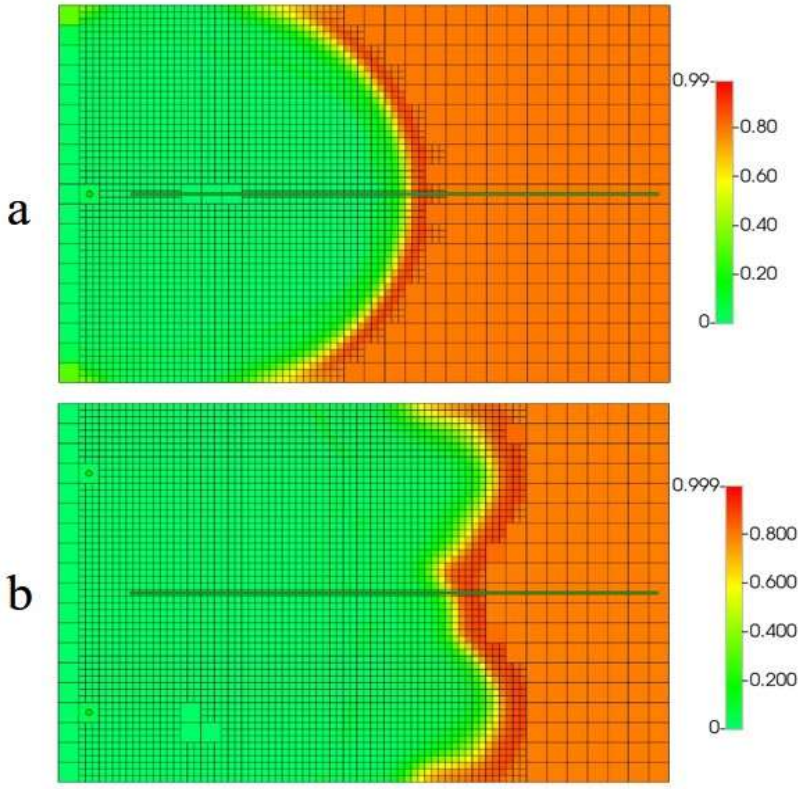


Figure 3.13. The predicted aerial view of oil saturation profile for the DLD-THAI (a) and the SLD-THAI (b) processes

Figure 3.13 shows the predicted aerial view of oil saturation profile, at the top horizontal plane, for the DLD-THAI (a) and the SLD-THAI (b) field scale simulations at the end of the simulated period. It is evident that a larger volume of the reservoir, two-thirds of that on top horizontal layer, was fully swept by the combustion front in the SLD-THAI compared to that in the DLD-THAI. The swept oil was then forced to flow to the horizontal producer well by the pressure gradient and gravity drainage. This is reflected in the predicted oil production profile for both simulated cases, reported in Section 3.3.5.3 in this study.

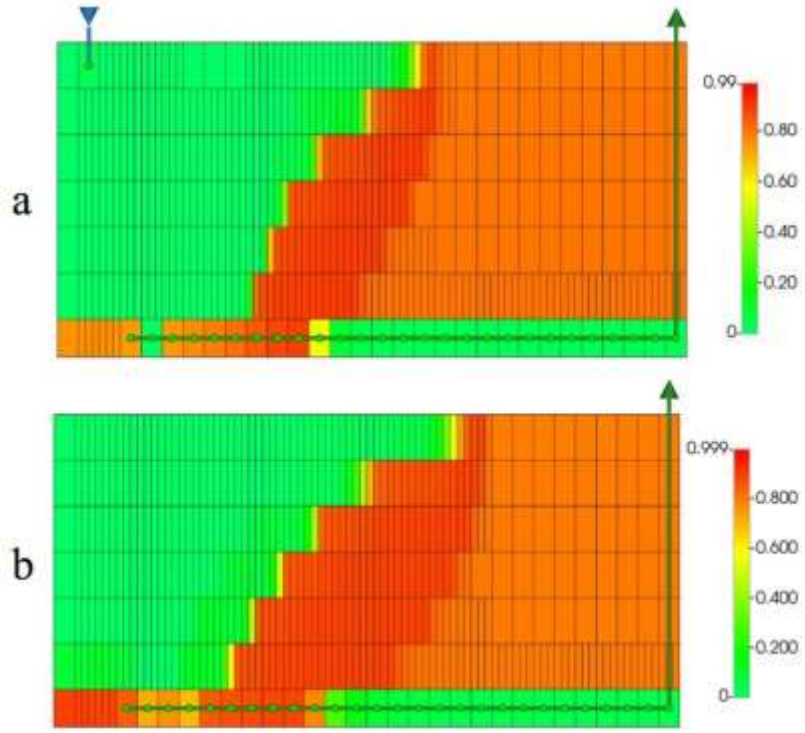


Figure 3.14. The predicted cross-sectional view of the oil saturation profile for the DLD-THAI (a) and the SLD-THAI (b) processes

Figure 3.14 shows the cross-sectional view of the oil saturation profile, at the vertical mid-plane of the reservoir, for the DLD-THAI (a) and the SLD-THAI (b) field scale simulations at the end of the simulated period. It is clear that the size of mobile oil zone (MOZ), where the oil saturation is between 0.8 and 1, is larger in the SLD-THAI application compared to that in the DLD-THAI. This means that a larger portion of cold heavy oil, ahead of the combustion front, was mobilised and then drained into the horizontal producer in the simulated SLD-THAI process. This is due to the efficient in-situ combustion performance that had taken place in the simulated SLD-THAI process. Achievement of an efficient in-situ combustion performance is directly related to the oxygen consumption throughout the THAI process.

3.3.5.3 Oil production

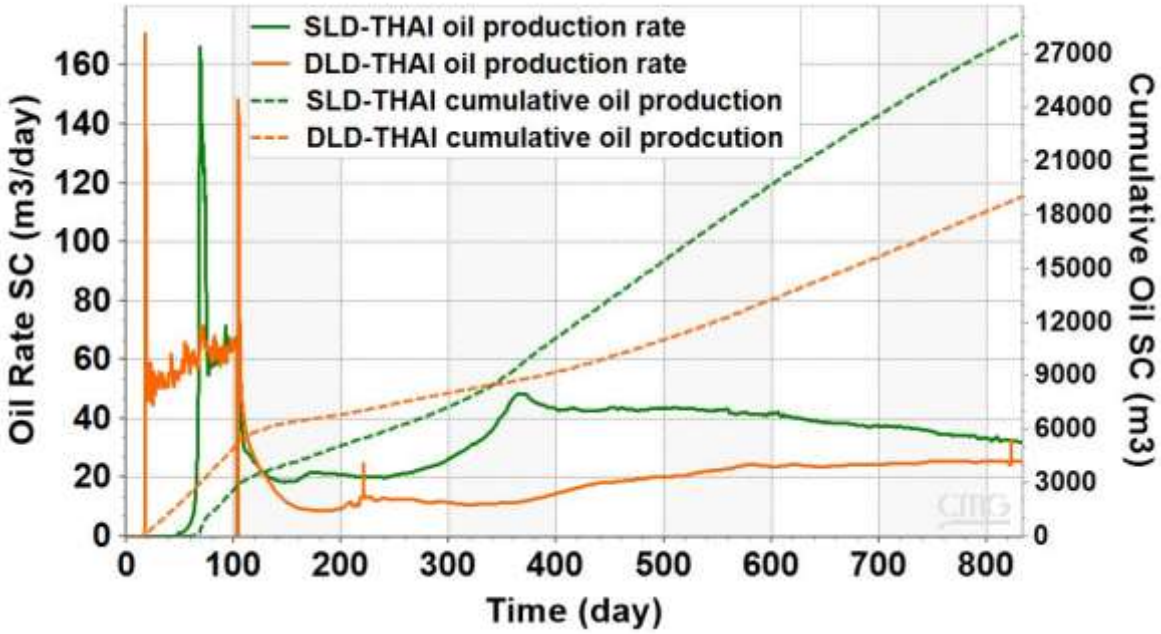


Figure 3.15. The predicted oil production profile for the DLD-THAI and SLD-THAI processes

Figure 3.15 shows the oil production profile for the DLD-THAI (a) and the SLD-THAI (b) field scale simulations during the simulated period. The DLD-THAI well arrangement resulted in an earlier oil production compared to the SLD-THAI well arrangement. During the PIHC, some oil has to be displaced form the inlet region of the reservoir in order to achieve gas communication with the producer well in the THAI process (Ado M. R., 2020). Petrobank (2009) reported that oil production started after almost three months of steam injection at the Whitesnads Experimental pilot project, where the THAI operator employed the DLD-THAI well arrangement. However, it can be seen in Figure 3.15 that the DLD-THAI simulation predicted after 18 days from the start of steam injection into the reservoir. This difference is due to various parameters that are involved in a field THAI operation, which are listed in Section 4.2 in this study. The SLD-THAI simulation predicted the first oil production after 67 days from the start of the PIHC. Both models predicted high initial oil production rates (up to

65 m^3/day). The high initial oil production rates are related to built-up pressure difference between the inlet zone (around injector well) and the outlet zone (around the toe section of the horizontal producer) in models. The oil production rates dropped rapidly (to 10 m^3/day and 20 m^3/day in the DLD-THAI and SLD-THAI applications, respectively) as soon as the air injection commenced (104th day). The deviation between the oil production rates for both models was around 10 m^3/day until 260th day of the THAI process. However, better in-situ combustion efficiency predicted in the SLD-THAI resulted in an increase in oil production rates (to up to 50 m^3/day) from 260th to 370th day of the THAI process. This was a direct result of a rise in volume of mobilised oil due to the heat transfer via the THAI process (rather than that caused by the PIHC earlier). The SDL-THAI oil production rate remained higher than in the SLD-THAI simulation until the end of simulated period. The predicted cumulative oil production for the SLD-THAI model was 50% higher than that in the DLD-THAI model.

3.3.5.4 Oxygen utilisation

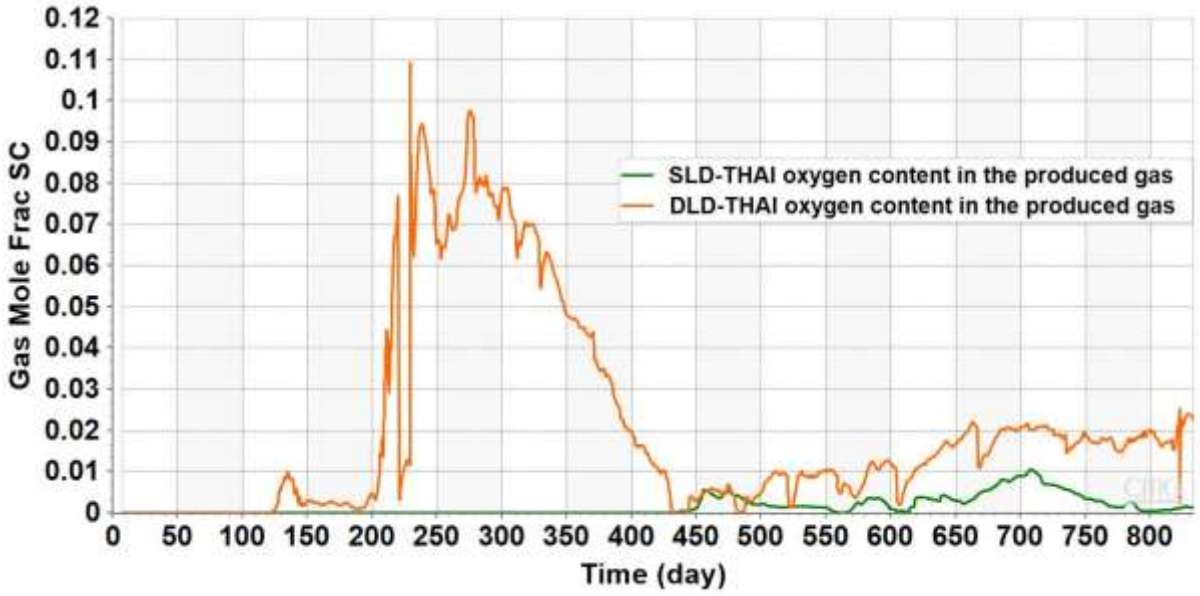


Figure 3.16. The predicted oxygen content in the produced gas for the DLD-THAI and SLD-THAI processes

Figure 3.16 shows the predicted oxygen content in the produced gas in the DLD-THAI and SLD-THAI models. It is clear that considerable oxygen channelling has taken place from early stages of the THAI process in the DLD-THAI model. This was because of its well arrangement, in which there is a short offset distance between the vertical injector well and the toe section of the horizontal producer. This led to a poor oxygen consumption in the DLD-THAI model, which was reflected in its lower oil production rate compared to the SLD-THAI model. Also, in Figure 3.16, it can be seen that oxygen channelling into the horizontal producer only occurred after the 440th day of the THAI process, where produced O_2 was remained below 1% until the end of the simulated period. The effective oxygen utilisation in the SLD-THAI model was reflected in its higher oil production rate in Figure 3.15. It was found that there is a direct relationship between the coke deposition around the toe section of the horizontal producer and oxygen channelling into the producer well, which will be discussed in detail in Section 4.5.3 of this study.

3.3.5.5 Coke deposition

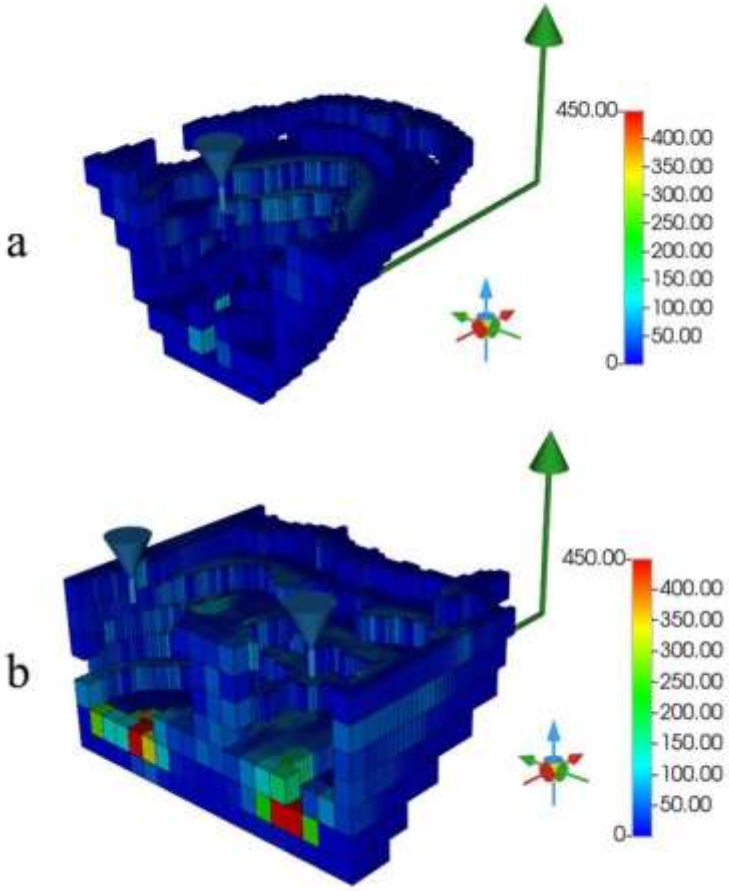


Figure 3.17. The predicted coke deposition profile (in kg/m^3) for the DLD-THAI (a) and the SLD-THAI (b) processes

Figure 3.17 shows the predicted coke deposition profile for the DLD-THAI (a) and the SLD-THAI (b) field scale models. Coke is formed, primarily, from thermal cracking of the heavy residue, which remains after all of the lighter-oil components and water have been vaporised by the approaching combustion front (Greaves, Dong, & Rigby, 2012 b). Coke deposition provides the fuel to sustain in-situ combustion, which is continuous throughout the THAI process. It can be seen in Figure 3.17 that for both models coke deposition acts as a seal, which prevents oxygen breakthrough ahead of the combustion front. The coke concentration profile, however, varies in areas immediately ahead of the combustion front to that at the base section of reservoir for both models. The SLD-THAI model predicted higher coke concentration

compared to the DLD-THAI model at the base section of the reservoir. It is evident that most of heavy faction of the oil was left behind and cracked to coke by the high temperature of the combustion front, occurring below the injector wells, in the SLD-THAI model. On the other hand, the fuel availability (coke deposition) is not sufficient in the DLD-THAI model, which was related to its poor in-situ combustion development.

3.3.5.6 In-situ steam generation

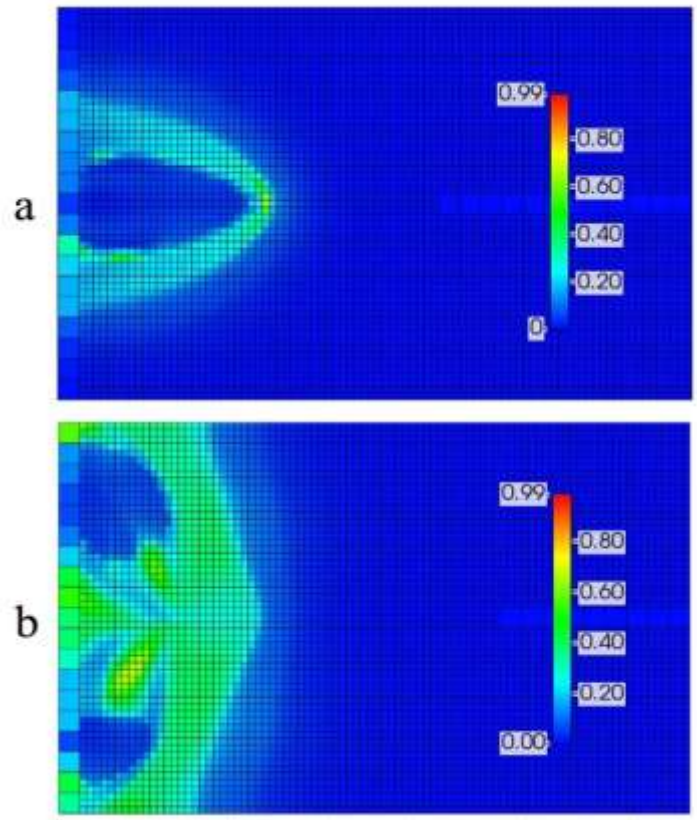


Figure 3.18. The predicted in-situ steam generation profile (steam mole fraction) for the DLD-THAI (a) and the SLD-THAI (b) processes

Figure 3.18 shows the predicted steam mole fraction profile for model the DLD-THAI (a) and the SLD-THAI (b) field scale models. The thermal sweep efficiency is largely governed by the steam-gas front generated ahead of the combustion front (Greaves & Al-Honi, 2000). The steam zone is the major heat transfer mechanism in the THAI process, transporting large

amounts of energy from the combustion gases into the downstream, cold oil zone, mobilising the viscous/immobile oil (Greaves, Dong, & Rigby, 2011). Figure 3.18 shows the steam concentration profile at the horizontal mid-plane for the DLD-THAI (a) and SLD-THAI (b) models when the combustion front propagation has fully stabilised. It was found that, in both simulations, the in-situ steam generation took place over the entire combustion period. However, the size of steam zone in the SLD-THAI model was noticeably larger than that in the DLD-THAI model. The larger steam zone indicates that the THAI process has been more efficient in the SLD-THAI model, in which the oxygen utilisation was greater. The larger mobile oil zone (shown in Figure 3.14 in dark red) for the SLD-THAI simulation is directly related to the size of the in-situ generated steam zone in this model. This is due the high reduction in oil viscosity via the heat which was supplied from the steam zone.

3.3.6 Conclusion

Starting from laboratory scale, a new field scale THAI model was constructed to study the DLD and SLD THAI well arrangements. It was found that a broader combustion front propagation can be achieved in the SLD-THAI arrangement compared to that in the DLD-THAI arrangement. This was directly linked to poor oxygen consumption in the DLD-THAI application. The oxygen channelling into the horizontal producer occurred from early stages of the THAI process in the DLD-THAI model. It was found that a larger volume of the reservoir was swept by the combustion front in the SLD-THAI compared to that in the DLD-THAI. The predicted cumulative oil production for the SLD-THAI model was 50% higher than that in the DLD-THAI model. It was found that, for both models, coke deposition acted as a seal, which prevented oxygen breakthrough ahead of the combustion front. Additionally, the size of steam zone in the SLD-THAI model was distinctly larger than that in the DLD-THAI model. Overall, the predicted results showed that SLD-THAI well arrangement has superiority over the DLD-THAI well arrangement.

4. Field performance and numerical simulation of the Kerrobert THAI pilot

Technological developments, such as toe to heel air injection (THAI), have been shown to efficiently recover heavy oil with reduced environmental footprint. The Kerrobert project was the first to utilise the THAI technology in presence of bottom water (BW) in the reservoir. The project demonstrated a good performance (with average oil production rate of 10 m^3/day per well) compared to the conventional ISC operations in a BW situation. Lessons taken from the Kerrobert operational experience can assist forthcoming THAI operations explicitly in the presence of BW. Dynamic field data for one of the best performing THAI pilot well pairs (K2), were analysed in this work. It was found that the K2 pilot must have experienced interference from K5, which is the closest neighbouring THAI well pair to the K2. Previously developed THAI models have not been validated against actual field data. A new field-scale THAI model in the presence of BW was constructed and, for the first time, validated against the field data from the Kerrobert project in this work. In addition, the quasi-staggered line drive well arrangement, as used for the K2 pilot, was studied. The daily and cumulative oil production rates were predicted well (the final agreement with field data was within 3 percent). The history matched model was then used to investigate the effect of the variation in air injection rates on THAI performance in presence of BW. Major developed zones during the propagation of the combustion front were numerically examined. It was demonstrated that extra air ingress from the neighbouring THAI well pair has caused a reduction in oxygen utilisation throughout the process. As a result, the simulated temperature profile declined with the increasing combustion time. The oxygen profile around the horizontal producer (HP) well was studied via the new history-matched model. An inversely proportional relationship was detected between the coke concentration and the oxygen profile around the HP well. It was found that the size of the steam zone, ahead of the combustion front, differs with variation in air injection rates. It was observed

that some of the mobilised oil sank into the BW, leaving a significant amount of oil trapped in the reservoir. To prevent such an event, the location of the HP well was altered as a potential strategy to optimise the THAI efficiency. Consequently, the oxygen utilisation was improved by 13%, resulting in 73% higher cumulative oil production in comparison with the history-matched model.

4.1 Introduction

Extra-heavy oil and bitumen (EHOB) comprises 30 percent (only 4% less than conventional crude oil) of remaining technically recoverable fossil fuel resources on the earth (International Energy Agency, 2021). The attention has been shifting towards unconventional oil such as EHOB with the decline in conventional light oil reserves (Adam, et al., 2020). However, EHOB are difficult to recover due to high intrinsic viscosity. Thermal enhanced oil recovery (EOR) methods are designed to reduce the viscosity of the remaining oil in place by increasing its temperature, requiring the injection of steam or air (in-situ combustion) (Greaves & Al-Shamali, 1996). Shah et al, (2010) reviewed novel thermal techniques for heavy oil recovery and bitumen extraction/upgrading. The methods that employ steam are steam flooding, cyclic steam stimulation (CSS), and steam assisted gravity drainage (SAGD), which were discussed in Section 2.3. The main limitation for steam-based methods, is that they are very energy intensive as they use natural gas to provide the required energy. Also, surface steam generation processes can cause release of significant quantities of greenhouse gases. Donnelly & Pendergast (1999) reported an average of around 0.10 tonnes of CO_2 equivalent per barrel of oil recovered by SAGD process, mainly to supply the latent heat requirement of steam generation. Additionally, large volumes of water are needed to run SAGD, with between 2 to 10 barrels of water injected as steam for every barrel of oil produced (Shah A. , et al., 2010).

In-situ combustion (ISC) involves injection of air into the reservoir and creation of a combustion front, in which a fraction of the oil in the reservoir is combusted to generate heat

downhole. The high-volume combustion gases (produced from low volume oil) push fluids (including gas from injected air, e.g., nitrogen, and by-products of combustion, e.g., mobilised oil) ahead of the combustion zone. In the original concept of ISC, which uses a vertical injector well-vertical producer well arrangement, the combustion zone moves from the injector well towards the producer well over time. The conventional ISC process suffers from serious operational problems, with gas over-riding and channelling being especially problematic (Nasr & Ayodele, 2005; Xia & Greaves, 2006). Toe to Heel Air Injection (THAI) technology integrates in-situ combustion with advanced horizontal well concepts. A horizontal producer well is used instead of a vertical producer well (as in conventional ISC), and this difference is the main feature of the THAI process. Also, the toe of the horizontal producer is positioned close to the injection point. Thus, as the combustion front propagates along the horizontal production well, from the 'toe' position to the 'heel', only short, gravity-driven vertical displacement of oil is necessary compared to the longer, horizontal displacement needed for conventional ISC (Xia & Greaves, 2000). Controlled gas over-ride, high sweep efficiency, production of thermally upgraded heavy oil, and less environmental footprint have been reported as potential benefits of the THAI process (Xia & Greaves, 2006). Other beneficial attributes of the THAI process can be found in a study by Greaves et al, (2001), including its environmental benefits through recycling CO_2, reduction in energy requirement, and eliminating the water requirement compared to steam injection based heavy oil recovery technologies (e.g., SAGD). The water produced within the SAGD process must be cleaned up at the water treatment facilities at the surface. This is another loss associated with SAGD which can be eliminated by employing the THAI process. The THAI process can reduce the surface facility requirement leading to a dramatic reduction in capital and operational costs of heavy oil production, while diminishing emission intensity.

There have been seven THAI pilots/projects, located in 3 countries, since 2006 (Turta A. , 2021). Canada was the pioneer in field testing of THAI. The Whitesands Experimental THAI project (2006-2011), located in Conklin, Alberta province, was the first field pilot of the THAI process. The main objective for the Whitesands project was to evaluate the THAI process under actual reservoir conditions, in order to advance the technology sufficiently to undertake a commercial project (Ayasse, et al., 2005). Based on the lessons taken from the Whitesands project, the Kerrobert project, located in Saskatchewan province, Canada, commenced in 2009 (and is still ongoing after 13 years). The Kerrobert THAI project is the first THAI pilot in a conventional heavy oil reservoir underlain by a relatively thick bottom water zone. The effect of bottom water on THAI performance was tested in the piloting stage of the Kerrobert project. So far, from both Canadian THAI projects, over half a million barrels of partially upgraded oil has been produced. However, the oil rate per well (10-30 m^3/day) was lower than in the SAGD projects (Turta, Greaves, & Strakov, 2021). China (with 3 THAI projects since 2012) and India (with 2 THAI projects since 2016) are other countries that have also been utilising THAI technology for heavy oil recovery (Turta A. , 2021).

Numerical simulations are a key tool to investigate the THAI operating mechanism due to limitations in experimental (3D combustion cell) THAI investigations. Previously developed field-scale THAI models (Coates & Zhao, 2001; Greaves , Dong, & Rigby, 2012 a; Greaves, Dong, & Rigby, 2013; Ado M. R., 2020) used data from 3D combustion cell experiments to first validate their laboratory scale THAI simulation and only then scale-up experimental scale models to field-scale models. However, none of the aforementioned models consider a bottom water zone. Although, Araujo et al. (2016), Ado (2019), and Ado et al (2022) carried out THAI simulations in the presence of bottom water in the reservoir, their results were not validated against actual field data. Ado et al (2022) found that the oil recovery is affected by how large the thickness of the bottom water layer is, and the severity of such was determined to be

proportional to the thickness of the bottom water layer. Ado (2019) reported that the critical BW thickness, when the THAI process is implemented in a staggered line drive pattern, should lie in the range of 50% OL (oil layer thickness) < BW < 100 OL. *Ab initio* field-scale model development using direct history matching of a field-scale THAI process with BW has never been published by other workers. This was due to insufficient published data concerning the oil production trends experienced in the field. It is hypothesised (from the above former numerical studies) that reducing the air injection rate will lead to lower oil production rates. On the other hand, Wei et al, (2020) carried out a detailed analysis of the Kerrobert THAI field data including air injection and oil production rates. Their findings can be summarised as the following: 1. there is no clear relationship between air injection and oil production rates, 2. more air injection into the reservoir does not promote higher oil production, which is related to combustion zone development, 3. higher gas saturation caused by excessive air injection increases gas relative permeability which hinders the oil production, and 4. higher air injection promotes greater cooling of system. Their analysis was purely based on analysing field data and no simulation work was carried out to explore the dynamic mechanism of the THAI process. A more detailed investigation of the oxygen utilisation, and its effect on the THAI performance, has been recommended by other workers in order to study how other real reservoir factors such as bottom water may impact the overall stability of THAI process.

This chapter focuses on the operational aspect of the THAI process. This work, for the first time, presents a field-scale THAI model that was validated against data obtained from the Kerrobert THAI project. The model includes the existing relatively thick bottom water in the studied formation. The first aim of this study is to determine whether variation in the air injection rates can promote the oil production rates during the THAI operation. It is highly likely that excessive air injection causes reduction in oxygen utilisation throughout operation. This means the ISC overall performance will be compromised if improper volume of air is

injected into the reservoir (for the sake of higher oil recovery). A secondary aim of this study is to numerically develop and test scenarios for optimisation purposes. A real life quasi-staggered line drive (QSLD) THAI well configuration (namely the K2 THAI well pair in the Kerrobert project) is studied in this work. The potential outcomes of this research are that it could improve the understanding of operational aspects of the THAI process and enhance recovery efficiency of the process for the forthcoming projects.

4.2 Field data analysis

Primary oil recovery of 1.5% was achieved in the Kerrobert field, located in Southeast Saskatchewan, Canada. This low production has been linked to high viscosity of the oil and presence of bottom water, which leaves a significant amount of resource left for secondary recovery/ enhanced oil recovery (EOR) schemes. Many operators in Western Canada employ thermal methods to recover remaining heavy oil in the reservoir after primary extraction has become uneconomic (Wikel & Kendall, 2012).

The Kerrobert THAI project is located at the Waseca Channel, Saskatchewan. The geological setting and stratigraphy of the Waseca sandstone formation were investigated by Hill (2017). The Waseca reservoir is a fine-grained sandstone reservoir with depth to the top of the formation varying between 758 and 774 m (oil-water contact is at 789). The oil zone thickness is 12-20 m in the Western part and increases up to 25-30 m in the Eastern part. The depth of bottom water is approximately 20 m in the Western part and around 10 m in the Eastern part (Turta, Greaves, & Grabowski, 2018).

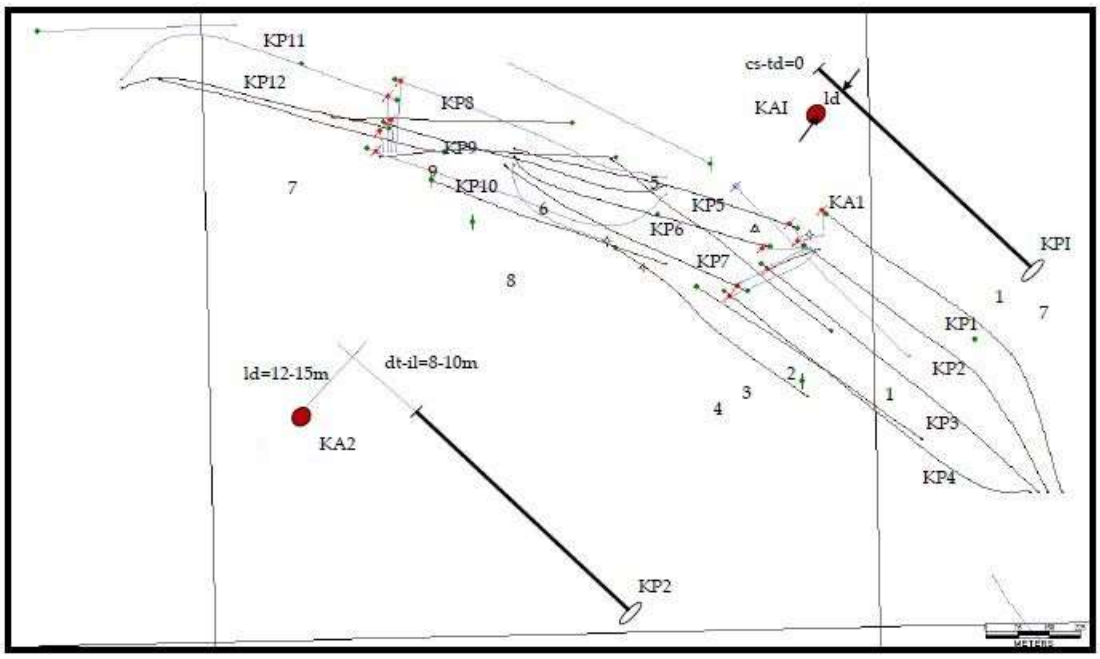


Figure 4.1. The location of THAI well pairs (K1-K12, where KA is vertical injector and KP is horizontal producer). Old horizontal wells are marked from 1 to 9 (Turta, Greaves, & Grabowski, 2018)

There were several old legacy horizontal wells in the area prior to the THAI project. The old horizontal wells are marked as 1 to 9, in order, starting from the south-east corner in Figure 4.1. The THAI project consists of 2 pilot well pairs (WPs) (denoted K1 and K2) and 10 semi-commercial WPs (denoted K3-K12) within Eastern and Western pads (shown in Figure 4.1). The operation started with pilot WPs in 2009. The semi-commercial wells were drilled in 2011 (Wei, Wang, Afshordi, & Gates, 2020).

Figure 4.2 shows a schematic of the Kerrobert THAI project. The vertical air injector well (2) was placed near the toe section of the horizontal production well (1) that was drilled at the base of the reservoir. Following a steam preheat period (pre-ignition heating cycle (PIHC)), air was injected to initiate combustion (3). The vertical combustion front broadens and moves horizontally through the reservoir from the toe of the production well to the heel (4). The heat generated reduces the viscosity of the heavy oil in the mobilised oil zone (MOZ) ahead of the

combustion front and enables it to flow by pressure gradient and gravity drainage into the horizontal production well (5). The oil flows to the surface plant facilities where it is treated and sent to market (6) (Petrobank Energy & Resources Ltd, 2012).

The K2 pilot THAI well pair was placed at the Eastern part of the Kerrobert formation. The K2 well pair consists of KA2 and KP2, denoting the vertical injector and horizontal producer wells, respectively. Both KA2 and KP2 were favourably positioned as they were located relatively far from any of the old wells in the region. Therefore, no external interference in the K2 pilot operations was expected from the old wells. The K2 well pair was considered as the ideal THAI pilot. This was due to its quasi-staggered line drive (QSLD) well arrangement (shown in Figure 4.1). Figure 4.1 shows that the lateral distance between the injector well and the horizontal section of producer well (Id) is 12-15 m, and that from the toe to the line of injection (dt-il) there is a distance of 8-10 m. The lateral well spacing between horizontal producers is 70-90 m, while the lengths of the horizontal sections are 400-450 m. The closest injector well to KA2 is KA5 (which belongs to K5, one of 10 semi-commercial THAI well pairs that were drilled and operated later). The KP2 well has its horizontal section located towards the top of the pay zone to minimise water production. There were 20 thermocouples installed in the KP2. Progressive cavity pumps (PCP) were installed in the heel region of KP2 for artificial lifting of heavy oil (Turta, Greaves, & Grabowski, 2018).

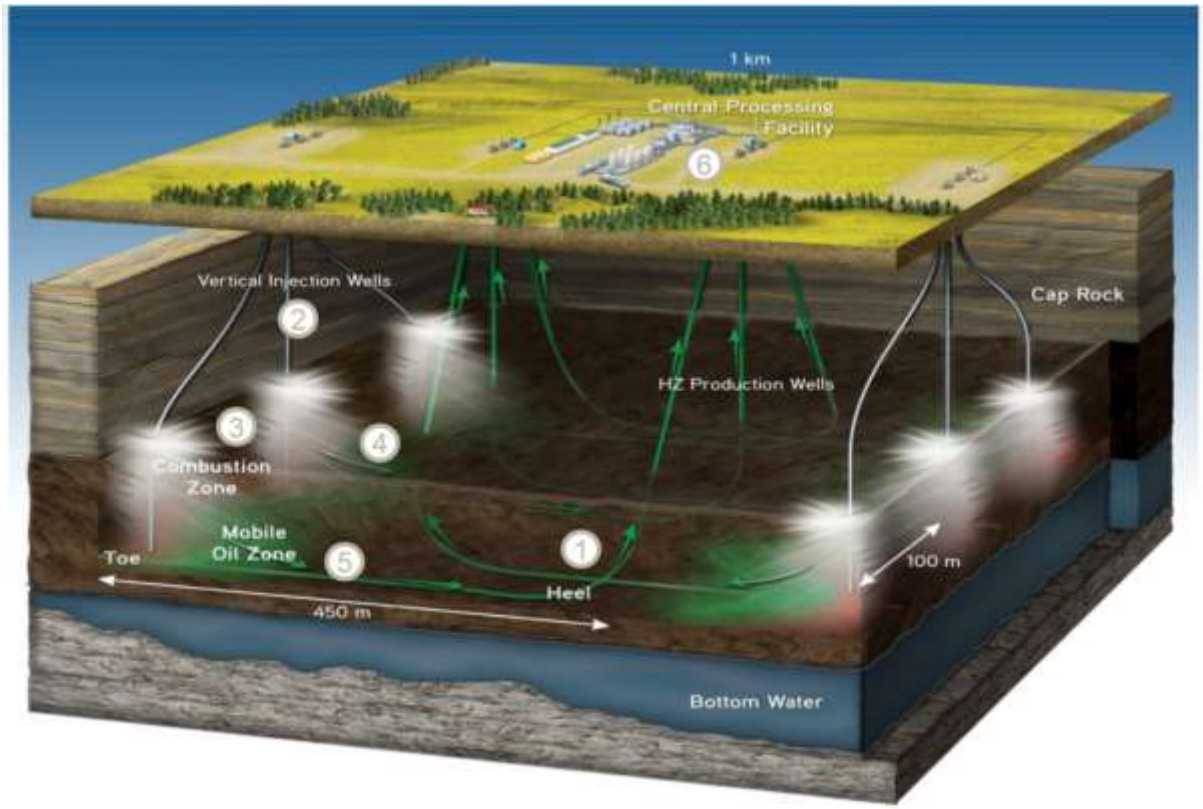


Figure 4.2. Schematics of the Kerrobert THAI project (Petrobank Energy & Resources Ltd, 2012)

The operational history of the Kerrobert THAI project is available in a study by Wei et al, (2020). The K2 pilot operation started with the PIHC in September 2009. Cumulatively, 3132 m^3 steam was injected for 51 days via KA2 (the steam injection rate was 62 m^3/day on average). The air injection began in late October 2009. The initial air injection rate was 5,000 m^3/day, with a projected maximum injection rate of 80,000 m^3/day. The in-situ combustion front was generated relatively slow in the K2 pilot. The ignition delay was up to 1-2 months. The quality of ignition was very good. The ISC behaviour of K2 was in a toe-to-heel propagation fashion. The ISC toe-to-heel propagation did not take place in the case of K5 (neighbouring semi-commercial THAI well pair) and a combustion chamber around the toe of KP5 was developed. It is believed that the KP5 combustion chamber has influenced the K2 pilot overall performance, which will be discussed later in this chapter.

Figure 4.3 shows the daily air injection and oil production profile for the K2 THAI pilot well pair from Nov 2009 to May 2016 (Petrobank Energy & Recources Ltd, 2021). A wide range of air injection rates were tried for K2 during the first year of the project. The project's operator did not rely upon any numerical model and the air injection profile was mainly based on trial and error. The air injection rates were larger in late 2009 and 2010 (up to 85,000 m^3/day in August 2010). The operator had to reduce air injection rates because temperatures as high as 1100 °C were observed at the toe section of KP2. It must be noted that the maximum operating temperature for KP2's instrument string was 1200 °C. In addition, initial high injection rates led to surges of gas production from KP2 (which could not be handled by the operator, Petrobank, at the surface properly). Consequently, the oil production trend was not consistent for the initial stage. However, daily oil rates up to 25 m^3/day were recorded in late 2010, implying the potential of THAI process.

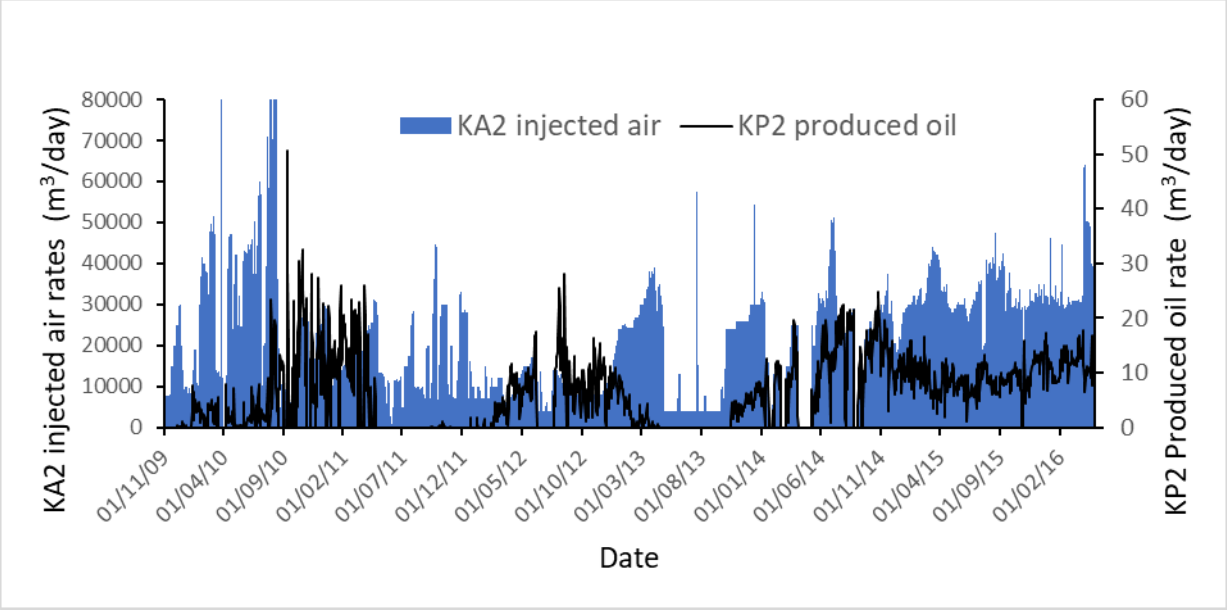


Figure 4.3. K2 air injection and oil production profiles

The air injection rates were not primarily varied to improve the oil production rates during the THAI operation in the K2 case, according to Petrobank. The decision-making regarding any change in air injection rates was based on the following criteria in order of importance:

1. Ability of the production pumps to handle a high gas factor (>500 GOR), temperature (around 170-200 °C), and sand content (>2%) in the flow
2. Downhole temperatures (900 °C was a limit for the integrity of the wellbore)
3. Handling produced gas from KP2 at the surface (depending on the gas production rates, the surface temperature can be relatively high)

The KP2 well was out of operation many times in 2011. The operational interruptions were mostly related to pump changes and issues with downhole equipment due to high temperatures. Eventually, the long instrument string was repaired in 2011, meaning no production from late-April 2011 to mid-Feb 2012. Nevertheless, the air injection into KA2 was not stopped while KP2 was down. This was because of concerns regarding the advancement of the in-situ combustion front. The air was injected in order to maintain the combustion front while the producer well was down. The KA2 air injection rates were between 4,000 to 20,000 m^3/day in 2012. The reduction in air injection rates was in conjunction with the preparation of the neighbouring semi-commercial K5 THAI well pair. Despite low injection rates, the daily oil production remained in the range of 3-16 m^3/day. The KP2 well was down due to operating issues from April to September 2013. Likewise, the air injection was not stopped then either due to the aforementioned reasons.

The benefits of having a steady or constant oil production profile are: (a) the income stream is maintained at a high level and (b) use of surface facilities is more cost efficient (Greaves , Dong, & Rigby, 2012 a). The operator had a better understanding of THAI performance from late 2013, allowing for less operation-caused fluctuations. The injected air profile was more stable (on average 25,000-30,000 m^3/day) and it was not interrupted from September 2014 to May 2016. Consequently, good/steady oil production rates were achieved. 6067 m^3 oil was produced in 590 days of operation (in average 10.3 m^3 per day).

Figure 4.4 shows the air injection profile, cumulative air injected, gas production profile, and cumulative gas produced (Petrobank Energy & Recources Ltd, 2021). The cumulative volume of produced gas by KP2 is compared with the cumulative volume of air injected into KA2. The cumulative volume of produced gas from KP2 is 30% higher than the cumulative air injected into the corresponding injector well (KA2). Previously, it was assumed that the 30% additional produced gas is made up of hydrocarbon gas injected into KP2 annulus (mainly methane to mitigate corrosion) (Turta, Greaves, & Grabowski, 2018). This conclusion, however, was not verified at the time.

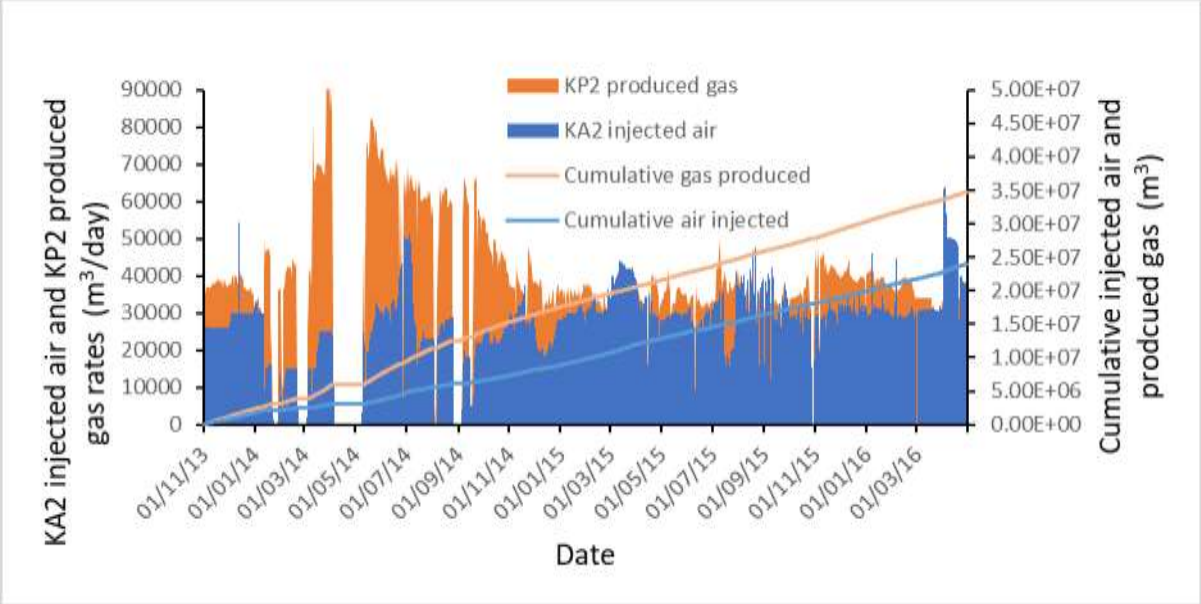


Figure 4.4. The air injection profile, cumulative air injected, gas production profile, and cumulative gas produced for the K2 (form November 2013 to April 2016)

The imbalance between the cumulative air injection and gas production for K2 is too high to be neglected. It is thought that K2 has experienced interference from K5, which is the closest neighbouring THAI well pair to K2 at the Eastern part of Kerrobert project. The likely well-to-well interference is because of the very short distance between KA5 and KP2 and the fact that the air injection into KA5 developed a combustion chamber around the toe section of KP5 (instead of toe-to heel propagation). Therefore, some of the KA5 injected air might have been

channelled towards KP2. It is difficult to approximate the exact channelled air volume flowing from KA5, but it is considered reasonable that the extra 30% produced by KP2 can be taken as a rough estimate. The good oil production profile (shown in Figure 4.3) achieved could reflect the combined contribution of air injection from both KA2 and KA5.

Hence, the interaction between neighbouring air injectors must be considered for a successful prediction of the performance of a THAI project, and this can validate previous speculation. This will be investigated here using a history-matched THAI numerical model. The new field-scale THAI model, for the first time, considers a relatively thick bottom water layer. The effect of air injection rates on the overall efficiency of the THAI process in the presence of bottom water will be explored in this chapter. It will be shown that achieved oil production rates can be significantly improved (36% cumulatively) by employing an appropriate air injection profile during the THAI operation. The effect of oxygen utilisation on the various zones developed during the ISC will be studied numerically. The location of the horizontal producer will be examined to enhance the THAI performance in the Kerrobert project. It will be seen how the well-validated field-scale model can be used to investigate scenarios for more efficient operation.

4.3 THAI simulation

4.3.1 Model development

The STARS software, developed by Computer Modelling Group (CMG), was used for this study. STARS is a three-phase multi-component thermal and steam additive simulator. ISC simulations are sensitive to grid block size. Ado (2020 a) carried out a study on the effect of the grid system on THAI simulation. The grid system used in this study (shown in Table 4.1) is based on a grid design for the field-scale THAI simulation studied by Ado (2020 a) (Model P).

Table 4.1. Grid block refinement system

Reservoir Dimension (i × j × k)	220m × 100m × 38m
Number of original grid block (i × j × k)	45 × 19 × 11
Number of refined grid block (i × j × k)	135 × 57 × 11
Total number of grid blocks	91782

The reservoir model is a regular Cartesian grid (with 45, 19, 11 blocks in the i, j, and k directions, respectively). The original grid blocks were then split into 3 refined grid blocks in the i direction, and 3 refined blocks in the j direction. The original grid blocks were not refined in the k direction. Grid refinement was not conducted for the grid blocks in which the vertical injector (VI) and horizontal producer (HP) wells were located. The aim of the grid refinement was to provide a better flood front resolution and reservoir description. The properties of the fundamental blocks were transferred to the corresponding constituent refined grid blocks. A single porosity type was assigned for the formation. The sink/source well model was used for both VI and HP. Only the horizontal section of the horizontal producer well was perforated. Aquifer modelling (bottom water section) was done by adding cells that contain only water. Figure 4.5 represents the dimensions of reservoir model and quasi-staggered line drive (QSLD) well arrangement of the K2 pilot. The model consists of three main sections (namely the pay, transition, and bottom water zones) based on their fluid saturation (shown in Figure 4.5). The simulation was made for a homogenous oil layer. No steam was injected into the reservoir model prior to air injection. An electrical heater was used to preheat the inlet zone (around injector well) of the reservoir and to bring it up to ignition temperature.

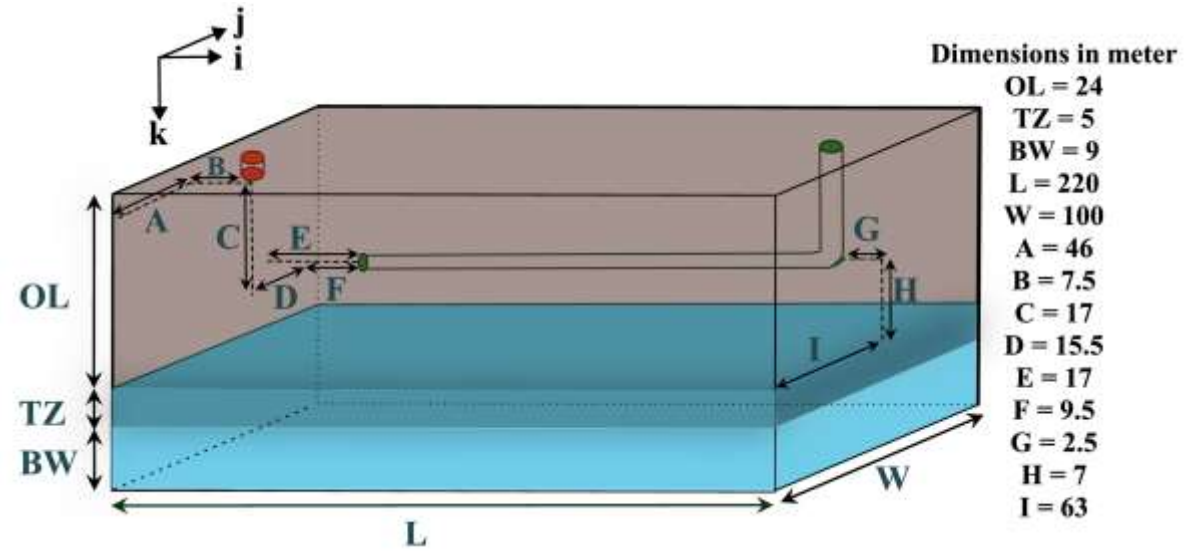


*Figure 4.5. Reservoir model dimensions and VI and HP configuration in quasi-staggered line drive (SQLD) fashion. Notes: *The oil layer (pay zone), transition zone, and bottom water zone are shown in grey, dark blue, and light blue, respectively.*

4.3.2 PVT and petrophysical properties

Athabasca heavy oil pressure, volume, and temperature (PVT) data, reported by Ado et al, (2017), were used for this study. They defined LC, MC, and IC as the Light, Mobile, and Immobile pseudo-Components, respectively. Likewise, the molecular fraction, temperature-dependent viscosity, and equilibrium *K*-values for each heavy oil pseudo-component have been taken from the study by Ado et al, (2017). Water (steam) , oxygen, inert gas (CO_x), and coke were the other four components in the model. The petrophysical properties used for this study are shown in Table 4.2 (taken from studies by Turta et al, (2018) and Wikel & Kendall, (2012)). The oil/water and gas water relative permeability curves are based on rock-fluid data by Ado et al, (2017).

Table 4.2. Properties and initial conditions of the Eastern Kerrobert reservoir

Reservoir porosity		0.32	
Horizontal permeability, k_h (mD)		4948	
Vertical permeability, k_v (mD)		3793	
Initial reservoir temperature (°C)		20	
Initial reservoir pressure (kPa)		3000	
Dead oil viscosity at reservoir temperature (mPa.s)		33491 - 89000	
Live oil viscosity (mPa.s)		>21000	
The asphaltene content		14%	
Reservoir zones	Pay zone	Transition zone	Bottom water zone
Initial oil saturation, S_{oi}	0.74	0.55	0
Initial water saturation, S_{wi}	0.26	0.45	1
Initial gas saturation, S_{gi}	0	0	0

The composition of air injected into the reservoir, as well as its injection pressure and temperature, are shown in Table 4.3. A minimum bottom hole pressure and a maximum surface liquid rate were also set as the horizontal producer constraints.

Table 4.3. Injected air properties and production well constrains

Injected fluid composition (%)	Injected fluid pressure (kPa)	Injected fluid temperature (°C)	Production well minimum bottom hole pressure (kPa)	Production well maximum surface liquid rate (m^3 day^{-1})
CO_x (79) & O_2 (21)	3500	25	3000	300

4.3.3 Kinetics scheme

Ado (2020) used a new upscaling procedure to carry out a comparative study between the predictions for two different types of validated kinetics schemes. Two models (model P and G) were proposed. The kinetics scheme used for Model G was heavily dependent on the stoichiometric coefficient of the product of the reaction. It was concluded that Model P provided a more realistic prediction of the THAI process. Model P employed a direct conversion thermal cracking scheme together with the combustion reactions for field-scale THAI modelling. Another merit of model P was to include low temperature oxidation (LTO) reactions as well as high temperature oxidation (HTO) reactions. Table 4.4 a and b present similar THAI kinetics to those proposed by Ado (2020), with the minor adjustment, that was used for this study. The default setting of the STARS software was used in order to calculate the enthalpies of the thermal cracking reactions. The heats of reaction for the combustion reactions were taken from the study by Ado et al, (2017).

Table 4.4 a and b. THAI Kinetics scheme. Note*: IC is Immobile pseudo-Component, MC is Mobile pseudo-Component, and LC is Light pseudo-Component.

a. Thermal cracking reactions	Frequency factor (min^{-1})	Activation energy ($J\ mole^{-1}$)
IC → 2.0471 MC	6.4726×10^{15}	239.01×10^{3}
MC → 0.4884 IC	5.7004×10^{13}	215.82×10^{3}
MC → 2.3567 LC	1.9171×10^{10}	184.88×10^{3}
LC → 0.4243 MC	2.5809×10^{10}	180.45×10^{3}
IC → 77.4563 Coke	3.9289×10^{10}	180.88×10^{3}

b. Combustion reactions	Frequency factor ($min^{-1}\ kPa^{-1}$)	Activation energy ($J\ mole^{-1}$)	Heat of Reactions ($J\ mole^{-1}$)
IC + 106.68 O_2 → 83.32 CO_x+ 46.90 H_2O	3.0686×10^{5}	138×10^{3}	4×10^{7}
MC + 37.06 O_2 → 29.74 CO_x+ 22.36 H_2O	3.0686×10^{6}	138×10^{3}	1.6×10^{7}
LC + 17.46 O_2 → 11.81 CO_x + 14.5 H_2O	3.0686×10^{7}	138×10^{3}	4.91×10^{7}
Coke + 1.22 O_2 → 0.97 CO_x+ 0.565 H_2O	1.6935×10^{7}	123×10^{3}	3.9×10^{7}

4.4 Model validation by history matching

In this section, two models (Model S and D) were constructed using the actual field data from the Kerrobert THAI project. Both Model S and D used the same physical properties as described earlier in Section 4.3.1. Model S was history matched and validated against the K2 THAI pilot well. Model D was built to investigate the effect of variation in air injection rates on the overall performance of the THAI process in the presence of bottom water.

4.4.1 Modelling the K2 THAI pilot

Geostatistical models built with static data only tend to give a very wide range of production profiles, but utilisation of dynamic data, such as production rates, will more substantially constrain a model (Baker, Chugh, Mcburney, & Mckishnie, 2006). A direct comparison between the KA2 air injection rates and the KP2 gas production rates (shown in Figure 4.4), suggests that a THAI model successfully matching air injection and oil production profiles is not reliable unless it considers the gas production profile. Petrobank reported that the imbalance between cumulative air injection and gas production in the K2 pilot was most likely caused by interference with its neighbouring semi-commercial THAI well pair (K5). This was possible due to the short distance between K2 and K5 well pairs (shown in Figure 4.1). Hence, the produced gas rates for KP2 must be assumed as contributing to air injection rates for KA2 for history matching purposes. This is to incorporate the effect of extra air from KA5. Henceforth, the history matching model is referred to as Model S in this work. The data of particular interest for Model S was from November 2013 to April 2016, since minimal operational interruptions occurred during this period. No steam was injected into the reservoir model prior to air injection.

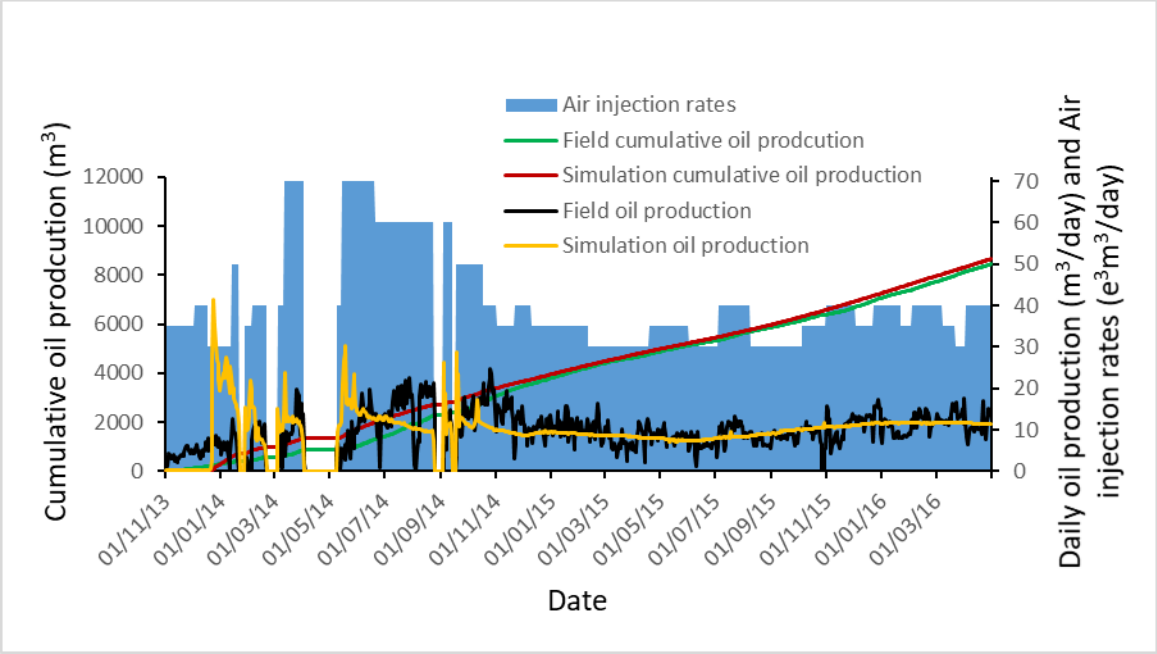


Figure 4.6. Comparison of simulation results for Model S with field data for the K2 pilot

Figure 4.6 provides a comparison of simulation results from model S with field data from the K2 THAI pilot. Apart from the initialisation period, the developed model was able to replicate daily oil production closely. The initial deviation in oil production rate between the predicted result and field data is due to: a. the communication between injection and production well was achieved 50 days after commencing air injection in Model S, which led to a short delay in oil production. It must be noted that the K2 pilot well pair was operating and producing oil prior to the simulated period, b. the higher initial oil production in Model S compared to field data is due to the pressure build up in the model before the establishing of communication between injection and production wells. However, good agreement was achieved for daily oil production rates from late January until mid-July 2014. The simulated produced oil rates were slightly lower than the field data from mid-July to early-December 2014. This was due to a change in oxygen utilisation in the model, which will be discussed when the combustion front is considered in detail in Section 4.5.2. later in this chapter. The simulated oil production rates tracked field data quite closely from early-December 2014 onwards. This narrowed the earlier

difference between simulated cumulative oil production and field cumulative oil production data (final agreement within 3%).

The good performance of K2 in terms of the oil production is a clear indication that a strong in-situ combustion front had occurred. It is plausible that temperatures higher than 800 °C were generated (Turta, Greaves, & Grabowski, 2018). Substantial data were generated by 20 thermocouples, which were placed along the horizontal section of the KP2 well (5 of them within 15 m from the toe and the remainder at the larger intervals up to the heel). Figure 4.7 shows the variation in temperature along KP2 from Jul 2011 to Nov 2016. Thermocouples located at the toe region of KP2 experienced a very high temperature, leading to their failures. Model S, as shown in Figure 4.8, predicted high temperatures up to 650 °C within 15 m of the toe section of the HP too. Similar to seen in the field data, a lower range of temperatures was observed around the perforations closer to the heel of the HP well in Model S. The simulation results showed excellent agreement with the temperature profile for the toe section between July 2014 and January 2015.

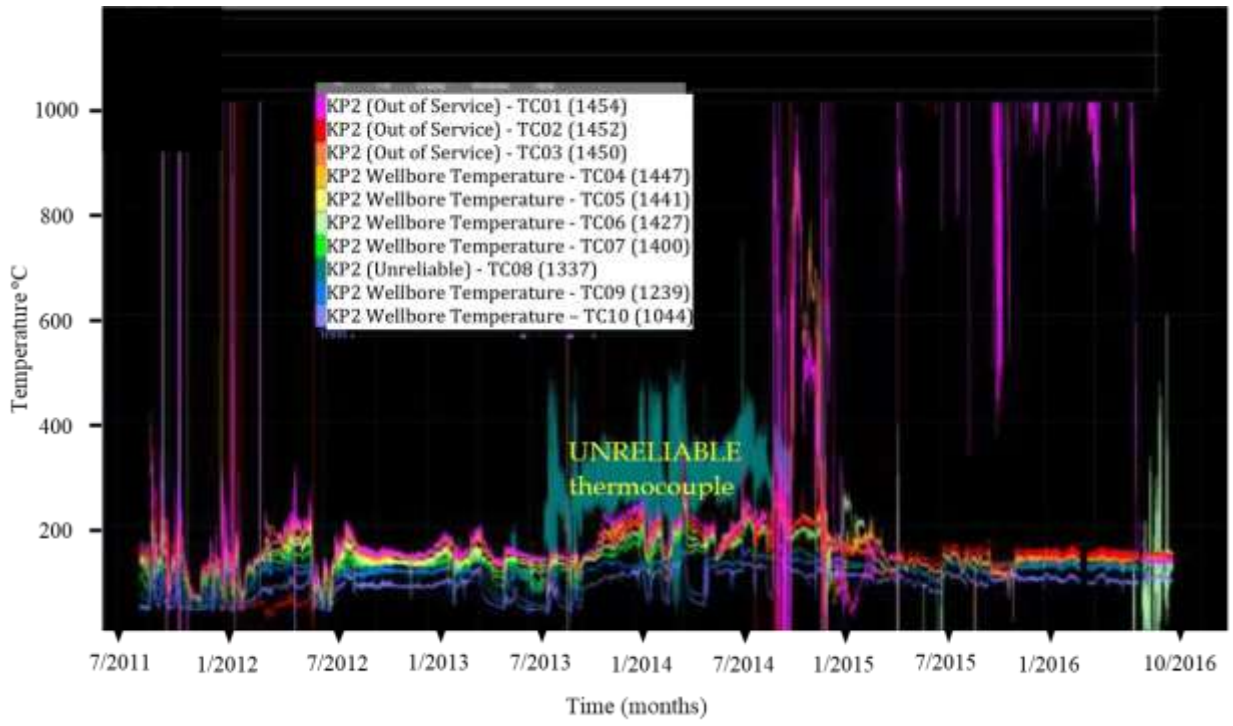


*Figure 4.7. Actual variation of temperature along KP2 versus time. Notes: * TC01 is located at the toe of HP.*

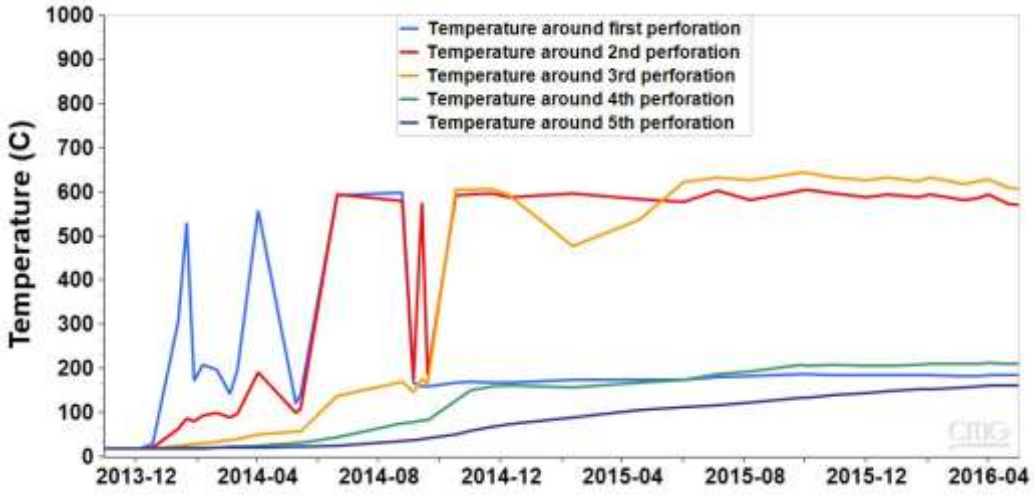


*Figure 4.8. Predicted variation of temperature around the toe section of HP in model S against time. Notes: * Order of perforation is from the toe side of HP.*

4.4.2 Effect of additional air ingress from KA5 on the overall performance of K2

A recent field data analysis by Wei et al, (2021) suggests that more air injection does not promote higher oil production. Their analysis was purely based on field data and no simulation work was carried out to explore the dynamic mechanism of the THAI process. A constant air injection rate of 20,000 m^3/day was used for a THAI numerical study by Ado (2019). Araujo et al, (2016) reported results for different continuous air injection rates from 0 to 40,000 m^3/day for their simulations. They reported a maximum limit of air injection of 35,000 m^3/day for their THAI models with thickness of 26 m (oil zone of 20 m and water zone of 6 m). However, both previous published THAI numerical studies with BW were not validated against field data. In the present study, the history-matched simulation (Model S) was used to numerically investigate the effect of air injection rates on THAI performance in the presence of bottom water. A new model is designated as Model D, and consisted of the restriction of air injection to only that into KA2 alone itself (hence, injected air rates were lower compared to Model S). The physical and petrophysical properties of Model D were the same as for Model S. No steam was injected into the reservoir model prior to air injection.

Figure 4.9 shows a comparison of the simulation results from Model D with field data from the K2 THAI pilot. The oil production started after 130 days of air injection, in early March 2014. Oil production was delayed for 70 days compared to Model S results. This indicated that it takes a longer time for oil to become mobile and drain into the HP well when it is subjected to lower air injection rates. A sharp peak in oil production was observed at the initial stage, which was in line with field data. However, Model D predicted higher oil production (up to 35 m^3/day) compared to field data after reopening the producer well in early May 2014. This was due to the pressure built up around the toe section prior to the closure of the HP. The simulated oil production rates declined from early-July to late-August 2014. Oil production rate was even lower than field data before HP closure in late-August 2014. The simulated oil production time

series was higher than field data during the uninterrupted K2 operation period (early-Sep 2014 to May 2016). The final cumulative oil production predicted by model D was 36% higher than K2 field data and 33% higher than Model S results, respectively. The predictions from Model D in the present study are consistent with the suggestion previously by Wei et al, (2020) and Araujo et al, (2016), namely that more air injection into the reservoir does not promote higher oil production. On the other hand, Figure 4.10 shows the simulated water cut against air injection rates for Model S and Model D. The predicted water cut profile for history-matched model (Model S) was in line with field data reported by Turta et al, (2018). They reported that water cut decreased from 70-90% to as low as 30-50% for the KP2 well. The earlier oil production reduced the water cut in the produced fluid in Model S at an earlier stage of the THAI process. However, the predicted results (from mid-May 2014) show that excessive increase in air injection rates led to an increase of water cut in Model S compared to model D.

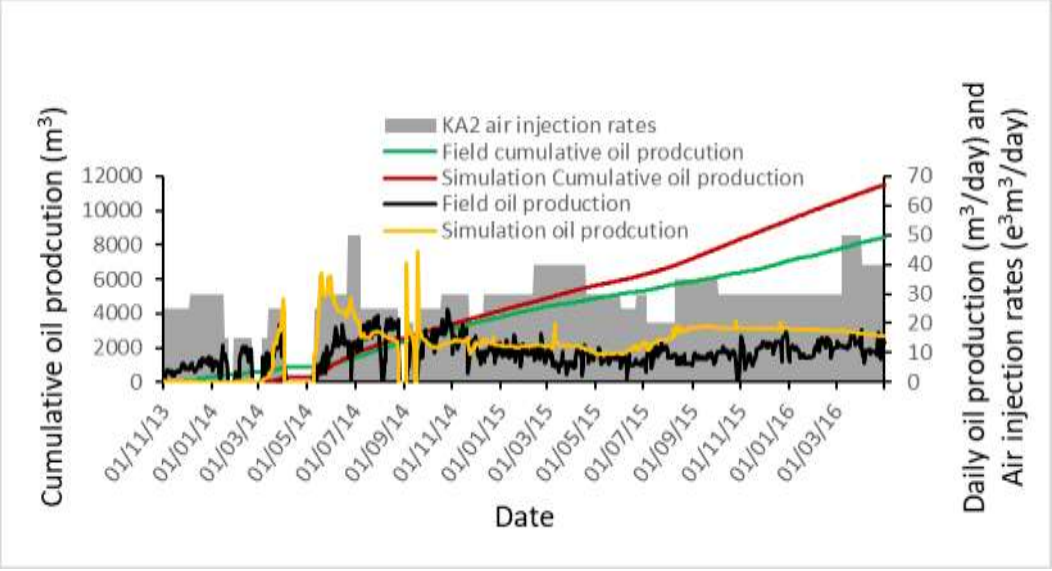


Figure 4.9. Model D simulated oil production profile compared with corresponding field data for K2

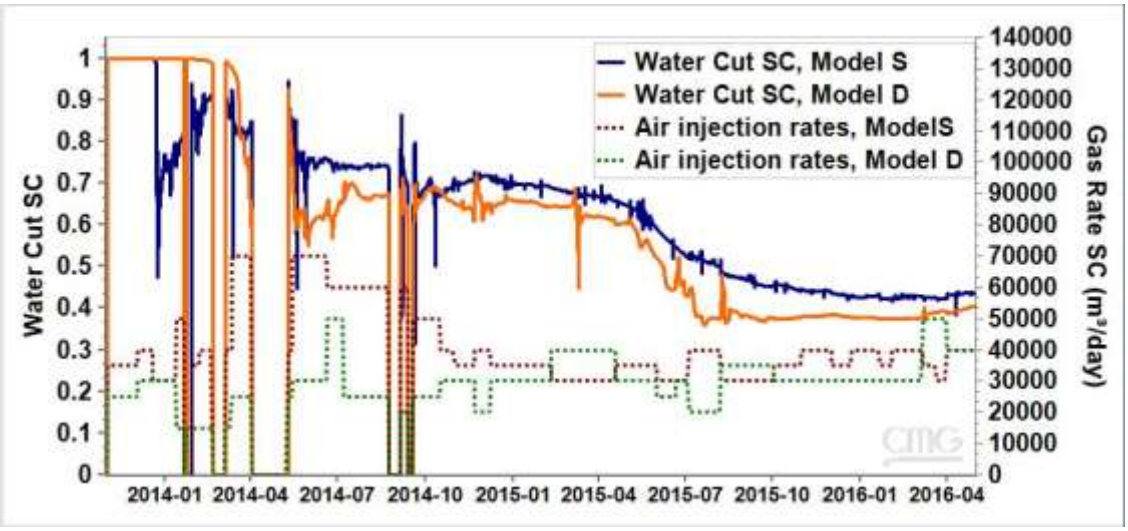


Figure 4.10. Simulated water cut against air injection rates for Model S and Model D

4.5 Results and discussions

In this section, simulation results from both Models S and D are examined. The effect of air injection rates on the overall performance of the THAI process will be studied. Detailed analyses are carried out for all the distinct zones established during the THAI process. Greaves et al, (2012 b) proposed a schema consisting of a series of zones that develop during the steady-state operation of the THAI process when the combustion front propagates from the inlet end to the production end of the reservoir (shown in Figure 4.11). The zones that were developed during the in-situ combustion (ISC) process include:

1. Combusted zone, the area that has already been in contact with the combustion front. All the oil has been displaced, meaning that there is only clean sand there.

2. Combustion zone, the leading edge of the combusted zone is where the oxygen is completely consumed.

3. Coke zone, the area that coke (a product of thermally cracked heavy oil) is deposited ahead of the combustion front.

4. Steam zone, the water supplying this zone comes from the resident reservoir water and from the combustion reactions.

5. Mobile oil zone, this area contains two regions; (region 1) thermally cracked oil as well as lighter vaporised fractions and (region 2) banked oil zone where the oil saturation is close to 100%.

6. Cold oil zone, this area contains the original crude oil.



Figure 4.11. Areal schematic of zones developed in the THAI process

The proposed schema by Greaves et al, (2012 b) was based on an experimental scale THAI simulation. It must be noted that their experimental scale model did not consider a bottom water zone. The major zones developed in the THAI process (as outlined above), in presence of bottom water will be probed using the history matched field-scale THAI simulation (Model S) in this section. The predictions from Model S and Model D (that excludes the additional air ingress from KA5) will then be compared. This comparison is to study the effect of including extra air ingress from KA5 on the developed zones during the THAI process. 3D, areal and cross-sectional views were used for the following investigations.

4.5.1 Combusted zone (swept region)

Figure 4.12 (a) shows a 2D simulated ternary oil-water-gas profile for Model S (top) and Model D (bottom) in May 2016. The region (in red) with 100 % gas saturation in the ternary profile is a good proxy indicator of the combusted zone. The oil initially in the inlet zone of the reservoir was swept by the combustion front, leaving only clean sand behind. It is evident that

the combusted zone is larger in Model D compared to Model S. However, comparing the Model S and D ternary profiles, the combusted zone shapes were approximately similar. In contrast, the swept zone for Model D was more advanced into the reservoir (particularly, at the first and second top horizontal planes). Similarly to the past THAI field-scale simulations by Greaves et al, (2013) (i.e. 25 m pay zone case), the combusted zone was mainly restricted to the inlet section leading to the toe section of the HP. Good volumetric oil sweep, with uniform oil displacement, can be identified across the inlet section of the reservoir for both Models S and D in Figure 4.12 (b). Temperatures as high as 600 ºC were predicted at the toe section of the HP for both models (mostly during the uninterrupted air injection period) (shown in Figure 4.8). This high temperature is related to the extensive gas saturation in the region. The grid block became nearly fully saturated with hot gas, thereby resulting in the prediction of elevated temperatures. The relative permeability of the oil phase dropped to zero as the large amount of air in the reservoir pushed the oil away from the producer. A similar event was reported by Wei et al, (2020). Additionally, the simulation indicated that some oil sank into the bottom water zone (shown in both Figure 4.12 (a) and (b)). The mobilised oil replaced some of the water originally in place in the bottom water area of the reservoir. This will be investigated in detail here later in Section 4.5.5.

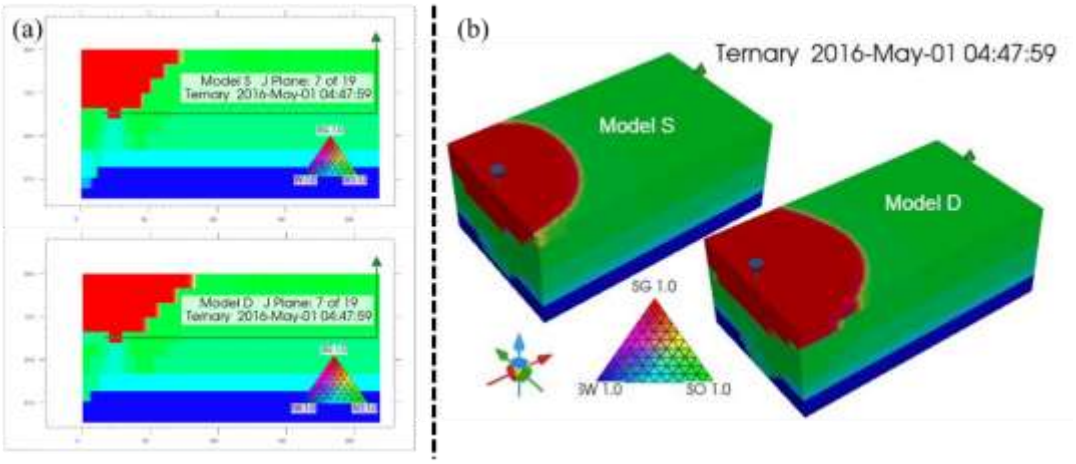


*Figure 4.12. Simulated ternary profile for model S and D in vertical midplane view (a) and in 3D (b) in May 2016. Notes: * SO, SW, and SG represent oil saturation, water saturation, and gas saturation, respectively.*

4.5.2 Combustion zone

Figure 4.13 shows the predicted oxygen profile for both models (Model S on left side and model D on right), during November 2014, July 2015, and May 2016. The oxygen profile is an accurate proxy representation of the combustion front shape. This is because, at the leading edge of the combustion front, the O_2 concentration drops to zero, and this is coincidental with the leading edge of the oxygen front (Greaves, Dong, & Rigby, 2012 b). The region behind the combustion front (combusted zone) was occupied by the injected air. Comparing the oxygen profile for both models in Figure 4.13 (a), it can be observed that the combustion front was already touching the toe section of the HP in model D in Nov 2014, whereas no O_2 was in the vicinity of the toe section of the HP in model D at the same time. This is due to higher air injection rates in the history-matched model. Thus, the combustion front was more advanced into the reservoir in model D compared to model S in Nov 2014. This is related to the migration of oxygen into the HP in model S and higher O_2 consumption in model D, which will be analysed below in this section. Figure 4.13 (b) shows the combustion front expansion in model S and D in July 2015. The same trend in oxygen profile (as in Figure 4.13 (a)) can be identified

in Figure 4.13 (b) for both model S and D, leading to larger horizontal propagation of the combustion front in model D (particularly, the top horizontal layers) in comparison with model S. Simulated results in Figure 4.13 (c) shows that the combustion front has a forward leaning shape meaning that a larger areal section was swept by the combustion front at the top of reservoir in both models. Also, Figure 4.13 (c) shows that the leading edge of the combustion front in model D was in the vicinity of the toe section of HP in May 2016.

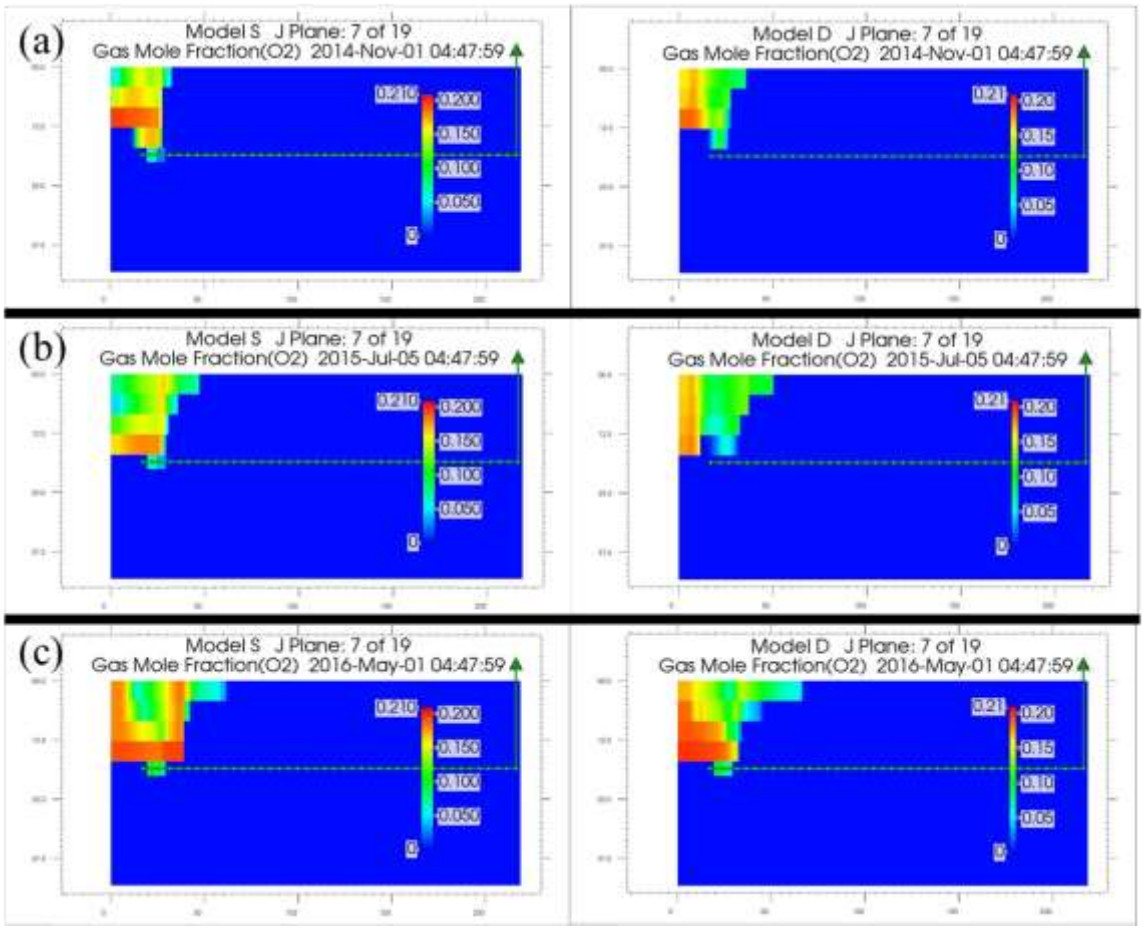


Figure 4.13. Change in predicted oxygen profile for Model S (left) and Model D (right) at vertical midplane from November 2014 to May 2016 (uninterrupted air injection period)

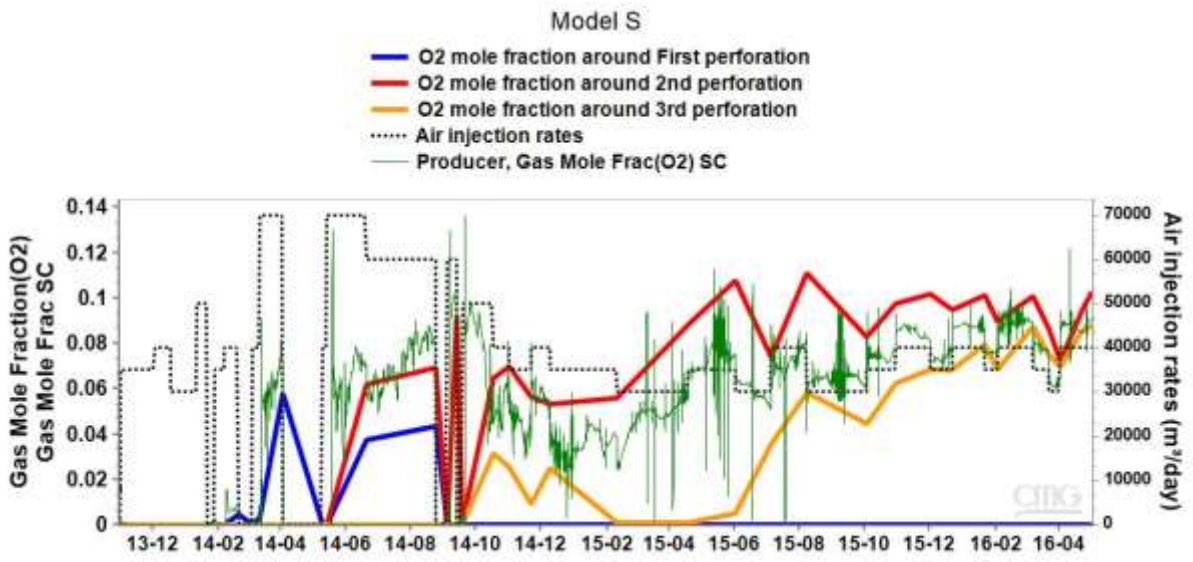


*Figure 4.14. Variation over time of injected air rates and predicted change in O_2 concentration at toe section of the HP by Model S. Notes: * Order of perforation is from the toe side of the HP.*

Figure 4.13 (c, left) shows a vertical midplane of the predicted combustion front for model S in May 2016. High values of oxygen concentration appear to exist around the second and the third perforation from the toe side of the HP. This can be examined in detail by looking at the change in oxygen concentration for the grid blocks in which the toe section of the HP is placed. Figure 4.14 shows the variation in the oxygen profile during the THAI process at the first, second and third grid blocks from the toe side of the HP in Model S. Understandably, the shift in oxygen concentration at the toe section of the HP is related to the air injection rates (Figure 4.14). The highest oxygen mole fraction around the first perforation of the HP toe section was around 6%, which occurred because of injecting 70,000 m^3/day air into the reservoir in March 2014. As the combustion front propagated along the HP (considering air injection rates of 60,000-70,000 m^3/day from mid-May to mid- Sep 2014), higher oxygen concentrations were detected around the second perforation of the HP toe section (maximum of 9 % in September 2014). There was no oxygen around the first perforation of the HP's toe during the uninterrupted air injection period (air injection rates of 30,000-50,000 m^3/day). Although, a

significant concentration of oxygen continued to exist around the second perforation of the HP toe section (maximum of 11% in August 2015). The initial oxygen presence around the third perforation occurred in late-Sep 2014 but it remained below 3% until early-July 2015. However, there was a substantial increase in oxygen mole fraction around the third perforation during last 10 months of simulated THAI process (up to 9% in late-April 2016).

Figure 4.14 also shows the predicted oxygen concentration in the produced gas for Model S. It is evident that a high O_2 concentration around the toe section of the HP in model S has caused oxygen channelling into the HP (up to 10%). In contrast, Greaves et al, (2013) reported no evidence from their simulation of any oxygen being produced for the 25 m thick oil layer over nearly 6 years operating period. Further, Greaves et al, (2012 a) predicted breakthrough of oxygen into the production well would occur only after 10.8 years of oil production. However, in both aforementioned previous field-scale THAI simulation studies, the predicted results were for a reservoir model with no bottom water. Additionally, the vertical offset between the injector well and toe section of horizontal producer was around 22 m in both previous studies (5 m longer compared to this work). Moreover, none of the previous field-scale THAI numerical works had been validated against actual field results due to the lack of published data. A more detailed investigation of the oxygen effect has been recommended by other workers, to study how other real reservoir factors, such as bottom water, may impact the overall stability of THAI process.

Table 4.5. KP2 average gas compositions from 2009 to 2015 in mole% (HMWG represents high molecular weight gas)

H_2	O_2	N_2	CO	CH_4	CO_2	H_2S	HMWG
1.33	0.40	73.85	0.35	9.26	12.71	0.41	1.10

Unlike the conventional ICS process, THAI is a short-distance oil displacement process. The THAI process has a very extended, long zone for the chemical reactions, displaying a considerably longer residence time (Turta, kapadia, & Gadelle, 2020). The unexpectedly high concentration of produced oxygen in this work can be explained by the particular reactions that may have been taking place in the producer wellbore. Recently, Wei et al, (2020) reported a summary of time-averaged gas composition from each producer well in the Kerrobert THAI project from 2009-2015 (shown in Table 4.5). The recorded produced oxygen from KP2 was only 0.4% (the injected air into KA2 contained 21% O_2 and 79% Nitrogen). They concluded that the low oxygen concentration in the production well was due to either a good combustion performance within the reservoir or leaving oxygen behind in the reservoir. It must be noted that the oxygen concentrations in the produced gas from KP2 does not necessarily correspond to the O_2 profile around the toe section of the HP, according to the Kerrobert THAI pilot operator (Strakov, 2021). The K2 operator confirmed the low O_2 (almost close to zero) production from KP2 (Strakov, 2021). However, they recorded problems with downhole equipment corrosion caused by oxygen. The high methane gas concentration in produced gas from KP2 was due to injection of methane to prevent corrosion. Direct oxygen channelling into the production well was also confirmed by the operator when the combustion front was too close to the wellbore. Petrobank was not able to measure downhole O_2 as it was difficult to locate where the inflow point was. It was also expensive to install oxygen sensors and be able to move O_2 sensors closer to/further away from the inflow zone. The assumption was that oxygen and hydrogen reacted within the wellbore and were then produced as water, which cannot be investigated through this numerical work. This is because of (a) an absence of H_2 in input components (as well as chemical reactions related to H_2 (coke gasification and water gas shift reactions)) and (b) O_2 does not undergo any chemical reaction within the wellbore in the present simulation study. Hence, the excessive predicted O_2 concentration in the producer in

the present simulation study can be explained. The effect of O_2 utilisation on THAI performance in the presence of bottom water, will be discussed later in this section.

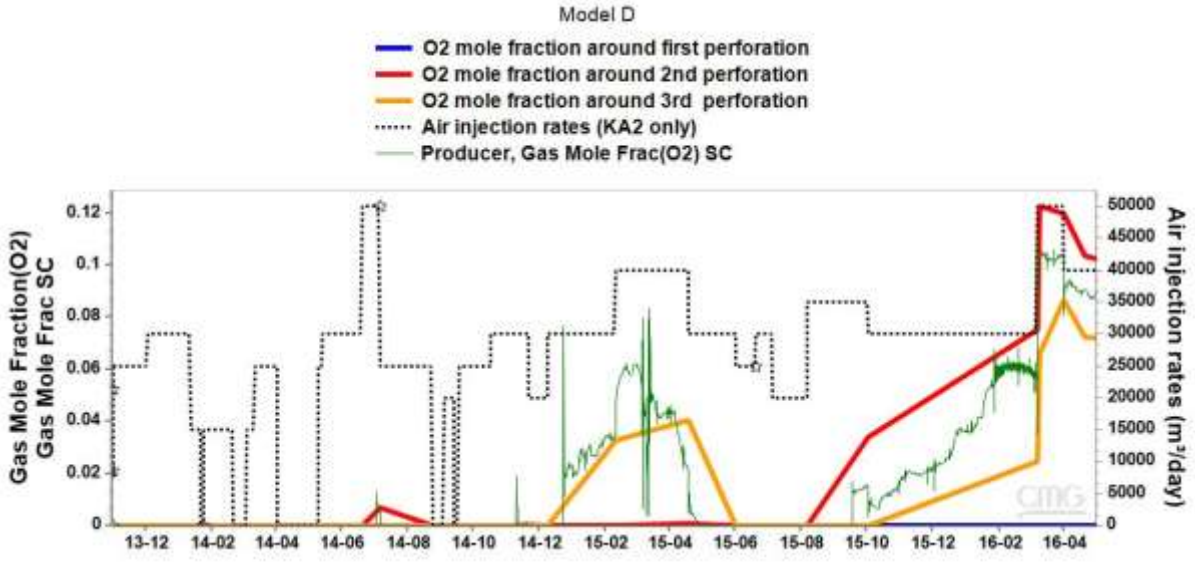


*Figure 4.15. Variation over time of injected air rates and predicted change in O2 concentration at the toe section of the HP by Model D. Notes: * Order of perforation is from the toe side of the HP.*

Figure 4.13 (c, right) shows the position predicted by model D for the combustion front in the vertical midplane of the reservoir in May 2016. The combustion front has better horizontal propagation at the top layer of the pay zone (around 70 m distance) compared to model S (around 60 m distance). The forward-leaning shape of the combustion front is clearly demonstrated as well. The variation in the O_2 concentration at the first, second and third grid blocks from the toe side of HP, is shown in Figure 4.15. Unlike with Model S, the oxygen breakthrough did not occur from the first HP perforation. The dramatic change in air injection rates (to 50,000 m^3/day in early-July 2014) led to oxygen channelling into the second HP perforation, although it amounted to less than 1% in overall comparison. The first significant oxygen breakthrough was seen at the third HP perforation (up to 3% and 7 % following air injection rates of 30,000 and 40,000 m^3/day, respectively) from late-Dec 2014 to May 2015).

No oxygen was produced from May to September 2015 in response to a reduction in air injection rates to as low as 20,000 m^3/day. Following another air injection rise from 20,000 to 35,000 m^3/day in Sep 2015, the O_2 concentration around the second and third HP perforation increased rapidly. The combustion front was very close to the HP at this point. The uninterrupted air injection accelerated the oxygen breakthrough, and consequently, significant amounts of oxygen channelled directly into the HP through the second and third perforations during the next 7 months.

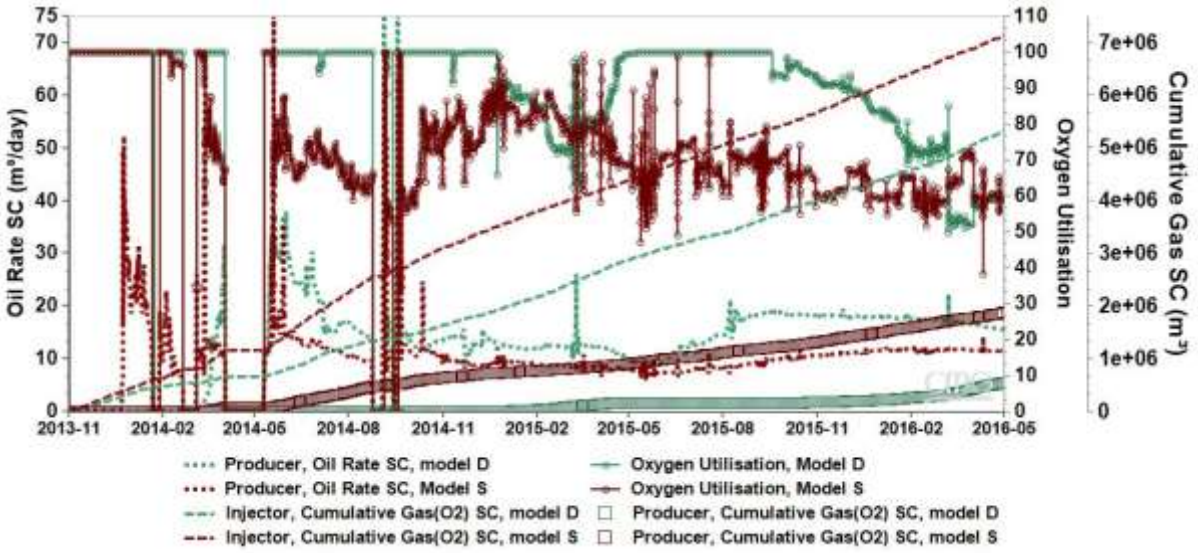


*Figure 4.16. Cumulative oxygen injected, cumulative oxygen produced, predicted oxygen utilisation, and oil production profile by Model S and Model D. Notes: * The illustrated parameters are distinguished with different line styles.*

The impact of the effective oxygen consumption throughout the THAI process was investigated in both models. Figure 4.16 shows the data predicted by Model S in red and Model D in green. Comparing cumulative injected oxygen rates, as well as cumulative produced oxygen rates, for Model S and Model D, a higher amount of oxygen was injected into Model S compared to Model D. It is not surprising to see then that the total produced oxygen in Model D is less than Model S. However, the O_2 utilisation by each model is less straightforward. The predicted

results show oxygen consumptions of 74% and 90% for Model S and Model D, respectively. It has been mentioned previously, earlier in this section, that the oxygen breakthrough into the HP occurred differently in Model S and Model D. This contributes to the difference in O_2 consumption predicted by Model S and Model D. Looking at Figure 4.16, it is apparent that the simulated oil production profile was directly affected by the oxygen consumption throughout the THAI process in both models. This is more noticeable during the uninterrupted air injection period. Apart from two periods of THAI operation (Feb-April 2015 and Mar-May 2016, when excessive air was injected to Model D), the simulated O_2 consumption by Model S was lower than the results predicted for Model D. This is a clear indication of better in-situ combustion (ISC) performance in Model D compared to model S. The higher daily and cumulative oil production profile by Model D (shown in Figure 4.9) is a direct result of a good overall ISC performance in Model D.

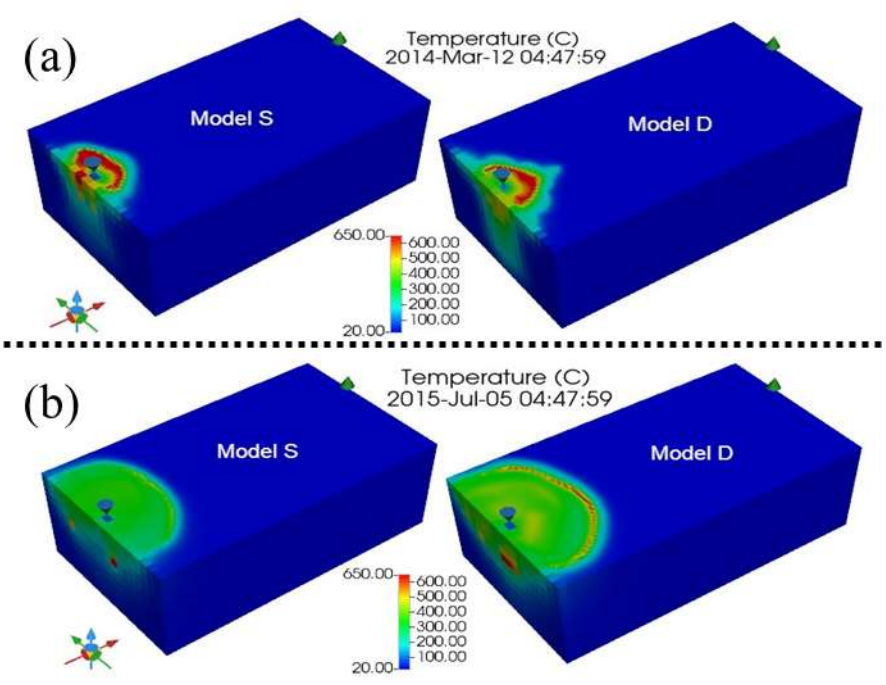


Figure 4.17. 3D simulated temperature profile by Model S and Model D in (a) March 2014 and (b) July 2015

Another indication of poor combustion front propagation in model S can be seen in its temperature profile. Figure 4.17 shows the predicted 3D temperature profiles for Model S and Model D in (a) March 2014 and (b) July 2015. High temperature regions can be seen ahead of the combustion front in both models in March 2014. Although, due to inadequate oxygen utilisation in Model S (approximately 70% from Figure 4.16), a poor combustion front advancement was predicted for Model S in July 2015. The experimental study by Greaves & Al-Shamali (1996) found that, irrespective of the extent of the combustion front established initially, the size of the high temperature region during ISC tends to decrease progressively with increasing combustion time. Because of the higher oxygen consumption by Model D (100% shown in Figure 4.16), a high-temperature leading edge of combustion front is still detectable even though it was narrower (in July 2015). This is consistent with findings by Greaves & Al-Shamali (1996). The predicted temperature profile (above 650 °C) shows that the combustion front propagation was more stable in Model D. This implies that the overall ISC performance is directly related to the O_2 consumption during the THAI process.

Both simulated oxygen and temperature profiles by Model S and Model D indicate that selection of proper air injection rates are key for a sufficient oxygen utilisation during the ISC, leading to a successful THAI operation. The findings in this section clearly show that the short distance between the K2 and K5 THAI well pairs, and subsequent extra air ingress from KA5 towards KP2, have had a negative impact on the performance of the THAI process. Therefore, for forthcoming projects, THAI well pairs must be drilled at a sufficient distance to avoid unwanted interference from each other, unless the operation is based on intended interaction between air injector wells (e.g., staggered line drive (SLD) THAI well arrangement).

4.5.3 Coke zone

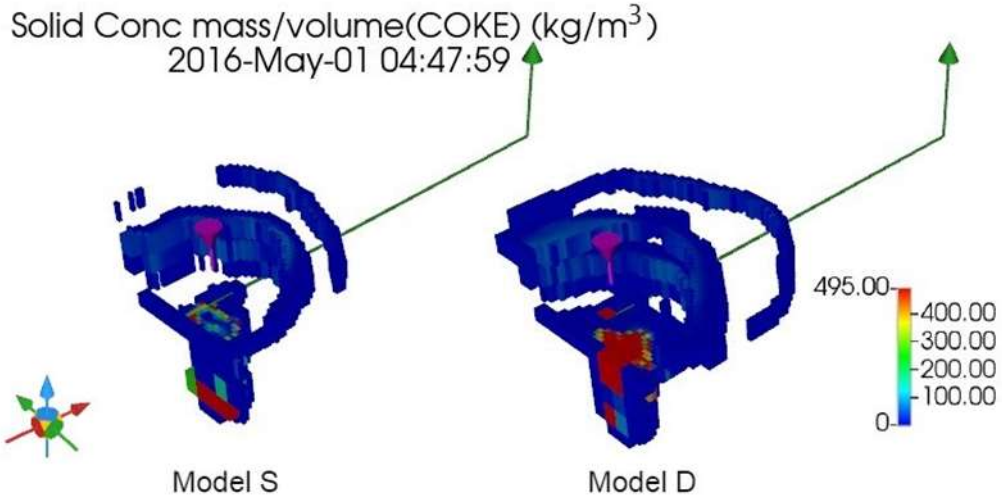


Figure 4.18. Simulated 3D structure of coke zone in Model S and Model D in May 2016

The coke zone provides the fuel for the in-situ combustion process. Coke is formed immediately ahead of the combustion front as a result of the precursor processes leading to oil displacement, including vaporisation and thermal cracking (Xia, Greaves, Turta, & Ayasse, 2003). Figure 4.18 shows the structure of the simulated coke zone in 3D for both models S and D. The area swept by the combustion front contained no coke. Coke deposition, with higher concentration (around 500 kg/m^3) and thickness occurred mainly in the lower part of inlet zone. The highest coke concentration was developed in the transition zone layer in Model S, while high coke concentrations were observed within the HP layer down to the transition zone layer in Model D. In other words, the high coke concentration zone (displayed in red in Figure 4.18) in Model D was larger compared to Model S in May 2016. It can be seen that coke concentration was high at the toe of HP in Model D, which matches the observation of Greaves et al, (2013)(i.e., 25m thick pay zone reservoir). The heavy oil thermal cracking reactions dominate downstream of the combustion front. This is due to the heat transportation to the base

of reservoir via conduction from the reservoir rock, and convection from the mobilised oil zone (Ado M. R., 2020). As the combustion front is limited to the upper portion of the reservoir, the immobile oil originally in place (below the combustion front) has a higher tendency to thermally convert to coke. This resulted in the rise in a higher conversion of heavy oil to coke beneath the combustion front, which is more evident in the predicted coke profile for Model D. A thinner coke zone with lower coke concentration was formed ahead of the combustion front for both models S and D. The average coke concentration ahead of the middle and upper parts of the combustion front was in the range of 50 to 60 kg/m^3 for both models. The high-performance in-situ combustion in Model D resulted in a uniform coke zone generation ahead of the combustion front. Some instability was identified in the upper part of the coke zone in Model S. The extra air ingress from KA5 caused direct migration of the injected oxygen into the HP in Model S, which consequently led to a reduction in cracking reaction of heavy oil (coke generation).

There was no evidence of oxygen ahead of the coke zone in this study. Xia et al, (2003) reported that coke acts as a gas seal in the horizontal producer, preventing air channelling through (from behind the combustion front). Therefore, there was no oxygen production in their study. Jinzhong et al, (2012) experimentally showed that the sealing ability of the coke zone and the operating parameters are closely related. It was reported that after the combustion front propagates beyond the toe position of HP, the oxygen will break through the coke zone and flow directly into the HP if the injection parameters are improper (e.g., too high air injection rates and/or injection pressure). The coke layer served as a gas seal ahead of the combustion front in the present study. However, coke did not prevent O_2 breakthrough into the HP when the combustion front was beyond the toe section of the HP. Hence, the relationship between coke generation and oxygen concentration around the horizontal producer was investigated in models S and D. The same area around the HP, in both models S and D, was selected for this

examination. Figure 4.19 presents this analysis for the third perforation from the toe side of the HP as well as air injection rates for both models.

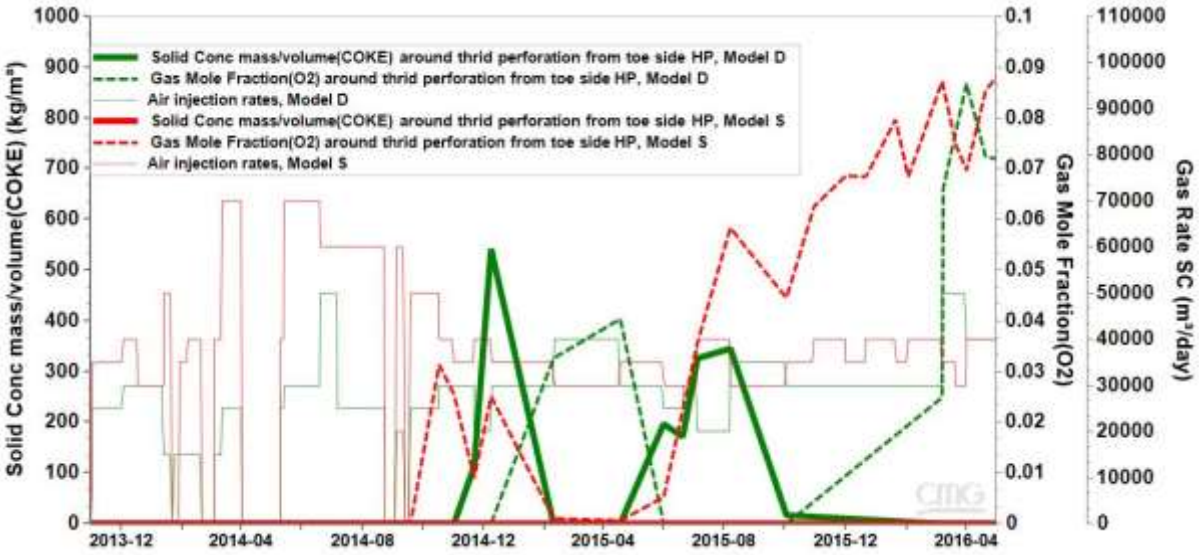


*Figure 4.19. Predicted coke concentration and oxygen profile around the third perforation from the toe side of HP in Model S and Model D. Notes: *SC stands for standard condition.*

Model S predicted no coke deposition around the targeted area for the whole 30 months of simulated period. This indicates that insufficient heavy oil thermal cracking took place at this region during the THAI process, which will be investigated later in detail. The primary oxygen breakthrough (although below 3%) into the region was detected in late-Sep 2014 (start of uninterrupted air injection). Simulated results by Model S indicate that the O_2 profile within the region experienced some fluctuations purely because of the variations in air injection rates until early-Feb 2015. The oxygen concentration was close to zero between early-Feb 2015 and mid-Apr 2015. This is most likely due to lower air injection rates during this period (30,000 m^3/day) and higher O_2 concentration around the second perforation from the toe side of the HP (shown in Figure 4.14). The variation in air injection was within 10,000 m^3/day from the mid-Apr to May 2016. Despite minor changes to injected air amounts in Model S, the oxygen profile rapidly amplified (up to around 9%) until May 2016 (end of simulation). This is due to the

propagation of the combustion front and connection of the HP with a combusted zone that is 100% saturated with injected air.

The simulated results for Model D (shown in Figure 4.19) demonstrated coke deposition from early-Nov 2014, with concentrations as high as around 500 kg/m^3 in Dec 2014. The oxygen breakthrough into the area (around the third perforation of the HP) began mid-Dec 2014 (with a sharp rate). Interestingly, this event coincided with a sharp decrease in coke concentration (as low as zero in early-Feb 2015) in the region. Coke concentration remained zero until late-Apr 2015, while the O_2 concentration in the gas phase increased up to 4%. It must be noted that air injection rates rose from 20,000 to 40,000 m^3/day between early-Dec 2014 and mid-Apr 2015, which contributed to oxygen breakthrough into the area. The second phase of coke deposition started in mid-April 2015 followed by a reduction in O_2 concentration in the area. It can be seen that the secondary coke build-up (up to 340 kg/m^3) happened immediately after a reduction in air injection rates from 40,000 to 20,000 m^3/day between mid-Apr 2015 and early-Aug 2015 in Model D. This emphasises the importance of air injection rates in providing the required heat for thermal cracking reactions in the reservoir. An increase in air injection existed

rates, from 20,000 to 35,000 m^3/day, caused a drastic decrease in the deposited coke (as low as 15 kg/m^3 in early-Oct 2015) in the region. This was the point when the secondary oxygen breakthrough began. Another decline in air injection rates (even though it was minor) in early-Oct 2015, reduced the rate at which coke deposition was declining. During the next 5 months some coke deposition occured in the area, but this was below 15 kg/m^3. This kept oxygen concentration below 2.5% until early-Mar 2016. The sharp increase in O_2 profile that took place until the end of the simulated period is mainly related to the following three factors; (a) no coke was present in the area, (b) air injection rates increased to 50,000 m^3/day, and c. the area was in contact with the combusted zone with 100% gas saturation.

The above findings from models S and D in the present work clearly indicate that a lack of coke deposition around the exposed section of the HP leads to the development of high oxygen concentrations in the HP. Insufficient thermal cracking of crude oil is the main contributor to the low coke laydown. Thermal cracking of heavy oil was closely related to injected air rates. Model S had poor in-situ combustion performance at the toe section of the HP leading to the absence of coke deposition. This was due to the extra air ingress from the KA5 injector well towards the KP2 producer well in Model S. Better thermal cracking took place around the toe section of the HP in Model D generating (even though only partially) a coke seal around the exposed section of the HP. Consequently, serious oxygen breakthrough into the region was delayed in Model D compared to Model S. This means, for existing THAI projects such as the Kerrobert project, the selection of air injection must be made considering air flowing from neighbouring injector wells (it can be done by pausing air injection for a short period and recording the produced gas from the corresponding producer well).

4.5.4 Steam zone

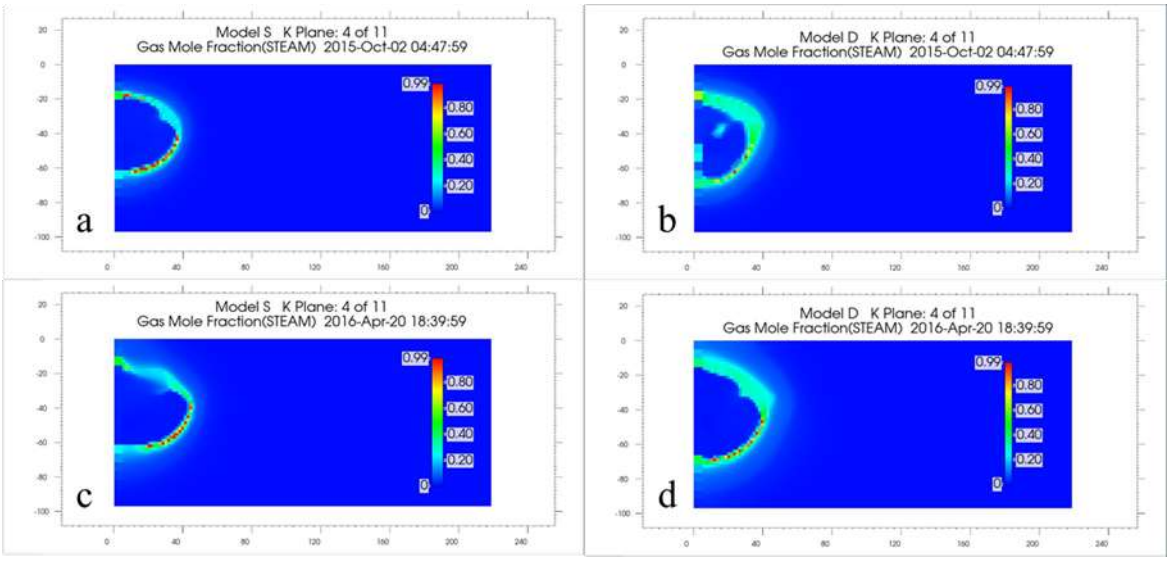


Figure 4.20. Predicted steam profile by model S and D during THAI process

The steam zone, that is generated during the THAI process, and its relationship with extra air flowing from KA5 are investigated in this section. Greaves et al, (2013) numerically studied the THAI process at field-scale, in which a steam zone was formed as the combustion front developed and propagated through the oil layer. They reported that steam was generated by evaporation of reservoir water and as a product of the combustion reactions. It was found that the steam zone was responsible for transporting the heat created by combustion reactions to the heavy oil. Three-dimensional studies of ISC by Greaves & Al-Honi (2000) showed that the thermal sweep efficiency is largely governed by the steam-gas front generated ahead of the combustion front, developing over the entire combustion period during ISC. They used a sand pack that had an initial water saturation of approximately 30% for their experiments. Both above studies did not consider bottom water in the reservoir. Therefore, it is important to study the generated steam zone during a THAI process in the presence of bottom water. The initial water saturation in the pay zone used for the present study is 26%. A transition zone (with 45% initial water saturation) and a bottom water zone (with 100% initial water saturation) are considered for the reservoir in this work.

Figure 4.20 (a) and (b) show the steam profile at the horizontal midplane above the HP for models S and D, respectively, in Oct 2015. It is evident that the steam zone was larger in Model D compared to Model S. The expansions of the steam zone in models S and D (predicted in Apr 2016) are shown in Figure 4.20 (c) and (d). A similar trend to that in Oct 2015 was observed for the formation of the steam zone in Apr 2016 (shown in Figure 4.20 c and d). Poor ISC performance in Model S resulted in a smaller steam zone, compared to Model D. It is fair to assume that the narrow steam zone was mainly generated from evaporation of reservoir water in Model S. Water vaporisation did not occur due to heat generation by ISC in model S. Reservoir water (in the pay zone) evaporated because of having contact with hot mobilised oil that was draining (downward) into the HP. On the other hand, a relatively large and constant

extension of the steam zone took place during the THAI process simulated by Model D. This is more attributed to good ISC performance than evaporation of reservoir water in Model D. Subsequently, a higher amount of heat was transferred to the cold oil zone which led to greater thermal heavy oil mobilisation. The displacement of hot mobilised oil will be examined in Section 4.5.5 in detail. It must be noted that the predicted temperature profile for the bottom water zone, for both models, was below the boiling temperature for water at reservoir pressure during the simulated period. This means that the bottom water did not contribute to "extra" steam generation during the ISC process in Model S and Model D. Temperatures as high as 80 ^{o}C were predicted at a small portion of the BW area below the inlet zone. However, the temperature of the vast majority of the BW zone was unchanged during the simulated period for both models. This implies that the bottom water does not act as a heat sink during the ISC operation in both models, despite the consequences of the variation in air injection rates.

The THAI's in-situ combustion nature has advantages over SAGD (in which surface-generated steam is injected into the reservoir). Successful ISC can dramatically lower the need for water and natural gas, with potentially smaller surface footprint, in comparison with steam injection (Kovscek, Castanier, & Gerritsen, 2013). The predicted steam profiles in this present study once again indicates the importance of air injection rates for a successful THAI project. Effective steam generation is key for in-situ heat transfer, and this can be achieved by injecting the right amount of air that would maintain ISC propagation throughout THAI operation, even with the presence of bottom water in the reservoir.

4.5.5 Mobile oil zone (MOZ)

Figure 4.21 shows the predicted oil saturation profile in the vertical midplane of models S and D. The region behind the combustion front (combusted zone with 100% gas saturation) was excluded from the vertical midplanes in Figure 4.21. It is evident that, as the combustion front expanded in size and moved further away from the inlet zone, heat (coming either by

conduction via the combustion front or by convection via steam) was transferred into the downstream oil region. This caused the MOZ to develop for the whole duration of the ISC. The MOZ contains two regions, namely region 1, which consists of the thermally cracked oil as well as lighter vaporized fractions, and region 2, which consists of the banked oil zone (BOZ) where the oil saturation is close to 100% (Greaves, Dong, & Rigby, 2012 b). Earlier water production, from the inlet zone of the reservoir (where initially $S_o = 0.74$), formed the BOZ ($S_o = 1$) during the initialisation period of ISC. This is due to higher mobility of water compared to oil. The oil flux vectors, shown in Figure 4.21, represent the direction in which the mobilised oil flow into the horizontal producer within the reservoir.

As discussed earlier, the extra air ingress from the neighbouring air injector well impacted the ISC efficiency in a negative way in Model S. Therefore, the BOZ, that was developed and extended by steam, is the major source for the MOZ in Model S. Good oil production rates were predicted for Model S (a peak of approximately 30 m^3/day shown in Figure 4.6) in late-Sep 2014. This was caused by (1) reinjection of a high volume of air into the reservoir (after a short break in mid-Sep 2014) and (2) oil flow into the toe of the HP from the previously established BOZ in model S (displayed by the forward directed horizontal vector in Figure 4.21 (a)). Also, the gravity drainage of mobilised oil into the exposed section of the HP closer to the heel (shown by vertically downwards vectors in Figure 4.21 (a)), contributed to the prediction of peak oil rate. Figure 4.21 (d) exhibits a similar pattern of oil displacement as simulated for Model S at the same time. However, a greater volume of oil flowed into the toe section (bigger oil flux vector shown in Figure 4.21 (d)) which resulted in a peak of 45 m^3/day in oil production. This was related to the larger BOZ (higher oil saturation) around/below the toe section of HP in Model D. Looking at Figure 4.21 (b) and (e), the BOZ ahead of the combustion front in model S was the same as Model D in size. The predicted oil production by model S was mainly limited to gravity drainage in Aug 2015. Whereas, a considerable amount of oil was produced

from the toe section of the HP in Model D during the same period. Another noticeable event was that the second and third perforation of HP from the toe side in Model S were fully saturated by gas in Aug 2015. Mobilised oil was produced from the same location (flowed from beneath the HP), at the same time, in Model D. The second and third perforations of the HP from the toe side in Model D became 100% saturated by gas in Model D in late 2015. Although a lower amount of oil was produced from below the HP in Model D (almost equal to Model S), higher volumes of mobilised oil drained into the HP from the upper part of the reservoir in Apr 2016 (demonstrated in Figure 4.21 c and f). This was due to the significant increase in the size of the BOZ ahead of the combustion front in Model D compared to its size in Aug 2015. Also, the BOZ ahead of the combustion front is larger in Model D compared to Model S in Apr 2016, displaying better combustion front advancement along the HP in Model D. The cold oil zone (COZ) was undisturbed during the THAI process in this study as no oil displacement was detected by both models in the COZ. The substantial difference in predicted daily oil production rates by models S and D (shown in Figure 4.16), from Aug 2015 until the end of simulated period, reflects the abovementioned events.

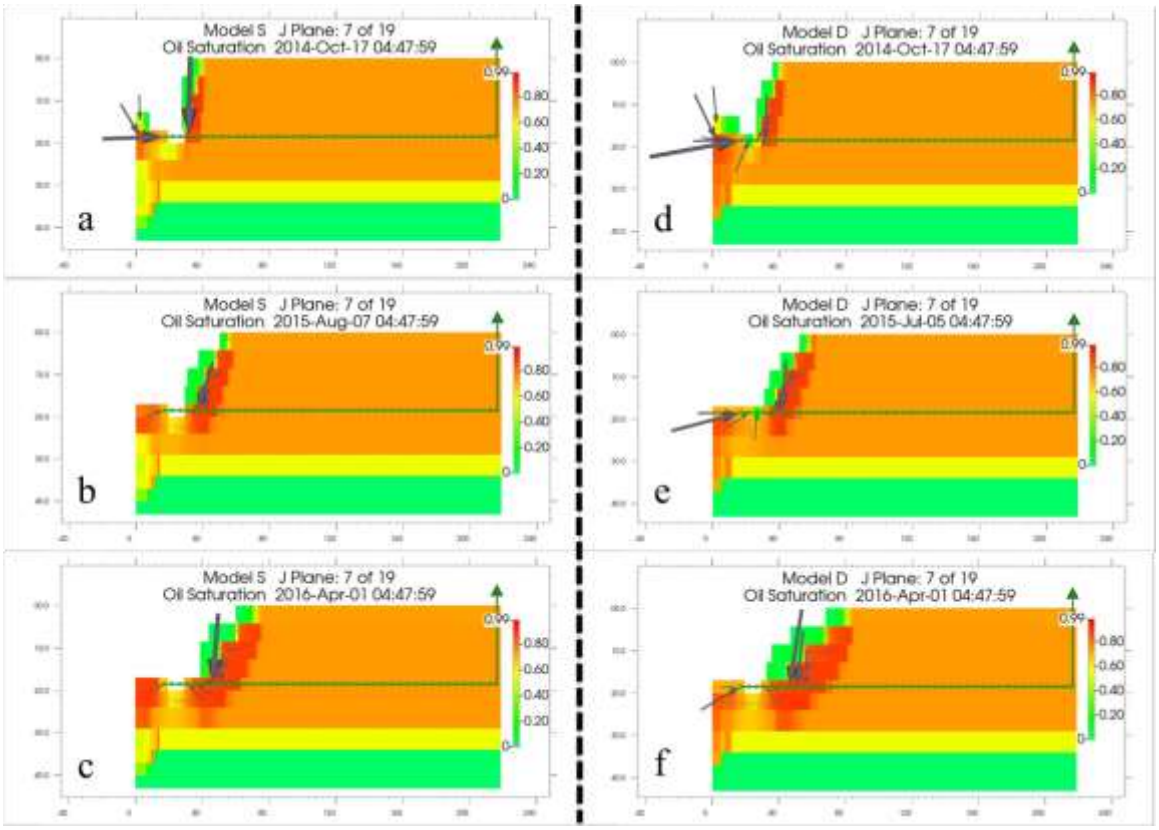


Figure 4.21. Predicted oil saturation profile by model S and D during uninterrupted air injection period

Additionally, the oil saturation profile in Figure 4.21 illustrates that some of the mobilised oil sank into the transition and bottom water zones in both models throughout the THAI process. Hence, a considerable amount of oil was left behind (trapped) in the deeper portion of the reservoir. This was a common issue for models S and D. This means that variation in air injection rates, employing the same THAI well arrangement, could not prevent mobilised oil sinking to the bottom water. A potential solution, to capture the maximum possible mobilised oil, is to move the HP closer to the transition zone. Model S was used to investigate the effect of HP location. It was also examined whether poor oxygen utilisation in Model S can be improved by adjusting the HP position. Two models were constructed (based on operating parameters of Model S) with adjusted HP positions, referred to as Model HP6 and Model HP7. It must be noted that the horizontal producer was placed 5 and 10 m closer to transition zone

in models HP6 and HP7, respectively. Figure 4.22 shows simulated results by models HP6 and HP7. It is evident that mobilised oil sank into bottom water zone in both model HP6 and HP7, no matter how close to the transition zone that the HP was (displayed in Figure 4.22 (a) and (b)). Therefore, a variation in HP location could not prevent oil sinking into deeper layers in the reservoir.

Figure 4.22 c shows that all three models predicted a similar initial oil production profile. However, from May 2014, a deviation in simulated cumulative oil production profiles occurred. Model HP6 predicted 28% higher cumulative oil production compared to Model S. The oxygen utilisation was improved by 5% in model HP6, in comparison with Model S. Model HP7, with the HP placed just above the transition zone, predicted the better oil recovery performance amongst the three models. The oxygen utilisation was improved to 86% in model HP7 resulting in 73% higher cumulative oil production compared to Model S. Overall, the simulation results demonstrate that the closer the HP was located to the transition zone, the higher the oil recovery that was achieved. In other words, the K2 THAI pilot well pair could have produced more oil by placing the KP2 well at a level closer to the transition zone, including the effect of extra air ingress from KA5.

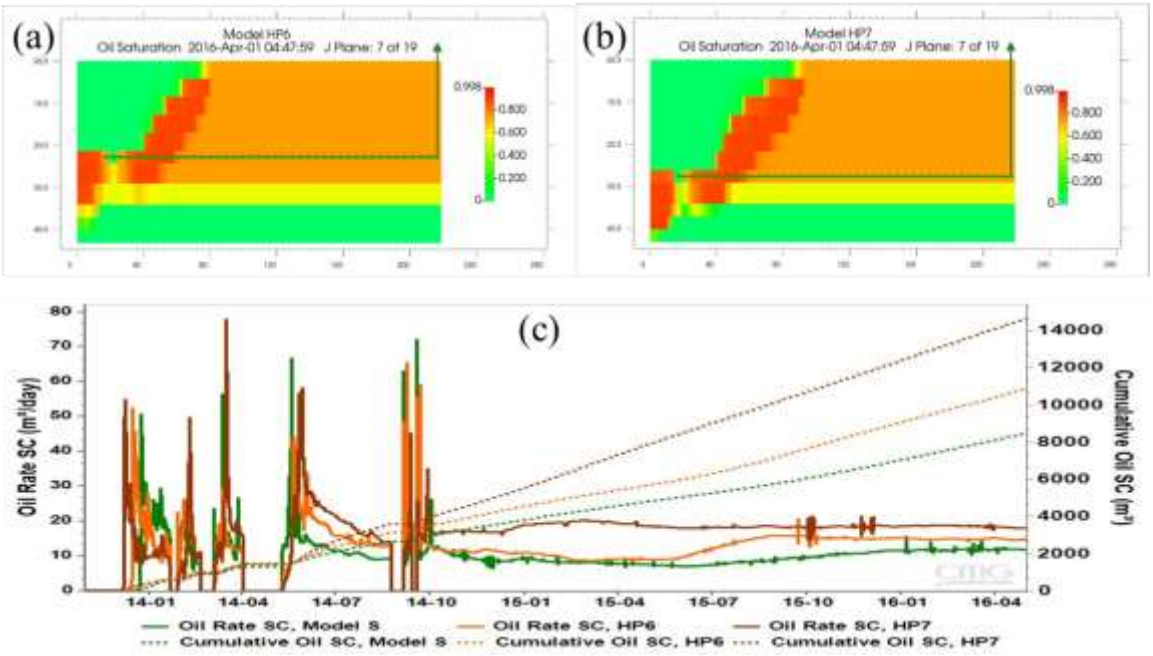


Figure 4.22. Predicted oil saturation profile (a and b) and oil production profile by model S with varied HP location (c)

4.6 Conclusion

The field data analysis in this work indicates that the K2 pilot, one of the best performing THAI well pairs in the Kerrobert project, suffered interference from a neighbouring K5 semi-commercial THAI well pair. The air injected through KA5 flowed in a direction opposite to that intended, namely towards the K2 pilot. This caused a significant imbalance between injected air and produced gas for KA2 and KP2, respectively. Previously developed field-scale THAI models lacked (a) consideration of a bottom water zone in the reservoir and (b) validation against the actual field data. In present work, a new field-scale THAI model with relatively thick bottom water layer was developed and validated against the Kerrobert field data. The simulation was used to probe whether the air injection rates impact the overall performance of the THAI process in the presence of bottom water. It was found that excessive air injection reduced oxygen utilisation resulting in a poor ISC efficiency with combustion time. This means more air injection does not necessarily promote oil production in the THAI process in a bottom

water situation. The O_2 utilisation was improved from 74 to 90% by restricting air injection to only that into KA2 alone itself. This means the interference from the KA5 has negatively impacted the overall performance of the K2 pilot. Various developed zones throughout the combustion front propagation were investigated in this study. It was numerically shown that extra air ingress from KA5 has had a negative impact on the combustion temperature profile. Similar to previous studies, the coke zone served as a gas seal preventing oxygen channelling ahead of combustion front in the new model. An inversely proportional relationship was detected between coke concentration and oxygen profile around the horizontal producer (HP) in this work. It was also found that the size of the steam zone varies with changes in air injection rates. The MOZ analysis demonstrates that a large BOZ was developed below the HP during THAI operation. Relocation of the horizontal producer was proposed as a potential strategy to capture as much mobilised oil as possible. The oxygen utilisation was improved by 13 %, resulting in 73% higher cumulative oil production in comparison with the history matched model.

Therefore, the following suggestions can be made for optimisation purposes: a. for forthcoming projects, THAI well pairs must be drilled at a sufficient distance to prevent unwanted interferences from each other, unless the operation is based on intended interaction between air injector wells (e.g., staggered line drive (SLD) THAI well arrangement), b. for existing THAI projects such as Kerrobert, the selection of air injection must be made considering air flowing from neighbouring injector wells (it can be done by pausing air injection for a short period and recording the produced gas from the corresponding producer well), and c. HP locations closer to the transition zone could be considered in order to produce from the large BOZ developed below the HP and enhance oil recovery.

5. In-situ microwave-assisted CAPRI using Hydrodesulphurisation catalyst

The history-matched THAI simulation showed that the in-situ combustion alone may not provide sufficient heating for downhole catalytic upgrading of heavy oil in the THAI-CAPRI process. Therefore, an additional heating source is required for a successful THAI-CAPRI process. As a strategy to provide the needed heating, a microwave heating technique has been proposed in this chapter. With its selective and volumetric nature, microwave technology can provide fast heating which can be targeted at the catalyst packing and/or the incoming oil in its neighbouring area. It was demonstrated that heavy oil can be heated directly with microwaves to 425°C, which is the temperature needed for successful catalytic upgrading. Contrary to previous assertions, the microwave heating of heavy oil was done without the need for an additional microwave susceptor. A commercially available hydrodesulphurization (HDS) catalyst was used for microwave-assisted catalytic upgrading experiments. The characterisation of the treated oil showed an upgrading of more than 3.2° API points, a 90% reduction in viscosity to less than 100 cP, and more than 12% reduction in sulphur content. Approximately 19% hydrogen was detected in the gas product which originated from the dehydrogenation of heavy oil by using the HDS catalyst. The in-situ produced hydrogen within the THAI-CAPRI process can be used to facilitate hydrodesulphurization as well as improving API gravity upgrading by hydrogenation of the treated oil.

5.1 Introduction

Starting in 1996, the investigations leading to the development of the catalytic add-on of THAI process, CAtalytic upgrading PRocess In situ (CAPRI), began at the University of Bath (Turta, Greaves, & Grabowski, 2018). Figure 5.1 and Figure 5.2 show the schematic of the CAPRI and THAI-CAPRI processes, respectively. The CAPRI process acts as a radial in-flow reactor

or in-situ upgrader. This process potentially provides in-situ upgrading by surrounding the horizontal producer with a catalyst packing. A catalyst bed/packed can be emplaced, or pre-engineered sections can be used. As the partially cracked THAI oil flows through the annular catalyst layer, it is further upgraded, before being produced by the horizontal well. Hart et al, (2017 b) reported that the THAI-CAPRI process significantly reduces the viscosity of the heavy oil by several orders of magnitude. Hence, it can be pipelined to a refinery without the need for a diluent. There have been seven THAI pilots/projects, located in 3 countries, since 2006. However, so far, the THAI-CAPRI process has only been tested once, which will be studied in detail in the next chapter.

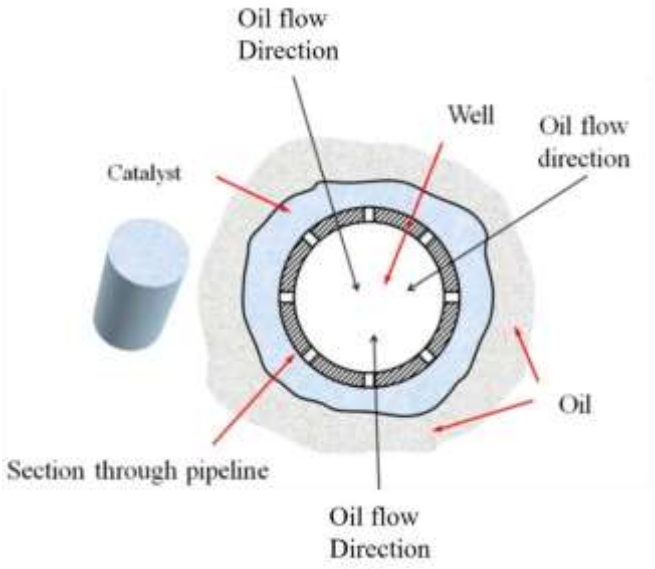


Figure 5.1. Schematic of the CAPRI process, taken from (Hart, Shah, Leeke, Greaves, & Wood, 2013)

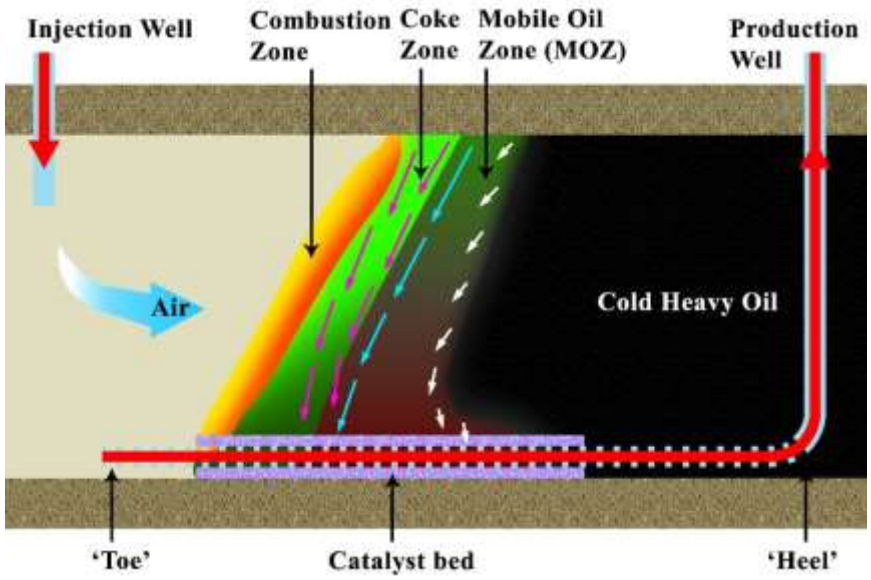


Figure 5.2. Schematic of the THAI-CAPRI process

Turta et al, (2018) listed the potential benefits of the CAPRI process as follows:

1. The CAPRI is an add-on process to the THAI process, so no other special adjustments are required.
2. Toe to heal combustion front propagation continually exposes fresh catalyst in the CAPRI process.
3. The CAPRI process partially upgrades heavy oil and bitumen to lighter oil, in one-step reservoir process during the oil recovery process. In addition, the CAPRI produces hydrogen and does not need any outside heat sources.
4. In the CAPRI process, the oil flowing over the catalyst is partially upgraded oil, with the majority of heavy ends removed (the coke burned or left behind in the reservoir), and significant reductions also in sulphur, Ni, and V.
5. As well as fresh standard refinery catalyst, spent/regenerated/fluid cracking catalyst (FCC) can be used for the CAPRI process. Improved catalysts could enable upgrading to light oil (API° greater than 30).

6. The CAPRI process substantially reduces the cost of surface upgrading plant.

Hart et al, (2017 b) reported an overall THAI-CAPRI in-situ upgrading of the produced oil of between 6 and 9° API, with potential worth of up to $12/barrel, depending on crude oil price. They also reported that an optimum temperature of 425 °C and pressure of 20 bar for the CAPRI process. Hydrodesulphurisation (HDS) catalysts such as CoMo/γ-Al_2O_3 and NiMo/γ-Al_2O_3, which are commonly used in oil refineries, have given positive results when used in CAPRI tests at lab-scale (Shah A. A., et al., 2011; Tare & Greaves, 2002). Using ultrafine particles and pelleted CoMo/γ-Al_2O_3 catalyst at reaction temperature of 425 °C, the API gravity and viscosity of the produced oil was found to improve by respectively 9° API and 96% viscosity reduction with ultrafine particles compared to 5° API and 79% viscosity reduction achieved with pelleted fixed-bed catalyst (Al-Marshed, Hart, Leeke, Greaves, & Wood, 2015). However, the history matched simulation of the THAI process (Model S) in this study, as well as the experimental scale THAI model, previously developed by Ado et al (Dynamic Simulation of the Toe-to-Heel Air Injection Heavy Oil recovery Process, 2017), suggest that the temperature of the oil passing through catalyst packing around the horizontal well does not exceed 300 °C.

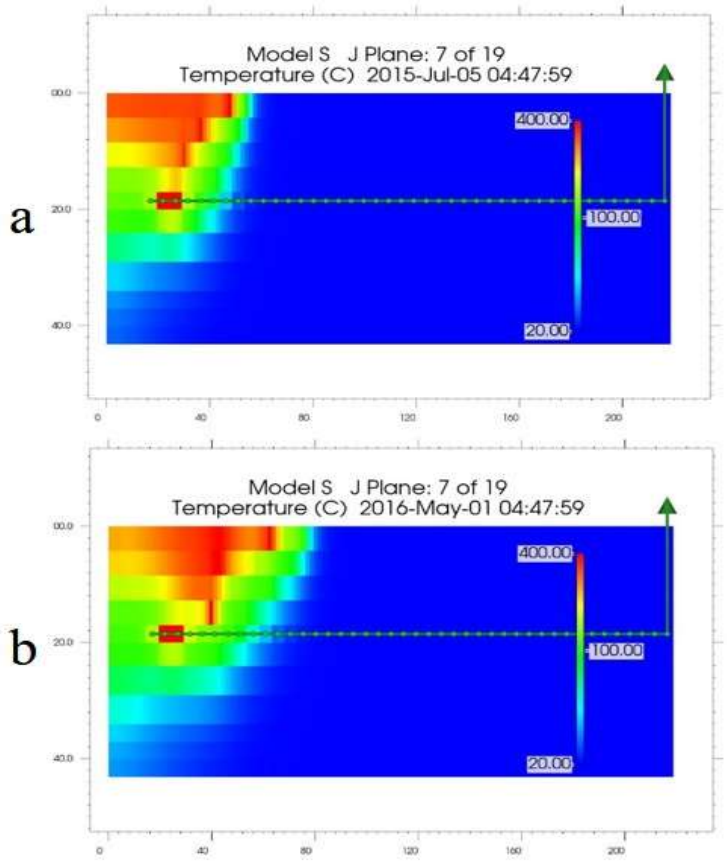


Figure 5.3. The predicted temperature profile alongside the HP well in the history matched model (Model S) in July 2015 (a) and May 2016 (b)

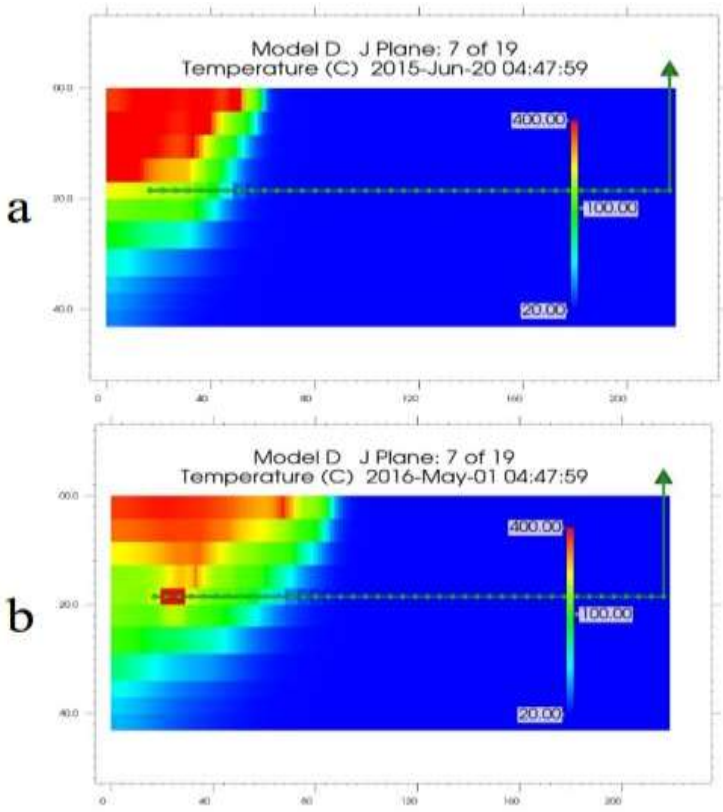


Figure 5.4. The predicted temperature profile alongside the HP well in Model D in July 2015 (a) and May 2016 (b)

Figure 5.3 shows the predicted temperature profile alongside the horizontal producer well for the history matched model (Model S as discussed in Chapter 4) in this study in July 2015 (a) and May 2016 (b). Apart from the toe section of the HP well, that was touched by the combustion front, the predicted temperatures are below 300 °C. A similar HP temperature profile was predicted for Model D (as discussed in Chapter 4) in which the in-situ combustion performance was more efficient. Figure 5.4 shows the predicted temperature profile alongside the horizontal producer well for Model D (with better oxygen utilisation during the ISC, compared to Model S) in this study in July 2015 (a) and May 2016 (b). Hence, there is a need to provide extra heating of the field-scale CAPRI reactor, which is contrary to previous assertions by Turta et al, (2018).

Marroquin et al (A batch reactor study to determine effectiveness factors of commercial HDS catalyst, 2005) carried out a series of experiments to determine effectiveness factors of commercial hydrodesulphurisation catalysts for catalytic heavy oil upgrading. They summarised two reviews of characteristics and classification of common batch reactors and their advantages and disadvantages when using them for screening of catalyst and catalytic reactions as follows:

a) The catalyst and the reactants are charged into a vessel and brought to react as function of time, under specific conditions of temperature and pressure.
b) The progress of the reaction is monitored by periodically analysing the vessel content.
c) Batch reactors are efficient, cheap, and easy to operate.
d) The catalyst can be either suspended in the liquid (the so-called slurry reactor) or kept in a spinning or static basket inside the reactor. A sufficient agitation is needed to keep the catalyst suspended in the liquid.
e) The reactor pressure is controlled at the desired level during the catalytic reaction.
f) There are neither intrareactor nor interphase gradients within perfectly mixed batch reactors.

Hart et al, (2020) demonstrated, in lab-scale tests, that inductive heating can be used to provide the heating needed for the catalytic upgrading. However, neither the oil nor the HDS catalyst interacted with the applied magnetic field at levels that were high enough to generate the heat needed to raise and maintain the temperature at 425°C. They also had to mix the catalyst with steel balls to act as a susceptor, with a catalyst-to-steel-balls volume ratio of about 2:1.

Electromagnetic heating methods have recently been proposed as possible strategies to overcome this deficiency and provide the additional heating needed for a successful CAPRI process (Adam, Hart, Wood, Robinson, & Rigby, 2019; Zhang, et al., 2018). In the current

study, microwave heating is used to provide the requisite additional heating and increase the temperature at the catalyst packing and/or the oil in its immediate vicinity to the required 425 °C or more, without needing addition of susceptors.

Commercially available microwave equipment are usually used by many scientists for carrying out high throughput syntheses or reducing the time required to undergo particular reaction steps, without concern for the reproducibility of the experiments or the underlying physio-chemical mechanisms (Robinson, et al., 2010). Robinson and co-workers (Understanding microwave heating effects in single mode type cavities—theory and experiment, 2010) reported a number of phenomena that must be considered in order to understand the mechanisms of microwave assisted synthesis. A new lab-scale microwave-heated reactor, developed by Dr. Mohamed Adam and co-workers at the Faculty of Engineering at University of Nottingham (Adam, Hart, Wood, Robinson, & Rigby, 2019), was used to examine the possibility of heating THAI-produced oil directly with microwaves to 425 °C in order to achieve catalytic upgrading. The system developed involves a single-mode microwave applicator, which has the advantage of a well-defined standing wave configuration with the ability to provide high electric field intensity focused within the oil. Adam et al, (2019) used electromagnetic simulations to model and adjust the electric field configuration inside the cavity and within the heated sample.

The current study also investigates the effect of coke and sulphur deposition on the porosity and activity of the catalyst. Gas sorption and TGA analysis were employed to characterize fresh and spent HDS catalyst with the aim to study the effect of coke deposition on blocking the porous space within the HDS catalyst.

5.2 Microwave (dielectric) heating

There are many frequency bonds, in the range of 6.78 MHz to 245 GHz, which have been allocated for Industrial, Scientific, and Medical (ISM) use. The frequency bond allocations were made to avoid interfering with communications signals. Microwaves are electromagnetic waves with frequency range from 300 MHz to 300 GHz (Metaxas & Meredith, 1983; Adam, 2017). Adam (2017) reported that the most commonly used frequency bond for industrial equipment are 896 MHz (in the UK) and 2450 MHz. High frequency oscillating electric and magnetic fields (microwaves) are generated when electrons resonate at high frequencies. The fundamentally distinct methods of transferring energy from the source to the sample is the main advantage of utilising microwave energy in comparison to conventional thermal processing (Mutyala, Fairbridge, Pare, & Belanger, 2009). In conventional heating, energy is delivered to a material via conductive, convective, and radiative heat transfer. Whereas, in dielectric heating, energy is delivered volumetrically and instantaneously due to interaction of material with the alternating electric field (Robinson, et al., 2010). By directly delivering energy to microwave-absorbing materials, conventional issues such as long heating periods and energy loses can be minimised (Mutyala, Fairbridge, Pare, & Belanger, 2009). As a result, the targeted materials can be heated rapidly, delivering an advantage in energy efficiency and processing time (Zhang, et al., 2018). A microwave heating process is not restricted by the temperature gradient and the heat transfer coefficient, as in the cases of conventional conductive and convective heating methods, allowing for rapid heating (Adam, et al., 2018).

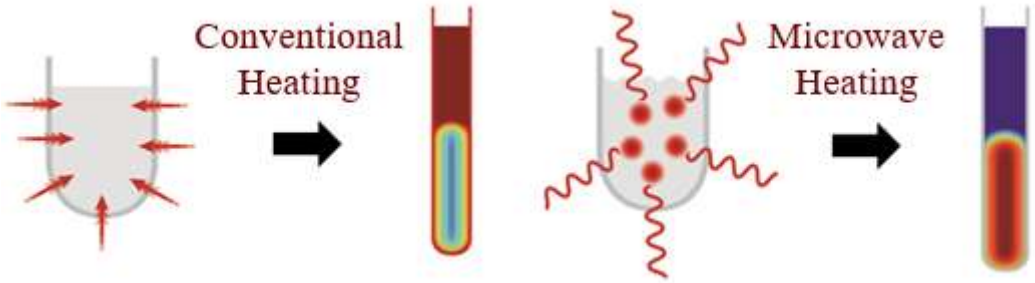


Figure 5.5. Selective nature of microwave heating

The extent to which a material interacts with an electric field can be characterised by the dielectric properties of that material. The dielectric constant (ε′) is the ability of a material to store electromagnetic energy through polarisation and the dielectric loss factor (ε″) is the ability of a material to convert the stored energy to heat. The loss tangent (tan δ) is the ratio of ε″ to ε′. The loss tangent can be used to assess the general ability of a material to heat in a microwave field. Materials can be broadly classified based on their response to microwaves as: transparent to microwaves (with a low value of tan δ) such as sulphur, reflects microwaves such as copper, and absorbs microwaves (with a high value of tan δ) such as water. When a matrix of materials is present then selective heating will occur based on the relative dielectric properties of the individual components (Robinson, et al., 2010; Mutyala, Fairbridge, Pare, & Belanger, 2009).

The electromagnetic field can penetrate the rock matrix, allowing heating to take place at a significant distance away from the electromagnetic source (Zhang, et al., 2018). Therefore, in a THAI-CAPRI setting, heating can be targeted at the catalyst packing, and/or the incoming oil in its immediate vicinity, at any desired section along the horizontal well to correspond to any part of the combustion front and successive layers.

Where a number of studies have been published on microwave-assisted processing and upgrading of heavy oils, many of these studies have erroneously concluded that microwaves can only be used for heating the oil by indirect means, i.e. via the use of a microwave susceptor

such as activated carbon (Nasri, 2019), silicon carbide (SiC) (Jeon, et al., 2012) or carbon nanoparticles (Li, Hou, Wang, & Cui, 2014). The need for microwave susceptors is supposedly because of the relatively low microwave-absorbing ability of the oils themselves, and also because of the lack of proper applicator/cavity design since most of the previous studies were conducted in modified domestic microwave ovens. Domestic ovens are built with limited power and low levels of electric field intensity, and they lack a well-defined electric field configuration.

However, Zhang et al, (2018) showed that, at high temperatures, which is the case in THAI-CAPRI, heavy oils are themselves more susceptible to being heated directly with microwaves. Furthermore, Porch et al, (2012) showed, through electromagnetic simulations, that microwave heating devices for processing heavy oils could be designed and optimised to provide relatively high microwave absorption efficiencies without the need for added susceptors.

5.3 Materials and methods

5.3.1 Materials

5.3.1.1 Heavy oil produced through THAI technology

As discussed earlier in Section 5.1, the CAPRI process is an add-on to the THAI process. In the CAPRI process, oil flowing over the catalyst has already been partially upgraded by the THAI process. The heavy oil used in this study was supplied by Touchstone Exploration Inc. Canada (previously Petrobank) which was produced through the THAI technology. The properties of the THAI oil used in this study are listed in Table *5.1*.

Table 5.1. Properties of the heavy oil used for this experimental work

API gravity at 20 ºC	Viscosity at 25 ºC (cP)	Sulphur content (wt. %)
14.3	880	3.2

Zhang et al (Impact of Oil Composition on Microwave Heating Behavior of Heavy Oils, 2018) previously conducted SARA analysis (analysis of saturates, aromatics, resins, and asphaltenes content) for the same heavy oil as shown in Table *5.2*.

Table 5.2. SARA analysis of THAI oil used in this study

Saturates (wt %)	Aromatics (wt %)	Resins (wt %)	Asphaltenes (wt %)
32.34 ± 0.34	33.19 ± 1.77	15.86 ± 0.44	7.91 ± 0.40

5.3.1.2 Hydrodesulphurisation (HDS) catalyst

The word "catalyst" is used to describe many phenomena but in all instances an agent (the catalyst) exerts a more-than-proportional influence over some change (Twigg, 1993). The essential features of a heterogenous catalyst (a catalyst with solid material) are as follows Twigg (1993):

a) The presence of a heterogeneous catalyst changes the rate of an overall chemical reaction.
b) The products of the catalysed reaction can, in principle, be obtained from uncatalysed reactions under the same conditions.
c) Any useful catalyst must have a high productivity (the catalysed reaction steps must occur many times before catalytic activity is lost).
d) The catalyst reaction steps take place very close to the solid surface.

It is too optimistic to define catalysts as materials that accelerate chemical reactions without themselves undergoing change (Twigg, 1993). In other words, the properties of all real catalyst change with use. The nature of the catalytic process depends on catalyst's essential properties including its activity (ability to convert feedstock to products), selectivity (ability to give the

desired product, and life (time for which the catalyst keeps a sufficient level of activity and/or selectivity) (Twigg, 1993).

The size and shape of the catalyst pieces is a compromise between the wish to minimise pore diffusion effects in the catalyst particles (requiring small particle sizes) and pressure drop across the reactor (requiring large particle sizes). Once the operating conditions of a catalytic reactor have been determined, it is necessary to decide the form of catalyst that should be used for the catalytic reaction (Twigg, 1993).

$CoMo/\gamma\text{-}Al_2O_3$ catalyst is a bifunctional hydrodesulphurization/hydrotreating (HDS/HDT) catalyst (i.e., metal and acidic sites), which is favourable for hydrocracking and hydrogenation in catalytic heavy oil upgrading (Hart, Shah, Leeke, Greaves, & Wood, 2013). The acidic sites of the support promote cracking reaction through a carbocationic mechanism, whereas the metal side promote hydrogen addition. Hart et al, (2013) reported that catalytic upgrading occurs by breaking the larger molecules to give fragmented free radicals, which then react with hydrogen radicals to stabilise the hydrocarbon chains and terminate the reaction. Hart et al, (2017 a) used $Ni\text{-}Mo/Al_2O_3$, another type of HDS/HDT catalyst, for their heavy oil catalytic upgrading experiments. They reported that splitting of C—C, C—S, C—N, and C==C bonds, within heavy oil, is facilitated by the acid sites of the Alumina support. They also reported that thermal and catalytic cracking, hydrogen-transfer reactions, ring opening and closure, desulphurisation, demetallisation; lead to bond scission reactions.

A commercially available mesoporous $CoMo/\gamma\text{-}Al_2O_3$ catalyst with a BET surface area of ~ 210 $m^2\ g^{-1}$ was used. The HDS catalyst contained Cobalt oxide (4.5%), molybdenum oxide (14.5%), and Alumina (81%). The catalyst is a quadra-lobe shaped extrudate of length ~6 mm and diameters (a,b) ~1.3, ~1.5. However, for the microwave upgrading experiments smaller particles were used to enable homogeneous mixing of the reactor contents. The extrudates were

crushed using a pestle and a mortar, and then divided into different particle size groups ranging from 75 µm to 1180 µm.

5.3.2 Experimental setup

Figure 5.6 shows a schematic of the microwave heating system which was built to examine the catalytic upgrading of the heavy oils in this study. This system provides many benefits over similar commercially available microwave heating systems. The reactor has a maximum operating temperature and pressure of 450 °C and 20 bar. Also, the microwave heating system used in this study allows the study of a wider range of power and temperature.

The microwave system involves a flanged 30 mm i.d quartz tube inside a single-mode microwave applicator. The quartz tube with a length of 150 mm, shown in Figure 5.10, was manufactured by Robson Scientific (Hertfordshire, UK). The quartz flange was supported and sealed against stainless steel flanges using Perfluoroelastomer (FFKM) O-rings (Polymax ltd, Hampshire, UK). A 2.45 GHz generator (GU020, IMS Ltd., Buckinghamshire, UK) with a maximum power input of 2 kW was used to supply the microwave power, which was transported to the applicator through a standard WR340 waveguide.

For impedance matching to improve the microwave power delivery efficiency, a sliding short-circuit and a three-stub motorized Homer analyzer/tuner (STHT 2.45 GHz, S-TEAM, Bratislava, Slovakia) were used. The sliding short-circuit allows for shifting the standing wave configuration within the waveguide, while the 3-stub tuner enables amplifying the electric field intensity in the cavity. The Homer analyser/tuner also samples and analyses the microwave power signal to determine the absorbed and reflected power, as well as frequency.

To measure temperature during microwave heating, an IR pyrometer was used (Optris CT 3MH, Berlin, Germany). The IR pyrometer operates with radiation at a wavelength of 2.3 µm, which is able to pass through the quartz wall and measure the temperature of the oil inside the

tube. The reactor pressure was monitored using a pressure transducer (Omega PXM409, Manchester, UK). The temperature from the IR sensor, pressure from the transducer, and the forwarded/reflected power from the tuner are displayed on a monitor connected to a PC. The process monitoring and control setup is shown in Figure 5.11.

The experiment consists of a water-cooled reactor placed inside a single-mode cavity. The quartz tube is covered with a stainless-steel flanged cap with PTFE gasket and FFKM O-rings. The stainless-steel flange is water cooler through an embedded jacket (shown in Figure 5.8). The metallic cap of the reactor with its seals are cooled during heating using cooling water. To mix the reactor contents during the experiments, a magnetic stirrer (as shown in Figure 5.7) together with a glass-coated magnetic bar were used.

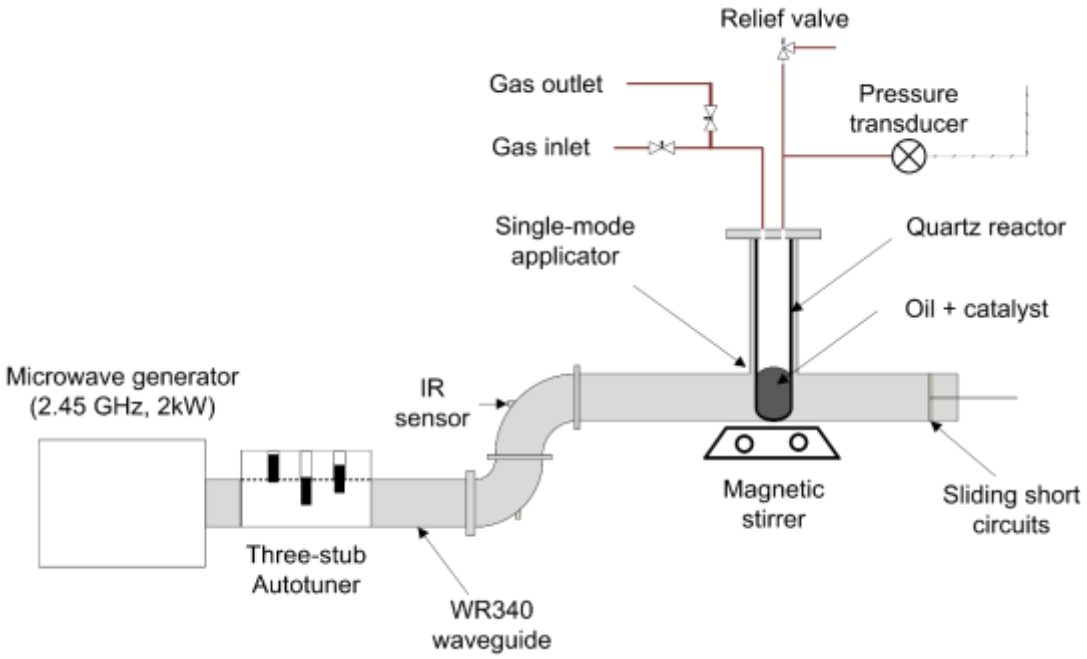


Figure 5.6. Schematic diagram of the laboratory-scale microwave-assisted heavy oil upgrading experiment setup

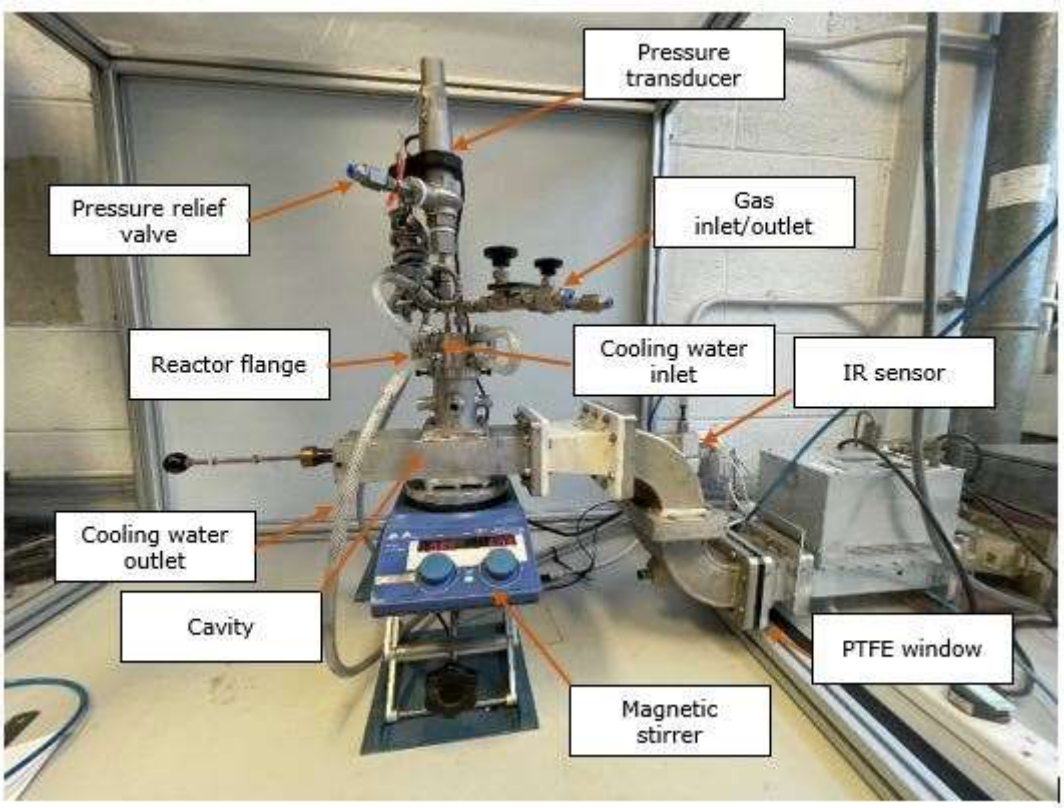


Figure 5.7. Front view of the experimental setup

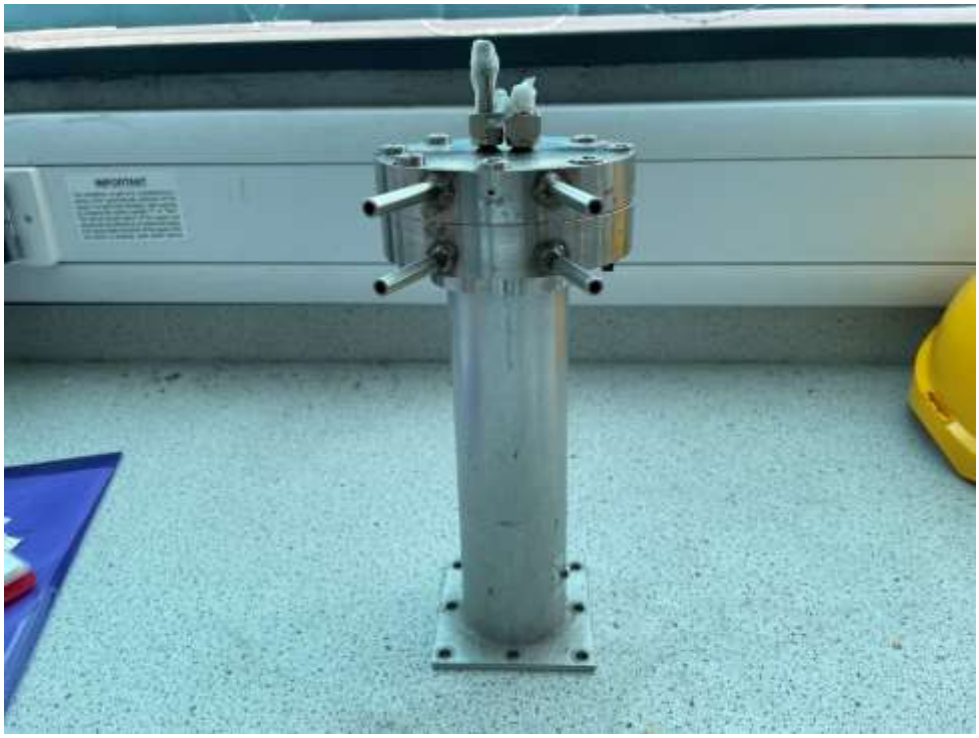


Figure 5.8. Batch reactor

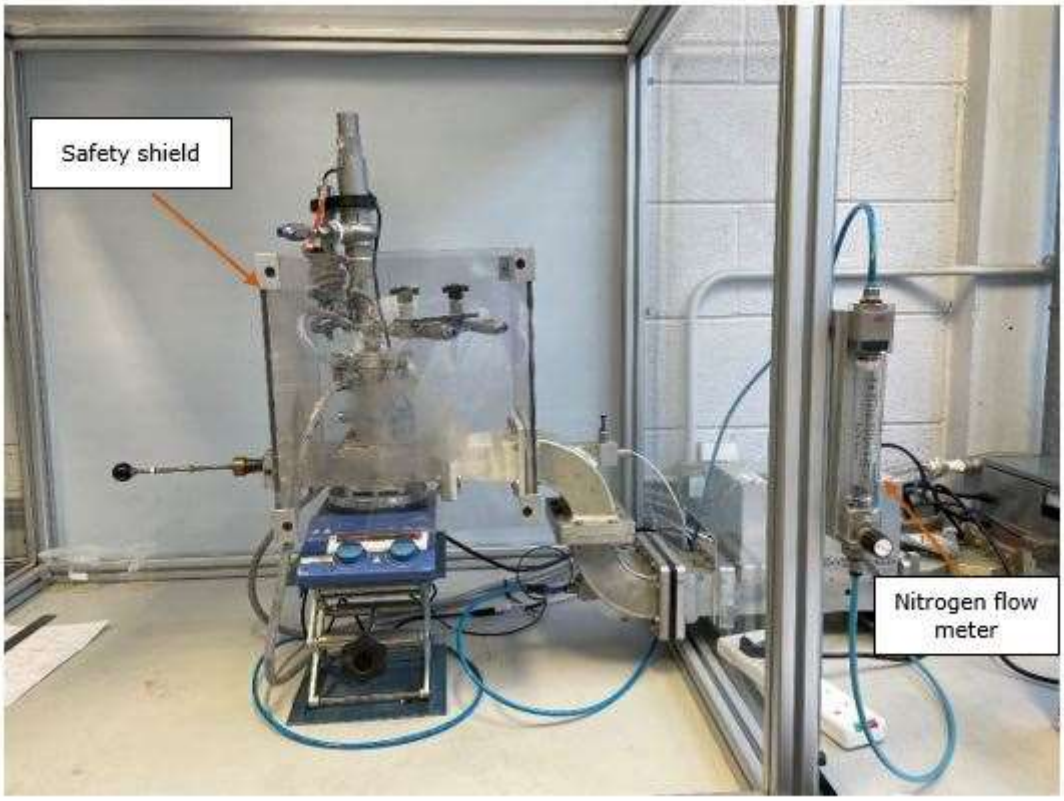


Figure 5.9. Front view of the experimental setup with safety shield



Figure 5.10. Quartz tube

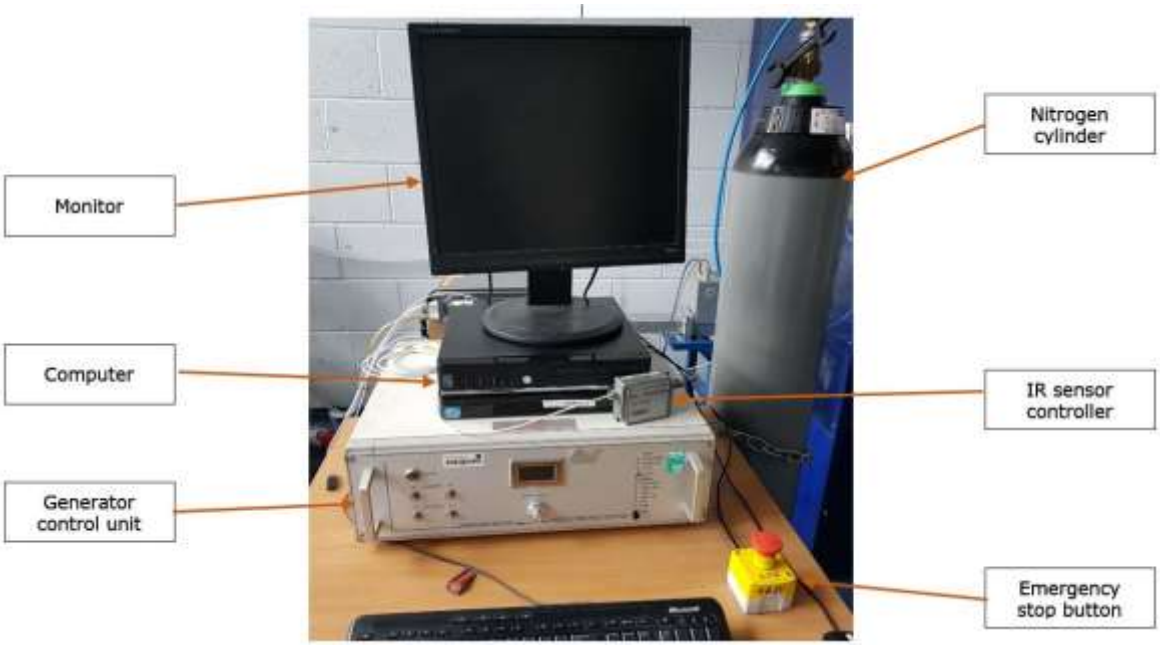


Figure 5.11. Process monitoring and control

In each experiment typically 15 g of oil was mixed with 1.0 g of solid catalyst in the quartz reactor (shown in Figure 5.10). The system was then assembled as shown in Figure 5.7 and Figure 5.9. Prior to heating the reactor was purged with nitrogen. This was performed through the pressure-swing method (CEN/TR 15281:2006) in three cycles up to 2.0 barg. The waveguide and cavity were purged continuously with nitrogen (10 L min^{-1}) during microwave heating for safety purposes in order to maintain an inert environment in case of reactor failure. The heating rate and temperature were controlled during the experiments by manually changing the microwave power input, using generator control unit shown in Figure 5.11.

After heating, the reactor and its contents were left to cool down to room temperature. Before taking the reactor out of the cavity gas samples were collected in 12 mL glass sampling vials (Labco Exetainer, Lampeter, UK) (shown in Figure 5.12). The treated oil was poured into a conical centrifuge tube leaving most of the solid catalyst in the reactor. Fine particles in the oil were settled at the bottom of the tube after centrifuging at 3900 RPM for 30 minutes. The oil was then poured into a glass vial and stored for further analysis. The spent catalyst was washed

with xylene until no further colour change was observed, then dried in a vacuum oven at 100 °C and stored for further analysis.



Figure 5.12. Gas sample vials



Figure 5.13. Washing the spent catalyst

5.4 Characterization

The density of the oil and water were measured using a 5 ml Fisherbrand glass pycnometer (as shown in F) according to ASTM D5355-95. The specific gravity of crude oil is defined as the

ratio of the density of oil to that of water. Both densities are measured at standard conditions (Ahmed, 2001).



Figure 5.14. 5 ml Fisherbrand glass pycnometer

The density and specific gravity are used extensively in the oil and gas industry. However, the American Petroleum Institute (API) gravity is the preferred density scale. The API gravity is related to the specific gravity of oil and was calculated accordingly via the following formula:

$$\text{API gravity} = \frac{141.5}{\text{Specific Gravity}} - 131.5$$ (Ahmed, 2001)

The API gravities of crude oils usually ranges from 47 º API for the lighter crude oils to 10 º API for the heavier asphaltic crude oil (Ahmed, 2001).

The oil viscosity is an important physical property that controls and influences the flow of the oil through porous media and pipes. In general, the viscosity is defined as the internal resistance of the fluid to flow. It is a strong function of the temperature, pressure, oil gravity, gas gravity, and gas solubility (Ahmed, 2001).

The oil viscosity was measured in a cone and plate viscometer (NμLine, ATAC, Wiltshire, UK). Figure 5.15 shows the viscometer used in this study, in which fluid is sheared between a shallow cone (< 2 ° angle θ) and fixed plate which is usually temperature controlled.



Figure 5.15. NµLine, ATAC cone and plate viscometer

Figure 5.16 shows a schematic of the cone and plate geometry for viscometer. The shear rate is the linear velocity of the cone surface divided by the gap at that point. Using a conic probe allows for a constant shear rate across the width of the sample because shear rate is a function of the cone speed and the angle. Shear stress is the shear force per unit area. The viscometer calculates the viscosity via dividing shear stress by shear rate (ATAC Group, 2023). The viscosity of oil was measured at atmospheric pressure, 20 ºC, and 20 rpm for this study.

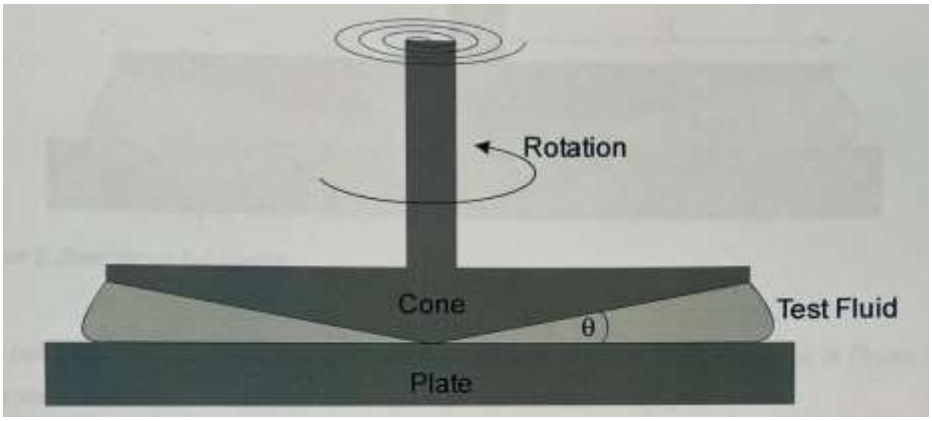


Figure 5.16. Cone and plate geometry for viscometer (ATAC Group, 2023)

The sulphur content of the treated oil was measured using a calibrated energy-dispersive X-ray fluorescence spectrometer XFS (Epsilon 3, PANalytical B.V, Almelo, Netherlands) following ASTM D4294-16.

The composition of the gas produced after the microwave processing was determined by using gas chromatography (Clarus 580 GC, PerkinElmer, Inc., US) equipped with a flame ionization detector (FID) and a thermal conductivity detector (TCD) for determination of the hydrocarbon and non-hydrocarbon gases, respectively. Figure 5.17 shows a basic flow pattern of gas chromatography.

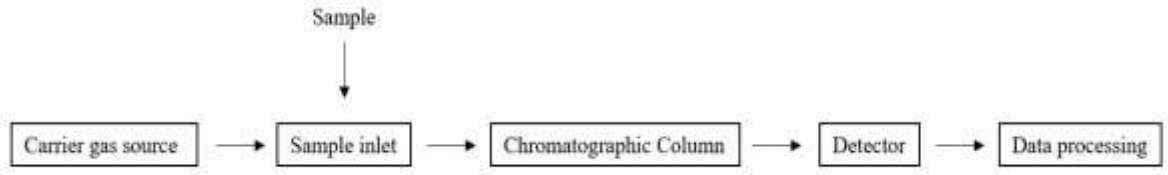


Figure 5.17. basic flow pattern of gas chromatography (Science Direct, 2023)

Gas chromatography (GC) is a column chromatography technique that utilizes an inert gas such as nitrogen, helium, argon, hydrogen, etc. as the mobile phase. The mixed gas is separated based on differences in physical and chemical properties, such as the boiling point, polarity, and adsorption of the substance. The process involves the pure carrier gas source, sampling inlet, chromatographic column, and detector (for separation over time). The signal output value of the detector changes to respond to the components, as the components pass through. Figure 5.18 shows an example of the change in output value in response to gas sample components obtained from microwave-assisted catalytic upgrading experiments in this work. The obtained chromatograms were recorded and processed in an interactive software, TotalChrom (Clarus 580 GC, PerkinElmer, Inc., US).

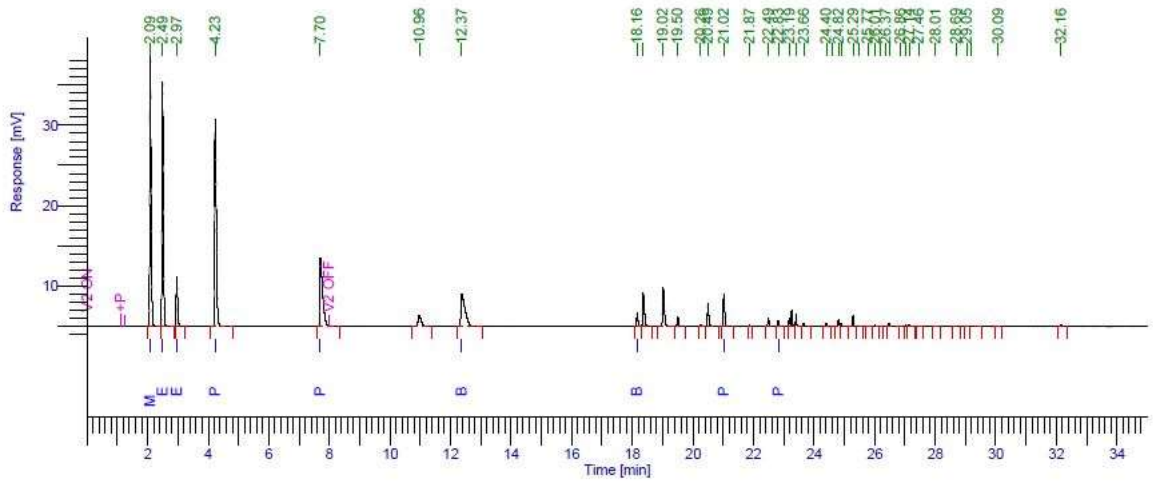


Figure 5.18. Changes in output value of GC in response to gas sample components (each peak in the graph above represents a different component)

Gas sorption analysis for fresh and spent HDS catalyst was carried out using a Micromeritics 3Flex instrument (Micromeritics Instrument Corp., USA).

The Micromeritics 3Flex instrument (shown in Figure 5.19) is a high-performance analyser for measuring surface are, pore size and pore volume of powders and particle materials. Standard methods or used customised protocols can be utilised to characterize a wide variety of porous and non-porous materials such as catalysts. The 3Flex is ideally suited for gas and vapour adsorption analysis of microporous (< 2nm) and mesoporous (2 to 50 nm) materials. It has three microprobe ports that can be used to characterise 3 samples simultaneously, within a single run (Micromeritics, 2023).

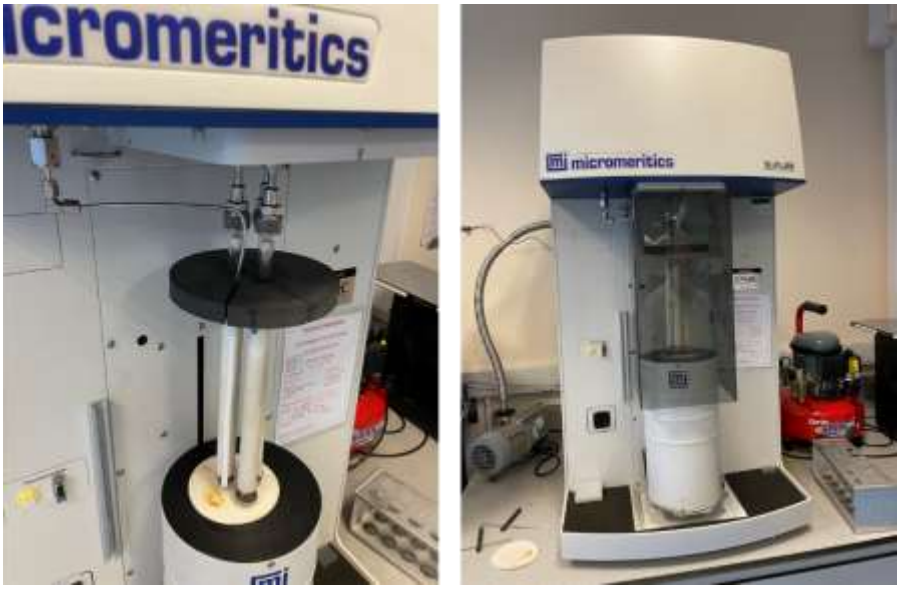


Figure 5.19. The Micromeritics 3Flex instrument

Prior to analysis, the catalyst samples were outgassed at 120 °C overnight under vacuum conditions in order to remove moisture content within the catalyst (as shown in Figure 5.20). N2 adsorption isotherms were obtained at -196 °C.

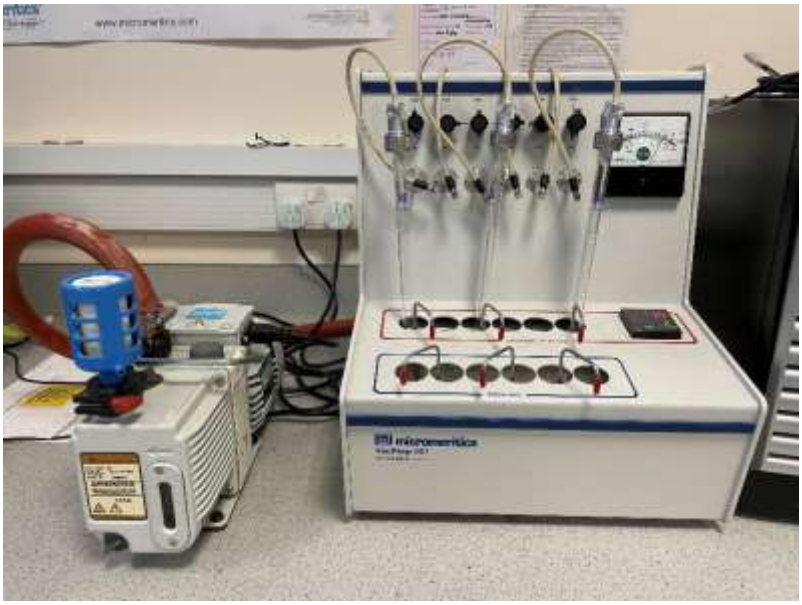


Figure 5.20. Outgassing and vacuuming the catalyst

The Brunauer–Emmett–Teller (BET) model (Brunauer, Emmett, & Teller, 1938) was used for calculating the specific surface area. The calculations were performed using interactive data analysis software, 3Flex analyser V.5 (Micromeritics Instrument Corp., USA).

The coke content of the spent catalyst was determined using thermogravimetric analysis (TGA 550, TA Instruments, US). The 550 TA thermogravimetric analyser measures weight change (either loss or gain) and the rate of weight change as a function of temperature, time, and atmosphere. The common usages of the TGA includes thermal and oxidation stability of the materials, moisture and volatile contents, composition of multicomponent materials, decomposition kinetics and estimated lifetime of a product, and effect of reactive or corrosive atmospheres (TA Instruments, 2023). The samples were heated under air flow to 900 °C at 10 °C min^{-1}, and held at 900 °C for 20 min. Coke content (hard coke) was identified as the mass loss above 520 °C (Hart, Lewis, White, Greaves, & Wood, 2015).

Sulphur deposition on the spent catalyst was determined by using a sulphur analyser (SC632, Leco Corp., USA). SC632 sulphur analyser series determine sulphur content deposited on material using direct combustion/infrared detection. It allows for performing sulphur analysis for many applications including coal, coke, cement, soil, and fuel oil (Leco Corporation, 2023).

The sulphur content of the treated oil and sulphur deposition on the spent catalyst, and the coke content of the spent catalyst were analysed by Dr. Mohamed Adam.

5.5 Results and discussion

5.5.1 Dielectric properties

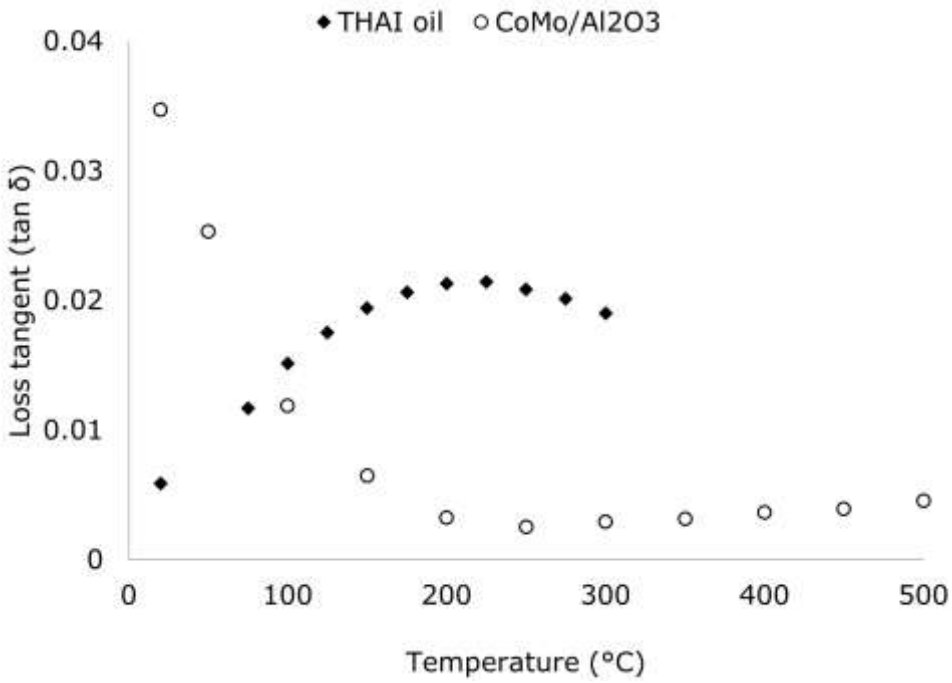


Figure 5.21. Dielectric loss tangent of the CoMo/γ-Al_2O_3 catalyst and the THAI oil (Adam, et al., 2020)

Figure 5.21 shows the loss tangent of the THAI oil and the CoMo/γ-Al_2O_3 catalyst as a function of temperature (Adam, et al., 2020). As it was discussed earlier, dielectric properties define the interaction of the material with the electromagnetic field. The dielectric constant is a measure of the ability of the material to be polarised and store electromagnetic energy, whilst the loss factor defines the material's ability to convert electromagnetic energy into heat. The loss tangent (tan δ), which is the ratio of the loss factor to the dielectric constant, is a measure of the efficiency of energy conversion. The loss tangent of the THAI oil was calculated using the dielectric constant and the loss factor data from study by Zhang et al, (2018). The dielectric properties of CoMo/γ-Al_2O_3 catalyst were measured at temperatures from 20 to 500 ºC.

It can be seen in Figure 5.21 that that the loss tangent of the catalyst gradually drops with temperature up to 200 °C, above which it stays low with no significant change. This drop in

the loss tangent with temperature can be attributed to the moisture evaporation as water is considered a good microwave absorber. The loss tangent of the THAI oil, on the other hand, increases with temperature, reaching a peak at around 200 – 250 °C. The increase of the loss tangent of the oil with temperature is linked to a corresponding reduction in its viscosity, whereas the drop above 250 °C is attributed to evaporation and transition in relaxation frequency (Zhang, et al., 2018). Also, the results shown in Figure 5.21suggest that above 100°C or when a dry catalyst is used microwaves will selectively heat the heavy oil in an oil-catalyst ($CoMo/\gamma\text{-}Al_2O_3$) mixture.

5.5.2 Heating profile

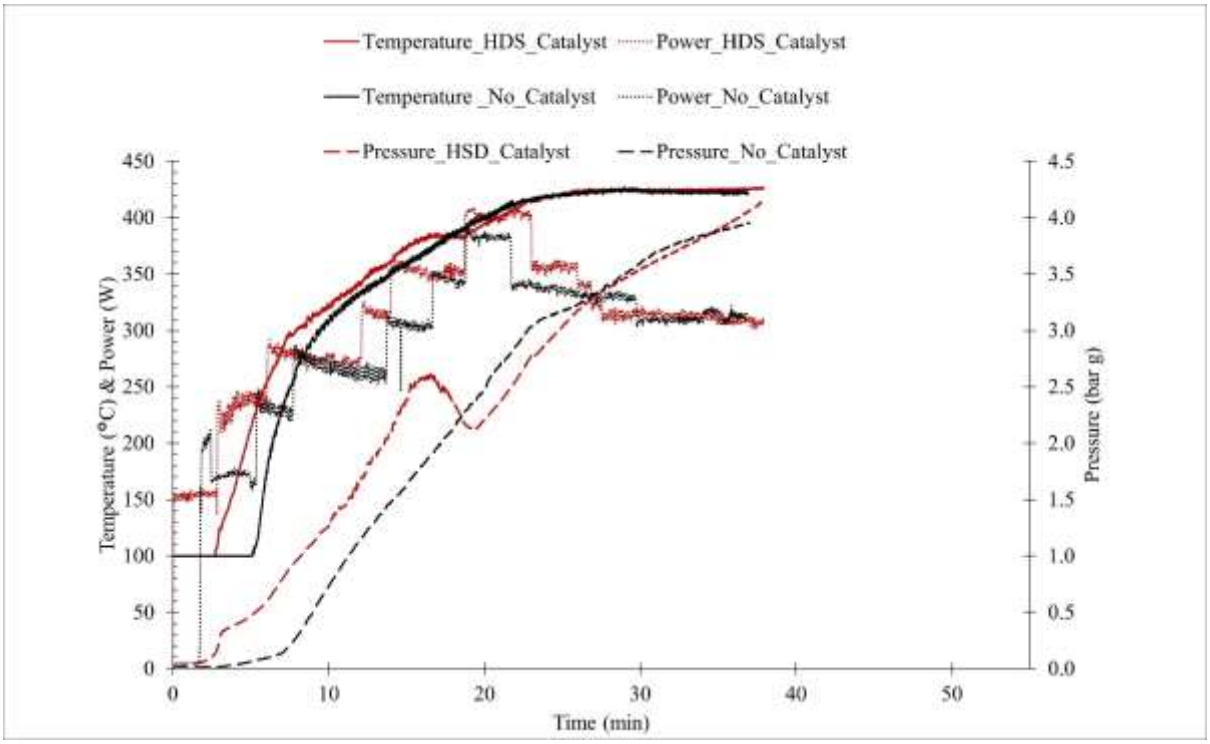


Figure 5.22. A typical power, temperature, and pressure profile during microwave heating of the heavy oil with and without using HDS catalyst

Figure 5.22 displays a typical power, temperature, and pressure profile during microwave heating of the heavy oil. It shows that under the applied power profile it was possible to heat the heavy oil, with and without using HDS catalyst, to the target temperature of 425 °C in about

30 minutes. Heating in the range between 100 °C to 300 °C is the fastest which can be linked to the dielectric properties of the Oil and HDS catalyst. Despite the increase in absorbed power, the decreasing rate of temperature rise above 300 °C can be attributed to the boiling/condensation cycles of the lighter fractions within the oil. The increase in heat loss to the surroundings, due to the increase in temperature difference, is another reason for the slowing-down of the rate above 300 °C. The results shown in Figure 5.22 demonstrate, contrary to previous assertions that heavy oil can be heated to such high temperatures with no need for an additional microwave susceptor. Figure 5.22 also shows that the temporal profile of the pressure within the batch reactor increases, with a constant rate, during the heating of the heavy oil when no catalyst is used. However, a pressure drop (from 2.6 to 2.1 bar g) can be noticed at temperatures around 385 °C, from 16^{th} to 20^{th} minutes of the heating when the HDS catalyst is used. The temperature remained constant during this period when the HDS catalyst is used. It can be seen that pressure and temperature start to increase form 20^{th} minutes of the heating. The change in pressure profile during the use of HDS catalyst for microwave-assisted heating can be attributed to chemical reactions taking place within the batch reactor. This will be investigated in more detail in Chapter 6.

5.5.3 Catalytic upgrading and catalyst activity

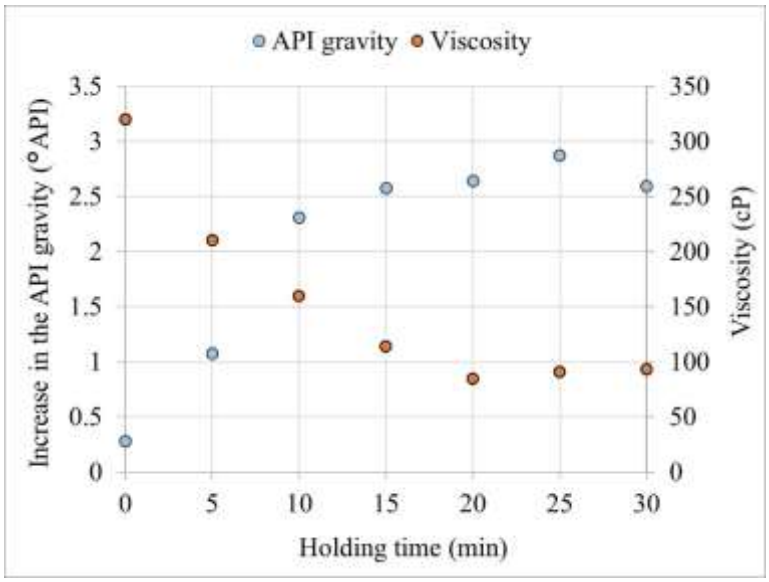


Figure 5.23. Effect of holding time at 425 °C on API gravity & viscosity

The degree of upgrading at 425°C was evaluated by running a series of batch microwave heating experiments. The HDS catalyst with 212 – 600 µm particle size (1.0 g), as well as THAI oil (15 g) were used for experiments in this Section. Figure 5.23 and Figure 5.24 show the effect of holding time on the degree of upgrading and desulphurization using a catalyst with particle sizes in the range 212 – 600 µm. It can be seen in Figure 5.23 that the API gravity increased with time up to 15 minutes, beyond which no further significant increase could be seen. The viscosity of the THAI oil dropped from 325 cP to less than 100 cP with the holding time. The level of upgrading after 15 minutes holding time did not change substantially which can be attributed to catalyst deactivation due to pore blockage and loss of activity as will be discussed in further detail later in this chapter. It can be seen in Figure 5.24 that the increase in API gravity and reduction of viscosity were correlated correspondingly with desulphurization of the treated oil and an increase in sulphur deposition on the spent HDS catalyst.

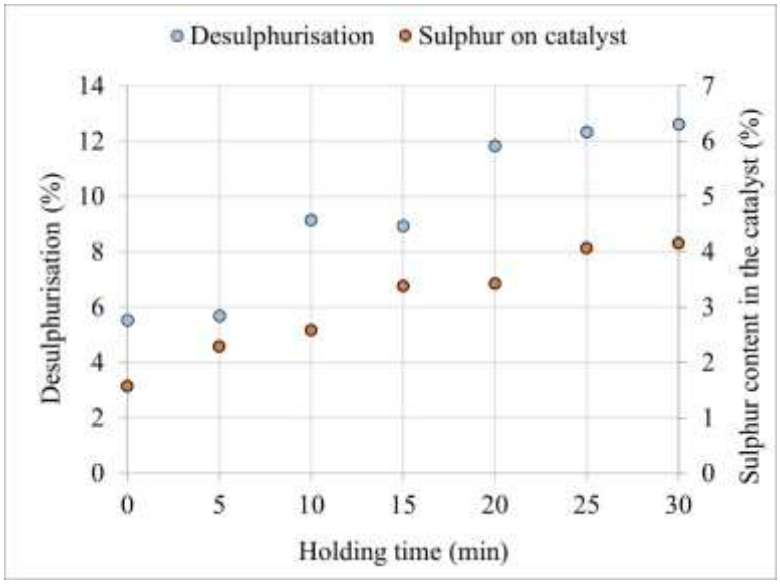


Figure 5.24. Effect of holding time at 425 °C on sulphur content

Raybaud & Toulloat (2013) reported that sulphided CoMo catalysts have better HDS activity compared to unsulphided catalysts. This means that sulphur deposition on the solid catalyst could be useful. They also reported that one of the strategies for sulphidation of HDS catalysts is heating them in sulphur-containing hydrocarbons. This explains the sulphur deposition on HDS catalyst used for thermal catalytic upgrading of heavy oil (containing 3.2 wt. % sulphur) in this study. Two following competing factors can be identified in influencing the activity of the catalyst in the current situation: (a) the increase in the degree of sulphidation, which improves the catalyst activity and (b) the pore blockage due to coke deposition, which makes the active sites unreachable by the reactants.

In order to evaluate the catalytic activity of the HDS catalyst, γ-Al_2O_3 (Alumina) support was employed for a series of batch microwave heating experiments. Table *5.3* shows results obtained under similar conditions using the HDS and Alumina at 425 °C and 15 minutes holding time. The obtained results shows that higher API gravity and lower viscosity was achieved when γ-Al_2O_3 was employed, compared to when CoMo/γ-Al_2O_3 catalyst was used. However, higher desulphurization was obtained when the HDS catalyst was used.

Table *5.3* also displays variations in the gas composition between the two cases indicating variations in the process chemistry. The gas composition arising from use of Alumina is a typical product of thermal cracking while that arising from use of $CoMo/\gamma\text{-}Al_2O_3$ is typical of the composition of gases originating from catalytic cracking (acid-activated) (Greensfelder, Voge, & Good, 1949). In general, thermal cracking gives high yields of C_1 and C_2 gases (methane, ethane, and ethylene), whereas C_3- C_6 are the major light hydrocarbon products in catalytic cracking (Greensfelder, Voge, & Good, 1949).

Table 5.3. Comparison of the performance of CoMo/γ-Al_2O_3 to that of γ-Al_2O_3 (Experiments were run under similar conditions at 425 °C and 15 minutes holding time with particles of 212 – 600 µm size)

	CoMo/γ-Al_2O_3	γ-Al_2O_3
Increase in API	2.58 ± 0.14	3.03 ± 0.06
Viscosity (cP)	114.1 ± 1.16	86.50 ± 7.71
Reduction in sulphur (%)	8.90 ± 0.41	6.71 ± 0.35
Sulphur deposition on solid (%)	3.38 ± 0.12	0.70 ± 0.06
Gas composition (mole %)		
Methane	0.018	12.792
Ethane	0.013	5.753
Ethene	0.000	1.226
Propane	0.013	4.139
Propene	0.007	2.436
Butane	0.005	0.000
Butene	0.002	0.633
Pentane	0.003	0.500
Pentene	0.015	0.427
Hydrogen	18.879	0.779
Carbon dioxide	0.632	1.036
Carbon monoxide	0.790	1.065
Hydrogen sulphide	6.782	11.896

A significantly higher hydrogen content occurred in the CoMo/γ-Al_2O_3 produced gas when compared to that for γ-Al_2O_3 as can be seen in Table *5.3*. Hart et al, (2020) reported that, in an inert atmosphere (nitrogen), CoMo/γ-Al_2O_3 induces dehydrogenation, whereas, under a hydrogen atmosphere it catalyses hydrogenation. The induced dehydrogenation by CoMo/γ-

Al_2O_3 in this study allowed unsaturated compounds to be produced. This explains the lower API obtained by using the HDS catalyst compared to results obtained by using Alumina for the equivalent experiments.

Table *5.3* also shows that the HDS catalyst was more active in desulphurisation of the treated oil compared to Alumina. On the other hand, the HDS catalyst produced less hydrogen sulphide compared to the Alumina support. Also, the results shows that higher sulphur was deposited on the spent HDS catalyst compared to the spent Alumina support. It can be concluded that, when HDS catalyst was employed, the sulphur content in the treated oil was first converted to H_2S. The produced hydrogen sulphide was then led to considerable sulphur deposition on the HDS catalyst.

Hart et al, (2014) reported that as well as its ability to improve the API gravity and reduce viscosity, hydrogen can reduce coke formation and deposition on the catalyst. Table *5.3* shows that the HDS catalyst has produced approximately 19 % hydrogen in the gas product, compared to less than one percent hydrogen content in the produced gas when Alumina was used. The produced gas composition, with a particular focus on the quantity and origin of the produced hydrogen content, will be studied in more detail in Chapter 6, where a low temperature shift (LTS) catalyst will be employed for microwave-assisted catalytic upgrading experiments.

5.5.4 Effect of particle size on upgrading

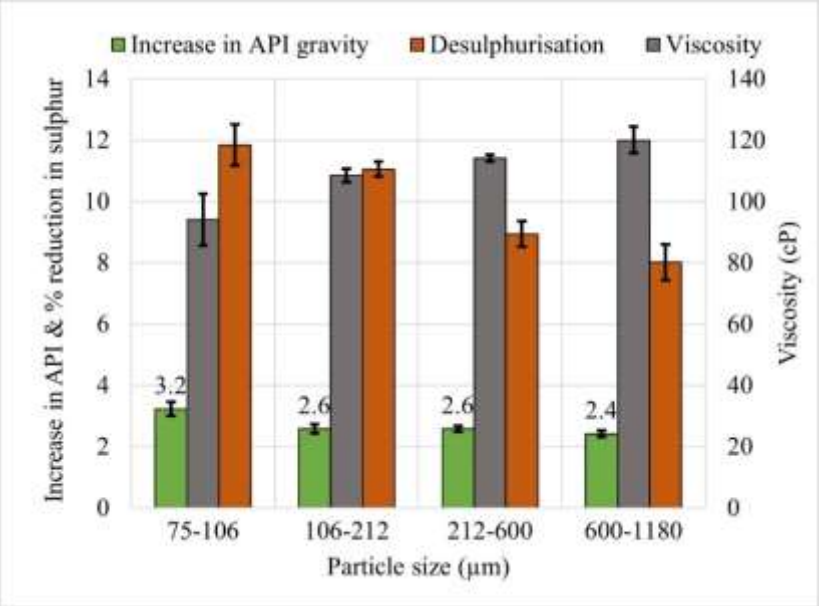


Figure 5.25. Effect of particle size on API gravity, viscosity & desulphurisation (HDS catalyst)

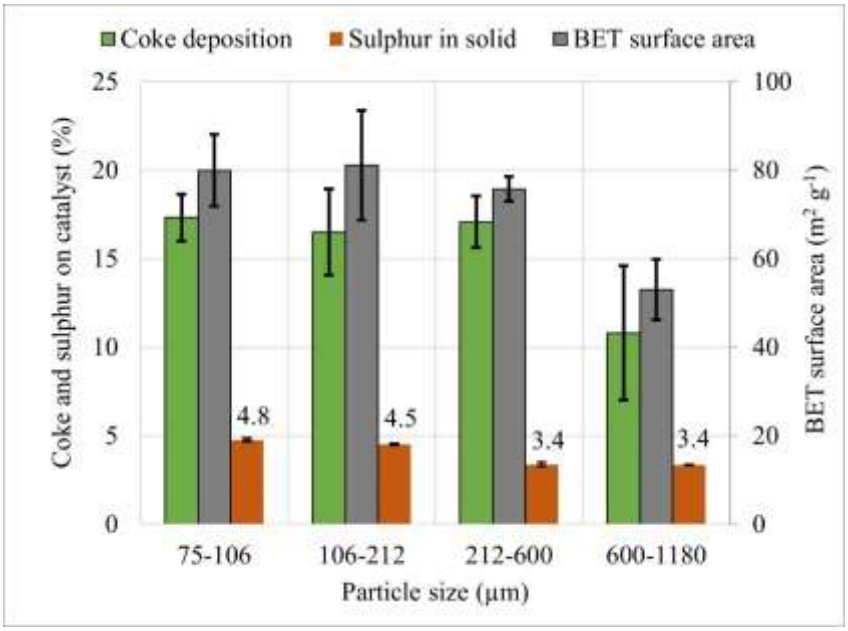


Figure 5.26. Effect of particle size on coke and sulphur deposition, and BET surface area of the spent catalyst using (HDS catalyst)

In this section, the effect of coke deposition on the catalyst porosity and activity was further investigated. Compared to conventional oil and lighter hydrocarbons, heavy oils have a higher

tendency to produce coke during thermal treatment, which can lead to pore blockage and loss of activity when deposited on the catalyst. Hence, gas absorption and TGA analysis, as well as a sulphur analyser were employed to characterise fresh and spent catalyst samples.

Figure 5.25 and Figure 5.26 display the effect of particle size on the catalytic activity and the catalyst performance (results are at 425 ºC and 15 minutes holding time). Figure 5.25 shows that using smaller particles leads to better upgrading, i.e. higher API, lower viscosity and higher desulphurization. Upgrading with up to ~3.2° increase in API, ~90% reduction in viscosity to less than 100 cP, and ~12% reduction in sulphur content (desulphurisation) were achieved when 75-106 µm particles were used. Figure 5.26 shows that coke and sulphur deposition on the spent catalyst is higher for smaller particles, which is in line with the catalytic activity and improvement in the degree of upgrading noted from Figure 5.25. However, as can be seen in Figure 5.26, larger particles demonstrate lower surface area despite their lower catalytic activity and smaller coke deposition. The results presented here, as well as additional analysis by Adam et al, (2020), indicate that most of the coke deposition happens on the outer layers of the catalyst particle.

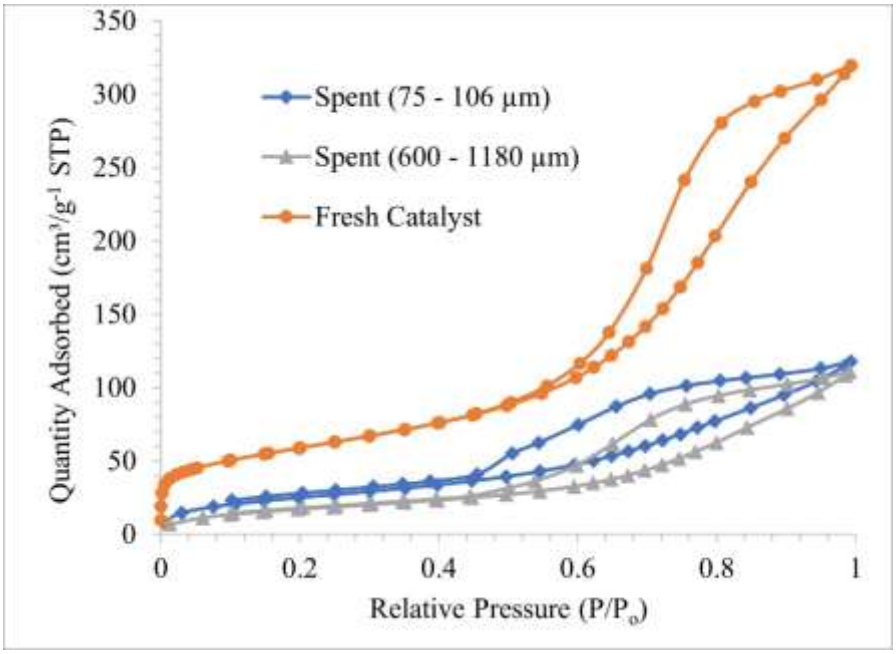


Figure 5.27. N_2 sorption isotherms for the fresh and spent HDS catalyst

Figure 5.27 displays N_2 isotherms of fresh and spent HDS catalysts. A sharp increase in the gas uptake at low pressure can be noticed in the case of fresh catalyst, which indicates the presence of micropores. However, the spent catalysts do not have the same sharp increase at low relative pressure, which suggests that the majority of the micropores have been filled, or their access blocked, with coke. Adam et al, (2020) found that the spent HDS catalysts experienced over 70% reduction in their micropore volume based on that of the fresh catalyst.

In summary, the obtained results shows that catalyst particle size has a direct impact on the degree of upgrading. It was due to a larger external surface available for catalytic reactions when a smaller particle size was employed. The viscosity reduction was linked to API upgrading and the highest reduction in viscosity occurred when the smallest particle size was used. Additionally, the highest desulphurisation was achieved by using the smallest particle size. Likewise, the larger available surface area facilitated the sulphur deposition on the smaller particle size. In catalytic heavy oil refining, coke deposition and its effect on the activity of HDS catalysts remains one of the challenges that requires further research. Adam et al, (2020)

reported that one of the options to improve intra-particle diffusion and avoid coke deposition on the external layers is either using smaller catalyst particles and/or engineering catalysts with more uniform larger pore sizes as mentioned earlier. However, both options may have their disadvantages (separation difficulties and reduction in surface area, respectively). Hart et al, (2014) found that, alongside further upgrading and desulphurisation, hydrogen may reduce coke formation and deposition on the catalyst. As injecting hydrogen into the reservoir could be a challenging and costly task, further work is required to examine hydrogen production downhole, which will be discussed further in Chapter 6.

5.6 Conclusion

This study demonstrated that microwave heating could provide the additional required heat for a successful THAI-CAPRI process. It was shown that, without adding a microwave supplemental susceptor, temperatures up to 425 °C could be achieved. Upgrading in API gravity with more than 3.2° increase, 90% reduction in viscosity to less than 100 cP, and more than 12% reduction in sulphur content was achieved using a commercially available HDS catalyst.

Alumina support demonstrated a better upgrading and viscosity reduction performance compared to the HDS catalyst. This was due to dehydrogenation induced by the HDS catalyst. However, it was found that the HDS catalyst is more active in desulphurisation of the treated oil, compared to Alumina support. Higher amount of sulphur was deposited on the spent HDS catalyst compared to the spent Alumina support, resulting in less H_2S content in the produced gas. Majority of the hydrogen sulphide generated via the chemical reactions was produced in gas form when Alumina support was employed. This indicate that HDS catalyst has experienced sulphidation by sulphur transfer, via H_2S, from the treated oil to solid catalyst.

Gas sorption analysis was performed to analyse pore network connectivity within fresh and spent HDS catalyst. It was demonstrated that the spent HDS catalyst has experienced significant reduction in their porous volume. Further analysis showed that coke deposition led to blockage of most of the porous volume that initially existed in the fresh HDS catalyst.

With increasing hydrogen demand across the globe, further cost-effective hydrogen production technologies are required to be developed. The high hydrogen content in the produced gas in this study demonstrated that the THAI-CAPRI process could potentially be a new route for in-situ hydrogen production form heavy oil reservoirs. However, further research is required to examine the mechanisms involved in hydrogen production via the microwave-assisted THAI-CAPRI.

6. In-situ hydrogen production via the microwave-assisted THAI-CAPRI

Environmental concerns with regard to hydrocarbon consumption, as fuel, have shifted attention to cleaner energy supplies. Hydrogen, the most abundant element in the universe, is essential for several chemical processes such as hydrogenation, hydrocracking, and hydrotreating. H_2 could also be combusted as fuel, leaving steam, the cleanest combustion by-product, behind. The characteristics of the toe to heel air injection (THAI) process are suitable not only for in-situ upgrading but for hydrogen production downhole as well. Compared to other commercial and experimental in-situ combustion processes, a combination of the produced hydrogen and methane, at high values, has not been seen anywhere but through the THAI process. Employing the catalytic add-on of the THAI process (the CAPRI process) could potentially result in even higher in-situ hydrogen production. Previously, we demonstrated the upgrading capacity of the CAPRI process at experimental scale by a microwaved-assisted catalytic upgrading batch reactor. In this study, the hydrogen production potential of the CAPRI process was investigated further. A commercial low shift temperature ($ZnO/CuO/Al_2O_3$) catalyst were used for a new series of the upgrading experiments. The experimental results were compared to those previously obtained from employing either a hydrodesulphurization ($CoMo/\gamma\text{-}Al_2O_3$) catalyst or an Alumina support.

6.1 Introduction

Russia's invasion of Ukraine in early 2022 has amplified energy security concerns, with physical supply constraints for natural gas in Europe and a surge in natural gas prices, following a price surge in the second half of 2021, as demand recovered from the COVID-19 pandemic. This has changed the economics of producing hydrogen from natural gas, for both with and without carbon capture utilisation storage (CCUS) (Internation Energy Agency (IEA), 2023).

Global hydrogen demand in 2021 was 94 Mt, a 5 % increase from 2020. There was a considerable increase in low-emission hydrogen production in 2021 (almost 20 % increase compared to 2020, including hydrogen from natural gas with CCUS and water electrolysis). However, the production of renewable based hydrogen is very low, accounting for approximately 0.1 % of the total H_2 production. More than 80 % of hydrogen is produced from fossil fuels, with remainder largely from refineries where hydrogen is produced as a by-product of processes that use fossil fuels as inputs (Internation Energy Agency (IEA), 2023; Cho, Strezov, & Evans, 2023).

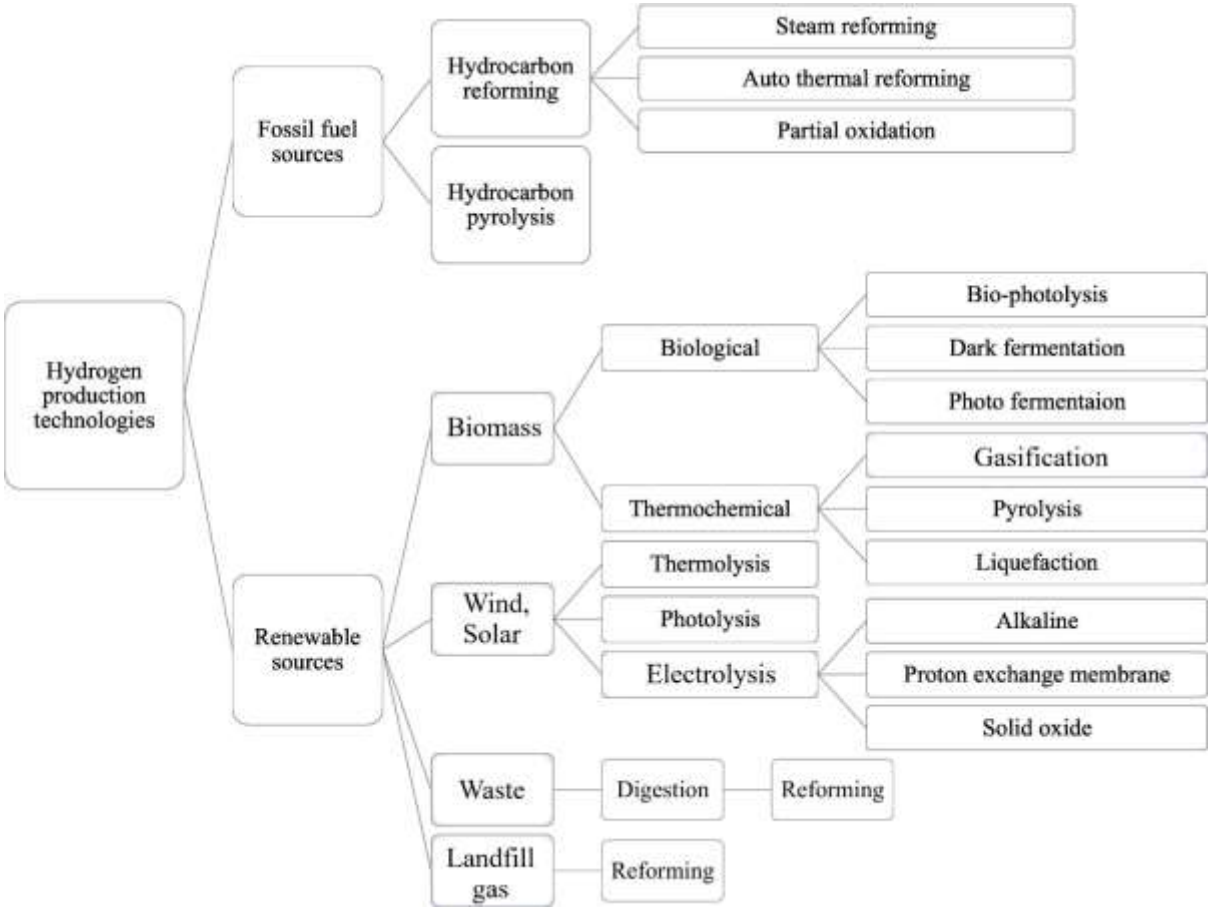


Figure 6.1. Hydrogen production technologies (Cho, Strezov, & Evans, 2023)

Cho et al, (2023) reviewed hydrogen production technologies (shown in Figure 6.1) from the fossil fuel and renewable sources. The IEA (2021) reported the cost of hydrogen production by technology in 2021, 2030, and 2050. It must be noted that the ranges of hydrogen production

cost estimates in the IEA report reflect the regional variation in costs and renewable resource conditions. The published data showed that hydrogen production from fossil fuels will remain the cheapest H_2 production process until at least 2050.

Steam reforming of natural gas is the most commonly used hydrogen production technology. In reforming of natural gas, steam reacts with methane in the presence of a catalyst at temperatures between 700 and 1100 ºC generating synthesis gases (CO_2 and H_2) (Kapadia , Kallos, & Gates, 2011). In steam reforming, additional hydrogen can be recovered from steam via the water gas shift reaction (WGSR). This requires an excessive amount of water to be employed. Kapadia et al, (2011) reported the other challenges associated with the steam reforming of methane as following:

a) Steam reforming of natural gas uses large quantities of methane.
b) It generates excessive carbon dioxide which is often emitted to the atmosphere.
c) The process of steam reforming of natural gas requires high temperature and pressure.
d) It involves multiple catalytic steps to make the process cost and energy efficient.

The recent development in carbon capture, utilisation, and storage (CCUS) technologies may address the CO_2 emissions associated with the steam reforming of methane. However, other concerns with regards to the hydrogen production via the steam reforming of natural gas still remain to be addressed.

Demand for hydrogen in new applications such as in the heavy industry, transport, power generation, and the building sectors, was very low (about 0.04 % of global hydrogen demand) in 2021. Most of the recent increase in hydrogen demand has been from traditional applications such as in chemicals, with 3 Mt increase (taking it to 54 Mt), and in refining, with about 2 Mt increase (taking it to 40 Mt) from 2020. Refineries use hydrogen to remove impurities such as sulphur and to upgrade heavy fractions into lighter products. Hydrogen demand in refining

reached its historic maximum at 40 Mt in 2018 (when refinery throughputs were at their all-time peak) and once again in 2021 (led by recovery in global crude processing from COVID-19 pandemic). Almost all the hydrogen used in refineries is produced from unabated fossil fuels, resulting in more than 200 Mt CO_2 emitted in 2021 (International Energy Agency, 2021).

Hydrogenation (adding hydrogen) and decarbonization (removing carbon) are two main reactions involved in heavy oil upgrading technologies. Decarbonization reactions are often used in refineries such as delayed coking, while hydrogenation reactions are often used in combination with various catalysts. The former involves inhibiting the generation of carbon or coke because heavy oil has a high carbon and hydrogen ratio, resulting in a light oil with a low carbon and hydrogen ratio. In the latter reaction, the yield of liquid products increases due to hydrogenation, while suppressing the formation of coke (Zhao, et al., 2022).

Processing the produced heavy oil requires its transfer from the production facilities to the refineries or upgrading units. It cannot be done without the reduction of heavy oil viscosity to a value that ensures its transportation by pipelines (250 cSt at 100 °F or 225 cP at 37 °C). Therefore, excessive amounts of energy are required to overcome the high-pressure drop in pipelines due to the high viscosity of heavy oil. This challenge has motivated the development of new technologies to improve the flow properties of heavy oil through three main mechanisms; fraction reduction, viscosity reduction, and in-situ upgrading (Alemán-Vázquez, Torres-Mancera, Ancheyta, & Ramírez-Salgado, 2016).

There are studies in literature, such as patent work by Magine (United States of America Patent No. 4241790, 1980) in which direct hydrogen injection was proposed to decrease the viscosity of crude oil in-situ. Although there have been improvements in industrial hydrogen production, a large amount of hydrogen is needed for such a process. Additionally, hydrogen is a highly

flammable and explosive gas, resulting in issues with its operation and transport. Hence, direct hydrogen injection for hydrogenating heavy oil has rarely been considered as feasible option.

It is now well established that hydrogen production is a constant feature in the THAI process, but not in the conventional in-situ combustion process. In fact, the THAI process is the first ever EOR process to produce underground upgraded oil and hydrogen on a constant basis (Turta, kapadia, & Gadelle, 2020). The THAI process exhibits a short-distance character for oil displacement but has a long-distance behaviour for the oxidation pathway. This is significant for in-situ upgrading, coke deposition mechanisms, and hydrogen production (Turta, Greaves, & Grabowski, 2018). Comparing the gas composition recorded in other commercial and experimental in-situ combustion processes, the main characteristics of the THAI process are the simultaneous production of relatively high percentages of hydrogen, methane, and CO. A combination of these three components at these high values has not been seen anywhere (Turta, Greaves, & Grabowski, 2018). Only when using a particular form of in-situ combustion process, namely pressure cycling ISC with oxygen injection, high hydrogen content in the produced gas was recorded in the Marguerite Lake ISC pilot in Canada (Turta, Greaves, & Grabowski, 2018).

In-situ combustion generates high temperatures which enables hydrogen generation reactions. During the THAI process, since heavy oil, water and oxygen are all present downhole, there are multiple reactions accountable for both the production and consumption of the hydrogen (Kapadia, Kallos, & Gates, 2014). It must be noted that the SARA (saturates, aromatics, resins, asphaltenes) fraction of heavy oil would also influence the gas products after the high temperature steam treatment of heavy oil within the thermal heavy oil recovery techniques (Kapadia, Kallos, & Gates, 2012).

Turta et al, (2020) proposed certain families of reactions that contribute to the production of coke, gas, and treated oil in different capacities, depending upon extent of reaction, which is the function of temperature and pressure. They reported that four categories of hydrogen can be produced in-situ within the THAI process which will be studied in detail below.

1. Pyrolysis (thermolysis or thermal cracking)

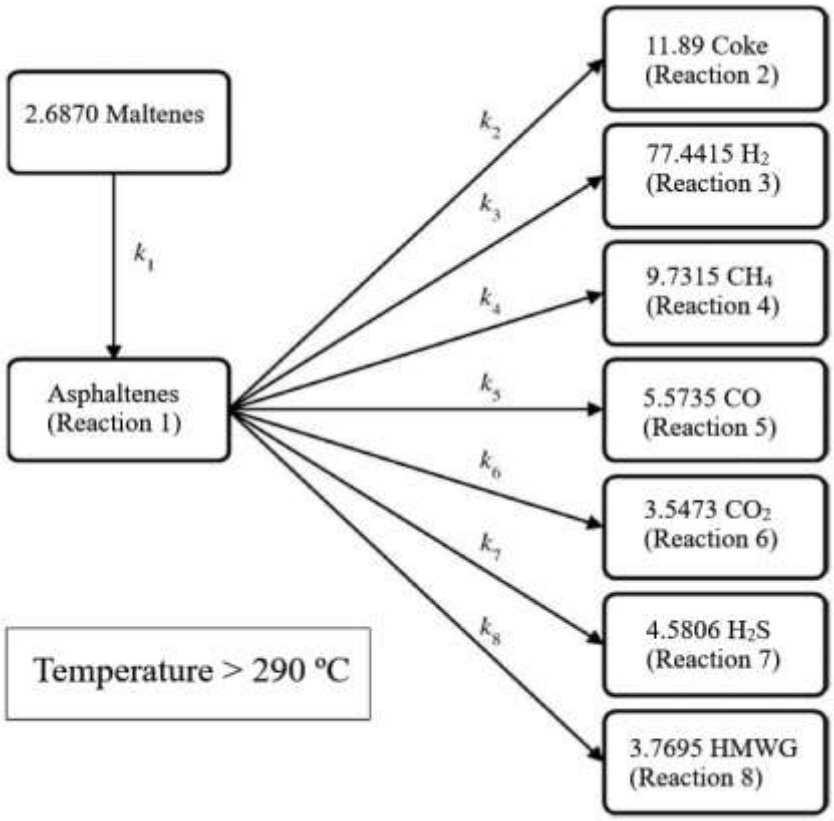


Figure 6.2. Bitumen pyrolysis reaction scheme, taken from (Turta, kapadia, & Gadelle, 2020), High Molecular Weight Gas (HMWG) represents all C2+ combustible gases.

Unlike the conventional in-situ combustion process, the THAI process is a short-distance oil displacement process with a long zone allowing the chemical reactions such as pyrolysis reactions to take place (Turta, kapadia, & Gadelle, 2020). Pyrolysis is the thermochemical decomposition of heavy oil at elevated temperatures in the absence of the oxygen (Kapadia, Kallos, & Gates, 2014). Kapadia et al, (2013) carried out a study to understand and optimize

hydrogen generation by in-situ gasification from bitumen reservoirs. It aimed to examine the potential to generate hydrogen directly from the bitumen reservoirs. They proposed a bitumen pyrolysis reaction scheme, involving two pseudo-components: maltenes and asphaltenes, which are displayed in Figure 6.2. Reactions 2-8 conserve the moles of all elements involved in the reactions (Kapadia, Wang, Kallos, & Gates, 2013). The pyrolysis reaction largely occurs at temperatures greater than 300 ºC. The asphaltene pseudo-component, itself, represents many individual components in the bitumen pyrolysis reaction scheme. Asphaltene can be converted into different products through a parallel reaction system when it reacts (Kapadia, Wang, Kallos, & Gates, 2013).

Kapadia et al, (2011) reported that just beyond the combustion zone, the heavy oil is heated by conduction within the in-situ combustion process. Because the oxygen is not present, the pyrolysis reaction converts maltenes to asphaltene (as shown in Figure 6.2) and then the elevated temperature (surrounding the combustion zone) gasifies asphaltene, which generates hydrogen.

2. Aquathermolysis (hydrous pyrolysis)

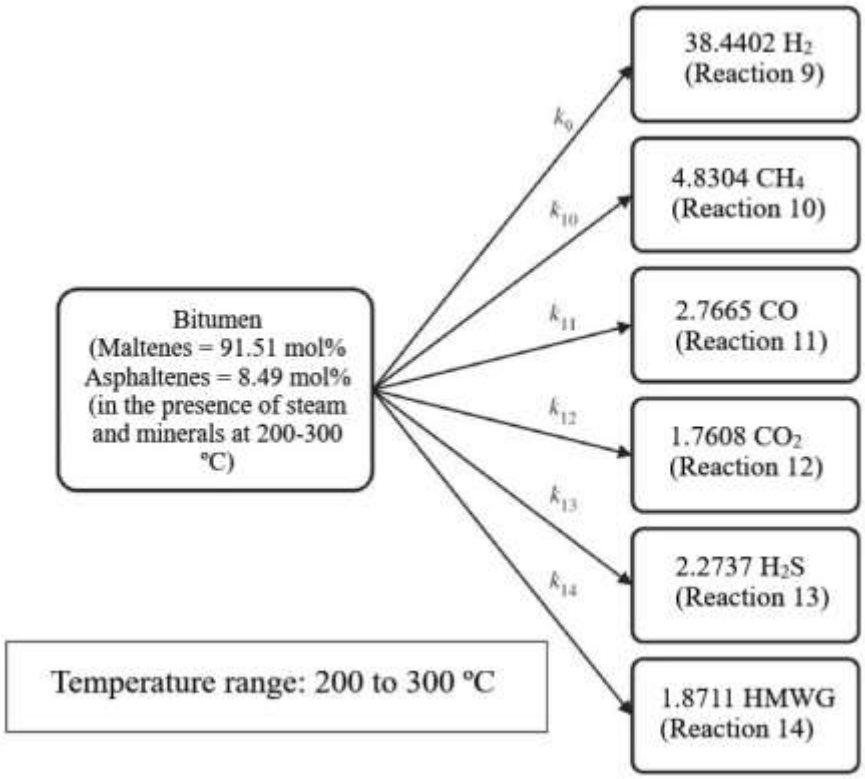


Figure 6.3. Bitumen aquathermolysis reaction scheme, taken from (Turta, kapadia, & Gadelle, 2020), High Molecular Weight Gas (HMWG) represents all C2+ combustible gases.

During in-situ combustion heavy oil recovery processes, pyrolysis, aquathermolysis, and oxidation mechanisms coexist because of coexistence of heavy oil, water, and oxygen in the presence of high temperature and high pressure (Kapadia, Kallos, & Gates, 2014). Aquathermolysis (aqua – water; thermos = heat; lysis = loosing) of heavy oil occurs when it is thermally cracked in the presence of water. The aquathermolysis of heavy oil occurs at the temperature ranges between 200 and 300 ºC (Hajdo, Hallam, Vorndran, & BP Resources Canada Ltd, 1985). The major physical effect of steam, within the in-situ technologies for heavy oil production, is the heating of heavy oil which mobilises it. Along with physical interactions, steam also chemically reacts by aquathermolysis (also referred as hydrous pyrolysis) with heavy oil. Kapadia et al, (2013) proposed the bitumen aquathermolysis reaction

scheme, which is shown in Figure 6.3. Reactions 9-14 conserve the moles of all elements involved in the reactions (Kapadia, Wang, Kallos, & Gates, 2013). The chemical effect consists of steam heating which produces acid gases, such as CO_2, CO, sulphur dioxide, and hydrogen sulphide along with a small amount of hydrogen and methane.

Turta et al, (2020) reported that the effect of the aquathermolysis can safely be neglected during the THAI process because other reactions such as pyrolysis are faster and dominating. The amount of gas produced during the aquathermolysis of heavy oil is less than 1% of that produced during the pyrolysis of heavy oil. Figure 6.4 displays the aquathermolysis and pyrolysis regimes for the system heavy oil and water, which was taken from study by (Kapadia, Kallos, & Gates, 2012).

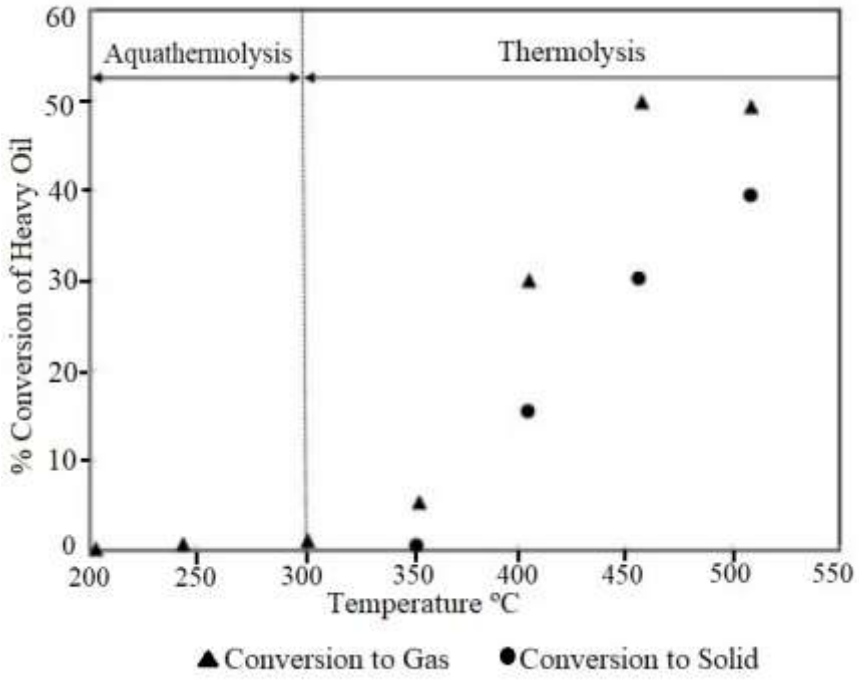


Figure 6.4. The aquathermolysis and pyrolysis regimes for the system of heavy oil and water (Kapadia, Kallos, & Gates, 2012)

3. Coke gasification

There are chemical interactions among the products of heavy oil pyrolysis and aquathermolysis reactions such as coke gasification (Kapadia, Wang, Kallos, & Gates, 2013). Hajdo et al, (1985) conducted adiabatic combustion tube tests in order to better understand the flow and reaction processes that generates hydrogen and thereby to suggest ways of influencing H_2 production via the heavy oil in-situ combustion processes. They concluded that the coke gasification is the most influencing process that generates the largest amount of hydrogen downhole.

Coke is the product of heavy oil pyrolysis (Kapadia, Kallos, & Gates, 2014). The coke gasification plays a significant role in the in-situ hydrogen production in the THAI process. Turta et al, (2020) reported that unlike conventional in-situ combustion, two categories of coke can be formed in the THAI process as following:

a) In-situ coke which is generated close to and burned at the combustion front within the THAI process.
b) Coke generated at high temperature oxidation areas within the THAI process, (other than currently present at combustion front location), so called “leftover coke”.

The in-situ coke may produce very little (negligible) hydrogen within in-situ combustion process. However, at high temperatures, the non-in-situ coke (leftover coke) is predominantly gasified if oxygen is not present (O_2 has already been consumed during the THAI process), and steam and/or carbon dioxide is present; this was, hydrogen is produced. The leftover coke may be burned if oxygen is present, e.g., at the sudden increase of the injected air/oxygen flux during the THAI process. The coke gasification reactions involved producing H_2 are listed below (Turta, kapadia, & Gadelle, 2020):

$C + H_2O = CO + H_2$ *endothermic reaction (Equation 6.1)*

$C + CO_2 = 2CO$ *endothermic reaction (Equation 6.2)*

4. Water gas shift reaction (WGSR)

Water gas shift reactions are other chemical interactions among the products of heavy oil pyrolysis and aquathermolysis reactions within in-situ combustion process (Kapadia, Wang, Kallos, & Gates, 2013). Hajdo et al, (1985) reported the WGSR as following:

$CO + H_2O = CO_2 + H_2$ *exothermic reaction (Equation 6.3)*

The WGSR requires that carbon monoxide and water, as the reactants, are in equal molar volume. There are three possible sources of carbon monoxide, (a) CO generated at the combustion front, (b) CO generated through heavy oil pyrolysis, and (c) CO generated through coke gasification. The CO generated in heavy oil aquathermolysis can be neglected as the total quantities of gasses produced by aquathermolysis are not large (less than 1% for their oil) (Hajdo, Hallam, Vorndran, & BP Resources Canada Ltd, 1985). The WGSR generates CO_2 which could be potentially sequestered in an in-situ gasification process so that emissions to the atmosphere are reduced (Kapadia , Kallos, & Gates, 2011).

Hajdo et al, (1985) reported that the position of equilibrium in the water gas shift reaction favours the products up to 810 ºC, whereas the coke gasification reactions does not favour hydrogen until about 675 ºC is reached. They also reported that CO must flow into a steam-laden region at temperature less than 750 ºC for the WSGR to proceed. Wet in-situ combustion (combined injection of steam and air/oxygen) widens the steam plateau for the WGSR. However, the dry in-situ combustion (injection of steam and air/oxygen only) could generate steam through the connate water in the reservoir (over regions downstream of the combustion front). The WGSR could also occur downstream of the coke gasification zone as long as the zone is wet (Hajdo, Hallam, Vorndran, & BP Resources Canada Ltd, 1985).

It is crucial to distinguish between the generation and production of hydrogen and other gases during in-situ combustion of heavy oil. There is no reason to suppose that the products of the pyrolysis, aquathermolysis, coke gasification, and WGSR reactions (as discussed earlier) are not subjected to further reactions such as oxidation and methanation reactions (Hajdo, Hallam, Vorndran, & BP Resources Canada Ltd, 1985). Hajdo et al, (1985) listed the methanation reactions within in-situ combustion of heavy oil as following:

$C + 2H_2 = CH_4$ *(Equation 6.4)*

$CO + 3H_2 = CH_4 + H_2O$ *(Equation 6.5)*

$2CO + 2H_2 = CH_4 + CO_2$ *(Equation 6.6)*

The methanation reactions consume hydrogen below temperature in the range of 540 to 630 ºC (Hajdo, Hallam, Vorndran, & BP Resources Canada Ltd, 1985). In addition, the generated hydrogen within in-situ combustion of heavy oil can react according to the reverse water gas shift reaction, generating carbon monoxide and water. Also, the generated hydrogen can react with the oxygen in a case of a sudden increase of the injected air/oxygen flux, forming water (Kapadia , Kallos, & Gates, 2011).

The field data on produced gas could assist in investigating how complete the WSGR has taken place in the reservoir throughout an in-situ combustion process. Hajdo et al, (1985) reported that, in the field, hydrogen was produced in the absence of large quantities of CO. This means either the WGSR has been very complete (leaving no CO for methanation reaction) or very little carbon monoxide was generated by the combustion front in the first place. For instance, the Kerrobert THAI pilot field data, as shown in Table 4.5, indicates that most of the in-situ generated CO was utilized in generating methane (9.6 mole% of the KP2's produced gas is methane). The produced hydrogen (1.33 mole%), on the other hand, implies that WGSR was not completed, leaving carbon monoxide to react with the in-situ generated hydrogen

(methanation reactions). Hajdo et al, (1985) found that in order to achieve a complete WGSR, and favour it over methanation reactions, the WGSR must rapidly follow the coke gasification reactions. This seems to be what happened in the Marguerite Lake in-situ combustion field pilot which contained 20 mole% hydrogen in the produced gases. They also reported that steam and CO undergo the WGSR at temperatures below 260 ºC. Another complicating element is the solubility of gases such as carbon dioxide, carbon monoxide and hydrogen in the heavy oil. The solubilities of aforementioned gases vary depending on the type of heavy oil (Hajdo, Hallam, Vorndran, & BP Resources Canada Ltd, 1985).

Even if the WGSR is complete and abundant hydrogen is generated downhole, the hydrogen needs to be moved to a production well rapidly to be ultimately detected. This means a pressure difference must exist to drive the hydrogen gas away from the combustion zone faster than the propagation of the combustion front (to avoid steam generation by reaction of the generated hydrogen and injected oxygen). Hence, faster gas mass transport velocity relative to the reaction zone propagation speed is needed (Kapadia , Kallos, & Gates, 2011).

Kapadia et al, (2011) proposed a reaction model which was used to determine the optimum temperature and pressure conditions that might be realized in an in-situ combustion process for hydrogen generation. They used Athabasca bitumen for their study. They found that there was a peak hydrogen generation range, which occurs in the temperature range of 320 to 380 ºC. They also reported a significant amount of coke production which accelerates the hydrogen generation reactions. It was found that, if temperature is elevated beyond 380 ºC, then more coke is consumed by the HTO reactions and therefore less coke is available for hydrogen generation.

In-situ catalytic upgrading involves the use of the reservoir as a reactor for heavy oil hydrogenation, which offers cost, energy, and environmental benefits as it utilises heat energy

from in-situ combustion to drive the catalytic upgrading. Most of the impurities such as sulphur, vanadium, iron, and nickel are left behind in the reservoir, thus lowering the environmental footprint and impact on downstream refining processes, and reducing the cost of diluents to improve pipeline transport (Al-Marshed, Hart, Leeke, Greaves, & Wood, 2015).

Heavy oil dehydrogenation (hydrogen production from heavy oil), within the CAPRI process, is the process of converting large/complex molecules of heavy hydrocarbon to more valuable products by removing hydrogen from heavy oil and/or bitumen molecules and breaking them to smaller products with more value. Heavy oil dehydrogenation is not a one-step straightforward process and involves stages which require thorough consideration to be taken into account prior to the implementation of the CAPRI process in forthcoming THAI projects.

Regarding the CAPRI process, there are many aspects to be further developed before considering systematic field pilots. The CAPRI process should be investigated mainly in an SLD-THAI configuration. This is due to the temperature profile around the horizontal producer associated with the SLD-THAI configuration. Additionally, it should approach in a correlating manner to the integration of the underground upgrading and hydrogen production, with the potential to control the process towards enhancing upgrading or enhancing hydrogen production (Turta, Greaves, & Grabowski, 2018).

The details of variations of the produced gas composition are needed to calculate the apparent atomic hydrogen-carbon (H/C) ratio and estimate the ignition delay, as well as, the intensity of combustion within and around the combustion zone, and whether low-temperature oxidation reactions were significant immediately after the start of air injection (Turta, Greaves, & Grabowski, 2018).

The Whitesands THAI pilot in Canada was carried out between 2006 and 2011. The project used a DLD THAI configuration. Inconsistent heavy oil upgrading (considerable variation

from one measurement to the other) was reported. Good oxygen utilization efficacy (lack of any oxygen short-circuiting into the horizontal producer) was reported. The produced gas composition was CO_2 = 12-13 %, CO = 0.8-3 %, hydrocarbon gases = 4-5 %, and the remainder nitrogen. In the first 3-6 months, the produced hydrogen content was 2 %. However, it exceeded to 8-14 % afterwards. The occurrence of hydrogen production was related to the water gas shift reaction and the coke gasification reactions (Turta, Greaves, & Grabowski, 2018).

Turta et al, (2018) reported that the heavy oil upgrading was associated with an increase of hydrogen content up to a maximum of 4-7 %. However, a typical average gas composition for the KP2 well (as shown in Table 4.5) show a 1.33 % hydrogen content in the produced gas. In average, the Whitesands pilot produced more hydrogen and CO than the Kerrobert project; hydrogen (3.5 % vs 1.25 %) and CO (1.3 % vs 0.35 %). The high hydrogen content in the Whitesands pilot is related to mechanisms involved in the in-situ hydrogen production (pyrolysis, aquathermolyisis, coke gasification, and WGSR) that were taking place at each case. However, the produced methane content is quite high in the Kerrobert project. This was mainly due to the injection of methane in the annulus in order to mitigate corrosion caused by hydrogen sulphide. It must be noted that oil displacement in the Kerrobert project was significantly more sufficient than that of the Whitesands pilot, as indicated by the air oil ratio (AOR) of 2000-3000 sm^3/m^3 and 5000-6000 sm^3/m^3, respectively.

Up to 20 % hydrogen percentage was also recorded in the Wolf Lake Pilot in Canada when in-situ combustion was conducted with oxygen injection. The hydrogen production phenomena was associated with three essential aspects as follows (Turta, Greaves, & Grabowski, 2018):

a) Existence of high peak combustion temperatures, which also causes thermal cracking of the heavy oil in-situ.

b) Flow of oil partially through the burned zone, which was intentionally carried out in pressure-cycling in-situ combustion pilots, therefore, no oxygen is present. In the THAI case, a long pathway for the flow of oil through the heated mobile oil zone, with only coke gasification and WGSR reactions on the last portion.
c) Short distance oil flow promoted by the horizontal producer, which also permits the preservation of the upgrading.

On the other hand, methanation reaction may take place as a result of high temperature thermo-cracking in the absence of oxygen on the portion close to the horizontal producer and/or of coke/superheated steam reactions. Hence, some methane may be produced as a product (Turta, Greaves, & Grabowski, 2018).

Turta et al, (2018) proposed preliminary screening criteria for the DLD-THAI, SLD-THAI, and THAI-CAPRI applications. They indicated that the proposed criteria may be slightly modified to account for the hydrogen generation in case this is regarded as a secondary task of the process, and there is interest in hydrogen production. The proposed criteria for the DLD-THAI applications were as follows:

- No excessive bottom water (preferably less than 40-50 % thickness of the oil zone
- Net pay thickness greater than 8 m
- Depth greater than 150 m
- Permeability greater than 200 mD
- Porosity greater than 0.2
- Water cut less than 85 %
- Oil viscosity grater than 200-300 mPa s
- Oil content (porosity × oil saturation) greater than 0.065

In the case of the SLD-THAI process, as the distance for flow is more extended, the following two modification may be required:

- Net pay thickness greater than 6 m
- Permeability greater than 400-500 mD

The screening criteria for the THAI-CAPRI process is more demanding. The reservoir first needs to be entirely acceptable for the THAI application (by meeting the above criteria). Turta et al, (2018) also proposed a preliminary screening criteria for the THAI-CAPRI applications. The proposed criteria is very preliminary as the CAPRI has only been tried in laboratory scale or simulations. They expressed the conditions under which the CAPRI application is worthwhile such as need for further oil viscosity reduction by in-situ upgrading and removal of pollutants e.g., sulphur, nitrogen, heavy metals. The proposed criteria for the THAI-CAPRI applications is as following:

- Net pay zone greater than 8 m
- Depth greater than 150 m
- Permeability greater than 1000 mD
- Porosity greater than 0.25
- Water cut less than 60 %
- Oil viscosity greater than 10000 mPa s
- Oil content greater than 0.125
- Sulphur content greater than 3 wt%
- Clay content greater than 3 % but less than 20 %

As discussed earlier, the feasibility of the CAPRI technology has been tested mainly in laboratory scale using a fixed bed of catalyst. Also, there are fewer experimental studies on the CAPRI process than laboratory investigations for the THAI process. Turta et al, (2018)

reported that to improve the catalyst performance and advance the CAPRI technology more in-depth considerations are required in the following aspects:

a) Understanding the main similarities and differences in surface (refinery type) and in-situ (CAPRI type) catalytic heavy oil upgrading processes in terms of thermodynamics, mechanisms, and kinetics. Processing of heavy oil may undergo a complex array of thermo-catalytic reactions associated with carbon removal by delayed coking, viscosity reduction by visbreaking, molecular weight reduction by thermal and/or catalytic cracking, hydrogen addition by hydrotreating/hydrocracking, etc.
b) Determining the catalyst loading or catalyst to oil ration (CTO) for the CAPRI process. The laboratory results have shown that increase in the CTO ratio results in increase in upgrading degree. On the other hand, the CTO ration from refineries may not be very relevant and/or directly applicable for the in-situ CAPRI application.
c) Examining the influence of less controlled conditions in the field such as in-situ steam generation, sand flux, etc. The THAI-CAPRI laboratory tests have been conducted under initial water saturation of less than 10-20 %. Further tests in combustion cells with initial water saturations greeter than 40 % are required in order to be representative of the field conditions.
d) Clarifying the production mechanisms favouring hydrogen production in case the potential of hydrogen production for THAI-CAPRI process is higher than that in the THAI process. The upcoming laboratory tests should be planned to precisely emphasis hydrogen production potential of the THAI-CAPRI process.

Turta et al, (2018) reported that Petrobank carried out a limited field pilot (for about 3 month) testing the CAPRI technology. The field testing of THAI-CAPRI occurred within the frame of the Whitesands pilot in Athabasca. Petrobank used one of the replacement wells, namely P3B as shown in Figure 6.5, for testing the process. A fixed-bed catalyst was enclosed between two

concentric slotted liner as shown in Figure 6.6 (exterior liner is 9 5/8 inches and interior liner is 5 ½ inches). The type of catalyst used for testing the THAI-CAPRI was not reported. The concentric slotted liners containing the catalyst were prefabricated before being installed in the well. The catalytic liners (or CAPRI liners) were introduced one by one for the whole length of the horizontal section of the producer well from the heal to the toe. It was believed that the CAPRI liners lasted a maximum of 3 months. The catalyst deactivation was related to poisoning of the catalyst and other factors. Turta et al, (2018) reported that the catalyst became mushy and possibly restricted the flow. They also reported that there was no significant increase/reduction in oil production during the CAPRI process. Also, no change of hydrogen or carbon monoxide contents in the produced gas was believed to be related to the catalyst presence. It was reported that the air injection interruption, before and after CAPRI testing, seemed to have a higher impact on the composition of the produced gas. Overall, the obtained incremental upgrading through the CAPRI test did not justify the upfront investment.

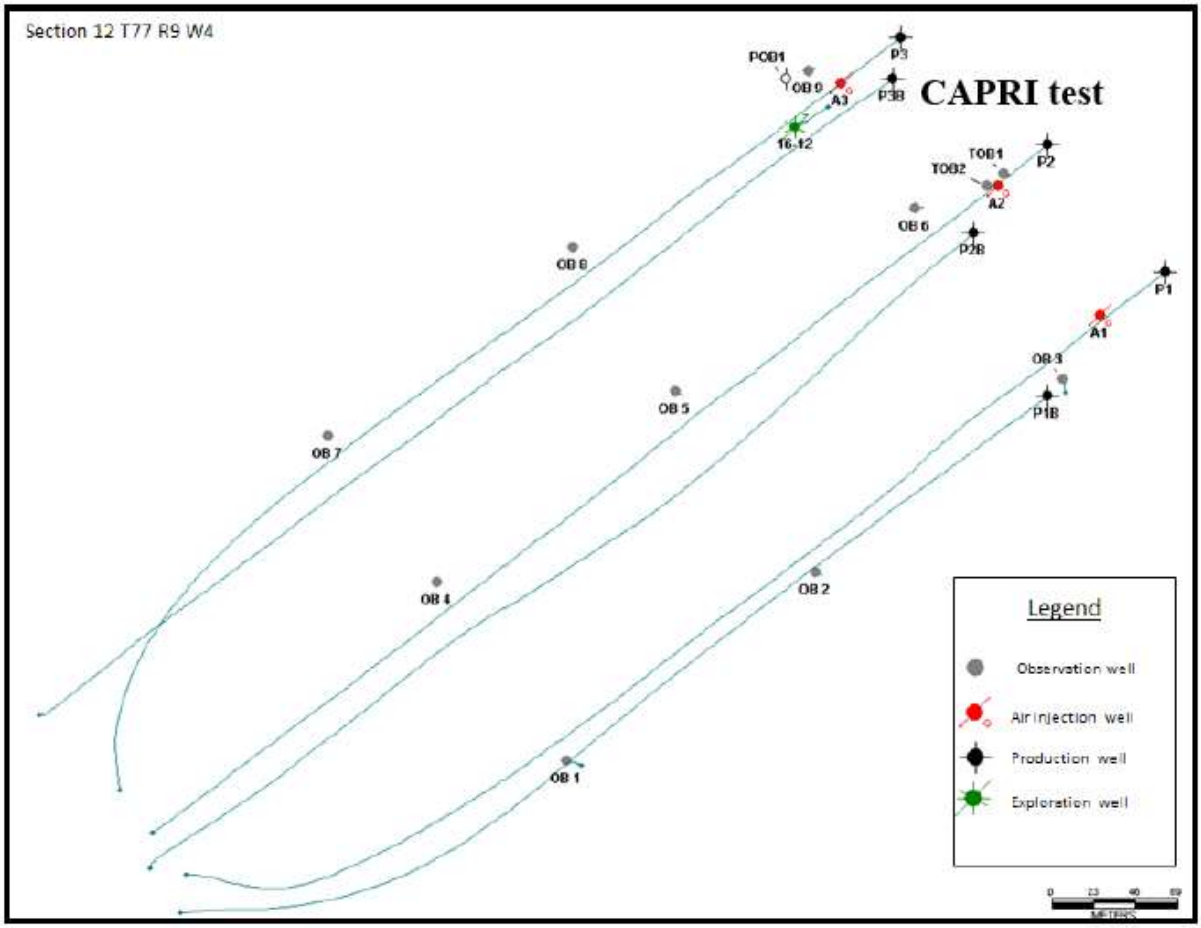


Figure 6.5. The Whitesands pilot well layout map. The operation of P3 was suspended and P3-B was drilled as a CAPRI well in 2008 (Petrobank Energy & Resources Limited, 2009)

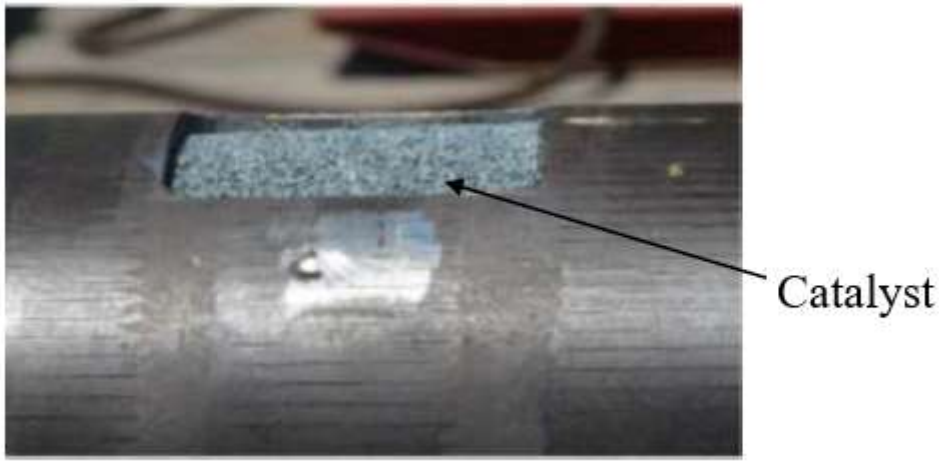


Figure 6.6. Horizontal section of P3-B well in the Whitesands pilot, which was converted to a catalytic downhole reactor in the CAPRI testing form August to October 2008 (Turta, Greaves, & Grabowski, 2018)

The underground upgrading can increase the value of the crude oil. The increase in value could be by at least US$ 0.5/bbl of oil for each point of API degree upgrading. As the average underground upgrading is 3-4 ° API through the THAI process alone. This is equivalent to the at least US$ 1.5-2/bbl of the upgraded oil. Of course, it may even be higher when efficient CAPRI process is developed and brings incremental upgrading (Turta, Greaves, & Grabowski, 2018). As Figure 6.7 shows that by the time of writing this thesis (early 2023) the oil price (US$ 80/bbl) is US$ 20/bbl more expensive than its price in early 2018 (US$ 60/bbl).



Figure 6.7. West Texas Intermediate (WTI) crude oil price change from 2018 to present (Macrotrends, 2023), the pricing is in US$/bbl

The results from the CAPRI test in the Whitesands pilot were not very conclusive, confirming that need for more laboratory investigations. On the positive side, the CAPRI test demonstrated that a catalyst pre-packed screen could be installed. The catalyst gravel packing concept was recommended to be tried in the future allowing the construction of a thicker wall of catalyst around the well. Hence, the catalyst to oil ratio and residence time for the following oil will be

increased. Additionally, it was recommended that the future investigation of the CAPRI process should be tightly correlated with the progress made in the application of the THAI process; they should monitor and follow the THAI advancements. Upcoming studies should approach, in a correlating manner with potential to control the process towards enhancing upgrading and hydrogen production (Turta, Greaves, & Grabowski, 2018).

Hart et al, (2015) reported that the dispersed ultrafine HDS catalyst has superiority over fixed-bed of pelleted catalyst in THAI-CAPRI process. They showed that dispersed ultrafine $CoMo/Al_2O_3$ catalyst promotes the cracking of larger molecular weight components (like resins and asphaltenes) to light components (such as saturates and aromatics) and produced oil thereafter was less viscous and higher in quality compared to that produced from a fix-bed of pelleted catalyst. Al-Marshed et al, (2015) reported that the hydrotreating catalysts used for the THAI-CAPRI process, in the form of fixed-bed around the horizontal producer, deactivated during reactions. This is due to poisoning of active sites by impurities and blocking of pores induced by coke and metal deposition resulting from cracking of heavy oil. Al-Marshed et al, (2015) also reported that as the catalyst particle size decreases to nanoscale, its specific surface area increases while the diffusion path length decreases. This improves the interaction between the macromolecules and cracking reaction. Hence, attention has been shifted towards the once-through process which is using an ultradispersed catalyst, prepared in-situ or injected as slurry into the reservoir, during the THAI process.

It was experimentally demonstrated, in Section 5.5.3, that $CoMo/\gamma\text{-}Al_2O_3$ is capable of dehydrogenating the heavy oil, producing nearly 20% hydrogen in the gas product as shown in Table *5.3*. Also, it was shown, contrary to previous assertions, that heavy oil can be heated directly with microwaves to 425°C, which is the temperature needed for successful catalytic upgrading, without the need for an additional microwave susceptor. Upgrading of > 3.2° API

points, a 90% reduction in viscosity to less than 100 cP, and > 12% reduction in sulphur content was achieved using commercially available hydrodesulphurization (HDS) catalyst.

It is, therefore, suggested that part of the oil-in-place could be targeted for 'deep' dehydrogenation within the CAPRI process (as shown in Figure 6.8). The produced hydrogen could then be directed to aid hydrodesulphurization and improve the upgrading. This concept is equivalent to in-situ combustion where part of the oil is sacrificed in combustion to produce the heat needed to mobilize the rest of the oil-in-place. Further, this could provide a new route for hydrogen production from oil reservoirs which can be used for chemicals synthesis and contribute to the efforts towards a hydrogen economy.

The microwave-assisted THAI-CAPRI process (as shown in Figure 6.8) provides an inert environment for boosting in-situ hydrogen generation reactions (as described earlier in this Section) in the absence of oxygen. This requires (a) selecting appropriate air injection rates to avoid oxygen channelling into the horizontal producer (as discussed in Chapter 4) and (b) employing the right catalyst (that favours hydrogen generation) and operating conditions for the CAPRI process. The activation energy required for the dehydrogenation reactions can be lowered by using an appropriate catalyst, which could make the catalytic hydrogenation process more cost and energy efficient. Also, methanation is known as a process that consumes the in-situ generated hydrogen via the THAI process. Hence, the choice of catalyst must target the reduction of the methanation reaction within the process. On the other hand, microwave technology is used to control the temperature profile (an important operating parameter for hydrogen generation downhole) around the horizontal section of the producer well.

The use of low temperature shift (LTS) catalyst for microwave-assisted catalytic upgrading experiments will be studied in this chapter. The experimental results will be compared to those previously obtained from employing either a HDS catalyst or an Alumina support (as shown

in Section 5.5). A comparison of the produced gas composition will be used to investigate hydrogen generation phenomena in the CAPRI process.

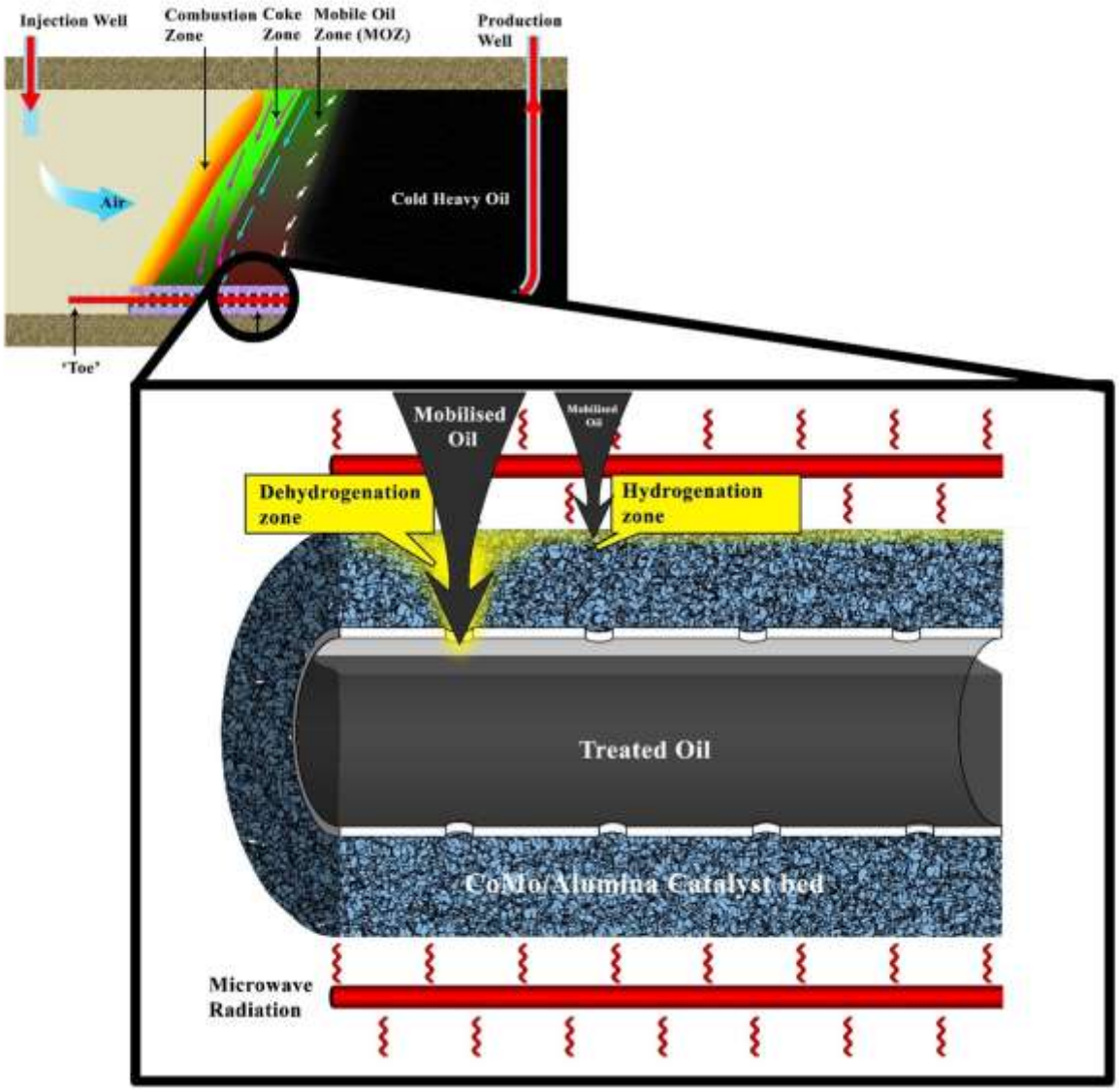


Figure 6.8. Schematic of dehydrogenation and hydrogenation within microwave-assisted THAI-CAPRI process

6.2 Materials

6.2.1 Heavy oil produced through the THAI process

The heavy oil, produced through the THAI process, was used for the microwave-assisted catalytic upgrading experiment in this chapter. The properties of the oil used can be found in Section 5.3.1.1.

6.2.2 Low Temperature Shift (LTS) catalyst

The ability of supported copper to catalyse the water-gas shift reaction has long been known. Copper-based catalysts have good activity for the water-shift reaction and have no methanation activity. This means they are well suited for use in water-gas shift duties (Twigg, 1993). The low temperature shift (LTS) catalysts, specifically the active copper-based LTS catalysts, are utilised to shift the equilibrium of the water gas shift reaction to the right ($CO + H_2O = CO_2 + H_2$). This means the active copper-based LTS catalysts could give equilibrium CO concentrations of less than 0.3% in the water gas shift reaction at low temperature. This could reduce the cost of synthesis hydrogen production and promote the overall efficiency of such a process. The LTS catalysts are used on all ammonia and refinery hydrogen plants. The LTS catalysts are supplied in the oxide form, and they must be reduced to metallic copper, which is the active species, before they are used. (Twigg, 1993).

A low temperature shift catalyst, Zinc oxide/Copper oxide/Aluminium oxide ($ZnO/CuO/Al_2O_3$) was used in this chapter. The LTS catalyst contained Copper Oxide (50-75%), Zinc Oxide (10-25%), Alumina (10%), Graphite (3%), and Magnesium Oxide (3%). It was aimed to (a) investigate the possibility of catalytic upgrading of heavy oil using the LTS catalyst and (b) further probe the in-situ hydrogen production within the catalytic upgrading of heavy oil using the LTS catalyst. The water gas shift reaction converts carbon monoxide and water to carbon dioxide and hydrogen. The reaction is catalysed by a number of different base metal catalyst, depending on the operating temperature and level of poisons in the feedstock

(Johnson Matthey, 2023 a). $ZnO/CuO/Al_2O_3$ catalyst is used in ammonia and hydrogen plants to maximise the hydrogen produced and minimise the gas purged from the ammonia synthesis loop. It combines high activity and poison resistance with excellent selectivity to give a low methanol by-product formation (Johnson Matthey, 2023 b). The properties and composition of the used catalyst can be found in (Dim, Fletcher, & Rigby, 2016). It must be noted that the catalyst used for this study had 3 % graphite content in its composition. The LTS catalyst was supplied in the form of pellets, which was then crushed and sieved to range of mean particle sizes from 106 to 1180 µm.

Graphite is a pure and two-dimensional crystalline form of carbon in which atoms are strongly bonded to each other. Graphite layers can easily slide past each other and, therefore, can be used a lubricant in catalyst manufacturing. It has been used as a preferred electronically conducting filler in polymer manufacturing because of its ability to increase the tensile strength as well as its conductivity (Torgut, Biryan, & Demirelli, 2019). Torgut et al, (2019) reported that dielectric properties (ε'' and ε') of their polymer was increased with a rise in the amount of graphite. Mitchell et al, (2013) reported that graphite is classified as lubricant additive in catalyst manufacturing. Its function is to reduce friction during mixing and shaping operations.. As it was mentioned earlier, the LTS catalyst used for this study contained graphite in its composition. Hu et al, (2012) reported that graphite behaves as an excellent microwave absorbent. The graphite content in the LTS catalyst suggests that it could be a good microwave absorber. On the other hand, graphite could potentially act as a source of carbon for coke gasification reactions (reacting with water (steam) supplied either oil or catalyst), leaving behind H_2 in the batch reactor. The coke gasification also generates CO which reacts with steam in WGSR reaction, generating additional hydrogen.

6.3 Experimental setup

The details of the experimental setup used for conducting experiments in this chapter can be found in Section 5.3.2.

6.4 Characterisation

The density, specific gravity, API gravities and viscosity of the treated oil was measured/calculated using the same procedure discussed in Section 5.4. The sulphur content of the treated oil was not measured. The cavity perturbation technique was used to measure the dielectric properties of the solid $ZnO/CuO/Al_2O_3$ catalyst.

Gases generated during microwave-assisted catalytic heavy oil upgrading experiments were collected with the aid of a syringe via a connector by opening the outlet gas valve and transferred to a gas vial with a pierceable septum. The gas was analysed on a Clarus 580 gas chromatograph (GC) fitted with a FID and TCD detectors operating at 200 °C, by introducing 5 ml of gas sample for hydrocarbon and non-hydrocarbon analysis. The GC used for this study can detect concentrations as low as 15 ppm. The hydrocarbon gases were analysed by automated injection of 100 µl of gas samples (split ratio 10:1) onto the FID by the instrument at 250 °C. Separation was performed on an Alumina plot fused silica 30 m x 0.32 mm x 10 µm column, with helium as the carrier gas. The oven temperature was programmed to ramp from 60 °C (13 min hold) to 180 °C (10 min hold) at 10 °C min^{-1}. Individual hydrocarbon gas yields were identified and quantified in relation to C_1-C_5 gases (injected separately) as an external gas standard. The non-hydrocarbon gases (H_2, and CO_2) were analysed also by automated injection of 500 µl onto the TCD by the instrument. Separation was performed on a Haysep N6 packed column, using argon as the carrier gas. The oven temperature was programmed from 60 °C (13 min hold) to 160 °C (2 min hold) at 10 °C min^{-1}. The hydrogen and carbon dioxide yields were also identified and quantified in relation to their individual gas standards (injected

separately) as a mixture of external gas standards. The gas chromatography analysis was carried out by Dr Clement Uguna.

The dielectric properties measurement of loss materials is widely done by the cavity perturbation method (Clarke, et al., 2003). A schematic of the dielectric measurement setup used for measuring dielectric properties of the LTS catalyst is shown in Figure 6.9 and Figure 6.10. In the cavity perturbation technique, the network analyser produces and sends electromagnetic signals to the cavity and measures the resultant resonant frequency and quality factor of the cavity. This is done before and after inserting the sample inside the cavity. The dielectric constant and the loss factor are calculated using the difference in the resonant frequency and quality factor of the cavity (Zhang, et al., 2018). The catalyst was loaded into the measuring tube (with a 4 mm diameter) in powder form. The tube was purged with nitrogen and closed at the top with a piece of sealing parafilm prior to the measurements. The purging was done to ensure that measurements were made in an inert atmosphere (like the laboratory-scale microwave-assisted heavy oil upgrading experiment).

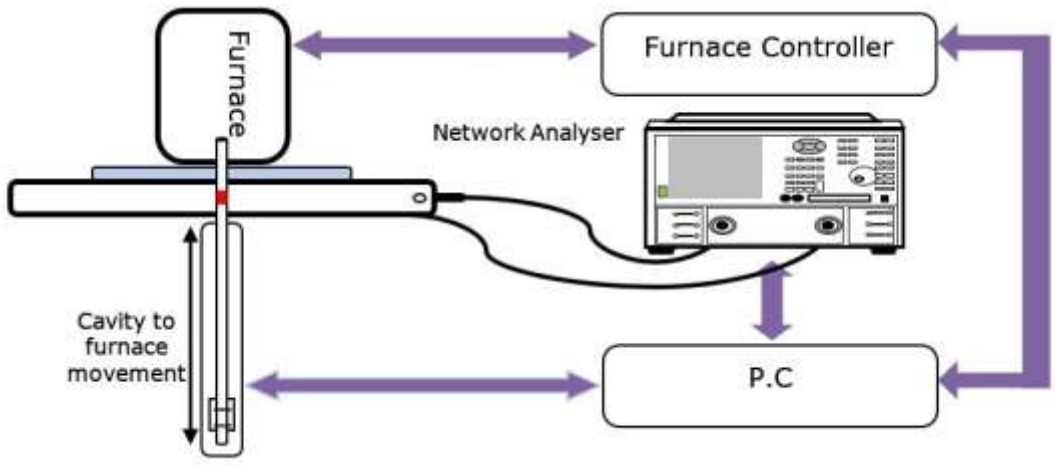


Figure 6.9. Schematic diagram of the dielectric properties measurement system

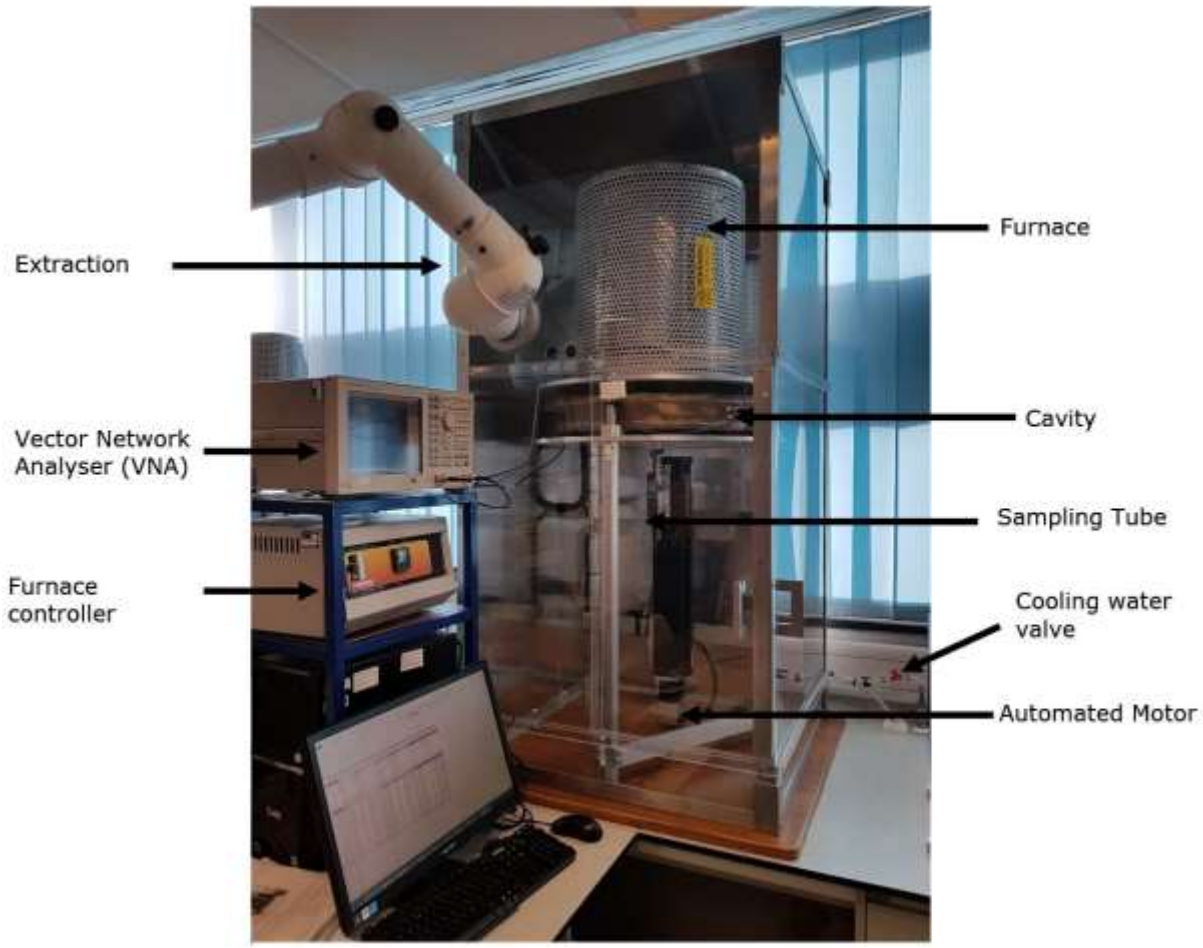


Figure 6.10. Dielectric measurement system setup

Gas sorption analysis for fresh and spent LTS catalysts was carried out as described in Section 5.4.

The thermogravimetric analysis (TGA) was used to determine the hard coke content of the spent LTS catalyst as described in Section 5.4.

6.5 Results and discussion

6.5.1 Dielectric properties

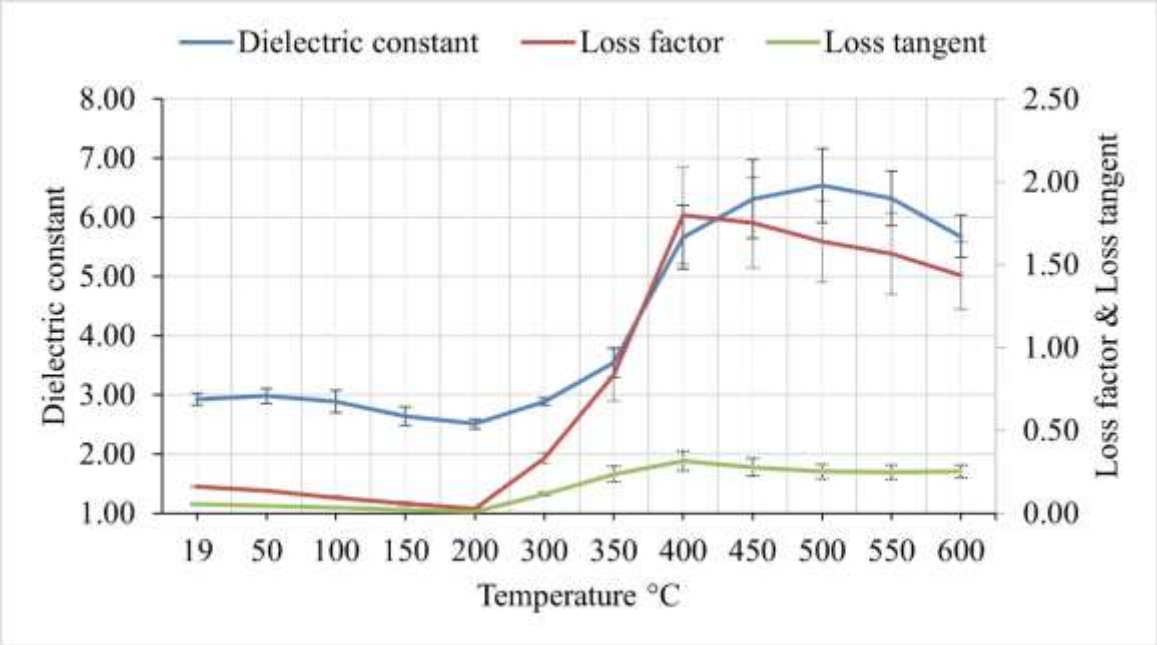


*Figure 6.11. Dielectric properties of the ZnO/CuO/Al_2O_3 catalyst. *Error bars represent standard deviation of a set of dielectric properties measurement for the LTS catalyst*

Figure 6.11 shows the loss tangent, dielectric constants, and loss factor of the ZnO/CuO/Al_2O_3 catalyst as a function of temperature up to 600 ºC. It can be seen that the loss factor initially drops with temperature up to 200 ºC. A similar event was observed for dielectric properties measurements of CoMo/γ-Al_2O_3 (shown in Figure 5.21). This was attributed to the evaporation of free water content within the catalysts as water is a good microwave absorber. This means that the ability of the ZnO/CuO/Al_2O_3 catalyst to heat, in response to the electric field, is slightly decreased from room temperature to 200 ºC (the energy is stored in the catalyst). This is due to the change in water content for reasons that will be explained as follow. Metaxas & Meredith (1983) reported that the nature of water absorbed in a material has a marked effect upon its dielectric properties. Absorbed water in wet materials can exist in two principle states: (a) free water, which resides in capillaries, cavities, etc, and (b) bound water, which is chemically combined to other molecules or physically adsorbed to the surface of the dry

material (Metaxas & Meredith, 1983). The tan δ increases with temperature from 200 to 400 ºC, with increasing dielectric loss factor and dielectric constant. This means that the ability of the LTS catalyst to heat, in response to the electric field, is rapidly increased from 200 to 400 ºC (less energy is stored in the catalyst and more energy is lost as heat). This can be attributed to the release of bound water within the catalyst resulting in an increase in the loss factor over the range of temperatures from 200 to 400 ºC. Morimoto & Morishige (1974) reported a change in water content, including that present as hydroxyl groups (bound water), of zinc oxide with increasing temperature up to 600 °C. They reported that only a small amount of the surface hydroxyl groups on zinc oxide can be desorbed by evacuation up to 300 °C, while most of them can be removed at temperatures ranging from 300 to 400 °C, due to co-condensation. Figure 6.11 shows a decreasing rate of increase of dielectric constant of the LTS catalyst above 400 °C, which can be attributed to the removal of bound water. Also, the loss factor of the LTS catalyst gradually decreases between 400 to 600 ºC.

Additionally, a clear change in the colour of catalyst (from dark brown to black) was observed after the dielectric properties measurement. The change in the colour of the catalyst might suggest some form of oxidation of residual copper. However, the dielectric properties measurements were conducted within an inert atmosphere (the sample tube was being purged with nitrogen gas during the measurements). The observed change in the colour of LTS catalyst could be related to the variation in crystal structure and matrix of the LTS catalyst in response to the applied heat.

6.5.2 Heating profile

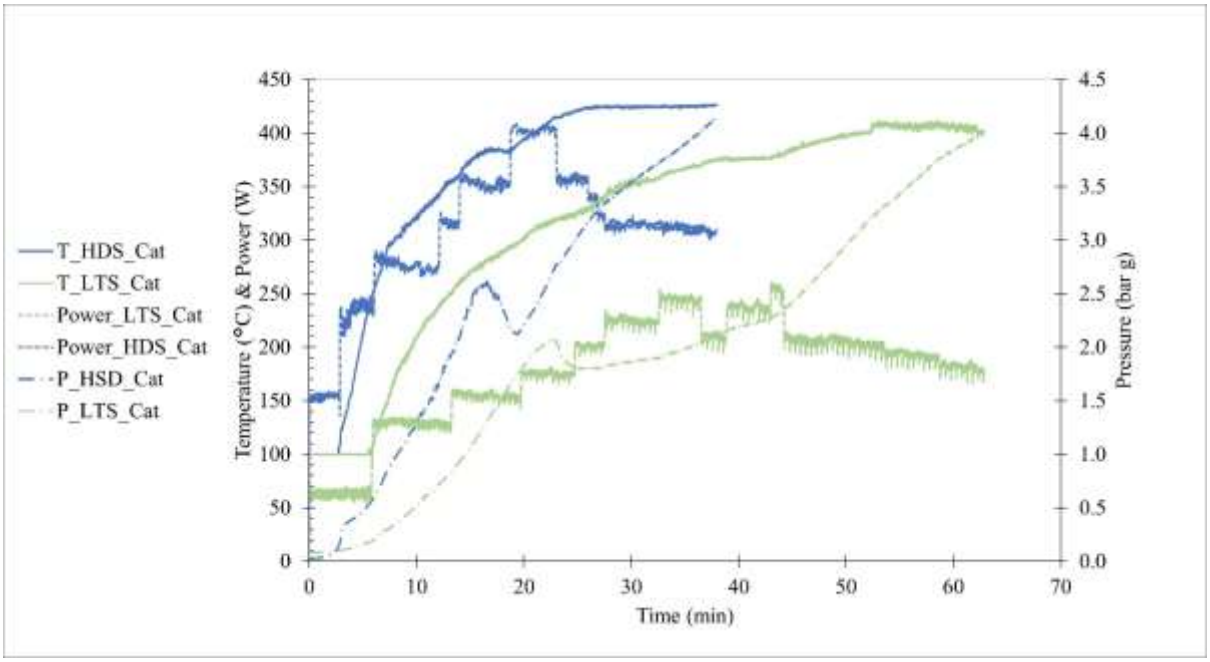


*Figure 6.12. Absorbed power, temperature, and pressure profile during microwave heating of the heavy oil with and without using LTS and HDS catalyst. * The abbreviations T, P and Cat in the legend represent temperature, pressure, and catalyst, respectively.*

Figure 6.12 shows a typical absorbed power, temperature, and pressure profile during upgrading experiments when either HDS or LTS catalysts were employed. It can be seen that the heating rate achieved by HDS catalyst is steeper than that achieved by the LTS catalyst. The observed difference in heating rate was mainly due to the varied position of the sliding short circuit of experimental setup. The heating rate for the LTS catalyst was slightly increased by conducting microwave heating simulations to find the best position for the sliding short circuit. However, it was not possible to reach the exact same heating rate initially achieved using the HDS catalyst. As discussed in Section 6.5.1, the LTS catalyst had different dielectric properties compared to the HDS catalyst. Considering that an identical input power profile was used during the upgrading experiments, the absorbed power profile shows that the HDS catalyst absorbed higher input power overall compared to the LTS catalyst. As a result, the temperature of heavy oil/catalyst mixture rapidly increased to 300 °C in less than 10 minutes when the HDS

catalyst was used. However, the temperature of the heavy oil/catalyst mixture only rose to 300 °C in more than 20 minutes when LTS catalyst was employed. The heating rate became even slower as the LTS catalyst lost its moisture content, taking 30 minutes to reach 400 °C, the temperature at which the holding time began. Due to the pressure build-up within the reactor, it was not possible to reach to 415 °C, the equivalent ultimate temperature at which the holding time began for the HDS catalyst.

Figure 6.12 also shows that the increase in the pressure profile was slower in the LTS catalyst case compared to the HDS catalyst case. However, both pressure profiles show a brief pressure drop, at 17th minute in the HDS catalyst case (at 385 °C) and at 23rd minute in the LTS catalyst case (at 320 °), before they start to increase again, at the 20th minute for the HDS catalyst case and at the 25th minute for the LTS catalyst case. Having the same volume (v), amount of substance (n), and idea gas constant (R), based on ideal gas law ($PV = nRT$), the sudden pressure drop suggests a phase change within the reactor (from gas phase to liquid or solid phase). To investigate the potential correlation of the observed pressure profile with the composition of the produced gas, a series of additional experiments were conducted to study the gas composition of the produced gas using the LTS catalyst. In addition, the effect of the pressure build-up, during the holding time, on the composition of the produced gas was studied. Figure 6.13 shows three points at which the upgrading experiment were terminated, and the produced gas samples were collected for the gas analysis.

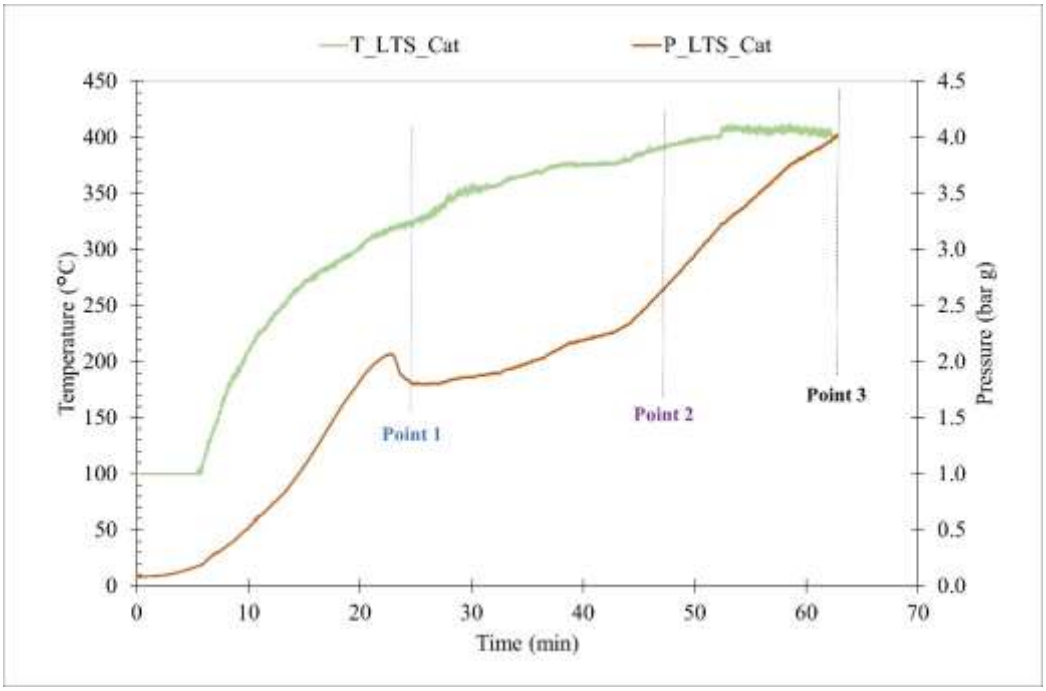


*Figure 6.13. Three different points for gas collection during upgrading experiments using LTS catalyst. * T, P and Cat represent temperature, pressure, and catalyst, respectively.*

6.5.3 Catalytic upgrading

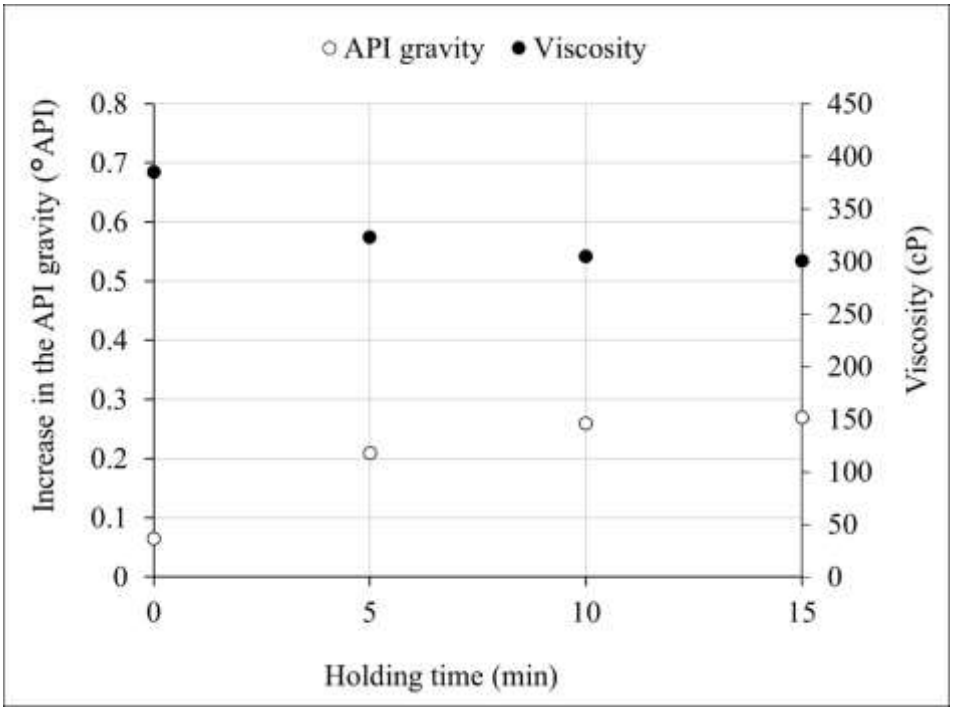


Figure 6.14. Effect of holding time at 400 °C on the original API gravity and viscosity

A series of batch microwave heating experiments were carried out to evaluate the degree of catalytic upgrading at 400 °C. The LTS catalyst was used for upgrading experiments in this section (Catalyst = 1.0 g, oil = 15 g). Figure 6.14 shows the effect of the holding time on the degree of upgrading using the $ZnO/CuO/Al_2O_3$ catalyst with particle sizes in the range 212 – 600 µm. The LTS catalyst particle size was in the same range as the HDS catalyst for upgrading experiments. It was only possible to investigate the effect of the holding time up to 15 minutes. This was mainly due to (a) the lower heating rate, as discussed in Section 6.5.2, to reach to the targeted 400 ºC and (b) the pressure build-up within the quartz tube making it impractical to hold the oil-catalyst mixture at 400 ºC for longer than 15 minutes (in order to avoid breaking the quartz tube during experiments).

The increase in API gravity obtained from using the LTS catalyst, as shown in Figure 6.14, was far less significant than that obtained from using the HDS catalyst, as shown in Figure 5.23. This was due to the significant difference in Alumina content of the HDS and LTS catalysts. Table *6.1* shows the composition of the HDS and LTS catalysts. The HDS catalyst contained 80% Alumina whereas the LTS catalyst contained only 10% Alumina.

Table 6.1.Composition of the HDS and LTS catalysts

Catalyst	Composition
CoMo/ γ-Al_2O_3 (HDS)	Cobalt oxide (4.5%), molybdenum oxide (14.5%), **Alumina (81%)**
$ZnO/CuO/\gamma$-Al_2O_3 (LTS)	Copper Oxide (50-75%), Zinc Oxide (10-25%), **Alumina (10%)**, Graphite (3%), magnesium Oxide (3%)

Table *6.2* shows the upgrading performance and gas analysis results obtained from the upgrading experiments using the HDS and LTS catalysts, as well as the Alumina support. Prior to any comparison, it is important to consider the operating conditions under which the

experiments were carried out. In the case of the HDS catalyst and Alumina support, the experiments were carried out under similar conditions (up to 415 °C and 15 min holding time with particles of 212 – 600 µm size). However, it was not possible to reach to 415 °C in the case of the LTS catalyst. Hence, the 15 min holding time started at 400 °C when the LTS catalyst was used for upgrading experiments.

In bifunctional catalysts such as CoMo/γ-Al_2O_3, the metals are responsible for hydrogenation/dehydrogenation, while the Alumina support provides the cracking functionality (Hart, Adem, Robinson, Rigby, & Wood, 2020). Comparing the upgrading results for Alumina, as shown in Table *6.2*, the insignificant upgrading achieved by the LTS catalyst is associated with a low amount of Alumina Support in LTS (10%). Whereas the HDS catalyst contained a high amount of Alumina support (80%) compared to the LTS catalyst, resulting in a higher degree of upgrading. Table *6.2* shows that the highest catalytic upgrading was achieved using Alumina support only.

In the case of the LTS catalyst, as shown in Figure 6.14, the viscosity of heavy oil was reduced to 300 cP (from original 880 cP) after the first 5 minutes of holding time. However, the reduction in viscosity was insignificant in the subsequent 5 to 15 minutes of holding time. This was due to the eventual deactivation of the LTS catalyst, as a result of coke deposition, which will be discussed in detail in Section 6.5.5. It was shown in Section 5.5.3 that the increase in API gravity and reduction of viscosity are coupled with the desulphurisation of the treated oil and an increase in sulphur deposition on the solid HDS catalyst. The characterisation for sulphur content of the treated heavy oil was not carried out when LTS catalyst was used for the experiment. Hence, in the case of the LTS catalyst, the relationship between the desulphurisation of the treated oil and the increase in API/reduction in viscosity was not examined.

Table 6.2. The performance of CoMo/γ-Al_2O_3, γ-Al_2O_3 and ZnO/CuO/Al_2O_3 catalysts including the gas composition

	CoMo/γAl_2O_3	γ-Al_2O_3	ZnO/CuO/Al_2O_3
Increase in API	2.58 ± 0.14	3.03 ± 0.06	0.3 ± 0.04
Viscosity (cP)	114.1 ± 1.16	86.50 ± 7.71	285 ± 10.15
Reduction in sulphur (%)	8.90 ± 0.41	6.71 ± 0.35	N/A
Sulphur deposition on solid (%)	3.38 ± 0.12	0.70 ± 0.06	N/A
Gas composition (mole %)			
Methane	0.018	12.792	6.64
Ethane	0.013	5.753	2.82
Ethene	0.000	1.226	0.64
Propane	0.013	4.139	1.97
Propene	0.007	2.436	1.20
C_4 Alkanes	0.005	1.880	0.83
C_4 Alkenes	0.005	1.660	0.77
C_5 Alkanes	0.004	0.883	0.31
C_5 Alkenes	0.015	0.639	0.23
Hydrogen	18.879	0.779	17.031
Carbon dioxide	0.632	1.036	15.39
Carbon monoxide	0.790	1.065	Not detected
Hydrogen sulphide	6.782	11.896	Not detected

In terms of the produced gas composition, both HDS and LTS catalysts produced high quantities of hydrogen, namely 19 and 17 mole %, respectively. Despite the higher degree of API upgrading achieved by Alumina support, its produced hydrogen was considerably lower than the other two catalysts (0.779 mole %). This indicates that the active (metallic) sites of the

HDS catalyst (CoMo) and the LTS catalyst (ZnO/CuO) have promoted the dehydrogenation of heavy oil during the experiments.

The high carbon dioxide and hydrogen content produced by the LTS catalyst indicates that the $ZnO/CuO/Al_2O_3$ catalyst has favoured the forward water gas shift reaction by shifting the equilibrium of the WGSR to the right (Equation 6.3). The WGSR required a water source to take place. It was earlier shown, in Section 5.5.1, that the LTS catalyst contained water within itself. The TGA analysis, that will be discussed in Section 6.5.5, also showed that the LTS catalyst had water content. In addition, the water condensation on the top flange of the reactor (after experiments), as shown in Figure 6.15, clearly indicates that water was available for the WGSR.

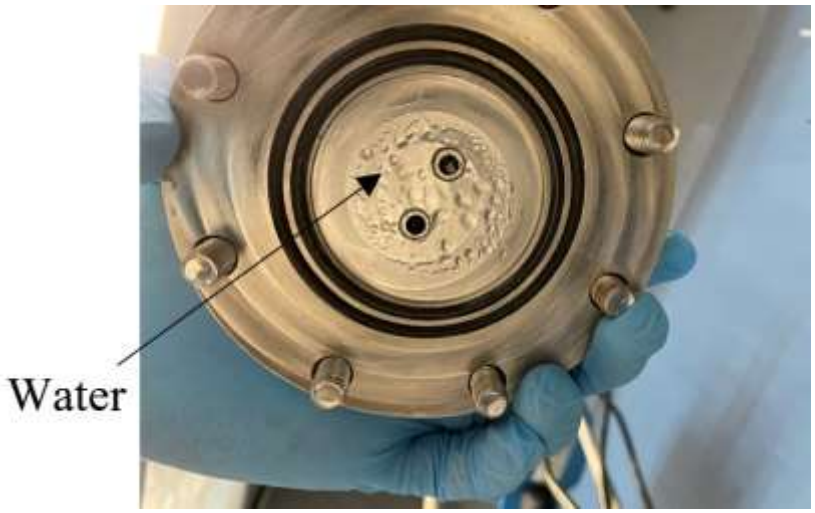


Figure 6.15. Water condensation on the top flange

Another potential reason for the observation of high CO_2 and low CO content in produced gas via the LTS catalyst could be the backward Boudouard reaction, as shown in Figure 6.16. Boudouard reaction is the reaction of C and CO_2 to produce CO:

$C + CO_2 = 2CO$ (Equation 6.7) (Hunt, et al., 2013)

However, due to a large positive enthalpy, typically reported to be 172 kJ/mol under standard conditions at 298 K, the equilibrium does not favour carbon monoxide production until temperatures greater than 700 °C (Hunt, et al., 2013). On the other hand, backward Boudouard reaction could result in carbon or coke generation. It will be shown, in Section 6.5.5, that high carbon content was deposited on the spent LTS catalyst.

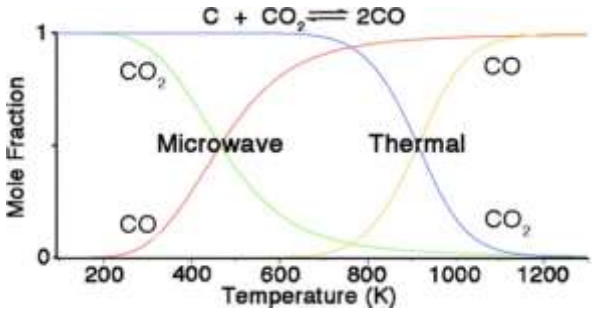


Figure 6.16. Boudouard reaction (Hunt, et al., 2013)

As it was discussed earlier in Section 6.1, the methanation reactions are known as hydrogen consumers within the CAPRI process. The high methane content produced by Alumina support suggests that most of the generated hydrogen within the reactor was consumed to produce methane (12.72 mole %). Alternatively, thermal cracking could be the main source of the produced methane obtained from the Alumina support. The HDS catalyst was more successful in avoiding methanation compared to the LTS catalyst, producing 0.018 and 6.64 mole % methane, respectively.

The composition of the produced gas obtained from the LTS catalyst, shown in Table *6.2*, indicates that hydrogen sulphide was either not present or below the detection limit of the GC instrument. Further, analysis is required to examine the sulphur content of the treated oil and the spent catalyst in the future studies of catalytic upgrading using $ZnO/CuO/Al_2O_3$ catalyst.

As it was discussed earlier in Section 6.5.2, a series of upgrading experiments were carried out to investigate the effect of the pressure profile, as shown in Figure 6.13, as well as the effect of

holding time on the composition of the produced gas. Table *6.3* shows the results for the gas analysis of collected gas samples at Point 1, Point 2, and Point 3 as shown in Figure 6.13. No H_2S was detected in any of three gas sample analysis. The hydrogen and methane contents obtained at Point 1 were insignificant. The highest carbon dioxide content was produced at Point 1.

The amount of produced hydrocarbon (HC) and non-hydrocarbon (NHC) gases, together, increased cumulatively by nearly 13 % from Point 1 to Point 2. This could explain the increase in the pressure profile within the reactor, as shown in Figure 6.13, from Point 1 to Point 2. The data for Point 2 shows that as hydrogen and methane start to be produced, the CO_2 produced drops from 24.08 to 22.81 mole %. This means that reactions that lead to H_2 generation activated between Point 1 and Point 2. Some of the generated hydrogen was consumed by methanation reactions (Equation 6.4, 6.5, and 6.6) to generate methane between Point 1 and Point 2, which suggests a slow rate of apparent production of hydrogen (H_2 was produced and then consumed within the reactor between Point 1 and Point 2).

The produced hydrocarbon and non-hydrocarbon gases increased cumulatively by nearly 70 % from Point 2 to Point 3 (holding time). This was reflected in the sharp pressure rise, as shown in Figure 6.13, during the holding time. The produced hydrogen increased from 1.90 to 17.03 model % from Point 2 to Point 3. The produced methane also increased from 1.5 to 6.64 model % during the holding time. The produced carbon dioxide was decreased by nearly 33 percent (from 22.82 to 15.39 mole %) from Point 2 to Point 3. It can be suggested that, up to Point 1, CO was mainly consumed due to a backward Boudouard reaction. However, from Point 1 to Point 3 (320 to 400 °C), carbon monoxide was consumed by the WGSR and methanation reactions to generate H_2 and CH_4, respectively.

Table 6.3. The gas composition of the produced gas collected at Point 1, Point 2, and Point 3 in Figure 6.13

Gas composition		Point 1 (mole %)	Point 2 (mole %)	Point 3 (mole %)
Hydrocarbon Gases (HC)	Methane	0.21	1.50	6.64
	Ethane	0.05	0.49	2.82
	Ethene	0.03	0.16	0.64
	Propane	0.09	0.41	1.97
	Propene	0.05	0.30	1.20
	C_4 Alkanes	0.2	0.28	0.83
	C_4 Alkenes	0.06	0.23	0.77
	C_5 Alkanes	0.13	0.25	0.31
	C_5 Alkenes	0.19	0.11	0.23
Non-hydrocarbon Gases (NHC)	Hydrogen	0.12	1.90	17.031
	Carbon dioxide	24.08	22.82	15.39
	Carbon monoxide	Not detected	Not detected	Not detected
	Hydrogen sulphide	Not detected	Not detected	Not detected
HC+NHC		25.21	28.45	47.83

6.5.4 Effect of particle size on upgrading

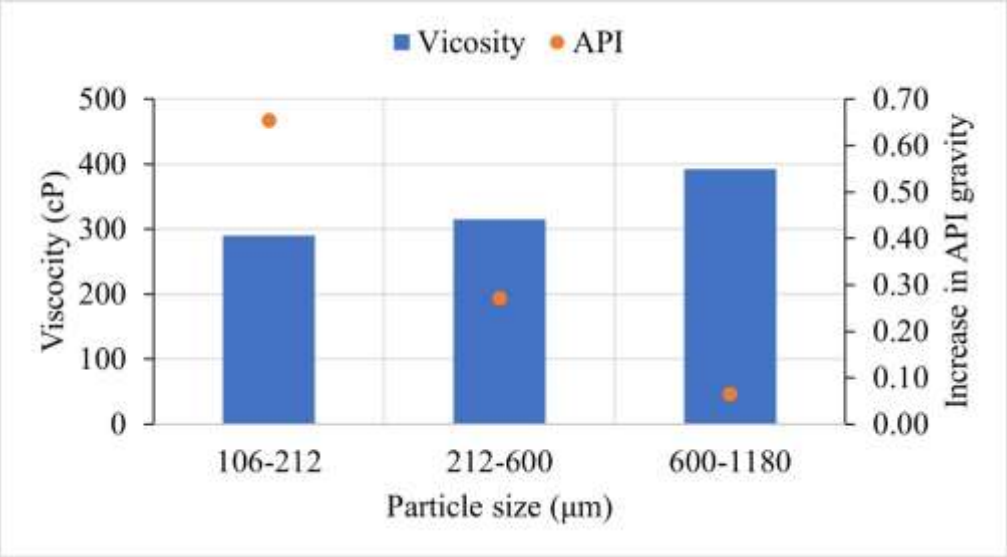


Figure 6.17. Effect of the LTS catalyst particle size on original API gravity and viscosity

The effect of the particle size on the catalytic activity and performance of the LTS catalyst is shown in Figure 6.17. Unlike the HDS catalyst, the 75-106 µm particles were not employed for investigating the effect of the particle size on upgrading. This was due to the physical nature (mechanical stability) of the LTS catalyst used for this study. The smallest used LTS catalyst particle size (106-212 µm) resulted in better upgrading of the treated oil, with regard to the API gravity and viscosity. However, the level of catalytic upgrading degree was not significant compared to the larger particle sizes. Catalytic upgrading , consisting of an up to ~0.7 ° increase in API gravity and ~70% reduction in viscosity to less than 280 cP, was achieved using the LTS catalyst.

The obtained upgrading degree using LTS catalyst, specifically in terms of API gravity, is considerably lower than that obtained using HDS catalyst (shown in Figure 5.25). In contrast, the upgrading degree, represented by the viscosity of the treated oil, was considerable (~70%) when the LTS catalyst with 106-212 µm particle size was used. It is unlikely that the catalytic performance and larger surface area of smaller particle size have led to such a reduction in the

viscosity of the treated oil. The thermal cracking played a major role in reducing the oil viscosity. In terms of API gravity, as discussed in Section 6.5.3, the low Alumina content of the LTS catalyst did not promote the catalytic upgrading during the experiments and, as a result, the API gravity did not change considerably with varied particle size.

Comparing the upgrading result obtained from the HDS (as shown in Section 5.5.4) and LTS catalysts, the lower increase in API gravity and reduction in viscosity of the treated oil, when the LTS catalyst was employed, can also be attributed to the slower mechanical stability of the LTS catalyst during experiments. Unlike the HDS catalyst, the LTS catalyst used for this study was not hardened enough to satisfy the mechanical strength demands of investigating the effect of particle size on upgrading performance. Only 0.1 gram of spent catalyst was recovered through filtrations, as shown in Figure 5.13, after each experiment regardless of the various particle sizes used for the experiments. Considering that the treated oil was centrifuged (after the experiments and before the specific gravity measurements), it is safe to assume that most of the spent catalyst were deposited at the bottom of the centrifuging tube. However, the dissolved LTS catalyst in the treated oil (even with minor quantities) may have resulted in a low increase in API gravity and decrease in viscosity.

6.5.5 Effect of coke deposition on catalyst activity

Dim et al, (2015) reported that the reactions involving heavy oil and catalysts are highly likely to produce carbonaceous deposits, generally called coke. The coke can smother active sites, and/or prevent access of reactants to the catalyst completely by blocking of the surface pores. The spatial distribution of coke depends upon the balance between the rates of reaction and mass transfer. A rapid coking, relative to the rate of mass transfer, is likely to lead to pore-mouth blocking, whereas a slower reaction is likely to lead to a more even distribution of coke. The rate of mass transfer is affected by the pore structure of the catalyst (Dim, Hart, Wood, Macnaughtan, & Rigby, 2015).

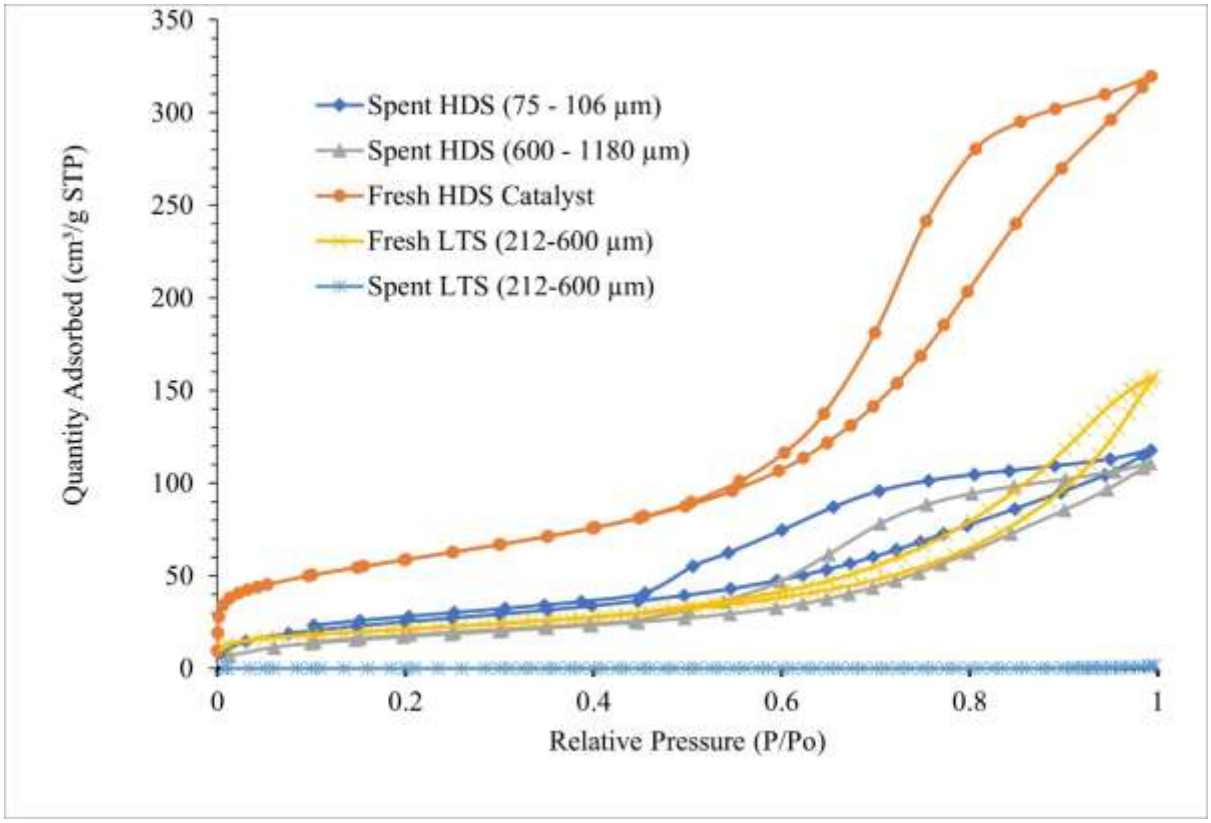
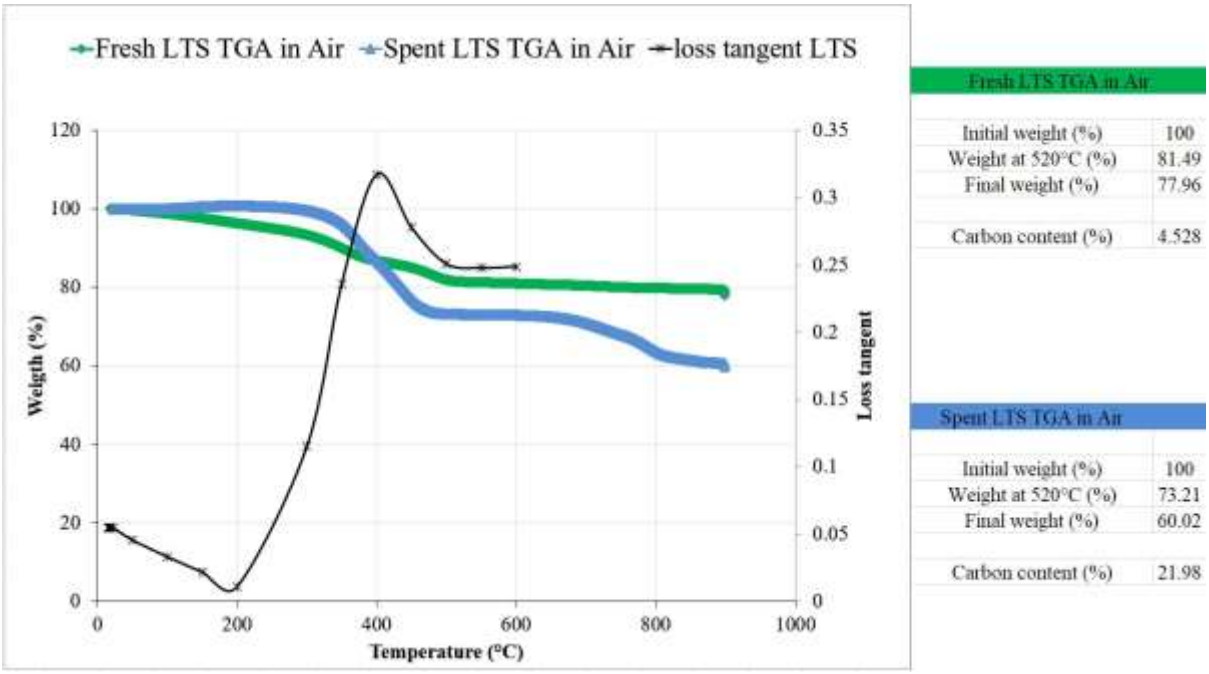


Figure 6.18. N_2 sorption isotherms for the fresh and spent HDS and LTS catalyst

Figure 6.18 shows the N_2 isotherms of the fresh and spent HDS and LTS catalysts. Same as the fresh HDS catalyst, as discussed in Section 5.5.4, a sharp increase in the gas uptake at low pressure can be seen in the case of the fresh LTS catalyst. This is an indication of the presence of microporosity within the fresh LTS catalyst. The BET surface area of the fresh LTS catalyst was 65 percent less than that for the fresh HDS catalyst. Figure 6.18 also shows that the micropores of the spent LTS catalyst have been completely filled, or their access were blocked, with coke. In comparison with the fresh LTS catalyst with a BET surface area of 72.8108 m^2/g, the BET surface area of the spent LTS was significantly reduced to 0.15863 m^2/g. TGA analysis was carried out to determine the coke deposition on the spent LTS catalyst.



Fresh LTS TGA in Air	
Initial weight (%)	100
Weight at 520°C (%)	81.49
Final weight (%)	77.96
Carbon content (%)	4.528

Spent LTS TGA in Air	
Initial weight (%)	100
Weight at 520°C (%)	73.21
Final weight (%)	60.02
Carbon content (%)	21.98

Figure 6.19. TGA results for the fresh and spent LTS catalysts and change in loss tangent of the fresh LTS catalyst with temperature

Figure 6.19 shows the TGA results for the fresh and spent LTS catalysts. Hart et al, (2015) reported that coke content (hard coke) can be identified as the mass loss above 520 °C. The coke deposition (%) was calculated by the following formula:

$$\text{Hard coke deposition (\%)} = \frac{(\text{Wt\% at 520 °C} - \text{final Wt\%})}{\text{final Wt\%}} \times 100$$

22% coke deposition (carbon content) was found in the spent LTS catalyst, which was higher than when HDS catalyst was employed (around 17% as shown in Figure 5.26). The TGA analysis showed 4.35% carbon content in the fresh LTS catalyst when air was used. It must be noted that quantities in a range of 4 to 6 mg were used for the TGA analysis.

In addition to carbon content, TGA analysis also shows that the fresh LTS catalyst originally contained water. The initial weight reduction in the fresh LTS catalyst was due to the vaporisation of the free water. As it was shown earlier in Figure 6.18, the fresh LTS catalyst had a larger porous media and BET surface area to store moisture within itself, compared to

the spent LTS catalyst. This means that water was available for the WGSR reaction (as discussed in Section 6.1) to take place within the reactor, boosting the observed hydrogen generation (as shown in Table *6.2*).

Further weight reduction, within the TGA analysis of the fresh LTS catalyst, between the boiling point of water and 520 °C could be attributed to dehydroxylation and/or soft carbon contents. Dehydroxylation involves the heating process through which the hydroxyl group (OH) is released by co-condensing and forming a water molecule (Frost & Vassallo, 1996). The water molecules formed from the dehydroxylation of the LTS catalyst then could be evaporated, once exposed to high temperatures. Figure 6.19 also shows the change of the loss tangent of the fresh LTS catalyst with increasing temperature in response to microwaves. As it was discussed earlier in Section 6.5.1, the tan δ initially dropped with temperature up to 200 ºC, which was attributed to the evaporation of loose-bound water, which is considered a good microwave absorber. The loss tangent then starts to increase up to 400 ºC, where it dropped again just before it plateaued. The dehydroxylation processes may have influenced the dielectric properties of the LTS catalyst, boosting the loss factor, as shown in Figure 6.11, resulting in an increase in tan δ between 200 and 400 °C. Hart et al, (2015) reported that soft coke content can be identified as the mass loss between 278 and 520 °C. It is hard to distinguish the major contributor to weight reduction for the fresh LTS catalyst between 278 and 520 °C. However, the first mass loss observed for the spent LTS catalyst can be safely classified as soft carbon, considering its temperature profile (300-470 °C). Further studies are required to investigate the effect of carbon deposition regarding the deactivation of LTS catalyst as well as the effect of dehydroxylation processes on altering the dielectric properties of the LTS catalyst with increasing temperature.

6.6 Conclusion

This study examined the potential of the microwave-assisted THAI-CAPRI for in-situ hydrogen production in experimental scale.

Analysis of the dielectric properties of the fresh ZnO/CuO/Al_2O_3 (LTS) catalyst showed that its loss factor and dielectric constant varied considerably with increasing temperature. This was due to the free and bound water contents within the LTS catalyst. The obtained results suggests that the loss factor of the LTS catalyst slightly decreased with the vaporization of the free water up to 200 °C. However, the release of the bound water within the LTS catalyst increased its ability to store electromagnetic energy (dielectric constant) up to 400 °C. With the complete release of the bound water, the general ability of the LTS catalyst to heat by microwave (loss tangent) decreased from 400 to 500 °C, where it plateaued.

Although the obtained increase in API gravity from using the LTS catalyst for upgrading experiments was not significant, a ~70% reduction in viscosity to less than 280 cP was achieved. Comparing to the upgrading results obtained from using the CoMo/ γ-Al_2O_3 (HDS) catalyst and Alumina support in the previous chapter, it was found that the low Alumina support content of the LTS catalyst has had a substantial impact on its catalytic upgrading potential. The achieved reduction in viscosity was mainly attributed to the thermal cracking rather than the catalytic cracking.

The gas analysis showed 17 mole % hydrogen content in the produced gas using the LTS catalyst. The hydrogen content produced by the LTS catalyst was comparable to that produced by the HDS catalyst (19 mole %). This indicates that active (metallic) sites of the LTS catalyst (ZnO/CuO) and the HDS catalyst (CoMo) have promoted the dehydrogenation of heavy oil during the experiments. It was shown that the pressure profile within the reactor was correlated to gas generation throughout the experiments. The produced hydrocarbon and non-

hydrocarbon gases increased cumulatively by 70 % during the holding time (at 400 °C) of the experiment.

Gas absorption analysis of the fresh and spent LTS catalysts showed that coke deposition during experiments completely blocked access to the available pore space of the catalyst. The TGA analysis of the fresh and spent LTS catalyst showed 22 % coke deposition (hard carbon content) on the spent LTS catalyst. The high coke deposition on the spent catalyst resulted in the deactivation of the catalyst and, consequently, low upgrading degrees.

This study confirms the potential of the THAI-CAPRI process to be a new route for in-situ hydrogen production form heavy oil reservoirs. However, in terms of scaling up and field trials, further research is required to (a) cost-effectively develop catalysts that could promote in-situ upgrading and hydrogen production simultaneously (catalysts such as CoMo/ γ-Al_2O_3), (b) conduct further microwave-assisted catalytic upgrading experiments to examine the applicability of the new catalysts as well as optimising the operating conditions of the experiments.

7. Conclusion and future work

7.1 Conclusion

In this study, a new field scale THAI model was developed to study the overall performance of the DLD and the SLD THAI well arrangements. The predicted results showed that the SLD THAI well arrangement has the following advantages over the DLD THAI well arrangement:

a) Steeper oxygen consumption, boosting the ISC process
b) Broader combustion front propagation, larger steam zone, and improved sweep efficiency
c) Up to 50% higher cumulative oil production

Dynamic field data, for one of the best performing THAI pilot well pairs (K2) within the Kerrobert THAI pilot project, were analysed in this work. It was found that the K2 pilot must have experienced interference from K5, which is the closest neighbouring THAI well pair to the K2. This caused a significant imbalance between injected air and produced gas for KA2 (K2's injector well) and KP2 (K2's producer well), respectively. The history-matched THAI model, developed in this work, was used to probe whether the air injection rates impact the overall performance of the THAI process in the presence of bottom water. It was found that excessive air injection reduced the oxygen utilisation resulting in a poor ISC efficiency with combustion time. This means more air injection does not necessarily promote oil production in the THAI process in a bottom water situation. The O_2 utilisation was improved from 74 to 90% by restricting air injection to that into KA2 alone. An inversely proportional relationship was detected between the coke concentration and the oxygen profile around the horizontal producer (HP). It was also found that the size of the steam zone varies with changes to the air injection rates. The MOZ analysis demonstrates that a large BOZ was developed below the HP during the THAI operation. Relocation of the horizontal producer was proposed as a potential strategy

to capture as much mobilised oil as possible. The oxygen utilisation was improved by 13%, resulting in 73% higher cumulative oil production in comparison to the history matched model. Hence, the following suggestions can be made for optimisation purposes:

a) For forthcoming projects, THAI well pairs must be drilled at a sufficient distance to prevent unwanted interference from each other, unless the operation is based on an intended interaction between air injector wells (e.g., staggered line drive (SLD) THAI well arrangement).
b) For existing THAI projects such as Kerrobert, the selection of air injection must be made considering air flowing in from neighbouring injector wells (it can be done by pausing air injection for a short period and recording the produced gas from the corresponding producer well).
c) HP locations closer to the transition zone could be considered in order to produce from the large BOZ developed below the HP and enhance oil recovery.

This study showed that microwave heating could provide the additional required heat for a successful THAI-CAPRI process. It was shown that, without adding a microwave supplemental susceptor, temperatures up to 425 °C could still be achieved with microwave heating. An upgrading in API gravity of more than a **3.2°** increase, a **90%** reduction in viscosity to less than **100 cP**, and a more than **12%** reduction in sulphur content, were achieved using a commercially available HDS catalyst. An alternative Alumina support demonstrated a better upgrading and viscosity reduction performance compared to the HDS and LTS catalysts. In comparison with the LTS catalyst, it was found that the high Alumina content within the HDS catalyst has resulted in higher upgrading. Examining the effect of the catalyst particle size on the catalytic upgrading revealed that the smaller particle sizes of the HDS catalyst resulted in higher upgrading degrees. This was due to a larger available external surface area for the

catalytic reactions. It was also found that the HDS catalyst is more active in desulphurisation of the treated oil, compared to Alumina support.

Gas sorption analyses were performed to analyse pore network connectivity within the fresh and spent HDS and LTS catalysts. It was demonstrated that the spent HDS and LTS catalysts have experienced significant reduction in their pore volume. TGA analysis showed that coke deposition led to blockage of most of the pore volume that initially existed in the fresh HDS and LTS catalysts. Up to **17% and 22%** hard coke content were found on the spent HDS and LTS catalysts, respectively.

In addition, this study demonstrated the potential of the in-situ hydrogen production using a microwave-assisted THAI-CAPRI process on the experimental scale. Up to **19 mole % and 17 mole %** hydrogen content was found in the produced gas using the HDS and LTS catalyst, respectively. However, an insignificant amount of hydrogen was detected when the Alumina support was employed. This means that that metallic sites of the LTS catalyst (ZnO/CuO) and the HDS catalyst (CoMo) have promoted the dehydrogenation of heavy oil throughout the catalytic upgrading experiments.

7.2 Future work

The proposed history matched model in this study provides a deep insight into the fundamental mechanisms involved in the THAI process. Alongside studying the operational aspects of the THAI process, the constructed simulation could be used for short- and long-term forecasting of the future THAI application in heavy oil reservoirs with underlaying bottom water. However, the following future research should be considered in terms of numerical investigation of the THAI process:

a) Expansion of the chemical reaction concerning the hydrogen production such coke gasification and WGSR reactions.

b) Examination of the solubility of the CO_2 and O_2 in the bottom water.

c) Implementation of the microwave-heating technology in the THAI model.

d) Implementation of the CAPRI process in a field scale THAI model.

In terms of experimental study of the CAPRI process, the following research should be considered microwave-assisted catalytic upgrading experiments:

a) Investigation of the scaling up the catalyst to oil ratio.

b) Further microwave-assisted catalytic upgrading experiments with tailored catalysts for hydrogen production through the CAPRI process (such as a modified CoMo/ γ-Al_2O_3 catalyst with higher CoMo content).

c) Investigating dielectric properties of a wider range of commercially available HDS/HDT catalyst.

d) Examining the application of hydrogen donor for future microwave-assisted catalytic upgrading experiments.

e) Implementation of the microwave-assisted THAI-CAPRI in the field

References

Adam, M. (2017). *Understanding microwave pyrolysis of biomass materials.* Retrieved 03 20, 2023, from https://eprints.nottingham.ac.uk/41301/1/Full%20Thesis%20final.pdf

Adam, M., Anbari, H., Hart, A., Wood, J., Robinson, J. P., & Rigby, S. P. (2020). In-situ microwave-assisted catalytic upgrading of heavy oil: Experimental validation and effect of catalyst pore structure on activity. *Chemical Engineering Journal, 413*, 127420. doi:10.1016/j.cej.2020.127420

Adam, M., Hart, A., Stevens, L. A., Wood, J., Robinson, J. P., & Rigby, S. P. (2018). Microwave synthesis of carbon onions in fractal aggregates using. *Carbon, 138*, 427-435. doi:10.1016/j.carbon.2018.07.066

Adam, M., Hart, A., Wood, J., Robinson, J. P., & Rigby, S. P. (2019). MICROWAVE-ASSISTED CATALYTIC UPGRADING OF HEAVY OIL. Houston, Texas: 4th American Symposium for Chemical Reaction Engineering.

Ado, M. (2017). *Numerical Simulation of Heavy Oil and Bitumen Recovery and Upgrading Processes.* Nottingham: University of Nottingham, Department of Chemcial and Environmental Engineering, PhD thesis.

Ado, M. (2019). Simulation study on the effect of reservoir bottom water on the performance of the THAI in-situ combustion technology for heavy oil/tar sand upgrading and recovery. *SN Applied Sciences*, 2-29. doi:10.1007/s42452-019-1833-1

Ado, M. R. (2020 a). A detailed approach to up-scaling of the Toe-to-Heel Air Injection (THAI) In-Situ Combustion enhanced heavy oil recovery process. *Journal of Petroleum Science and Engineering, 187*, 106740. doi:10.1016/j.petrol.2019.106740

Ado, M. R. (2020). Predictive capability of field scale kinetics for simulating toe-to-heel air injection heavy oil and bitumen upgrading and production technology. *Journal of Petroleum Science and Engineering, 187*(106843), 106843. doi:10.1016/j.petrol.2019.106843

Ado, M. R., Greaves, M., & Rigby, S. P. (2017). Dynamic Simulation of the Toe-to-Heel Air Injection Heavy Oil recovery Process. *Energy & Fuel, 31*(2), 1276-1284. doi:10.1021/acs.energyfuels.6b02559

Ado, M. R., Greaves, M., & Rigby, S. P. (2022). Numerical simulation investigations of the applicability of THAI in situ combustion process in heavy oil reservoirs underlain by bottom water. *Petroleum Research*. doi:10.1016/j.ptlrs.2022.06.001

Ado, R. M. (2020 a). A detailed approach to up-scaling of the Toe-to-Heel Air Injection (THAI) In-Situ Combustion enhanced heavy oil recovery process. *Journal of Petroleum Science and Engineering, 187*(0920-4105), 106740. doi:10.1016/j.petrol.2019.106740

Agarwal, A., Simonaitis, J., Goyal, V. K., & Berggren, K. K. (2023). Secondary electron count imaging in SEM. *Ultramicroscopy, 245*, 113662.

Ahmed, T. (2001). *Reservoir Engineering Handbook* (Second ed.). Woburn, MA: Butterworth-Heinemann.

Alemán-Vázquez, L. O., Cano, J.-L., & Garia-Gutierrez, J. L. (2012). Effect of Tetralin, Decalin and Naphthalene as Hydrogen Donors in the Upgrading of Heavy Oils. *Procedia Engineering, 42*, 532-539.

Alemán-Vázquez, L., Torres-Mancera, P., Ancheyta, J., & Ramírez-Salgado, J. (2016). Use of Hydrogen Donors for Partial Upgrading of Heavy Petroleum. *Energy & Fuel, 30*(11), 9050-9060.

Ali, A. F., Hauser, A. H., Abdullah, A., & Al-Adwani, A. (2006). Accelerated Solvent Extraction of Spent Hydrotreating Catalysts: A Study on Oil and Coke Fractions. *Energy Fuels, 20*(1), 45-53. doi:10.1021/ef0501905

Al-Marshed, A., Hart, A., Leeke, G., Greaves, M., & Wood, J. (2015). Optimization of Heavy Oil Upgrading Using Dispersed Nanoparticulate Iron Oxide as a Catalyst. *Energy & Fuels, 29*(10), 6306-6316. doi:10.1021/acs.energyfuels.5b01451

Anaya, I., Cruz, R. E., Alvarez, A. J., Gutierrez, D., Skoreyko, F. A., & Card, C. (2010). Simulation Study for Designing an In-Situ Combustion Pilot in the Orinoco Belt of Venezuela: From Laboratory Studies to the Field Scale. Calgary: Canadian Unconventional Resources and International Petroleum Conference. doi:10.2118/137491-MS

Anbari, H., Robinson, J. P., Greaves, M., & Rigby, S. P. (2022). Field performance and numerical simulation study on the toe to heel air injection (THAI) process in a heavy oil reservoir with bottom water. *Journal of Petroleum Science and Engineering, 220, Part B*, 111202.

Araujo, E. A., Diniz, A. R., Gurgel, A. R., Lima, D. S., Dutra, T. V., & Barillas, J. M. (2016). Analysis of oil production by applying in situ combustion. *Petroleum Science and Technology, 34*(1), 50-55. doi:10.1080/10916466.2015.1098664

Arthur, M. A., & Cole, D. R. (2014). Unconventional Hydrocarbon Resources: Prospects and Problems. *Elements, 10*, 257-264. doi:10.2113/gselements.10.4.257

ATAC Group. (2023). *NμLine cone and plate viscometer manual.* ATAC.

Ayasse, C., Bloomer, C., Lyngberg, E., Boddy, W., Donnelly, J., & Greaves, M. (2005). First Field Pilot of the THAI Process. Calgary, Canada: Petroleum Society/Canadian Institute of Mining, Metallurgy & Petroleum. doi:10.2118/2005-142

Aziz, K., & Settari, A. (1979). *Petroleum Reservoir Simulation.* Essex: Applied Science Publishers LTD.

Baker, R. O., Chugh, S., Mcburney, C., & Mckishnie, R. (2006). History matching standards; quality control and risk analysis for simulation. Calgary, Canada: Canadian International Petroleum Conference. doi:10.2118/2006-129

Barrett, E. P., Joyner, L. G., & Halenda, P. P. (1951). The Determination of Pore Volume and Area Distributions in Porous Substances. I. Computations from Nitrogen Isotherms. *Journal of the American Chemical Society, 73*(1), 373-380. doi:10.1021/ja01145a126

Belgrave, J. D., Moore, R. G., Ursenbach, M. G., & Bennion, D. W. (1993). A comprehensive approach to in-situ combustion modeling. *SPE, 1*(1), 98-107.

Borchardt, J. T., & Yen, T. F. (1989). Oil-Field Chemistry. Enhanced Recovery and Production Stimulation. *ACS Symposium, 396*.

bp. (2011, March). *http://tc.canada.ca.* Retrieved 08 09, 2022, from http://tc.canada.ca/sites/default/files/migrated/hres_3_10_11_lunch_learn_bp_heavy_oil1.pdf

Bravo-Sanchez, M., Romero-Galarza, A., Ramirez, J., Gutierrez-Alejandre, A., & Solis-Casados, D. A. (2019). Quantification of the sulfidation extent of Mo in CoMo HDS catalyst through XPS. *Applied Surface Science, 493*, 587-592. doi:10.1016/j.apsusc.2019.07.012

Brunauer, S., Emmett, p. H., & Teller, E. (1938). Adsorption of Gases in Multimolecular Layers. *Journal of the American Chemical Society, 60*(2), 309-319. doi:10.1021/ja01269a023

Cho, H. H., Strezov, V., & Evans, T. J. (2023). A review on global warming potential, challenges and opportunities of renewable hydrogen production technologies. *Sustainable Materials and Technologies, 35*, e00567.

Clarke, R., Gregory, A., Cannell, D., Patrick, M., Wylie, S., Youngs, I., & Hill, G. (2003). *A guide to the characterisation of dielectric materials at RF and microwave frequencies.* London: Institute of Measurement and Control/ National Physical Laboratory .

CMG. (2020). *STARS Manual* .

Coates, R., & Zhao, L. L. (2001). Numerical Evaluation of THAI process. Calgary, Canada: Canadian International Petroleum Conference. doi:10.2118/2001-021

Dim, P. E., Fletcher, R. S., & Rigby, S. P. (2016). Improving the accuracy ofc atalyst pore size distributions from mercury prosimetry using mercury thermoporometry. *Cheimcal Engineering Sceince, 140*, 291-298.

Dim, P., Hart, A., Wood, J., Macnaughtan, B., & Rigby, S. P. (2015). Characterization of pore coking in catalyst for thermal down-hole upgrading of heavy oil. *Chemical Engineering Science, 131*, 138-154. doi:10.1016/j.ces.2015.03.052

Donnelly, J. K., & Pendergast, D. K. (1999). Nuclear Energy in Industry: Application to Oil Production. *Annual Conference of the Canadian Nuclear Society.* Montreal, Canada.

Ferziger, J. H., & Peric, M. (2002). *Computational Methods for Fluid Dynamics.* Berlin: Springer.

Fogler, S. H. (2016). Diffusion and Reactions. In *Elements of Chemical Reaction Engineering.* Prentice Hall.

Frost, R. L., & Vassallo, A. M. (1996). The Dehydroxylation of the Kaolinite Clay Minerals using Infrared Emission Spectroscopy. *Clays and Clay Minerals, 44*, 635-651.

Ghoodjani, E., Kharrat, R., Vossoughi, M., & Bolouri, S. (2011). A Review on Thermal Enhanced Heavy Oil Recovery from Fractured Carbonate Reservoirs. *Journal of Petroleum & Environmental Biotechnology, 02*(02). doi:10.2118/150147-MS

Greaves , M., Dong, L. L., & Rigby, S. P. (2012 a). Determination of Limits to Production in THAI. Calgary, Canada: SPE Heavy Oil Conference Canada. doi:10.2118/157817-MS

Greaves, M., & Al-Honi, M. (2000). Three-Dimensional Studies of In Situ Combustion-Horizontal Wells Process with Reservoir Heterogenties. *Journal of Canadian Petroleum Technology, 39*(10), 25-32. doi:10.2118/00-10-01

Greaves, M., & Al-Shamali, O. (1996). In Situ Combustion (ISC) Process Using Horizontal Wells. *Journal of Canadian Petroleum Technology, 35*, 49-55.

Greaves, M., Dong, L. L., & Rigby, S. P. (2011). Upscaling THAI: Experiment to Pilot. Calgary, Canada: The Canadian Unconventional Resources Conference.

Greaves, M., Dong, L. L., & Rigby, S. P. (2012 a). Determination of Limits to Production in THAI. Calgary, Canada: SPE Heavy Oil Conference Canada. doi:10.2118/157817-MS

Greaves, M., Dong, L. L., & Rigby, S. P. (2012 b). Validation of Toe-to-Heel Air Injection Bitumen Recovery Using 3D Combustion-Cell Results. Vienna, Austria: SPE EUROPEC/EAGE Annual Conference and Exhibition. doi:10.2118/143035-PA

Greaves, M., Dong, L. L., & Rigby, S. P. (2012 c). Simulation Study of the Toe-to-Heel Air Injection Three-Dimensional Combustion Cell Experiment and Effects in the Mobile Oil Zone. *Energy & Fuels, 26*(3), 1656-1669. doi:10.1021/ef201925c

Greaves, M., Dong, L. L., & Rigby, S. P. (2013). Toe-to-Heel Air Injection- Effect of Oil Layer Thickness. St. Petersburg, Russia: 17th Eauropean Symposium on Improved Oil Recovery. doi:10.3997/2214-4609.20142628

Greaves, M., Saghr, A. M., Xia, T. X., Turta, A. T., & Ayasse, C. (2001). THAI- New Air Injection Technology for Heavy oi Recovery and In Situ Upgrading. *Journal fo Canadian Petroleum Technology, 40*(3), 38-47. doi:10.2118/01-03-03

Greaves, M., Tuwil, A. A., & Bagci, S. (1993). Horizontal Producer Wells In In Situ Combustion (ISC) Processes. *Journal of Canadian Petroleum Technology, 32*(4). doi:10.2118/93-04-04

Greensfelder, B. S., Voge, H. H., & Good, G. M. (1949). Catalytic and Thermal Cracking of Pure Hydrocarbons: Mechanisms of Reaction. *Indistrial & Engineering Chemistry, 41*(11), 2573-2584.

Hajdo, l. E., Hallam, R. J., Vorndran, L. D., & BP Resources Canada Ltd. (1985). Hydrogen Generation During In-Situ Combustion. *SPE*(13661).

Hart, A. (2014). The novel THAI–CAPRI technology and its comparison to other thermal methods for heavy oil recovery and upgrading. *Journal of Petroleum Exploration and Production Technology, 4*, 427-437. doi:10.1007/s13202-013-0096-4

Hart, A., Adam, M., Robinson, J. P., Rigby, S. P., & Wood, J. (2020). Tetralin and decalin h-donor effect on catalytic upgrading of heavy oil inductively heated with steel balls. *Catalysts, 10*(4), 393-409.

Hart, A., Adem, M., Robinson, J. P., Rigby, S. P., & Wood, J. (2020). Hydrogenation and Dehydrogenation of Tetralin and Naphthalene to Explore Heavy Oil Upgrading Using NiMo/Al2O3 and CoMo/Al2O3 Catalysts Heated with Steel Balls via Induction. *Catalyst, 10*(5), 497. doi:10.3390/catal10050497

Hart, A., Greaves, M., & Wood, J. (2015). A comparative study of fixed-bed and dispersed catalytic upgrading of heavy crude oil using-CAPRI. *Chemical Engineering Journal, 282*, 213-223.

Hart, A., Leeke, G., Greaves, M., & Wood, J. (2014 b). Downhole heavy crude oil upgrading using CAPRI: effect of steam upon upgrading and coke formation. *Energy & Fuel, 28*, 1811-1819.

Hart, A., Leeke, G., Greaves, M., & Wood, J. (2014). Down-hole heavy crude oil upgrading by CAPRI: Effect of hydrogen and methane gases upon upgrading and coke formation. *Fuel, 119*, 226-235. doi:10.1016/j.fuel.2013.11.048

Hart, A., Lewis, C., White, T., Greaves, M., & Wood, J. (2015). Effect of cyclohexane as hydrogen-donor in ultradispersed catalytic upgrading of heavy oil. *Fuel Processing Technology, 138*, 724-733. doi:10.1016/j.fuproc.2015.07.016

Hart, A., Shah, A., Leeke, G., Greaves, M., & Wood, J. (2013). Optimization of the CAPRI Process for Heavy Oil Upgrading: Effect of Hydrogen and Guard Bed. *Industrial & Engineering Chemsitry Research, 52*, 15349-15406.

Hart, A., Wood, J., & Greaves, M. (2017 a). In situ catalytic upgrading of heavy oil using a pelletized Ni-Mo/Al2O3 catalyst in the THAI process. *Jornal of Petroleum Science and Engineering, 156*, 958-965. doi:10.1016/j.petrol.2017.06.067

Hart, A., Wood, J., & Greaves, M. (2017 b). Laboratory investigation of CAPRI catalytic THAI-add-on process for heavy oil production and in situ upgrading. *Journal of Analytical and Applied Pyrolysis, 128*, 18-26. doi:10.1016/j.jaap.2017.11.004

Hart, A., Wood, J., & Greaves, M. (2017). Laboratory investigation of CAPRI catalytic THAI-add-on process for heavy oil production and in situ upgrading. *Journal of Analytical and Applied Pyrolysis, 128*(4), 18-26. doi:10.1016/j.jaap.2017.11.004

Hill, P. (2017). *Hydrocarbon Distribution in the Mannville Waseca Member, Edam Oil Field, West-central Saskatchewan.* Regina, Canada: Saskatchewan Geological Survey, Saskatchewan Ministry of the Economy. Retrieved from https://pubsaskdev.blob.core.windows.net/pubsask-prod/107073/107073-SOI_2017V1_Paper_A-3__Hill_Hydrocarbon_Distribution_Waseca_Member_Edam_Oil_Field.pdf

Hu, H., Zhao, Z., Zhou, Q., Gogotsi, Y., & Qiu, J. (2012). The role of microwave absorption on formation of graphene from graphite oxide. *Carbon, 50*(9), 3267-3273.

Hunt, J., Ferrari, A., Lita, A., Crosswhite, M., Ashley, B., & Stiegman, A. E. (2013). Microwave-Specific Enhancement of the Carbon–Carbon Dioxide (Boudouard) Reaction. *Journal of Physical Chemistry, 117*, 26871-26880.

Internation Energy Agency (IEA). (2023). *Global Hydrogen Review 2022*. Retrieved 01 25, 2023, from https://iea.blob.core.windows.net/assets/c5bc75b1-9e4d-460d-9056-6e8e626a11c4/GlobalHydrogenReview2022.pdf

International Energy Agency. (2021, October). *Energy Outlook 2021*. Retrieved 10 20, 2021, from IEA: https://www.iea.org/reports/world-energy-outlook-2021

Jeon, S., Kwak, N., Rho, N., Ko, C., Na, J.-G., Yi, K., & Park, S. (2012). Catalytic pyrolysis of Athabasca bitumen in H2 atmosphere using microwave irradiation. *Chemical Engineering Research and Design, 90*(9), 1292-1296. doi:10.1016/j.cherd.2012.01.001

Jiang, S., Liu, X., Lieohe Oilfield, Liu, Y., SPE, Zhong, L., & Daqing Petroleum Inst. (2005). In Situ Upgrading Hevay Oil by Aquathermolysis Treatment Under Steam Injection Conditions. Woodlands, Texas: SPE 91973.

Jinzhong, L., Wenlong, G., Youwei, J., Changfeng, X., Bojun, W., & Xiaoling, L. (2012). Progagation and control of fire front in the combustion assisted gravity drainage using horizontal wells. *Sinece Direct, 39*(6), 764-771.

Johnson Matthey. (2023 a). *Methanol synthesis catalysts*. Retrieved 01 12, 2023, from https://matthey.com/products-and-markets/chemicals/water-gas-shift-catalysts

Johnson Matthey. (2023 b). *Low temperature shif catalyst*. Retrieved 01 12, 2023, from https://matthey.com/products-and-markets/chemicals/low-temperature-shift-catalysts

Kapadia , P. R., Kallos, M. S., & Gates, I. D. (2011). Potential for hydrogen generation from in situ combustion of Athabasca bitumen. *Fuel, 90*, 2254-2265.

Kapadia, P. R., Kallos, M. S., & Gates, I. D. (2012). A New Reaction Model for Aquathermolysis of Athabasca Bitumen. *Canadian Society for Chemical Engineering, 91*(3), 475-482.

Kapadia, P. R., Kallos, M. S., & Gates, I. D. (2014). A review of pyrolysis, aquathermolysis, and oxidation of Athabasca bitumen. *Fuel Processing Technology, 131*, 270-289.

Kapadia, P. R., Wang, J., Kallos, M. S., & Gates, I. D. (2013). Practical process design for in situ gasification of bitumen. *Applied Energy, 107*, 281-296.

Kim, J. W., Longstaff, C. D., & Hanson, V. F. (1997). Upgrading of bitumen-derived heavy oils over a commercial HDN catalyst. *Fuel, 76*, 1143-1150.

Kovscek, A. R., Castanier, L. M., & Gerritsen, M. G. (2013). Improved Predictability of In-Situ-Combustion Enhanced Oil Recovery. *SPE Reservoir Evaluation & Engineering, 16*(2), 172-182. doi:10.2118/165577-PA

Larter, S. R., & Head, I. M. (2014). Oil Sands and Heavy Oil: Origin and Exploitation. *Elements, 10*(4), 277-283. doi:10.2113/gselements.10.4.277

Leco Corporation. (2023). *http://www.lecomexico.com/*. Retrieved 01 20, 2023, from http://www.lecomexico.com/organicos/sc632.pdf

Li, K., Hou, B., Wang, L., & Cui, Y. (2014). Application of Carbon Nanocatalysts in Upgrading Heavy Crude Oil Assisted with Microwave Heating. *Nano Letters, 14*(6), 3002-3008. doi:10.1021/nl500484d

Liu, H., & Seaton, N. A. (1992b). Determination of the connectivity of porous solids from nitrogen sorption measurements—III. Solids containing large mesopores. *Chemical Engineering Science, 49*(11), 1869-1878.

Liu, H., Zhang, L., & Seaton, N. A. (1992a). Determination of the connectivity of porous solids from nitrogen sorption measurements — II: Generalisation. *Chemical Engineering Science, 47*(17), 4393-4404.

Liu, Y., & Fan, H. (2002). The effect of hydrogen donor additive on the viscosity of heavy oil during steam stimulation. *Enegy Fuels, 16*(4), 842-846.

Liu, Y., Gao, L., Wen, L., & Zong, B. (2010). Recent Advances in Heavy Oil Hydroprocessing Technologies. *Recent Patents on Chimical Engineering, 2*(1), 22-36.

Liu, Y., Meirer, F., Krest, C. M., Webb, S., & Weckhuysen, B. M. (2016). Relating structure and composition with accessibility of a single catalyst particle using correlative 3-dimensional micro-spectroscopy. *Nature Communications, 7*, 12634.

Macrotrends. (2023). *WTI crude oil prices*. Retrieved 01 24, 2023, from https://www.macrotrends.net/2516/wti-crude-oil-prices-10-year-daily-chart

Magnie, R. L. (1980). *United States of America Patent No. 4241790.*

Mann, R. (1997). Catalyst deactivation by coke deposition: Approaches based on interactions of coke laydown with pore structure. *Catalyst Today, 37*(3), 331-349.

Marroquin, G., Ancheyta, J., & Esteban, C. (2005). A batch reactor study to determine effectiveness factors of commercial HDS catalyst. *Catalyst Today, 104*, 70-75.

Metaxas, A. C., & Meredith, R. J. (1983). *Industrial Microwave Heating* (4th ed.). London, UK: The Institution of Engineering and Technologuy.

Micromeritics. (2023). *https://www.micromeritics.com/*. Retrieved 01 20, 2023, from micromeritics.com/3flex/?utm_term=3flex&utm_campaign=MIC+Corporate+Campaign&utm_source=adwords&utm_medium=ppc&hsa_acc=2339074468&hsa_cam=14939750590&hsa_grp=129884671418&hsa_ad=554136485450&hsa_src=g&hsa_tgt=kwd-318393510225&hsa_kw=3flex&hsa_mt=b&hsa_net=

Mitchell, S., Michels, N. L., & Perez-Ramirez, J. (2013). From powder to technical body: the undervalued science of catalyst scale up. *Chemical Society, 42*(14), 6094-6112.

Mojarab, M., Harding, T., & Maini, B. (2011). Improving the SAGD performance by introducing a new well configuration. *Journal of Canadian Petroleum Technology, 50*(4), 9-18. doi:10.2118/146626-PA

Morimoto, T., & Morishige, K. (1974). Interaction between carbon dioxide and the zinc oxide surface. *Bulletin of the Chemical Society of Japan, 47*(1), 92-94.

Mutyala, S., Fairbridge, G., Pare, J., & Belanger, J. M. (2009). Microwave applications to oil sands and petroleum: A review. *Fuel Processing Technology, 91*, 127-135. doi:10.1016/j.fuproc.2009.09.009

Nasr, T. N., & Ayodele, O. R. (2005). Thermal Techniques for the Recovery of Heavy Oil and Bitumen. *SPE International Improved Oil Recovery Conference in Asia Pacific.* Kuala Lumpur, Malaysia: Society of Petroleum Engineers. doi:10.2118/97488-MS

Nasri, Z. (2019). Upgrading vacuum distillation residue of oil refinery using microwave irradiation. *Chemical Engineering and Processing - Process Intensification, 149*, 107675. doi:10.1016/j.cep.2019.107675

Natural History Museum. (2023). *https://www.nhm.ac.uk/*. Retrieved 01 20, 2023, from https://www.nhm.ac.uk/our-science/departments-and-staff/core-research-labs/imaging-and-analysis/electron-microscopy/fei-quanta.html#:~:text=The%20FEI%20Quanta%20650%20FEG,from%205%2D1%2C000%2C000x).

Nissen, A., Zhu, Z., Kovescek, A., Castanier, L., & Gerritsen, M. (2015). Upscaling Kinetics for Field-Scale In-Situ-Combustion Simulation. *SPE Res Eval & ENg, 18*(02), 158-170. doi:doi.org/10.2118/174093-PA

Orr, B. (2009). ES-SAGD; Past, Present and Future. *SPE*, 129518. doi:10.2118/129518-STU

Ovalles, C., Rengel, P., Bruzual, J., & Salazar, A. (2003). Upgrading of extra-heavy crude using hydrogen donor under steam injection conditions. Characterization by pyrolysis GC–MS of the asphaltenes and effects of a radical initiator. *Fuel Chem, 48*, 59-60.

Petrobank Energy & Recources Ltd. (2021, 05 05). *Kerrobert THAI project production history.* Retrieved 05 06, 2021, from https://petrobank.ca/

Petrobank Energy & Resources Limited. (2009). *Anuual report.* Calgary: Petrobank Energy & Resources Limited.

Petrobank Energy & Resources Ltd. (2012). *Annual report.* Calgary, Canada: Petrobank Energy & Recources Ltd.

Phillips, C. R., Haidar, N. I., & Poon, Y. C. (1985). Kinetic models for the thermal cracking of Athabasca bitumen: The effect of the sand matrix. *Fuel, 64*(5), 678-691. doi:10.1016/0016-2361(85)90055-9

Porch, A., Slocombe, D., Beutler, J., Edwards, P., Aldawsari, A., Xiao, T., . . . Almagati, N. (2012). Microwave treatment in oil refining. *Applied Petrochemical Research, 2*, 37-44. doi:10.1007/s13203-012-0016-4

Rahnama, H., Barrufet, M., & Mamora, D. D. (2017). Combustion assisted gravity drainage-Experimental and simualtion results of a promising in-situ combustion technology to recover extra-heavy oil. *Journal of Petroleum Science and Technology, 154*, 513-520. doi:10.1016/j.petrol.2017.01.044

Rahnema, H., & Mamora, D. (2010). Combustion Assisted Gravity Drainage (CAGD) Appears Promising. Calgary: Canadian Unconventional Resources and International Petroleum Conference. doi:10.2118/135821-MS

Raybaud, P., & Toulhoat, H. (2013). *Catalysis by Transition Metal Sulphides: From Molecular Theory to Industrial Application.* Paris: Editions TECHNIP.

Richardson, J. F., & Peacock, D. G. (1994). Gas-Solid Reactions and Reactors. In *Coulson and Richardson's Chemical Engineering Volume 3.* Elsevier.

Rigby, S. P. (2020). Gas Sorption. In *Structural Characterisation of Natural and Industrial Porous Materials: A Manual* (pp. 15-48). Springer International Publication.

Rigby, S. P. (2020). Nuclear Magnetic Resonance and Microscopy. In *Structural Characterisation of Natural and Industial Porous Materials: A Manual* (pp. 89-113). Springer International Publication.

Robinson, J. P., Kingman, S., Irvine, D., Peter, L., Smith, A., Dimitrakis, G., . . . Kappe, C. (2010). Understanding microwave heating effects in single mode type cavities—theory and experiment. *Physical Chemistry Chemical Physics, 12*, 7450-4758. doi:10.1039/b922797k

Rojas, J., Ruiz, J., & Jaime, V. (2010). Numerical simulation of an enhanced oil recovery process of toe to heel air injection THAI. Muscat: Society of Petroleum Engineers SPE. doi:doi.org/10.2118/129215-MS

Satter, A., & Iqbal, G. M. (2016). *Reservoir Engineering.* Oxford: Gulf Professional Publishing .

Science Direct. (2023). *https://www.sciencedirect.com*. Retrieved 01 20, 2023, from https://www.sciencedirect.com/topics/earth-and-planetary-sciences/gas-chromatography

Seaton, N. A. (1991). Determination of the connectivity of porous solids from nitrogen sorption measurements. *Chemical Engineering Science, 46*(8), 1895-1909. doi:10.1016/0009-2509(91)80151-N

Shah, A. A., Fishwick, R. P., Leeke, G. A., Wood, J., Rigby, S. P., & Greaves, M. (2011). Experimental Optimization of Catalytic Process In Situ for Heavy-Oil and Bitumen Upgrading. *Journal of Canadian Petroleum Technology, 50*(11), 33-47.

Shah, A., Fishwick, R. P., Leeke, G. A., Wood, J., Rigby, S. P., & Greaves, M. (2011). Experimental Optimization of Catalytic Process In-Situ for Heavy Oil and Bitumen Upgrading. Calgary: Canadian Unconventional Resources and International Petroleum Conference.

Shah, A., Fishwick, R., Wood, J., Leeke, G., Rigby, S., & Greaves, M. (2010). A review of novel techniques for heavy oil and bitumen extraction and upgrading. *Energy & Environmental Science*(3), 700-714. doi:10.1039/b918960b

Sharma, J., Moore, R. G., & Mehta, S. A. (2012). Effect of Methane Co-Injection in SAGD--Analytical and Simulation Study. *SPE, 17*(03), 687-704. doi:10.2118/148917-PA

Speight, J. G. (2011). *An Introduction to Petroleum Technology, Economics, and Politics.* Massachusetts: Scrivener.

Strakov, K. (2021, 05 21). Personal Communication.

TA Instruments. (2023). *https://www.tainstruments.com*. Retrieved 01 20, 2023, from https://www.tainstruments.com/products/thermal-analysis/thermogravimetric-analysis/?gclid=Cj0KCQiAlKmeBhCkARIsAHy7WVvxKhBNW2Pt2qGQlKxv-TUcOvMhd6Uy1e5c4-KX6rN5T3AcVj_I1GUaAkfCEALw_wcB

Tare, T. X., & Greaves, M. (2002). 3D Physical Model Studies of Downhole Catalytic Upgrading ofWolf Lake Heavy Oil Using THAI. *Journal of Canadian Petroleum Technology, 41*(8). doi:10.2118/02-08-03

Torgut, G., Biryan, F., & Demirelli, K. (2019). Effect of graphite particle fillers on dielectric and conductivity properties of poly(NIPAM-co-HEMA). *Bulletin of Materials Science*(42), 244.

Turta, A. (2021). *Toe-to-Heel Air Injection (THAI) Process: Lessons from 14-Year Field Experience.* Calgary, Canada: A T EOR Consulting Inc.

Turta, A. T., Lu, J., bhattacharya, R. N., Condrachi, A., & Hanson, W. (2005). Current Status of the Commercial In Situ Combustion (ISC) Projects and New Approaches to Apply ISC. Calgary: The Canadian International Petroleum Conference.

Turta, A., Greaves, M., & Grabowski, J. (2018). *Comprehensive Assessment of Toe-To-Heel Air Injection (THAI) Process. Guidelines for Development of Future Generations of In-Situ Combustion Processes.* Calgary, Canada: A CO-OPERATION BETWEEN A.T. EOR CONSULTING INC. SUILVEN OIL & GAS LTD AND PETRO MANAGEMENT GROUP (PMG). Retrieved from https://www.insitucombustion.ca/

Turta, A., Greaves, M., & Strakov, K. (2021, 02). *Advanced THAI Brochure.* Retrieved 10 10, 2021, from https://www.insitucombustion.ca/Advanced_THAI_Brochure.pdf

Turta, A., kapadia, P., & Gadelle, C. (2020). THAI process: Determination of the quality of burning from gas composition taking into account the coke gasification and water-gas shift reactions. *Journal of Petroleum Science and Engineering, 187*, 106638. doi:10.1016/j.petrol.2019.106638

Twigg, M. V. (1993). *Catalyst Handbook* (2nd Edition ed.). Roca Raton, FL: CRC Press.

Urazov, K. K., Sviridenko, N. N., Iovik, Y. A., Kolobova, E. N., Grebchenko, M. V., Kurzina, I. A., & Mukhamatdinov, I. I. (2022). Effect of Hydrogen-Donor of Heavy Crude Oil Catalytic Aquathermolysis in the Presence of a Nickel-Based Catalyst. *Catalysts, 12*(10), 1154.

Wei, W., Rezazadeh, A., Wang, J., & Gates, I. D. (2021). An analysis of toe-to-heel air injection for heavy oil production using machine learing. *Journal of Petroleum Science and Engineering, 197*(108109), 108109. doi:10.1016/j.petrol.2020.108109

Wei, W., Wang, J., Afshordi, S., & Gates, I. D. (2020). Detailed analysis of Toe-to-Heel Air Injection for heavy oil production. *Journal of Petroleum Science and Engineering, 186*(106704), 106704. doi:10.1016/j.petrol.2019.106704

Wikel, K., & Kendall, R. (2012). 4D study of secondary recovery utilizing THAI from a Saskatchewan heavy oil reservoir. *Search and Discovery Article*(90174). Retrieved from https://geoconvention.com/wp-content/uploads/abstracts/2012/079_GC2012_4D_Study_of_Secondary_Recovery_Utilizing_THAI.pdf

Xia , T. X., & Greaves, M. (2000). Upgrading Athabasca Tar Sand Using Toe-to-Heel Air Injection. *SPE/Petroleum Society of CIM International Conference on Horizontal Well Technology* . Calgary, Canada: Society of Petroleum Engineers.

Xia, T. X., & Greaves, M. (2006). In Situ Upgrading of Athabasca Tar Sand Bitumen Using THAI. *Chemical Engineering Research and Design, 84*(9), 856-864. doi:10.1205/cherd.04192

Xia, T. X., Greaves, M., Turta, A. T., & Ayasse, C. (2003). THAI- A Short-Distanced Displacement In Situ Combustion Process for the Recovery and Upgrading of Heavy Oil. *Chemical Engineering Research and Design, 81*(3), 295-304. doi:10.1021/acs.energyfuels.6b02559

Yao, J., Li, G., & Wu, J. (2018). Application of In-situ combustion for heavy oil production in China. *Journal of Oil, Gas and Petrochemical Sciences (JOGPS), 1*(3), 69-72. doi:10.30881/jogps.00014

Zhang, Y. S., Lu, X., Owen, R. E., Manos, G., Xu, R., Wang, F. R., . . . Bertt, D. J. (2020). Fine structural changes of fluid catalytic catalysts and characterization of coke formed resulting from heavy oil devolatilization. *Applied Catalyst, 263*, 118329.

Zhang, Y., Adam, M., Hart, A., Wood, J., Rigby, S. P., & Robinson, J. P. (2018). Impact of Oil Composition on Microwave Heating Behavior of Heavy Oils. *Energy & fuels, 32*(2), 1592-1599.

Zhao, F., Xu, T., Zhu, G., Wang, K., Xu, X., & Liu, L. (2022). A review on the role of hydrogen donors in upgrading heavy oil and bitumen. *Sustainable Energy & Fuels, 6*, 1866.

Appendices

Appendix 1

Reservoir simulation by computers allows for a detailed study of the reservoir by dividing the reservoir into several blocks (sometimes several thousands) and applying fundamental equations for flow in porous media to each block. Due to advancements in computing techniques, it is now possible to simulate some of the very complex processes that take place in reservoir during the hydrocarbon recovery schemes (Aziz & Settari, 1979). Aziz and Settari (1979) have reported the fundamentals of developing and using the computer models of petroleum reservoirs. The basic for reservoir simulation is a mathematical representation of the entire system, which integrates reservoir characterisation and fluid properties. The fluid flow and related equations used in the models are mostly nonlinear requiring iterative solutions (Satter & Iqbal, 2016).

The formulae and conservation equations of the thermal reservoir simulator, CMG's STARS, used in this study have been previously reported by Ado (2017). These equations are the result of expressing all the relevant physical phenomena in mathematical format. In STARS software, a conservation equation is constructed for each component of a set of identifiable chemical components that completely describe all the fluids of interest. All conservation equations are based on a region of interest, which is usually a discretised grid block (CMG, 2020). Ado (2017) reported equations concerning material balance, auxiliary relationship, energy balance, Darcy's law, chemical reaction terms, vapor-liquid equilibrium expression, physical properties of fluid (including density, viscosity, and enthalpy), and relative permeability in STARS software. In STARS, there is one conversion equation for each chemical component along with some equations describing the phase equilibrium between phases. Additionally, an equation is used to describe the operating conditions of each injection and production well (CMG, 2020).

The details of discretisation techniques to solve these equations are not the subject of this thesis. However, in this section, the fundamental of equation solution methods are briefly discussed.

The components of numerical solution methods have been reported by (Ferziger & Peric, 2002). The starting point of any numerical method is the mathematical model, i.e., the set of partial differential equations (PDEs). Fluid flow and related phenomena in a reservoir simulator can be described by PDEs (mathematical representation). The results of numerical solutions are not continuous and are obtained in discrete intervals of both space and time (Satter & Iqbal, 2016). Hence, the PDEs cannot be solved by analytical methods. This means to obtain an approximate solution numerically, a discretisation method must be used. The chosen discretisation method approximates the PDEs by a system of algebraic equations. The algebraic equations can then be solved on a computer. The accuracy of the numerical solutions is dependent on the quality of the used discretisation method. The most important discretisation method are finite difference (FD) method, finite volume (FV) method, and finite element (FE) method (Ferziger & Peric, 2002). Ado (2017) reported that any of abovementioned discretisation methods can be used to discretise the PDEs in reservoir simulations. However, the FD method is the most traditionally used discretisation method in reservoir simulations.

The finite difference method is the oldest method for numerical solution of PDEs (Ferziger & Peric, 2002). The PDEs are discretised for each grid block in the reservoir model leading to a large number of finite difference equations forming a matrix. It is solved by a suitable computational algorithm in order to obtain the variables such as fluid saturation or pressure at a particular time step. Discrete solutions are quite sensitive to the number of grid blocks and length of time steps. Use of rather large numbers of grid blocks and smaller time steps increases the accuracy and stability of simulation. However, the computational process is resource extensive in this case. Models based on irregularly shaped grid blocks would require more resources to run (Satter & Iqbal, 2016).

In the context of solving PDEs using the FD method, the explicit and implicit solution schemes can be used. The equation below shows the discretised form of single-phase Darcy flow of fluid in porous media in one direction (using the finite difference (FD) method) (Satter & Iqbal, 2016).

$$K\frac{P_i^{(t+1)} - P_i^{(t)}}{\Delta t} = \frac{P_{(i+1)}{}^{(t)} - 2P_i^{(t)} + P_{(i-1)}{}^{(t)}}{2\Delta x}$$

where K is a coefficient, t is time, x is distance over which flow occurs, and P is the fluid pressure, which varies over distance and time. It must be noted that subscripts i – 1 and i + 1 denote the relative location of grid blocks where the solution is sought. Also, superscripts t and t + 1 represent current and future time steps, respectively (Satter & Iqbal, 2016).

In the explicit solution, considering the above equation, the value of pressure at future time steps is based on the values obtained at the current step. Also, any coefficient appearing in the discretised equation is also evaluated at the current time step. In the implicit solution, reservoir pressure is assumed for the next time step, and any coefficient appearing in the equation is also calculated at the assumed pressure. Implicit solution of cell pressure is obtained by iterating the values of assumed cell pressure until a convergence between assumed values of pressure are obtained (Satter & Iqbal, 2016).

STARS reservoir simulations equations are formulated in two broad categories as follows.

a) Implicit pressure and explicit saturation (IMPES)

In IMPES methodology, the value of pressure in grid block for the current time step is computed implicitly, followed by explicit computation of fluid saturation for the grid block (Satter & Iqbal, 2016). Satter and Iqbal (2016) have reported the sequence of calculation for IMPES formulation.

b) Fully implicit

In the fully implicit method, the coefficients used in both pressure and saturation equations are evaluated at the current time step in an implicit manner. The implicit method is performed iteratively (via Newton's iteration method) until a convergence is achieved for both pressure and saturation values in a grid block. Also, the coefficients of the nonlinear PDEs in the simulation are updated in each iteration, which is in contrast to the IMPES methodology (Satter & Iqbal, 2016; CMG, 2020). Satter and Iqbal (2016) have provided a detailed outline of the fully implicit procedure.

STARS also benefits from a solution scheme called Adaptive-Implicit Method (AIM). The AIM method provides various degrees of explicitness for different grid block, which translates into CPU saving in comparison with a fully implicit method. Grid blocks that are experiencing large throughputs or rapid changes in primary variables (such as pressure, saturation, and temperature) are treated fully implicit. Grid blocks in which the changes or throughput are small are handled in an IMPES fashion (CMG, 2020).